# Molybdenum Quinonoid Complexes: Synthesis, Characterization, and Reactivity

Thesis by
Justin T. Henthorn

In Partial Fulfillment of the Requirements
for the Degree of Doctor of Philosophy

CALIFORNIA INSTITUTE OF TECHNOLOGY
Division of Chemistry and Chemical Engineering
Pasadena, California
2016
(Defended on 14 January, 2016)

*To my mother and father, Cheryl and Dave,*

*My sisters, Brittany and Heather,*

*And my wife, Kate*

*"A man who has been through bitter experiences and travelled far enjoys even his sufferings after a time"*

–Homer, The Odyssey

*"And now we are Free. I will see you again... but not yet... Not yet!"*
–Juba, Gladiator

## ACKNOWLEDGEMENTS

I would like to begin by thanking my family, who have always been a constant source of love, encouragement, and support. Thank you, mom and dad, for being amazing parents who presented me with so many wonderful opportunities. Growing up, I never thought there was something that I couldn't do. You taught me to believe in myself, and to follow my passion. Thank you for letting me drive across the country to California, and thank you for always welcoming me back home. To my sister Brittany, you are so talented and passionate, you astound me with everything you do. You are the best best man a brother could ask for. To my sister Heather, I don't think I will ever quite understand your love of sports, but thank you for showing me what it means to be dedicated and determined. I always admired your drive for softball and your belief in sisterhood.

Prof. Theodor Agapie, thank you for accepting me into Caltech, for taking me into your group, for your mentorship, and for your time. My road to Caltech was a bit unusual, I had applied late and hadn't participated in a visiting weekend, but you set up a phone call with me so that I might get a better feel for Caltech, and you might get a better feel for me as a student. You always tried to make yourself available to your students, which I greatly appreciate. You taught me what it meant to be rigorous, and I I value your emphasis on chalk talks and always having us, the students, present to visitors and speakers. Thank you for being patient with me at times, and thank you for being direct.

Prof. Jonas Peters, thank you for chairing my committee and for teaching me about EPR and nitrogenase. Profs. Brian Stoltz and Harry Gray, thank you for serving on my thesis committee. Thank you for encouraging my ideas, and pushing me intellectually.

Thank you Profs. Jeff Rack and Mike Jensen, for getting me into research as an undergraduate. Jeff, you were a great mentor to me and incredibly supportive. I certainly would not have come to Caltech were it not for you. You showed me how cool it was to be a chemist, and I met great friends and great people in your lab. You are the kind of professor I would want to be.

Thank you to all Agapie group members past, present and future. To my cohort in the group, thank you for your support and friendship. Guy Edouard, thank you for helping me to laugh at everything, for standing by me at the worst of times, and for never giving up. You always tried to help, and you did so much for this group. Kyle Horak, thank you for being a great colleague and labmate, and thank you for your inebriated shenanigans. Josh Wiensch, thank you for introducing me to rock climbing, and for playing Call of Duty with me, and thank you for being a great housemate.

To the students who came before us, thank you for leading the way. Emily Tsui, thank you for including me in dumplings and movies and drinking and Left 4 Dead. Paul Kelley, thank you for making the bad days better, and being a fantastic bay-mate and friend. Sibo Lin, thank you for showing me all of the benefits of the good schedule. Maddy Radlauer, thank you for serving as Safety Officer and for tolerating me in box 3. Jacob Kanady, thank you for being one of the few people in lab to yell at me. Davide Lionetti, thank you for teaching me about copper and $O_2$ reduction, and for great inebriated shenanigans with Kyle.

To the students who came after us, thank you for helping push us out the door. Josh Buss, I am convinced that you can fix anything in lab, and your mechanical as well as chemical skills will serve you well no matter where you end up. Jessica Sampson, thank you for working hard to keep us all safe, and for calling out people for their BS. Marcus Low, thank you for being so very sarcastic, and for your excellent party planning skills. Heui Beom Lee, thank you for your assistance with crystal samples and for being so laid back, your calm was noticeable in lab. To the even younger generation, Chris Reed, Nate Hirscher, and Ryan Ribson, and you have such youth and energy, I hope nothing but the best for you. And to the four horsemen of the Postdoc-alyse, Zhiji Han, Siti Riduan, Graham de Ruiter and Alejo Lifschitz, thank you for bringing such diverse and unique personalities to the group. I appreciate all that you've contributed, both in and out of lab. Special shout-out to the Chicken crew, I miss you already.

To the undergraduates I've overlapped with, Ruomeng Wan, Kurtis Carsch, Bogdan Dimitriu, Aya Buckley, Chung-Sun Chen, Jennifer Karolewski, Victor Zhao, Agnes Thorarinsdotter, Eva Nichols, Daniel Kim, Christine Cheng, Michael Desanker, Katherine Lee, and Jeff Rosenberg, thank you for showing me that we never stop learning, and that we never stop teaching.

I would also like to thank the many wonderful staff and administrators at Caltech who are often working tirelessly behind the scenes but without whom this work would have never been completed, including Margarita Davis and Julianne Just, Anne Penney, Agnes Tong, Joe Drew, David Vander Velde, Larry Henling and Michael Takase.

Finally, I would like to thank my best friend, my anchor, my love, Kate Gulino.

## ABSTRACT

π-bound Molybdenum-quinonoid complexes supported by pendant phosphines were prepared and investigated for metal-ligand cooperative reactivity and access to multiple equivalents of protons and electrons within a single transition metal complex. Chapters 3, 4, and 5 of this dissertation describe the synthesis, characterization, and reactivity of these complexes in the context of multiproton, multielectron chemistry and small molecule activation.

Chapter 2 presents the synthesis of an unprecedented bis-borane supported peroxide dianion, prepared from a mixture of ferrocenes, borane, and dioxygen. The peculiarity of such a structure is emphasized, and reactivity explored. While ferrocenes of varying reduction potential were found to lead to the peroxide, only tris(pentafluorophenyl)borane was found to yield isolable peroxide, with other boranes leading to oxygenation or borate formation.

Chapter 3 describes the synthesis of a series of π-bound Molybdenum-quinonoid complexes and explores their reactivity with dioxygen. The Mo-quinonoid interaction is probed and elucidated through a number of reactions and experiments, highlighting the importance of the electronic coupling of the metal center with the organic fragment on overall reactivity with $O_2$.

Chapter 4 further explores the π-bound Molybdenum-quinonoid complexes in various protonation and oxidation states, totaling four electrons and two protons accessible to the system. Proton-coupled electron transfer was demonstrated in two different

oxidation states, and the effects of the metal-quinonoid interaction on the transfer of protons and electrons investigated thermochemically.

Chapter 5 explores the potential for π-bound Molybdenum-quinonoid complexes to access inner-sphere reactivity. The activation of E–X bonds, including $H_2$ and $PhSiH_3$, is demonstrated, as well as catalytic hydrosilylation of aldehydes.

Appendix A describes initial investigations into the preparation of heterobimetallic complexes supported by the catechol-diphosphine ligand framework. The synthesis of heterobimetallic MoCu complexes is presented and their structural parameters discussed.

Appendix B outlines the synthesis of multinucleating ligand platforms based off bipyridine frameworks, for the preparation of biologically inspired multimetallic complexes. Dioxygen reactivity of a dicopper system is also briefly presented.

Appendix C contains relevant NMR spectra for the compounds presented in the preceding sections.

## PUBLISHED CONTENT AND CONTRIBUTIONS

Henthorn, J.T.; Agapie, T. *Angew. Chem., Int. Ed.* **2014**, *53*, 12893−12896.
J.T.H. developed the project, synthesized and characterized all compounds, designed and performed all experiments, analyzed and interpreted all data and wrote the manuscript.

Henthorn, J.T.; Lin, S.; Agapie, T. *J. Am. Chem. Soc.* **2015**, *137*, 1458−1464.
J.T.H. developed the project, synthesized and characterized all but one compound, designed and performed all experiments, analyzed and interpreted all data and wrote the manuscript. S.L. developed the ligand and synthesized one Molybdenum compound. Christine Cheng contributed to the development of the ligand.

Henthorn, J.T.; Agapie, T. *Inorg. Chem.* **2016**, *55*, 5337–5342.
J.T.H. developed the project, synthesized and characterized all but one compound, designed and performed all but one experiment, analyzed and interpreted all data and wrote the manuscript. Marcus Low synthesized and characterized a metal-free quinone and performed a control experiment with TEMPOH.

# TABLE OF CONTENTS

# LIST OF FIGURES

# LIST OF SCHEMES

# LIST OF TABLES

# CHAPTER 1

# General Introduction

This dissertation deals primarily with the synthesis, characterization, and reactivity studies of π-bound Molybdenum-quinonoid complexes. Emphasis is placed on multiproton, multielectron chemistry in the context of small molecule activation, as well as metal-ligand cooperation.

Small molecule activation, from $N_2$ or $O_2$ reduction to $H_2O$ oxidation requires the making and breaking of multiple chemical bonds, and thus requires the controlled transfer of multiple equivalents of protons and electrons. In nature, there are two basic startegies employed to facilitate the transfer of multiple equivalents of electrons: cooperative reactivity of multiple metal centers, or participation of non-innocent or redox active ligands. In the former case, several metal centers distribute the redox requirement so as not to build up charge at a single center, thus lowering the energy of the system and facilitating the desired chemistry, while in the latter, organic fragments are used to store and transfer redox equivalents in place of additional metal centers. The concept of non-innocent or redox active ligands has gained significant interest in past few years, with base metals demonstrating reactivity similar to their more noble counterparts.

Our group has investigated terphenyldiphosphine ligands which enforce metal-arene interactions, and in several instances observed unusual or non-innocent behavior. In the case of a Ni-H compound, the H was found to migrate reversibly from the metal center to the central arene of the ligand yielding an allyl moiety, a reversible transfer of formally protons and electrons between a transition metal and ligand. In an attempt to better control such a transfer of protons and electrons between a metal and ligand, the terphenyldiphosphine ligand was functionalized with a catechol or ortho-hydroquinone moiety. The two protons and two electrons potentially accessible from the hydroquinone/quinone couple, in addition to any redox states accessible at the metal center, was envisioned as a route to facile small molecule activation.

Low-valent molybdenum complexes were targeted for their ability to bind small molecules such as $N_2$ or $CO_2$, as well as their propensity to engage in metal-arene interactions. Reaction with $Mo(CO)_3$ precursors resulted in successful metalation of the functionalized diphosphine and access to Mo-quinonoid chemistry. In exploring the coordination chemistry of the Mo-quinonoid complexes, it was observed that the $Mo^0$-catechol complex reacts with $O_2$ to yield a $Mo^0$-quinone product and $H_2O$. This reactivity was explored in depth (Chapter 3). An outer-sphere reduction-initiated mechanism was elucidated through the use of an external Lewis acid combined with the unfunctionalized metal complex, which led to isolation of a bis-borane peroxide and $Mo^I$ compound. The bis-borane peroxide was investigated further (Chapter 2), while the investigation of the Mo-quinonoid complexes was also expanded.

Multiple oxidation and protonation states within the system were accessed, demonstrating a total of two protons and four electrons (Chapter 4). Thermochemical analysis was used to probe the effect of the metal-quinonoid interaction on the proton-coupled electron transfer chemistry of the organic fragment, with significant attenuation of the bond dissociation free energy of the first O–H moiety observed upon oxidation of the metal center. Changes in acidities and reduction potentials as a function of oxidation state and metal-quinonoid interaction could allow access to different mechanistic pathways within proton-couple electron transfer reactions.

From there, this dissertation continues with a discussion of efforts to access inner-sphere small molecule activation (Chapter 5). Two-electron reduction of a $Mo^{II}$-quinone complex was found to yield a $Mo^0$-quinone product that demonstrated E–X bond activation to yield Mo–Cl and Mo–H products. The same compound was also found to be a catalyst for the hydrosilylation of aldehydes, with a proposed mechanism involving Lewis-base catalysis. Finally, the dissertation discusses the potential of using the catechol-diphosphine ligand in the synthesis of bimetallic complexes, with initial successes including Mo-Cu bimetallic systems (Appendix A).

# CHAPTER 2

DIOXYGEN REDUCTION

## Dioxygen Redox Chemistry with the Ferrocene-Lewis Acid Combination: Reduction to a Boron Peroxide in the Presence of Tris(pentafluorophenyl)borane

Published in part as:
*Angew. Chem., Int. Ed.* **2014**, *53*, 12893−12896

**ABSTRACT**

Although several Group 13 peroxides have been reported, boron-supported peroxides are rare, with no structurally characterized examples of the $BO_2B$ moiety. Herein, the synthesis of a bis-borane supported peroxide and its structural and electrochemical characterization is described. Typically air-stable outer-sphere single-electron transfer reagents, ferrocenes were found to react with dioxygen in the presence of $B(C_6F_5)_3$, a Lewis acid unreactive to $O_2$, to generate bis-borane peroxide.

## INTRODUCTION

Dioxygen reduction to peroxide represents an important chemical transformation for energy generation and storage applications in fuel cells and Li-$O_2$ batteries[1]. Transition metal supported peroxides is an intermediate in the reduction of $O_2$.[2] Peroxides are also powerful oxidants that exhibit interesting and synthetically useful reactivity derived from the inherently weak O–O bond.[3] Next to carbon, organosilicon-based peroxides have been the most well studied and developed of the main group peroxides, and the combination of the weak O–O bond with the strong Si–O interaction has led to new and diverse reactivity.[4] Group 13 peroxides are comparatively less developed. Several examples of In,[5] Ga,[6] and Al[7] have been isolated and structurally characterized. These compounds are typically prepared by treatment of group 13 alkyl species with an organic hydroperoxide or inorganic superoxide, and by $O_2$ insertion to generate alkyl peroxide moieties. The isolation of these compounds is remarkable given the reducing power of the element-alkyl bonds and the oxidizing potential of the O–O bond are stored in the same molecule.[6c, 6d, 7a] Organoboron-based peroxides are very rare. There have only been three reports on structurally characterized compounds containing a peroxy-boranyl (RB–$O_2$) linkage.[8] This paucity of stable and structurally characterized molecules containing the peroxy-boranyl moiety is likely due to its propensity to undergo oxidative C–B bond cleavage.[9] Herein we report the synthesis and structural characterization of the first bis-borane supported peroxide dianion, wherein the source of the $[O_2]^{2-}$ moiety is dioxygen, generated in connection with decamethylferrocene ($Cp^*_2Fe$) and ferrocene ($Cp_2Fe$) as reductants.

## Results and Discussion

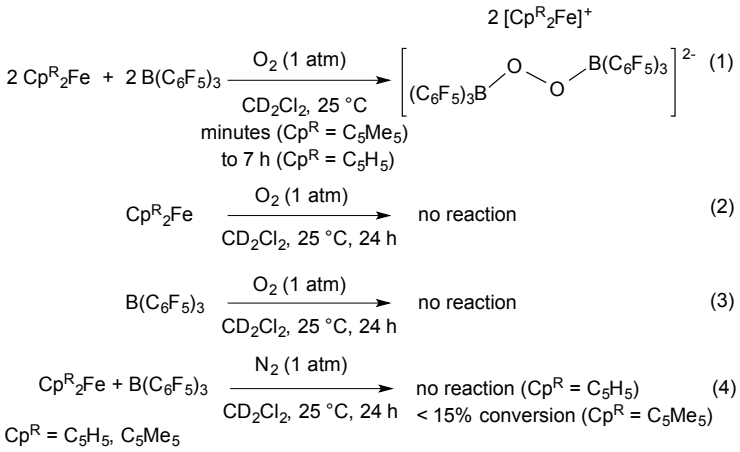


Exposure of an equimolar mixture of $Cp^*_2Fe$ and $B(C_6F_5)_3$ in deuterated dichloromethane to excess $O_2$ at room temperature led to a color change from yellow-orange to deep forest green upon addition (eq 1), consistent with oxidation of $Cp^*_2Fe$ to the decamethylferrocenium cation ($Cp^*_2Fe^+$). This assignment was further supported by $^1H$ NMR spectroscopic data that revealed the $Cp^*$ (pentamethylcyclopentadienyl) methyl peak had shifted upfield from 1.8 ppm to approximately -25 ppm. The $^{19}F$ NMR spectrum of the dark green solution revealed a set of new peaks at -130, -165, and -168 ppm, consistent with a tetrahedral boron center.[10] Toepler pump measurements indicate the consumption of 0.42 equiv of $O_2$, UV-Vis measurements show the generation of 0.85 equiv of $Cp^*_2Fe^+$ consistent with the two electron reduction of $O_2$. If the reaction is sufficiently concentrated, dichroic green/blue crystals precipitate from solution within minutes. An X-ray diffraction study of these crystals revealed the solid-state structure of the resulting product to contain an unprecedented bis-borane-supported peroxide dianion **2.1**$^{2-}$ with two decamethylferrocenium counter cations (Figure 2.1). The O–O (1.485(2) Å) and B–O (1.472(2) Å) distances are similar to the previously reported examples of B–O–O moieties supported by four coordinate boron, and consistent with the formation of a peroxide moiety. These distances

are 1.527(3) and 1.456(2) Å, respectively, for a B–O–O–C moiety resulted from the reaction of 9-boraanthracene with $O_2$.[8b] For a B–O–O–C motif resulted from a phosphine borane reaction with singlet $O_2$, the structural parameters are 1.454(6) and 1.473(4) Å, respectively.[8a] A B–O–O–Rh moiety resulted from the reaction of a Rh-peroxo with a boronic acid displays a trigonal boron,[8c] with the B–O distance shorter (1.400(2) Å) and the O–O distance longer (1.497(1) Å) than the above, likely because of the stronger interaction between O and three-coordinate boron. The B–O–O angle (106.9(1)°) is similar to the C–O–O angle (107.5(2)°) in bis(triphenylmethyl)peroxide[11].

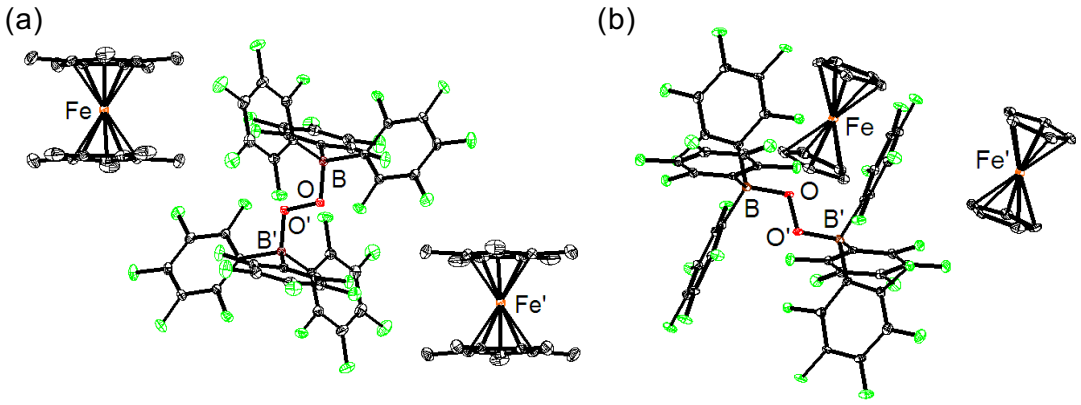


**Figure 2.1.** Solid state structures of [**2.1**$^{2-}$][$Cp^*_2Fe^+$]$_2$•2$CH_2Cl_2$ (a) and [**2.1**$^{2-}$][$Cp_2Fe^+$]$_2$ (b). Hydrogen atoms and solvent molecules omitted for clarity. Fluorine and carbon atoms depicted in light grey and black, respectively. Select bond distances and angles: (a) B–O = 1.472(2) Å, O–O' = 1.485(2) Å, ∠B–O–O' = 106.9(1)° (b) B–O = 1.472(5) Å, O–O' = 1.487(5) Å, ∠B–O–O' = 108.0(3)°.

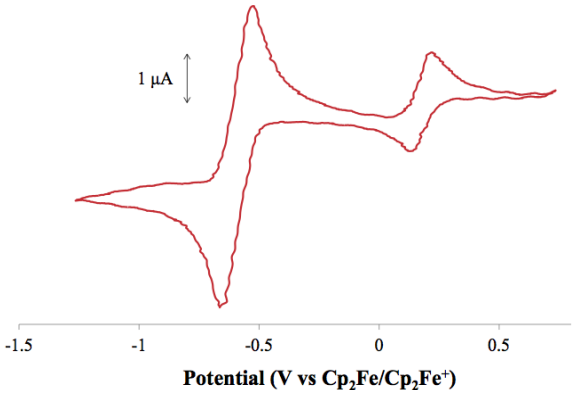


**Figure 2.2.** Cyclic voltammogram of [**2.1**$^{2-}$][$Cp^*_2Fe^+$] in 0.1 M [$nBu_4N^+$][$PF_6^-$] in DCM recorded with a glassy carbon electrode. Scan rate of 50 mV/s. Potentials referenced to $Cp_2Fe/Cp_2Fe^+$.

Electrochemical investigation of [**2.1**$^{2-}$][$Cp^*_2Fe^+$]$_2$ by cyclic voltammetry (Figure 2.2) revealed the reversible redox couple of $Cp^*_2Fe/Cp^*_2Fe^+$ referenced to -0.59 V (vs $Cp_2Fe/Cp_2Fe^+$)[12] and a quasi-reversible redox event centered at +0.17 V (vs $Cp_2Fe/Cp_2Fe^+$) assigned to the [**2.1**$^{2-}$] fragment. This event was assigned to a single-electron oxidation to form a superoxide species that is unstable in solution. The double concentration of $Cp^*_2Fe^+$ vs [**2.1**$^{2-}$] results in the observed relative peak size. Attempts to access the presumed superoxide via means of chemical oxidation have resulted in complex mixtures of diamagnetic species by $^{19}$F NMR spectroscopy. This redox potential is more positive than that of cryptand-encapsulated peroxide,[13] demonstrating greater stabilization of the anionic peroxo moiety by the Lewis acidic boranes over the cryptand hydrogen bonding.

The weaker reductant ferrocene was also found to react with dioxygen in the presence of $B(C_6F_5)_3$, yielding a species similar to [**2.1**$^{2-}$][$Cp^*_2Fe^+$]$_2$ by $^{19}$F NMR spectroscopy; however, the reaction is considerably slower, requiring several hours to complete.[14] The formation of

the peroxide dianion [**2.1**$^{2-}$] was confirmed crystallographically (Figure 1), with structural parameters very similar for the two versions differing in the nature of the cation. Additional experiments were performed with ferrocenes and boranes to better understand the formation of [**2.1**$^{2-}$]. As control reactions, solutions of $Cp_2Fe$, $Cp^*_2Fe$ and $B(C_6F_5)_3$ were exposed separately to an atmosphere of $O_2$ and monitored by $^1H$ NMR spectroscopy (eqs 2 and 3). No conversion was observed over 24 hours. A mixture of $Cp^*_2Fe$ and $B(C_6F_5)_3$ at room temperature, under $N_2$, led to slow formation of $Cp^*_2Fe^+$, with less than 15% conversion after 24 hours, and unidentified species by $^{19}F$ NMR spectroscopy. There is no observable oxidation of $Cp_2Fe$ in the presence of $B(C_6F_5)_3$ over similar timescales. These control experiments show that the reduction of $O_2$ (eq 1) requires both the reductant and the Lewis acid. The observed slow conversion of the stronger reductant $Cp^*_2Fe$ vs $Cp_2Fe$ in the absence of $O_2$ is reminiscent of the reduction of $B(C_6F_5)_3$ by $Cp^*_2Co$ to generate the $[B(C_6F_5)_3]^-$ radical anion[15] that decomposes to a complex mixture of species in dichloromethane;[16] however, attempts to detect the $[B(C_6F_5)_3]^-$ radical anion by EPR spectroscopy have been unsuccessful to date. Although $Cp^*_2Fe$ has a reduction potential significantly more positive than $B(C_6F_5)_3$ (vide infra), redox chemistry has been reported between $B(C_6F_5)_3$ and metal complexes that are weak reductants.[17]

Formation of [**2.1**$^{2-}$] is not inhibited by the presence of the bulky base 2,6-di-tert-butyl-4-methylpyridine (DTBMP) for either ferrocene or decamethylferrocene, inconsistent with a mechanism initiated by protonation of Fe[18] with adventitious strong acid.[19] Performing the reaction of $Cp_2Fe$, $B(C_6F_5)_3$, and $O_2$ in the presence of sub-stoichiometric strong acid $H(OEt_2)_2B[C_6H_3(CF_3)_2]_4$ resulted in conversion to a mixture of species by $^{19}F$ NMR spectroscopy, including the bis-borane-hydroxide anion $[[(F_5C_6)_3B]_2OH^-]$ as a major component.[20] With 50 mol % $H(OEt_2)_2B[C_6H_3(CF_3)_2]_4$, $[[(F_5C_6)_3B]_2OH^-][Cp_2Fe^+]$ was

isolated in 35 % yield, and its structure was confirmed crystallographically (SI). In an attempt to access [**2.1**$^{2-}$] via an alternative route, reaction of 4 equivalents of $B(C_6F_5)_3$ with 1 equivalent of DABCO•$2H_2O_2$ and 1 equivalent of DABCO (DABCO = [2.2.2]-diazabicyclooctane) resulted in a mixture of species by $^{19}F$ NMR spectroscopy. Treating the isolated peroxide [**2.1**$^{2-}$][$Cp^*_2Fe^+$]$_2$ with acid also resulted in a mixture of unidentified species by $^{19}F$ NMR spectroscopy. These results suggest that in the presence of Br*ønsted* acid, ferrocenes and $B(C_6F_5)_3$ different $O_2$ reduction pathways are operative. Moreover, the B–O–O–B moiety of [**2.1**$^{2-}$] is not stable in the presence of protons (or the combination with conjugate bases). Therefore, the reductive synthesis from $O_2$ is instrumental for the isolation of [**2.1**$^{2-}$].

The difference in rates for $Cp_2Fe$ vs $Cp^*_2Fe$ indicates that the stronger reductant better facilitates the reaction, even though neither reacts with $O_2$ directly. Several other boron-based Lewis acids were tested in combination with $Cp^*_2Fe$ or $Cp_2Fe$ for reactivity with $O_2$. $BF_3$•$OEt_2$, $B(C_6H_5)_3$, and $B(C_6F_5)_2(C_6H_5)$ show generation of the respective ferrocenium cations ($Cp_2Fe^+$ for $BF_3$•$OEt_2$, $Cp^*_2Fe^+$ for $B(C_6H_5)_3$ and $B(C_6F_5)_2(C_6H_5)$), indicating that electron transfer does occur. However, the only characterized boron products were borates resulting from ligand scrambling and oxygenation ($BF_4^-$, $B(OC_6H_5)(C_6H_5)_3^-$, and $B(C_6F_5)_2(C_6H_5)_2^-$, respectively), without a peroxide moiety.[21] These studies indicate that the electron deficient $C_6F_5$ moiety, less prone to migration, is instrumental for the isolation of the $B_2O_2$ species.

The formation of compound [**2.1**$^{2-}$] represents a rare example of using ferrocenes to reduce dioxygen to peroxide in the absence of additional transition metal catalyst or strong Brønsted acid. Although the reaction of ferrocene with $O_2$ in the presence of excess Lewis acids of the form $MX_3$ (X = Cl for M = Al, As, Bi, and Sb; X = F for M = B) to yield the

corresponding ferrocenium salts $[Cp_2Fe^+][MX_4^-]$ was previously reported, the oxygen-containing by-products eluded characterization.[22] More recently, Zheng reported the $B(C_6F_5)_3$ catalyzed disproportionation of superoxide into dioxygen and peroxide,[23] though the putative $B–O_2^{n-}$ species remained elusive. Activation of $O_2$ either inner-[24] or outer-sphere[25] by ferrocenes has been proposed. Additionally, the generation of reduced borane, $•B(C_6F_5)_3^-$ by species less reducing than $Cp^*_2Fe$ has been reported.[17, 26] Although the one-electron reduction potentials are mismatched with $Cp_2Fe$ or even $Cp^*_2Fe$ (-1.18 V vs $Cp_2Fe/Cp_2Fe^+$ in DMSO for $O_2^-/O_2$ couple[27] and -1.79 V vs $Cp_2Fe/Cp_2Fe^+$ in DCM for $•B(C_6F_5)_3^-/B(C_6F_5)_3$ couple[16, 28]), the presence of the Lewis acidic $B(C_6F_5)_3$ may facilitate direct reduction of $O_2$ by ferrocenes, as demonstrated for rates of electron transfer that increase with coupling to proton or metal transfer.[29]

## CONCLUSIONS

In summary, a facile synthesis and structural characterization of the bis-borane supported peroxide [**2.1**$^{2-}$] was reported. Taking advantage of readily available starting materials, reduction of dioxygen with ferrocenes in the presence of $B(C_6F_5)_3$ generates the $B_2O_2$ moiety. Notably, the precursors are separately unreactive with $O_2$ under ambient conditions, highlighting the reduction of $O_2$ facilitated by Lewis acid binding. Other boron based Lewis acids underwent ligand disproportionation, indicating that the electron deficient $C_6F_5$ moiety is important for the stability of the bis-borane peroxide.

## EXPERIMENTAL SECTION

### General considerations:

Unless indicated otherwise, reactions performed under inert atmosphere were carried out in oven-dried glassware in a glovebox under a nitrogen atmosphere purified by circulation through RCI-DRI 13X-0408 Molecular Sieves 13X, 4x8 Mesh Beads and BASF PuriStar® Catalyst R3-11G, 5x3 mm (Research Catalysts, Inc.). Anhydrous dichloromethane was purified by sparging with nitrogen for 15 minutes and then passing under nitrogen pressure through a column of activated A2 alumina (Zapp's). $CD_2Cl_2$ was purchased from Cambridge Isotope Laboratories, dried over calcium hydride, then degassed by three freeze-pump-thaw cycles and vacuum-transferred prior to use. $^1H$ and $^{19}F$ NMR spectra were recorded on Varian Mercury 300 MHz spectrometers at ambient temperature, unless denoted otherwise. $^1H$ NMR chemical shifts are reported with respect to internal solvent: 5.32 ppm for $CD_2Cl_2$. $^{19}F$ NMR chemical shifts are reported with respect to an external standard of $C_6F_6$ (-164.9 ppm). Elemental analysis was conducted by Robertson Microlit Labs (Ledgewood, NJ).

Electrochemical measurements were recorded with a Pine Instrument Company AFCBP1 bipotentiostat using the AfterMath software package. Cyclic voltammograms were recorded on ca. 2 mM solutions of the relevant complex in the glovebox at 20 °C with an auxiliary Pt-coil electrode, a $Ag/Ag^+$ reference electrode (0.01 M $AgNO_3$, 0.1 M [$^n$Bu$_4$N$^+$][$PF_6^-$] in MeCN), and a 3.0 mm glassy carbon electrode disc (BASI). The electrolyte solution was 0.1 M [$^n$Bu$_4$N$^+$][$PF_6^-$] in $CH_2Cl_2$. All reported values are referenced to an internal ferrocene/ferrocenium couple.

Unless otherwise noted all chemical reagents were purchased from commercial sources and used without further purification. Ferrocene, decamethylferrocene, 2,6-di-*tert*-butyl-4-methylpyridine (DTBMP), [2.2.2]-diazabicyclooctane (DABCO) and tris(pentafluorophenyl)borane were purchased from SigmaAldrich and sublimed prior to use; $B(C_6F_5)_3$ was sublimed twice prior to use. DABCO-$2H_2O_2$ and $H(OEt_2)_2BArF^{24}$ were prepared according to the literature methods.[30,31]

**NMR Scale Reactions of $Cp_2Fe$, $Cp^*_2Fe$, $B(C_6F_5)_3$, and $O_2$**

*$B(C_6F_5)_3$ and $O_2$*: A solution of $B(C_6F_5)_3$ (0.0203 g, 0.039 mmol) in $CD_2Cl_2$ (0.6 mL) was degassed via three freeze-pump-thaw cycles in a J. Young NMR tube. An atmosphere of $O_2$ was admitted to the headspace of the tube and the reaction was continuously inverted over 24 hours at room temperature, monitoring by $^{19}F$ NMR spectroscopy (see **Figure C2.1**).

*$Cp^*_2Fe$ and $O_2$*: A solution of $Cp^*_2Fe$ (0.0138 g, 0.042 mmol) in $CD_2Cl_2$ (0.6 mL) was degassed via three freeze-pump-thaw cycles in a J. Young NMR tube. An atmosphere of $O_2$ was admitted to the headspace of the tube and the reaction was continuously inverted over 24 hours at room temperature, monitoring by $^1H$ NMR spectroscopy (see **Figure C2.2**).

*$Cp^*_2Fe$ and $B(C_6F_5)_3$ under $N_2$ – NMR*: A solution of $Cp^*_2Fe$ (0.0130 g, 0.040 mmol) and $B(C_6F_5)_3$ (0.0202 g, 0.040 mmol) in $CD_2Cl_2$ (0.6 mL) was added to a J. Young NMR tube and monitored over time by $^1H$ and $^{19}F$ NMR spectroscopy (see **Figure C2.3-4**).

*$Cp^*_2Fe$ and $B(C_6F_5)_3$ under $N_2$ – UV-vis*: A mixed solution of $Cp^*_2Fe$ (0.0131 g, 0.040 mmol) and $B(C_6F_5)_3$ (0.0203 g, 0.040 mmol) in DCM (1 mL) was left standing in a sealed 1 dram vial in a nitrogen filled glovebox over 26 hours at room temperature. Aliquots of the reaction were diluted by a factor of 0.06 in DCM and the formation of $Cp^*_2Fe^+$ monitored by UV-vis spectroscopy (see **Figure C2.6**).

*$Cp^*_2Fe$ and $B(C_6F_5)_3$ under vacuum:* In the glovebox, a solution of $Cp^*_2Fe$ (0.0133 g, 0.041 mmol) in $CD_2Cl_2$ (0.3 mL) was added to a J. Young NMR tube and frozen in the cold well cooled by liquid $N_2$. A solution of $B(C_6F_5)_3$ (0.0211 g, 0.041 mmol) in $CD_2Cl_2$ (0.3 mL) was layered on top of the frozen $Cp^*_2Fe$ solution, and the tube frozen again in the cold well. The J. Young NMR tube was then sealed, removed from the glovebox and immediately submersed in an acetone/dry ice bath. The solution was degassed at -80 °C and then allowed to warm to room temperature. The reaction was monitored over time by $^1H$ and $^{19}F$ NMR spectroscopy (see **Figure C2.7-8**).

*$Cp^*_2Fe$, $B(C_6F_5)_3$, and $O_2$*: A solution of $B(C_6F_5)_3$ (0.0259 g, 0.051 mmol) and $Cp^*_2Fe$ (0.0188 g, 0.057 mmol) in $CD_2Cl_2$ (0.6 mL) was degassed via three freeze-pump-thaw cycles in a J. Young NMR tube. An atmosphere of $O_2$ was admitted to the headspace of the tube. Upon inversion of the tube an immediate color change from yellow-orange to

a dark green occurred. $^{1}H$ and $^{19}F$ NMR spectroscopy revealed a single new species (see **Figures C2.9-10**). After approximately 30 minutes a generous amount of dichroic green-blue crystals was observed in the tube.

*$Cp^{*}_{2}Fe$, $B(C_6F_5)_3$, and $O_2$ in the dark*: The above procedure was repeated using $B(C_6F_5)_3$ (0.0258 g, 0.051 mmol) and $Cp^{*}_{2}Fe$ (0.0196 g, 0.057 mmol) in $CD_2Cl_2$ (0.6 mL) with the modification that the J. Young tube was wrapped in aluminum foil to prevent the admittance of any light into the reaction, and the lights were turned off to prevent exposure during transfer into the NMR probe. The same new species was observed by $^{1}H$ and $^{19}F$ NMR spectroscopy as above (see **Figures C2.11-12**).

*$Cp_2Fe$, $B(C_6F_5)_3$, and $O_2$*: A solution of $B(C_6F_5)_3$ (0.0258 g, 0.050 mmol) and $Cp_2Fe$ (0.0109 g, 0.059 mmol) in $CD_2Cl_2$ (0.6 mL) was degassed via three freeze-pump-thaw cycles in a J. Young NMR tube. An atmosphere of $O_2$ was admitted to the headspace and the reaction was inverted continuously and monitored by $^{1}H$ and $^{19}F$ NMR spectroscopy over time. After 7 hours at room temperature the solution had darkened to a deep blue and all of the $B(C_6F_5)_3$ had been consumed and a single major new species was observed by $^{1}H$ and $^{19}F$ NMR spectroscopy (see **Figures C2.13-14**). After degassing the solution via three freeze-pump-thaw cycles the color had turned back to green-blue and significant decomposition was observed by $^{19}F$ NMR spectroscopy (see **Figures C2.15-16**). Repeating the experiment without degassing can result in the formation of crystals suitable for X-ray diffraction.

**NMR Scale Reactions in the Presence of Additives**

*$Cp^*_2Fe$, $B(C_6F_5)_3$, and $O_2$ with 2,6-di-tert-butyl-4-methylpyridine (DTBMP):* A solution of $B(C_6F_5)_3$ (0.0213 g, 0.0416 mmol), $Cp^*_2Fe$ (0.0142 g, 0.0435 mmol), and DTBMP (0.0084 g, 0.0409 mmol) in $CD_2Cl_2$ (0.6 mL) was degassed via three freeze-pump-thaw cycles in a J. Young NMR tube. An atmosphere of $O_2$ was admitted to the headspace of the tube. Upon inversion of the tube an immediate color change from yellow-orange to a dark green occurred. $^1H$ and $^{19}F$ NMR spectroscopy revealed the formation of [**1**$^{2-}$][$Cp^*_2Fe^+$]$_2$ (see **Figures C2.17-18**).

*$Cp_2Fe$, $B(C_6F_5)_3$ and $O_2$ with DTBMP in parallel with $Cp_2Fe$, $B(C_6F_5)_3$ and $O_2$:* A solution of $B(C_6F_5)_3$ (0.0202 g, 0.0395 mmol), $Cp_2Fe$ (0.0074 g, 0.0398 mmol), and DTBMP (0.0082 g, 0.0399 mmol) in $CD_2Cl_2$ (0.6 mL) was degassed via three freeze-pump-thaw cycles in a J. Young NMR tube. At the same time, a solution of $B(C_6F_5)_3$ (0.0214 g, 0.0418 mmol) and $Cp_2Fe$ (0.0082 g, 0.0441 mmol) was degassed via three freeze-pump-thaw cycles in a second J. Young NMR tube. An atmosphere of $O_2$ was admitted to the headspace of each tube, and the reactions followed by $^1H$ and $^{19}F$ NMR spectroscopy (see **Figures C2.19-20**). After approximately 2 hours at room temperature, crystals of the product [**2.1**$^{2-}$][$Cp_2Fe^+$]$_2$ began forming in both tubes, complicating qualitative comparison of the rate of the two reactions by NMR spectroscopy. Overall, the reaction appears unaffected by the presence of DTBMP.

*$Cp_2Fe$, $B(C_6F_5)_3$ and $H(OEt_2)_2BArF^{24}$:* A solution of $B(C_6F_5)_3$ (0.0119 g, 0.0232 mmol), $Cp_2Fe$ (0.0051 g, 0.0274 mmol), and $H(OEt_2)_2BArF^{24}$ (0.0017 g, 0.00168 mmol) in

$CD_2Cl_2$ was degassed via three freeze-pump-thaw cycles. An atmosphere of $O_2$ was admitted to the headspace and the reaction was inverted continuously, monitoring by $^1H$ and $^{19}F$ NMR spectroscopy over time. After approximately 3 hours the $B(C_6F_5)_3$ had been converted to a mixture of [**2.1**$^{2-}$][$Cp_2Fe^+$]$_2$ and other species (see **Figures C2.21-22**).

*$Cp_2Fe$, $B(C_6F_5)_3$ and $H(OEt_2)_2BArF^{24}$:* The reaction was repeated as above using $B(C_6F_5)_3$ (0.0113 g, 0.0221 mmol), $Cp_2Fe$ (0.0046 g, 0.0256 mmol), and $H(OEt_2)_2BArF^{24}$ (0.0095 g, 0.00938 mmol) in $CD_2Cl_2$ (0.6 mL). After approximately 2 hours the $B(C_6F_5)_3$ had been converted to a mixture of species with negligible [**2.1**$^{2-}$][$Cp_2Fe^+$]$_2$ observed (see **Figures C2.23-24**). Crystals formed from this reaction were identified by a preliminary crystal structure as [{$(F_5C_6)B$}$_2OH^-$][$Cp_2Fe^+$] in (see **Figure C2.36**).

**Miscellaneous Reactions**

*Reaction of [**2.1**$^{2-}$][$Cp^*_2Fe^+$]$_2$•2$CH_2Cl_2$ with $H(OEt_2)_2BArF^{24}$:* [**2.1**$^{2-}$][$Cp^*_2Fe^+$]$_2$•2$CH_2Cl_2$ (0.0095 g, 0.00506 mmol) was added to a solution of $H(OEt_2)_2BArF^{24}$ (0.0055g, 0.00543 mmol) in $CD_2Cl_2$ (0.6 mL), and the reaction products observed by $^1H$ and $^{19}F$ NMR spectroscopy (see **Figures C2.25-26**).

*Reaction of [**1**$^{2-}$][$Cp_2Fe^+$]$_2$ with $H(OEt_2)_2BArF^{24}$:* [**2.1**$^{2-}$][$Cp_2Fe^+$]$_2$ (0.0030 g, 0.00160 mmol) was added to a solution of $H(OEt_2)_2BArF^{24}$ (0.0023g, 0.00227 mmol) in $CD_2Cl_2$ (0.6

mL), and the reaction products observed by $^{1}H$ and $^{19}F$ NMR spectroscopy (see **Figures C2.27-28**).

*Reaction of $B(C_6F_5)_3$ with DABCO•$2H_2O_2$ and DABCO:* $B(C_6F_5)_3$ (0.0221 g, 0.0432 mmol) was added to a solution of DABCO•$2H_2O_2$ (0.0020 g, 0.0111 mmol) and DABCO (0.0016 g, 0.0143 mmol) in $CD_2Cl_2$ (0.6 mL) and the reaction products observed by $^{1}H$ and $^{19}F$ NMR spectroscopy (see **Figures C2.29-30**).

**Synthesis of bis(decamethylferrocenium) bis(tris(pentafluorophenyl)boranyl)peroxide [2.1$^{2-}$][$Cp^{*}_2Fe^{+}$]$_2$•$2CH_2Cl_2$**

$B(C_6F_5)_3$ (0.1336 g, 0.261 mmol) and $Cp^{*}_2Fe$ (0.0861 g, 0.264 mmol) were combined in DCM (2 mL) and added to a Schlenk tube charged with a stir bar. The tube was then removed from the glovebox and taken to the Schlenk line where the solution was degassed via three freeze-pump-thaw cycles. Next, an atmosphere of $O_2$ was added to the headspace with rapid stirring. After 5 seconds the solution had turned from yellow-orange to deep forest green. After 2 minutes the stirring was stopped and the solution left standing at room temperature. After 10 minutes at room temperature dichroic crystals began forming. After 30 minutes at room temperature the solution was degassed via three freeze-pump-thaw cycles, and the Schlenk tube was taken back into the glovebox and the crystals collected on a medium porosity glass frit, washing with minimal amounts of cold DCM. The crystals were then dried under vacuum to yield 0.1297g (53.9%) of the titular compound. $^{1}H$ NMR (300 MHz, $CD_2Cl_2$ , 25 °C): δ -34.7

ppm (br). $^{19}$F NMR (125 MHz, $CD_2Cl_2$ , 25 °C): δ -130.0 (br), -164.7 (br), -168.0 (br). $\lambda_{max}$ (DCM, nm), ε ($M^{-1}cm^{-1}$): 780, 1091; 710, 653; 650, 444. Anal. Calcd for [**2.1**$^{2-}$][$Cp^*_2Fe^+$]$_2$•$2CH_2Cl_2$, $C_{78}H_{64}B_2Cl_4F_{30}Fe_2O_2$: C, 49.87; H, 3.43. Found: C, 50.04; H, 3.49.

**Synthesis of bis(ferrocenium) bis(tris(pentafluorophenyl)boranyl)peroxide [2.1$^{2-}$][$Cp_2Fe^+$]$_2$**

$B(C_6F_5)_3$ (0.0113g, ) and $Cp_2Fe$ (0.0043 g, ) were combined in DCM (0.4 mL) and added to a J. Young NMR tube. The tube was removed from the glovebox and taken to the Schlenk line. The solution was degassed via three freeze-pump-thaw cycles and an atmosphere of $O_2$ was added to the headspace. The tube was then continuously inverted for several hours. Over the course of 30-60 minutes the solution changed from orange to green to dark blue. After 2 hours, some dark blue crystals began forming in the tube. After five hours, the reaction had gone to completion by $^{19}$F NMR spectroscopy. After 7 hours, the solution was degassed via three freeze-pump-thaw cycles and taken back into the glovebox. The crystals were then collected on a medium porosity glass frit, washing with minimal amounts of cold DCM. The crystals were then dried under vacuum to yield 0.0043 g (27%) of the desired compound. $^1$H NMR (300 MHz, $CD_2Cl_2$ , 25 °C): δ 31.9 ppm (br). $^{19}$F NMR (125 MHz, $CD_2Cl_2$ , 25 °C): δ -139.8 (br), -165.8 (br), -172.4 (br). Anal. Calcd for [**2.1**$^{2-}$][$Cp_2Fe^+$]$_2$•$CH_2Cl_2$, $C_{57}H_{22}B_2Cl_2F_{30}Fe_2O_2$: C, 45.25; H, 1.47. Found: C, 45.13; H, 1.56.

**Synthesis of ferrocenium bis(tris(pentafluorophenyl)boranyl)hydroxide [$[(F_5C_6)_3B]_2OH^-$][$Cp_2Fe^+$]**

$B(C_6F_5)_3$ (0.0113 g, 0.0221 mmol), $Cp_2Fe$ (0.0046 g, 0.0256 mmol), and $H(OEt_2)_2BArF^{24}$ (0.0095 g, 0.00938 mmol) were combined in DCM (0.5 mL) and added to a J. Young NMR tube. The solution was degassed via three freeze-pump-thaw cycles and an atmosphere of $O_2$ was added to the headspace. The tube was then continuously inverted for several hours, monitoring by $^{19}F$ NMR spectroscopy. After approximately 2 hours the $B(C_6F_5)_3$ had been converted to a mixture of species with negligible [**2.1**$^{2-}$][$Cp_2Fe^+$]$_2$ observed. After approximately 3 hours dark blue crystals formed in the tube, and after degassing were isolated by filtration on a fine porosity glass frit, washing with minimal amounts of cold DCM. The crystals were then dried under vacuum to yield 0.0047 g (35%) of the titular compound. A single crystal X-ray diffraction study was performed on this material (Figure S36). $^1H$ NMR (300 MHz, $CD_2Cl_2$ , 25 °C): δ 30.7 ppm (br). $^{19}F$ NMR (125 MHz, $CD_2Cl_2$ , 25 °C): δ -135.2 (br), -159.1 (br), -164.7 (br).

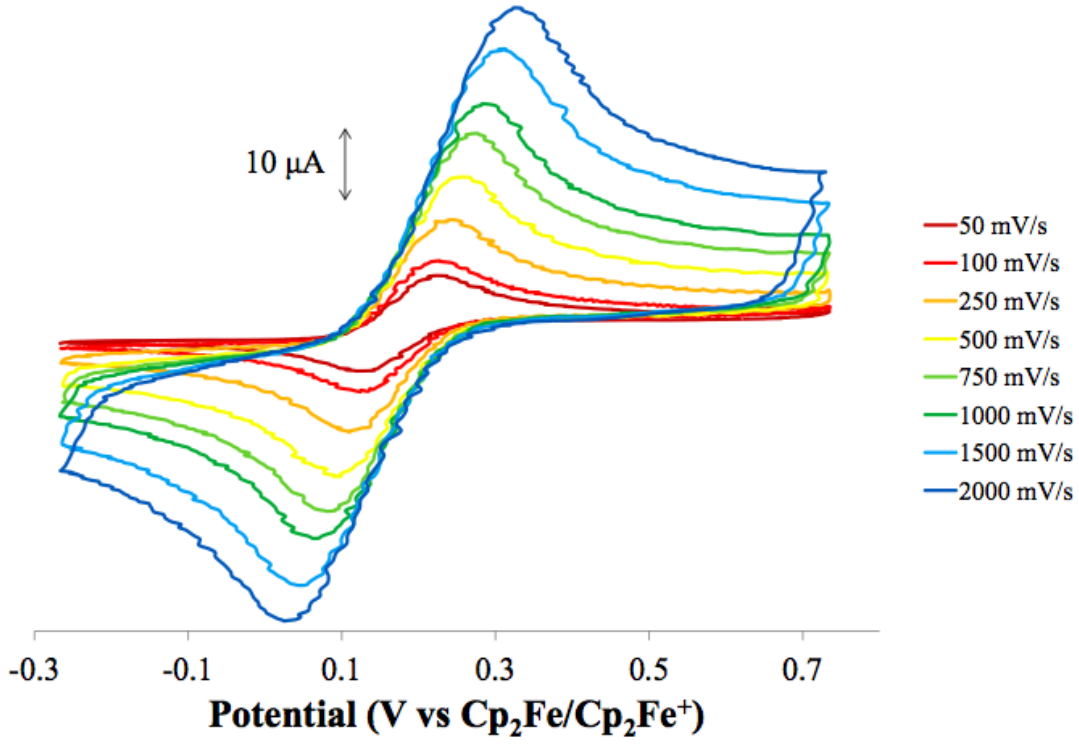


**Figure 2.3.** Variable scan rate cyclic voltammograms of [**2.1**$^{2-}$][$Cp^*_2Fe^+$]$_2$ in 0.1 M [$^n$Bu$_4$N$^+$][PF$_6^-$] in DCM with glassy carbon electrode. Potentials referenced to $Cp_2Fe/Cp_2Fe^+$.

## Crystallographic Information

CCDC 1000579 and 1023005 contain the supplementary crystallographic data for this paper. These data can be obtained free of charge from The Cambridge Crystallographic Data Centre via www.ccdc.cam.ac.uk/data_request/cif.

## Refinement Details

In each case, crystals were mounted on a glass fiber or nylon loop using Paratone oil, then placed on the diffractometer under a nitrogen stream. Low temperature (100 K) X-ray data were obtained on a Bruker APEXII CCD based diffractometer (Mo sealed X-ray tube, $K_\alpha$ = 0.71073 Å) or a Bruker SMART CCD based diffractometer (Mo sealed X-ray tube, $K_\alpha$ = 0.71073 Å). All diffractometer manipulations, including data collection, integration, and scaling were carried out using the Bruker APEXII software.[32] Absorption corrections were applied using SADABS.[33] Space groups were determined on the basis of systematic absences and intensity statistics and the structures were solved by direct methods using XS[34] or by intrinsic phasing using XT (incorporated into SHELXTL) and refined by full-matrix least squares on $F_2$. All non-hydrogen atoms were refined using anisotropic displacement parameters. Hydrogen atoms were placed in the idealized positions and refined using a riding model. The structure was refined (weighed least squares refinement on $F_2$) to convergence. Graphical representation of structures with 50% probability thermal ellipsoids was generated using Diamond visualization software.[35]

**Table 2.1.** Crystal and refinement data for complexes [**2.1**$^{2-}$][$Cp^*_2Fe^+$]$_2$•2$CH_2Cl_2$ and [**2.1**$^{2-}$][$Cp_2Fe^+$]$_2$.

| | [**2.1**$^{2-}$][$Cp^*_2Fe^+$]$_2$•2$CH_2Cl_2$ | [**2.1**$^{2-}$][$Cp_2Fe^+$]$_2$ |
|---|---|---|
| CCDC Number | 1000579 | 1023005 |
| Empirical formula | $C_{38}H_{32}BCl_2F_{15}FeO$ | $C_{28}H_{10}BF_{15}FeO$ |
| Formula weight | 1878.41 g/mol | 1428.04 |
| T (K) | 100 | 100 |
| *a*, Å | 11.330(2) | 10.5469(9) |
| *b*, Å | 14.003(3) | 10.646(1) |
| *c*, Å | 14.176(3) | 12.043(1) |
| α, deg | 114.17(3) | 77.024(3) |
| β, deg | 105.17(3) | 88.081(4) |
| γ, deg | 96.41(3) | 71.474(3) |
| Volume, Å$^3$ | 1918.3(7) | 1248.3(2) |
| Z | 1 | 1 |
| Crystal system | Triclinic | Triclinic |
| Space group | P-1 | P-1 |
| $d_{calc}$, g/cm$^3$ | 1.626 | 1.900 |
| θ range, deg | 2.20 to 43.57 | 2.38 to 30.58 |
| $\mu$, mm$^{-1}$ | 0.639 | 0.742 |
| Abs. Correction | Multi-scan | Multi-scan |
| GOF | 0.961 | 0.9420 |
| $R_1$,[a] $wR_2$ [b] [I>2 σ(I)] | 0.0599, 0.1920 | 0.0869, 0.2449 |

[a] $R_1 = \sum||F_o| - |F_c||/\sum|F_o|$. [b] $wR_2 = [\sum[w(F_o^2-F_c^2)^2]/\sum[w(F_o^2)^2]]^{1/2}$.

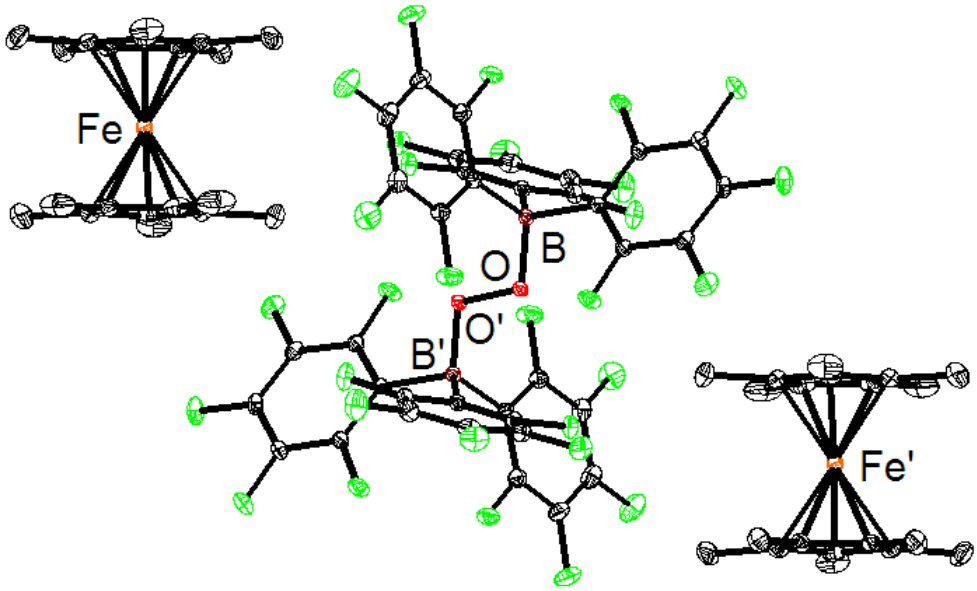


**Figure 2.4.** Structural drawing of [**2.1**$^{2-}$][$Cp^{*}_{2}Fe^{+}$]$_2$•2$CH_2Cl_2$ with 50% probability ellipsoids. Hydrogen atoms and solvent molecules not shown for clarity. Carbon and fluorine atoms shown in black and green, respectively.

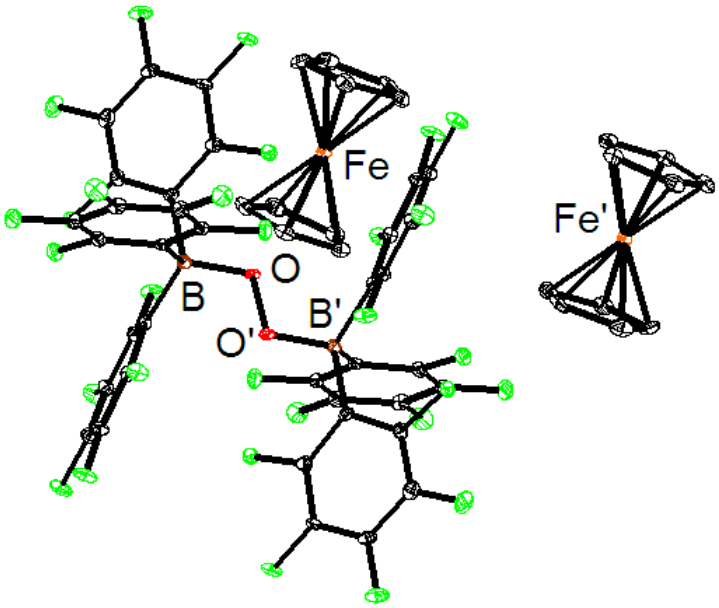


**Figure 2.5.** Structural drawing of [**2.1**$^{2-}$][$Cp_2Fe^+$] with 50% probability ellipsoids. Hydrogen atoms not shown for clarity. Carbon and fluorine atoms shown in black and green, respectively.

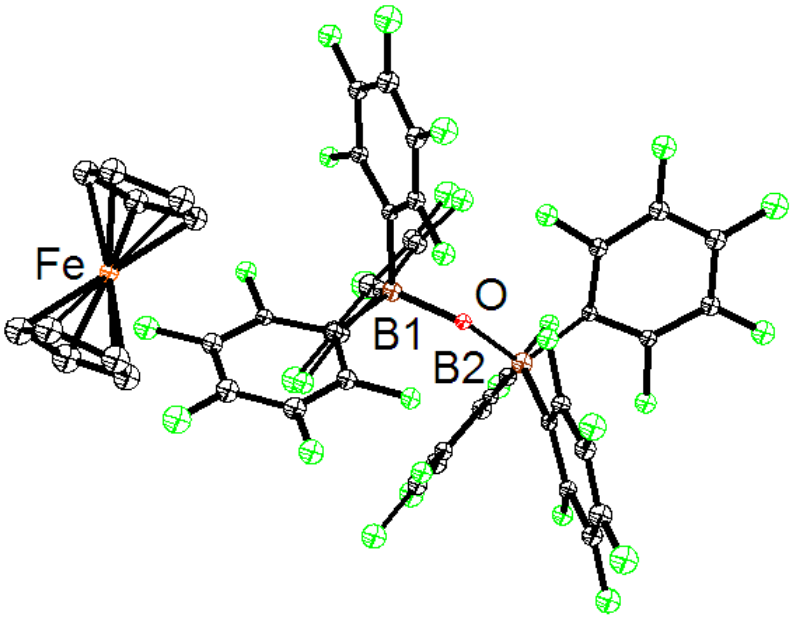


**Figure 2.6**. Preliminary crystal structure of $[\{(F_5C_6)_3B\}_2OH^-][Cp_2Fe^+]\bullet 2CH_2Cl_2$. Hydrogen atoms and solvent molecules not shown for clarity. Carbon and fluorine atoms shown in black and green, respectively.

## REFERENCES


[1] P. G. Bruce, S. A. Freunberger, L. J. Hardwick, J.-M. Tarascon, *Nat Mater* **2012**, *11*, 19-29.

[2] a) M. Sono, M. P. Roach, E. D. Coulter, J. H. Dawson, *Chem. Rev.* **1996**, *96*, 2841-2888; b) G. T. Babcock, M. Wikstrom, *Nature* **1992**, *356*, 301-309.

[3] a) *Peroxide Chemistry: Mechanistic and Preparative Aspects of Oxygen Transfer*, Wiley-VCH, Weinheim, Germany, **2000**; b) C. W. Jones, *Applications of Hydrogen Peroxides and Derivatives*, Royal Society of Chemistry, Cambridge, U.K., **1999**.

[4] a) A. G. Davies, *Tetrahedron* **2007**, *63*, 10385-10405; b) K. Tamao, *Science of Synthesis*, Thieme, Stuttgart, **2002**; c) P. S. Vankar, M. V. R. Reddy, Y. D. Vankar, *Organic Preparations and Procedures International* **1998**, *30*, 373-400.

[5] a) W. Uhl, B. Jana, *Eur. J. Inorg. Chem.* **2009**, *2009*, 3942-3947; b) W. M. Cleaver, A. R. Barron, *J. Am. Chem. Soc.* **1989**, *111*, 8966-8967.

[6] a) W. Uhl, M. R. Halvagar, M. Layh, *Chem. Commun.* **2009**, 4269-4271; b) W. Uhl, M. R. Halvagar, F. Rogel, W. Massa, *Eur. J. Inorg. Chem.* **2009**, *2009*, 489-492; c) W. Uhl, M. Reza Halvagar, M. Claesener, *Chem. Eur. J.* **2009**, *15*, 11298-11306; d) W. Uhl, M. Reza Halvagar, *Angew. Chem., Int. Ed.* **2008**, *47*, 1955-1957; e) W. Uhl, S. Melle, M. Prött, *Z. Anorg. Allg. Chem.* **2005**, *631*, 1377-1382; f) M. B. Power, J. W. Ziller, A. R. Barron, *Organometallics* **1993**, *12*, 4908-4916.

[7] a) W. Uhl, B. Jana, *Chem. Eur. J.* **2008**, *14*, 3067-3071; b) S. S. Kumar, S. Singh, H. W. Roesky, J. Magull, *Inorg. Chem.* **2005**, *44*, 1199-1201; c) J. Lewiński, J. Zachara, P. Goś, E. Grabska, T. Kopeć, I. Madura, W. Marciniak, I. Prowotorow, *Chem. Eur. J.* **2000**, *6*, 3215-3227; d) J. Lewiński, J. Zachara, E. Grabska, *J. Am. Chem. Soc.* **1996**, *118*, 6794-6795; e) D. C. Hrncir, R. D. Rogers, J. L. Atwood, *J. Am. Chem. Soc.* **1981**, *103*, 4277-4278.

[8] a) S. Porcel, G. Bouhadir, N. Saffon, L. Maron, D. Bourissou, *Angew. Chem., Int. Ed.* **2010**, *49*, 6186-6189; b) T. K. Wood, W. E. Piers, B. A. Keay, M. Parvez, *Angew. Chem., Int. Ed.* **2009**, *48*, 4009-4012; c) M. Ahijado, T. Braun, *Angew. Chem., Int. Ed.* **2008**, *47*, 2954-2958.

[9] a) H. G. Kuivila, *J. Am. Chem. Soc.* **1954**, *76*, 870-874; b) H. R. Snyder, J. A. Kuck, J. R. Johnson, *J. Am. Chem. Soc.* **1938**, *60*, 105-111; c) A. D. Ainley, F. Challenger, *J. Chem. Soc.* **1930**, 2171-2180.

[10] D. J. Parks, W. E. Piers, G. P. A. Yap, *Organometallics* **1998**, *17*, 5492-5503.

[11] C. Glidewell, D. C. Liles, D. J. Walton, G. M. Sheldrick, *Acta Crystallogr. Sect. B* **1979**, *35*, 500-502.

[12] N. G. Connelly, W. E. Geiger, *Chem. Rev.* **1996**, *96*, 877-910.

[13] N. Lopez, D. J. Graham, R. McGuire, G. E. Alliger, Y. Shao-Horn, C. C. Cummins, D. G. Nocera, *Science* **2012**, *335*, 450-453.

[14] Additionally, initial attempts to degass a solution of the presumed [12-][Cp2Fe+]2 resulted in a complex mixture of species by 19F NMR.

[15] R. J. Kwaan, C. J. Harlan, J. R. Norton, *Organometallics* **2001**, *20*, 3818-3820.

[16] E. J. Lawrence, V. S. Oganesyan, G. G. Wildgoose, A. E. Ashley, *Dalton Trans.* **2013**, *42*, 782-789.

[17] a) C. J. Beddows, A. D. Burrows, N. G. Connelly, M. Green, J. M. Lynam, T. J. Paget, *Organometallics* **2000**, *20*, 231-233; b) C. J. Harlan, T. Hascall, E. Fujita, J. R. Norton, *J. Am. Chem. Soc.* **1999**, *121*, 7274-7275.

[18] a) B. Su, I. Hatay, P. Y. Ge, M. Mendez, C. Corminboeuf, Z. Samec, M. Ersoz, H. H. Girault, *Chem. Commun.* **2010**, *46*, 2918-2919; b) L. H. Doerrer, M. L. H. Green, *Journal of the Chemical Society, Dalton Transactions* **1999**, 4325-4329.
[19] (H2O)B(C6F5)3 is a strong Bronsted acid and a common impurity of commercial B(C6F5)3 that can be difficult to completely remove even after repeated sublimation/recrystalization.
[20] A. Di Saverio, F. Focante, I. Camurati, L. Resconi, T. Beringhelli, G. D'Alfonso, D. Donghi, D. Maggioni, P. Mercandelli, A. Sironi, *Inorg. Chem.* **2005**, *44*, 5030-5041.
[21] Single crystals were isolated from reaction mixtures, which allowed for structural identification.
[22] G. Stolzle, Ludwig-Maximilians-Universitat **1961**.
[23] D. Zheng, Q. Wang, H.-S. Lee, X.-Q. Yang, D. Qu, *Chem. Eur. J.* **2013**, *19*, 8679-8683.
[24] B. V. Lokshin, I. I. Greenwald, *J. Mol. Struct.* **1990**, *222*, 11-20.
[25] D. S. Choi, D. H. Kim, U. S. Shin, R. R. Deshmukh, S.-g. Lee, C. E. Song, *Chem. Commun.* **2007**, 3467-3469.
[26] X. Zheng, X. Wang, Y. Qiu, Y. Li, C. Zhou, Y. Sui, Y. Li, J. Ma, X. Wang, *J. Am. Chem. Soc.* **2013**, *135*, 14912-14915.
[27] D. L. Maricle, W. G. Hodgson, *Anal. Chem.* **1965**, *37*, 1562-1565.
[28] a) A. E. Ashley, T. J. Herrington, G. G. Wildgoose, H. Zaher, A. L. Thompson, N. H. Rees, T. Kr√§mer, D. O,ÄôHare, *J. Am. Chem. Soc.* **2011**, *133*, 14727-14740; b) S. A. Cummings, M. Iimura, C. J. Harlan, R. J. Kwaan, I. V. Trieu, J. R. Norton, B. M. Bridgewater, F. J√§kle, A. Sundararaman, M. Tilset, *Organometallics* **2006**, *25*, 1565-1568.
[29] a) K. T. Tarantino, P. Liu, R. R. Knowles, *J. Am. Chem. Soc.* **2013**, *135*, 10022-10025; b) S. Fukuzumi, Y. Morimoto, H. Kotani, P. Naumov, Y.-M. Lee, W. Nam, *Nat Chem* **2010**, *2*, 756-759; c) S. Fukuzumi, K. Ohkubo, *Coord. Chem. Rev.* **2010**, *254*, 372-385; d) Y. Morimoto, H. Kotani, J. Park, Y.-M. Lee, W. Nam, S. Fukuzumi, *J. Am. Chem. Soc.* **2010**, *133*, 403-405.
**[**30] Dembech, P.; Ricci, A.; Seconi, G.; Taddei, M. *Org. Synth.* **1997**, *74*, 84.
[31] Brookhart, M.; Grant, B.; Volpe, A.F. *Organometallics* **1992**, *11*, 3920-3922.
[32] APEX2, Version 2 User Manual, M86-E01078, Bruker Analytical X-ray Systems, Madison, WI, June 2006.
[33] Sheldrick, G.M. "SADABS (version 2008/1): Program for Absorption Correction for Data from Area Detector Frames", University of Göttingen, 2008.
[34] Sheldrick, G.M. (2008). Acta Cryst. A64, 112-122.
[35] Brandenburg, K. (1999). DIAMOND. Crystal Impact GbR, Bonn, Germany.

# CHAPTER 3

DIOXYGEN REDUCTION

Combination of Redox-Active Ligand and Lewis Acid for Dioxygen Reduction with π-Bound Molybdenum Quinonoid Complexes

Published in part as:

*J. Am. Chem. Soc.* **2015**, *137*, 1458−1464

## ABSTRACT

A series of π-bound Mo quinonoid complexes supported by pendant phosphines has been synthesized. Structural characterization reveals strong metal-arene interactions between Mo and the π-system of the quinonoid fragment. The Mo-catechol complex (**3.2a**) was found to react within minutes with half an equivalent of $O_2$ to yield a Mo-quinone complex (**3.3**), $H_2O$ and CO. Si- and B- protected Mo-catecholate complexes also react with $O_2$ yielding **3.3** and $(R_2SiO)_n$ and $(ArBO)_3$ byproducts, respectively. Formally, the Mo-catecholate fragment provides two electrons, while the elements bound to the catecholate moiety act as acceptors for the $O_2$ oxygens. Unreactive by itself, the Mo-dimethylcatecholate analog reduces $O_2$ in the presence of added Lewis acid, $B(C_6F_5)_3$, to generate a $Mo^I$ species and a bis-borane supported peroxide dianion, $[[(F_5C_6)_3B]_2O_2^{2-}]$, demonstrating single electron transfer chemistry from Mo to the $O_2$ moiety. The intramolecular combination of molybdenum center, redox active ligand, and Lewis acid reduces $O_2$ with pendant acids weaker than $B(C_6F_5)_3$. Overall, the π-bound catecholate moiety acts as a two-electron donor. A mechanism is proposed where $O_2$ is reduced through an initial one-electron transfer, coupled with transfer of the Lewis acidic moiety bound to the quinonoid oxygen atoms to the reduced $O_2$ species.

## INTRODUCTION

Biological reduction of dioxygen is performed by active sites that employ redox non-innocent ligands, and proton relays to control the transfer of electrons and protons to substrate.[1] In synthetic transition metal chemistry, redox non-innocent ligands[2] and second coordination sphere acid/base moieties that facilitate proton transfer[3] engender novel reactivity at the metal center. However, ligand systems that engage in both electron and proton transfers to substrates are less common.[4] Metal-quinonoid complexes in which the metal is π-bound to the quinonoid fragment have the potential to access the two-electrons and two-protons of the hydroquinone/quinone couple in addition to any accessible metal-based redox couples. The study of π-bound metal-quinonoid complexes[5] has focused on polymeric metal–organometallic coordination networks,[5] with only rare examples of substrate based reactivity.[4b, 6] Although not directly coordinated to metal, hydroquinone has been employed as distal redox mediator.[4b]

We have previously reported ligand designs that employ the π-system of an arene to support metals in various coordination environments.[7] A Ni–H complex underwent reversible H-migration between the metal and pendant arene, demonstrating the reversible transfer of (formally) protons and electrons between the Ni center and the ligand.[8] Extending this chemistry to multi-proton, multi-electron processes at a single metal site with a pendant catechol moiety, we report herein the first synthesis of a series of Mo quinonoid complexes and their reactivity with dioxygen.

## RESULTS AND DISCUSSION

**Scheme 3.1.** Synthesis of π-bound Mo-quinonoid complexes.

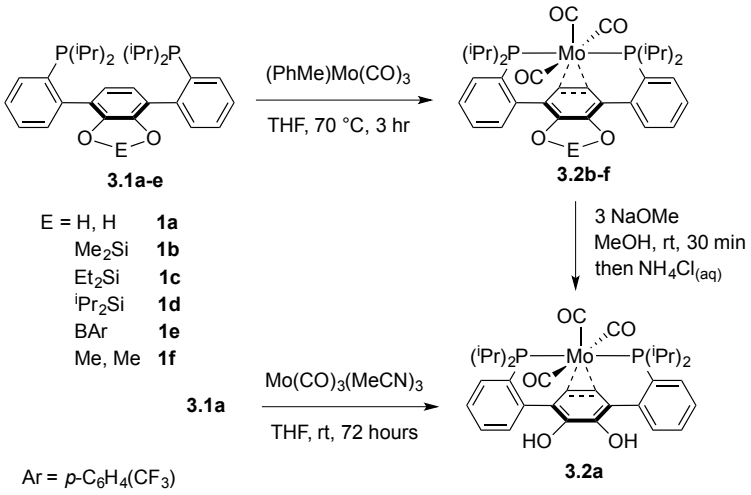


Access to the desired Mo-catechol complex **3.2a** was pursued through the use of the Si-protected catechol diphosphine **3.1b**, designed to avoid formation of oxygen-bound Mo-catecholate species. Heating diphosphine **3.1b** with $(PhMe)Mo(CO)_3$ (Scheme 3.1) in tetrahydrofuran (THF) generates a new species **3.2b** by NMR spectroscopy. A singlet (50.6 ppm) is observed by $^{31}P\{^1H\}$ NMR spectroscopy, while the protons assigned to the central arene ring in the $^1H$ NMR spectrum of **3.2b** resonate upfield (5.7 ppm, $CDCl_3$) compared to that of the free phosphine **3.1b** (6.8 ppm, $CDCl_3$) and have split into an apparent triplet ($J_{HP}$ = 4 Hz). Additionally, two singlets account for the methyl groups bound to silicon, indicating desymmetrization of the two faces of the central ring. These data are consistent with a $C_s$ symmetric molecule in which there is a strong metal-arene interaction with the central ring of the terphenyl moiety. The solution IR spectrum of **3.2b** reveals three bands in the region corresponding to CO stretches ($\nu_{CO}$ = 1959, 1843, and 1835 $cm^{-1}$) consistent with a $Mo(CO)_3$ fragment.

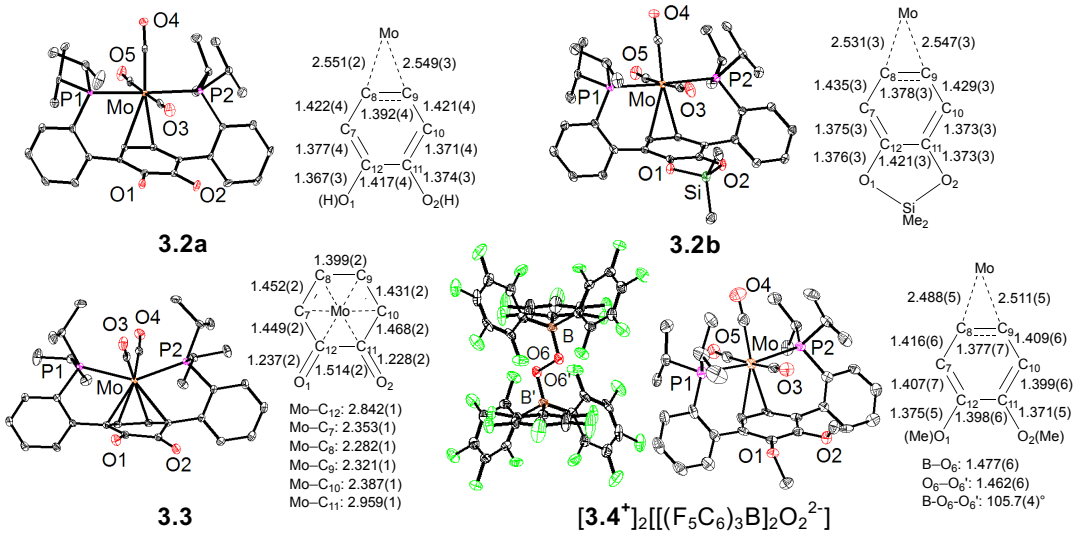


**Figure 3.1.** Solid-state structures of **3.2a**, **3.2b**, **3.3**, and $[\mathbf{3.4}^+]_2[[(F_5C_6)_3B]_2O_2^{2-}]$. Solvent molecules, hydrogen atoms, and second $\mathbf{3.4}^+$ cation are omitted for clarity. Carbon and fluorine atoms are depicted in black and green, respectively. Select bond distances (average values of two molecules in asymmetric unit for **3.2a**) are given in Å.

The single-crystal X-ray diffraction (XRD) study of **3.2b** (Figure 3.1) confirmed the spectroscopic findings, which are also consistent with the previously reported analog.[9] In the solid state, the metal center exhibits a *pseudo*-octahedral geometry with the coordination sphere comprised of two *trans* phosphines, three meridional carbonyls and an $\eta^2$-interaction with the π-system of the catechol fragment. Localization of double-bond character in the central arene ring suggests significant π-backbonding between Mo and the ring (the $C_7$–$C_{12}$ and $C_{10}$–$C_{11}$ bonds at 1.37 Å are considerably shorter than $C_7$–$C_8$, $C_9$–$C_{10}$, and $C_{11}$–$C_{12}$ at 1.43 Å). The aryl C–O bond distances at 1.37 Å are consistent with C–O single bonds.

The catechol complex **3.2a** can be accessed from **3.2b** by removal of the $SiMe_2$ group upon treatment with NaOMe in MeOH, followed by aqueous $NH_4Cl$ work-up. Alternatively, **3.2a** can be accessed directly from diphosphine **3.1a** through reaction

with $Mo(CO)_3(MeCN)_3$ at room temperature. The resulting product exhibits spectroscopic features similar to those of **3.2b**. A new broad resonance at 5.6 ppm ($^1$H NMR) is assigned to the catechol O*H* protons. This assignment was confirmed by loss of this resonance upon addition of $D_2O$. An XRD study of **3.2a** (Figure 3.1) revealed structural parameters nearly identical to those of **3.2b**.

**2.2 Reduction of $O_2$ by Mo-Catechol with Formation of Mo-Quinone.** While transition metal σ-bound catecholate complexes in general,[1a, 10] as well as Mo-catecholate complexes specifically,[10b, 11] have been reported to react with dioxygen to afford intra- and extra-diol cleavage products and oxidation to quinones, we are unaware of any reports on π-bound transition metal quinonoid complexes facilitating dioxygen reduction. To test the propensity of the metal-catechol moiety of **3.2a** to perform the transfer of multiple electrons and protons, its chemistry with $O_2$ was studied. Exposure of a solution of **3.2a** in DCM to an atmosphere of $O_2$ resulted in quantitative conversion to a new diamagnetic species **3.3** (eq 3) upon addition. The product displays a singlet at 72 ppm by $^{31}P\{^1H\}$ NMR spectroscopy. By $^1$H NMR spectroscopy, the resulting species exhibits a new apparent triplet at 4.9 ppm, assigned to olefinic protons coupled to the phosphines. The solution IR of **3.3** reveals bands at 1875 and 1605 $cm^{-1}$ consistent with the stretching frequency of metal-bound carbonyl and a quinone carbonyl stretch, respectively.[12] The solution $^{13}C\{^1H\}$ NMR reveals two resonances at ca. 240 ppm, consistent with two Mo-bound carbonyls. These spectroscopic features suggest conversion to a quinone-$Mo(CO)_2$ species, assignment confirmed by the solid-state structure (Figure 3.1). The Mo center exhibits a *pseudo*-trigonal prismatic geometry, with the vertices defined by two phosphine donors, two CO ligands, and two olefin moieties of the diene bound $\eta^4$ to the metal center. The C–O bonds of the organic fragment have contracted to 1.23 Å, consistent with carbon-oxygen double bonds. Formally, complex **3.2a** was oxidized by two electrons, coupled with the transfer of two

protons, to generate **3.3**, with the oxidation state of the metal center unchanged ($Mo^0$), and only the organic fragment undergoing the redox transformation.

To deconvolute the effect of the catechol vs metal moieties in the reaction with $O_2$, control experiments were performed with several species. 3,6-(Bis-2-bromophenyl)-catechol (**3.1$^{Br}$**, eq 1), a phosphine-free alternative to **3.1a**, exhibits no reaction under an atmosphere of $O_2$ in $CD_2Cl_2$ at room temperature, over 24 h ($^1$H NMR spectroscopy). Under similar conditions, the dimethyl-catecholate Mo complex **3.2f** and the parent complex **3.2g** (eq 2) also showed no conversion with $O_2$ over 24 hours. These experiments indicate that the Mo-catechol combination is required for the reactivity observed.

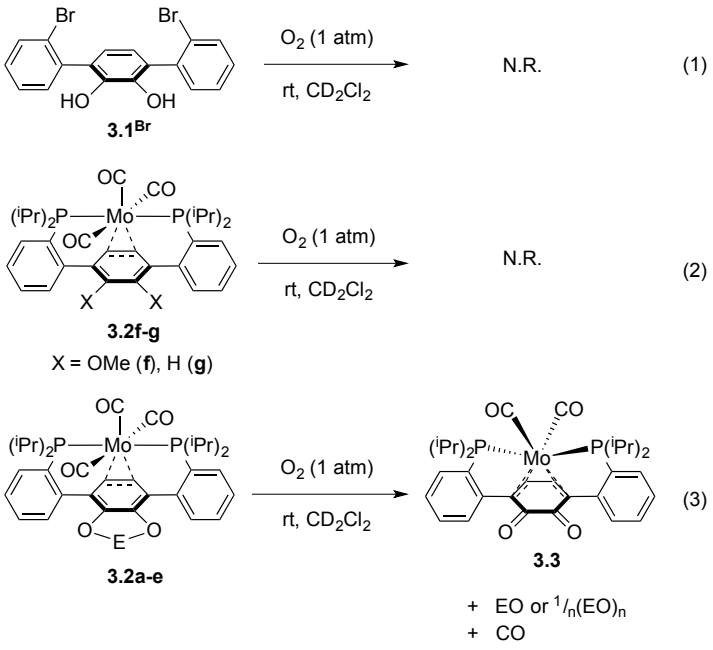


Toepler pump experiments were performed for the reaction of **3.2a** with $O_2$. Gas (0.48 ± 0.02 equiv) was generated in the reaction. Upon consumption of excess $O_2$ by reaction with a basic pyrogallol solution, the remaining gas (1.05 ± 0.05 equiv) was found to be combustible with CuO at 350 °C consistent with CO. The identity of the released gas was further confirmed by reaction with a $Cu^I$ precursor, to generate a previously reported $Cu^I$(CO) species.[13] Overall, the Toepler pump experiments reveal that 0.5 equivalents of

dioxygen are consumed and one equivalent of CO is released per mole of **3.2a**. This stoichiometry is consistent with four-electron reduction of $O_2$ to water, involving two equivalents of metal complex. This process could occur via partial reduction of $O_2$ by one equivalent of **3.2a** to $H_2O_2$, followed by reduction of $H_2O_2$ with a second equivalent of **3.2a**. Indeed, **3.2a** cleanly converts to **3.3** upon treatment with $H_2O_2$, while **3.3** exhibits only minor conversion to unidentified species (<20%) with $H_2O_2$ (1 equiv) within one hour. Thus it is plausible that $H_2O_2$ could be the initial $O_2$ reduction product, which is then rapidly consumed by a second equivalent of **3.2a**.

To understand the $O_2$ reduction process in more detail, **3.2b** was investigated as a metal complex with an electron rich central ring, yet without easily transferable protons. Compound 2b reacts with $O_2$ to also generate **3.3**, albeit slower than **3.2a** (over the course of several hours), with silyl-containing by-products identified by GC-MS as cyclo-oligomers of dimethylsiloxane. It has been reported that $O_2$ electrochemically reduced in the presence of $R_2SiX_2$ (R = Me, Et, and Ph, X = Cl, OMe) transiently generates silanones ($R_2Si{=}O$ species) that oligomerize to yield cyclopolysiloxanes.[14] As silanones are highly reactive and rapidly oligomerize, the presence of silanones in solution is typically deduced via trapping experiments with linear siloxanes, such as hexamethyldisiloxane. [14-15] Silanones insert into the Si–O bond of $Me_3SiOSiMe_3$ to yield longer linear chain siloxanes of the form $Me_3Si(OSiMe_2)_nOSiMe_3$ (n = 1, 2) which can be easily observed. An intermediate species (**3.2h**, Scheme 2) is observable by $^{31}P\{^1H\}$ and $^1H$ NMR spectroscopy during the reaction of **3.2b** with $O_2$, with a relative integration of the Si–$CH_3$ singlets to the central arene triplet of 6:2, rather than 3:2 in **3.2b**. These data are consistent with insertion of generated $Me_2Si{=}O$ into the Si–O bond of **3.2b** (Scheme 2.2), and was confirmed through independent synthesis. This observed species (**3.2h**) indicates that the $Me_2Si$ moiety acts as an oxygen acceptor to generate $Me_2Si{=}O$, as protons do when starting from **3.2a** to generate $H_2O_2/H_2O$.

**Scheme 3.2.** Reactivity of **3.2b** and **3.2c** with $O_2$.

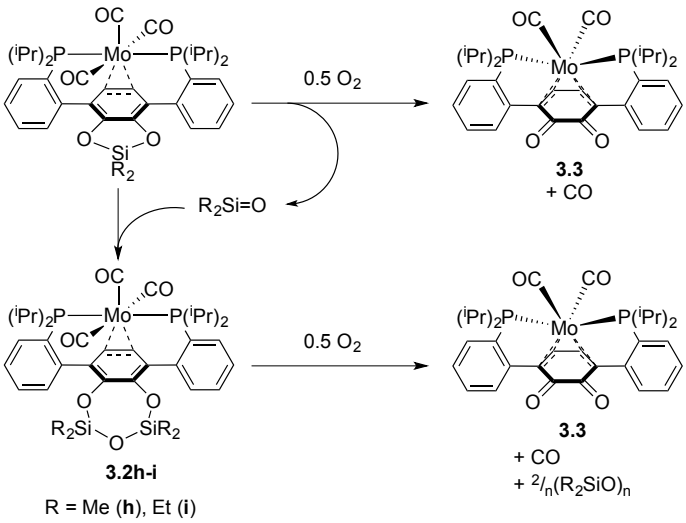


The effect of increasing the steric bulk at Si on the overall reaction with $O_2$ was investigated with the $Et_2Si$ and $^iPr_2Si$ analogues **3.2c** and **3.2d** (Scheme 3.1). Electrochemical measurements indicate that the nature of the alkyl group does not have a significant effect on the reduction potentials and, hence, the electronic properties of the complexes (Figure 3.2 and 3.7). Exposure of **3.2c** to an atmosphere of $O_2$ leads to consumption of starting material within hours, similar to **3.2b**, with the formation of a 1:1 mixture of **3.3** and the diethylsilanone insertion product **3.2i**; however, conversion of **3.2i** to **3.3** is much slower, requiring 48 hours for full conversion. Reaction of **3.2d** with $O_2$ is significantly slower, with <20% of **3.3** generated over the course of 5 days at room temperature. The observed effect in the rate of reaction due to increasing steric bulk indicates that the silicon center is accessed during a rate determining process; since the reduction potentials of **3.2b**, **3.2c**, and **3.2d** are very similar this process likely involves Si–O bond formation from $O_2$.

Reaction with $O_2$ was found to extend to boron-substituted **3.2e** as well, though compared to **3.2b** the reaction is slower. After 36 hours at room temperature **3.2e** had been consumed and **3.3** formed in ca. 80% yield. New unidentified species were observed by $^{31}P\{^1H\}$ NMR spectroscopy, in addition to multiple broad resonances by $^{19}F$ NMR spectroscopy. A

qualitatively similar set of spectra was obtained when **3.3** was combined with the boroxin $(ArBO)_3$ in $CD_2Cl_2$, likely due to the formation of Lewis acid-base adducts and **3.3**-mediated oligomerization of a "ArBO" moiety similar to the polysiloxanes observed for **3.2b**.

**2.3 Investigation of the Role of Lewis Acids in $O_2$ Reduction by Mo/quinonoid Compounds.** Considering that pendant $H^+$, $[R_2Si]^{2+}$, and $[RB]^{2+}$ moieties can act as Lewis acids and all engage in the $O_2$ activation process, more mechanistic insight was sought by addition of an external Lewis acid to target intermolecular reactivity. Compound **3.2f** does not undergo $O_2$ reactivity on its own. Addition of 2 equivalents of $B(C_6F_5)_3$ to **3.2f** under $N_2$ resulted in a broadening of the NMR spectroscopic features of **3.2f**, similar to what has been reported for a zirconocene complex.[16] This may be caused by a combination of effects, including electron transfer and coordination of borane to ether or carbonyl moieties. Exposure of this mixture to $O_2$ results in a mixture that is silent by $^1H$ and $^{31}P\{^1H\}$ NMR spectroscopy, and a gradual color change was observed from red-orange to brown to dark purple ($\lambda_{max}$ = 575 nm) over the course of 30 minutes at room temperature. Purple crystals of compound $[\mathbf{3.4}^+]_2[[(F_5C_6)_3B]_2O_2^{2-}]$ were isolated from the reaction mixture and an XRD study revealed a six-coordinate $Mo(CO)_3$ unit bound by the terphenyl-diphosphine with methoxy moieties intact analogous to **2.2a** and **2.2b** (Figure 3.1). The unit cell contains a bis-borane supported peroxide dianion,[17] in a ratio of 1:2 (peroxide to Mo), indicating that the metal complex is a mono-cation (formally $Mo^I$), consistent with the lack of diamagnetic resonances by NMR spectroscopy. The formation of the $[[(F_5C_6)_3B]_2O_2^{2-}]$ dianion was recently reported upon treatment of mixtures of ferrocenes and $B(C_6F_5)_3$ with $O_2$.[17] Observation of $[\mathbf{3.4}^+]_2[[(F_5C_6)_3B]_2O_2^{2-}]$ in reaction of **3.2f** and $B(C_6F_5)_3$ with $O_2$ demonstrates the ability of the Mo center to reduce $O_2$ via outer-sphere one-electron transfer.

**Scheme 3.3.** Reactivity of **3.2f** with $O_2$ in the presence of $B(C_6F_5)_3$.

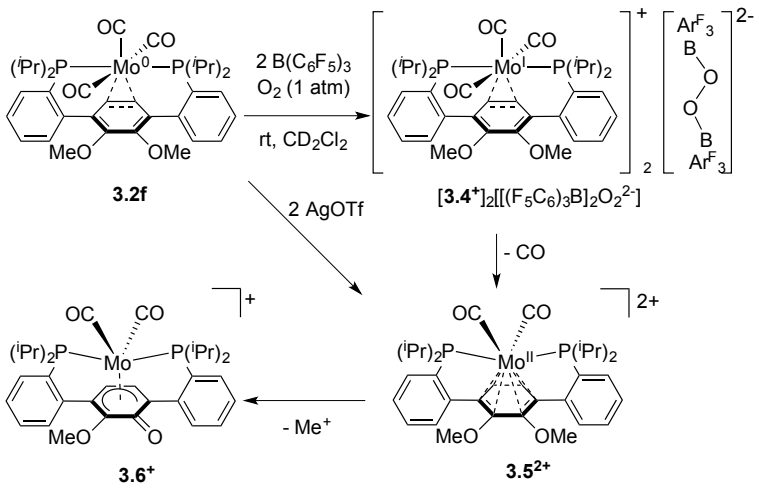


Over the course of several hours the purple solution of $\mathbf{3.4}^{+}$ generated a new diamagnetic ion $\mathbf{3.5}^{2+}$, which was independently synthesized by oxidation of **3.2f** with two equivalents of silver trifluoromethanesulfonate (AgOTf). Upon treatment of **3.2f** with AgOTf, the solution initially turned purple, consistent with formation of one-electron oxidized $\mathbf{3.4}^{+}$, then pale yellow-orange to yield $\mathbf{3.5}^{2+}$ via further oxidation and loss of CO. In the presence of the bis-borane supported peroxide dianion, $\mathbf{3.5}^{2+}$ partially converts to a new diamagnetic species, $\mathbf{3.6}^{+}$, resulting from ether demethylation. Independent synthesis by addition of MeOTf to **3.3** supports the structural assignment of $\mathbf{3.6}^{+}$. After complete conversion of intermediate $\mathbf{3.4}^{+}$ to a mixture of $\mathbf{3.5}^{2+}$ and $\mathbf{3.6}^{+}$, vacuum transfer of the volatiles to a J. Young NMR tube revealed the formation of $Me_2O$ and MeOH. To determine the origin of the O-atom in $Me_2O$, the oxidation reaction was performed with $^{18}O_2$ instead of natural abundance $O_2$. $Me_2O$ generated in the reaction was detected by GC-MS, and when performing the experiment with $^{18}O_2$, the major isotopolog observed was $Me_2{}^{18}O$. While not quantitative, observation of $Me_2O$ formation suggests that the peroxide moiety reacts with $\mathbf{3.5}^{2+}$ via abstraction of $Me^{+}$ to yield $\mathbf{3.6}^{+}$.[18] Conversion of $\mathbf{3.5}^{2+}$ to $\mathbf{3.6}^{+}$ demonstrates the ability of a reduced oxygen species to cleave the O–element bond of the resulting oxidized Mo complex, although cleavage of the aryl–O bond has not been ruled out.[18a]

The crystal structure of **3.4**$^+$ allows for an evaluation of the effect of the metal oxidation state on the interaction with the arene. While partial localization of double-bond character in the catechol moiety was observed for **3.2a** and **3.2b**, with C–C distances varying between 1.37 and 1.43 Å, the dimethyl catecholate moiety of **3.4**$^+$ displays C–C distances in a narrower range (1.40–1.42 Å). These structural parameters suggest that the Mo-arene interaction shifted from predominantly Mo-to-arene π-backbonding to arene-to-Mo σ-donation upon oxidation of the metal center.[19] The Mo–C distances are ca. 0.05 Å shorter in **3.2a** (ca. 2.55 Å) vs **3.4**$^+$(ca. 2.50 Å) indicating a strong interaction between the metal center and the ring. This interaction increases the electrophilicity of the arene and of group E bonded to the catecholate oxygens. It is proposed that this activation of E for nucleophilic attack facilitates the reaction with the $O_2$ fragment.

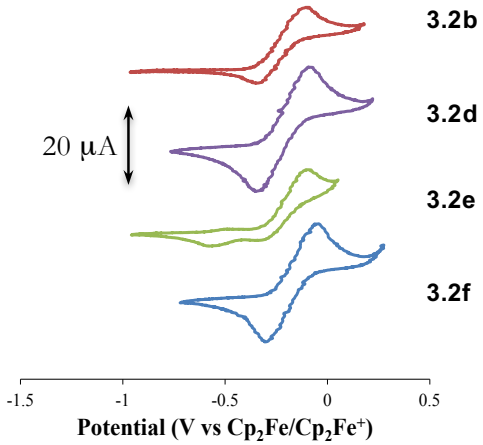


**Figure 3.2.** Cyclic voltammograms of compounds **3.2b** (red), **3.2d** (purple), **3.2e** (green), and **3.2f** (blue) in 0.1 M [$^n$Bu$_4$N$^+$][PF$_6^-$] in THF recorded with a glassy carbon electrode. Scan rate of 100 mV/s. Potentials referenced to $Cp_2Fe/Cp_2Fe^+$.

Further insight into the redox chemistry of the reported Mo complexes is provided by cyclic voltammetry studies (Figure 2.2). Compound **3.2f** shows a symmetric and fairly reversible couple, consistent with the isolation of both neutral and oxidized species and

relatively small structural reorganization. Compound **3.2b** exhibits a more asymmetric couple with less cathodic compared to anodic current. Increasing steric bulk at Si in **3.2d** shows a return to a symmetric couple, while the more sterically accessible **3.2e** shows a fully irreversible couple at all scan rates. This electrochemical behavior is reminiscent of the behavior of ($\eta^6$-arene)$Cr(CO)_3$ compounds, wherein the reversibility of the one-electron redox event is highly dependent on the presence of nucleophiles (additives such as MeCN, MeOH, $H_2O$, THF or the counteranions $ClO_4^-$ or $PF_6^-$),[20],[21] due to chemical decomposition of the generated radical cation by external nucleophiles. Consequently, reversibility can be achieved in non-coordinating solvents like $CH_2Cl_2$ by either lowering the temperature or employing less-nucleophilic electrolyte anions such as $[B(C_6F_5)_4^-]$.[21]

For compounds **3.2b-e**, we speculate that upon one-electron oxidation, the Si and B bound to the catecholate oxygens develop more electrophilic character and become susceptible to attack by external nucleophiles, either from the supporting electrolyte (tetrabutylammonium hexafluorophosphate) or even the solvent itself (THF), resulting in the observed electrochemical irreversibility. Indeed, chemical oxidation of **3.2b** with either one or two equivalents of Ag(OTf) or $[Cp_2Fe^+][PF_6^+]$ in THF resulted in a mixture of species by $^1H$ and $^{31}P\{^1H\}$ NMR spectroscopy, capable of polymerizing THF over the course of several hours, suggesting the generation of a very electrophilic species. Conversely, oxidation of **3.2d** with two equivalents of Ag(OTf) in THF yields a single major diamagnetic species by $^1H$ and $^{31}P\{^1H\}$ NMR spectroscopy and the resulting solution was not observed to polymerize THF. As the alkyl substituents bound to Si are oriented away from both the metal center and the catechol carbocyclic ring (Figure 2.1), the recovery of electrochemical reversibility from **3.2b** to **3.2d** and lack of solvent polymerization upon chemical oxidation of **3.2d** is suggestive of Si being the site of nucleophilic attack. The bulkier isopropyl groups of **3.2d** better impede the approach of nucleophiles to the Si center compared to the methyl groups of **3.2b**. These results are consistent with increased electrophilic character

developing on the Lewis-acidic E upon oxidation, indicative of ligand-metal cooperation by activation of the catechol moiety upon Mo-based electron transfer. The reactivity of $O_2$ of these species follows the trends observed electrochemically, with the bulky species displaying more reversible CV reacting slower.

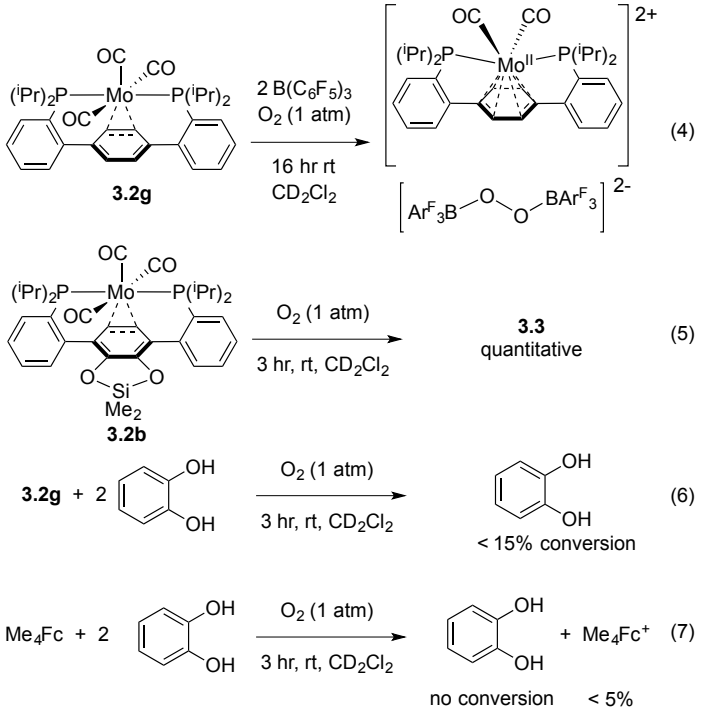


To further probe the role of metal-ligand cooperation for species with the quinonoid fragment connected to the Mo center on the reactivity with dioxygen, reaction of **3.2g** with $O_2$ in the presence of external catechol was investigated. Compound **3.2g** was selected for this experiment to limit potential complications due to loss of $Me^+$ as was observed during the reaction of **3.2f** and $B(C_6F_5)_3$ with $O_2$. Compound **3.2g** is competent for $O_2$ reduction in the presence of $B(C_6F_5)_3$, generating the same borane-supported peroxide, $[[(F_5C_6)_3B]_2O_2^{2-}]$, as **3.2f** according to $^{19}F$ NMR spectroscopy (eq 4).

Accordingly, exposure of an orange mixture of **3.2g** and catechol to an atmosphere of $O_2$ results in a slight darkening of the solution over the course of 3 hours (the time required for quantitative conversion of **3.2b** to **3.3**, eq 5). $^{31}P\{^1H\}$ NMR spectroscopy shows a complete

loss of signal, while $^{1}$H NMR spectroscopy reveals a broadening of the signals corresponding to **3.2g**; however, the majority of the catechol remains unaffected over the course of the reaction (eq 6) with less than 15% conversion. After 36 hours at room temperature, a new signal is observed by $^{31}P\{^{1}H\}$ NMR spectroscopy at 60 ppm, consistent with oxidation of the phosphine to free phosphine oxide, indicative of decomposition of the metal complex. These results suggest that the presence of external catechol is sufficient to facilitate $O_2$ reactivity at Mo, but this is a slow process and the low conversion of catechol and decomposition of the metal complex indicate that the resulting reduced oxygen species preferentially reacts with the Mo complex over the external catechol. Additionally, reaction of catechol with $O_2$ in the presence of 1,1',3,3'-tetramethylferrocene ($Me_4Fc$) as a surrogate outer-sphere reductant of similar potential as the reported Mo complexes was investigated (eq 7). Over the course of 3 hours at room temperature, slight oxidation of $Me_4Fc$ (< 5%) was observed by UV-Vis spectroscopy; however, no conversion of catechol was detected by $^{1}$H NMR spectroscopy. The low conversion of catechol oxidation chemistry observed in these intermolecular reactions emphasizes the cooperative nature of the reactivity observed for the Mo quinonoid complexes.

**2.4 Proposed Mechanisms for $O_2$ Reduction by Mo Quinonoid Complexes.** The intermolecular reactivity of **3.2f** and $O_2$ in the presence of $B(C_6F_5)_3$ (Figure 3.3) offers insight applicable to the intramolecular systems. The proposed mechanism for $O_2$ activation by **3.2f** and $B(C_6F_5)_3$ initiates via outer-sphere electron transfer from Mo to $O_2$, facilitated by the strongly Lewis acidic borane. While the reduction potentials of the $Mo^0/Mo^I$ couple and the $\bullet O_2^-/O_2$ couple are mismatched (-0.176 V vs $Cp_2Fe/Cp_2Fe^+$ for $Mo^0/Mo^I$ in THF vs -1.18 V vs $Cp_2Fe/Cp_2Fe^+$ for $\bullet O_2^-/O_2$ in DMSO),[22] it has been demonstrated that by coupling Lewis acid binding, electron transfer rates can be greatly increased.[23] This pre-equilibrium step is driven forward by the rapid disproportionation of the proposed borane supported superoxide into borane-supported peroxide and dioxygen, as has been previously

reported.[24] Disproportionation of the formally 17-electron **3.4**$^{+}$ yields the 18-electron complex **3.5**$^{2+}$ and regenerates starting material **3.2f**. While it is anticipated that the $Mo^{I}$ of **3.4**$^{+}$ should be an even weaker reductant than **3.2f**, further oxidation of **3.4**$^{+}$ via $O_2$ and $B(C_6F_5)_3$ to yield **3.5**$^{2+}$ cannot be ruled out.

$\eta^6$-Coordination of phenol to a $Cr(CO)_3$ unit resulted in a 4 $pK_a$ unit increase in acidity,[25] and thus it is presumed that similar activation of the catecholate unit in **3.5**$^{2+}$ results in increased susceptibility of the methyl groups toward nucleophilic attack. Both nucleophilic attack at the methyl carbon and at the aryl carbon have been proposed in $Cp^{*}Ir(\eta^6\text{-anisole})^{2+}$ complexes.[18] Based on our isotopic labeling studies, **3.5**$^{2+}$ is demethylated by the borane-supported peroxide via nucleophilic substitution at methyl to yield methylperoxide and **3.6**$^{+}$, with the former reacting further to yield the observed $Me_2O$ or $Me_2{}^{18}O$.

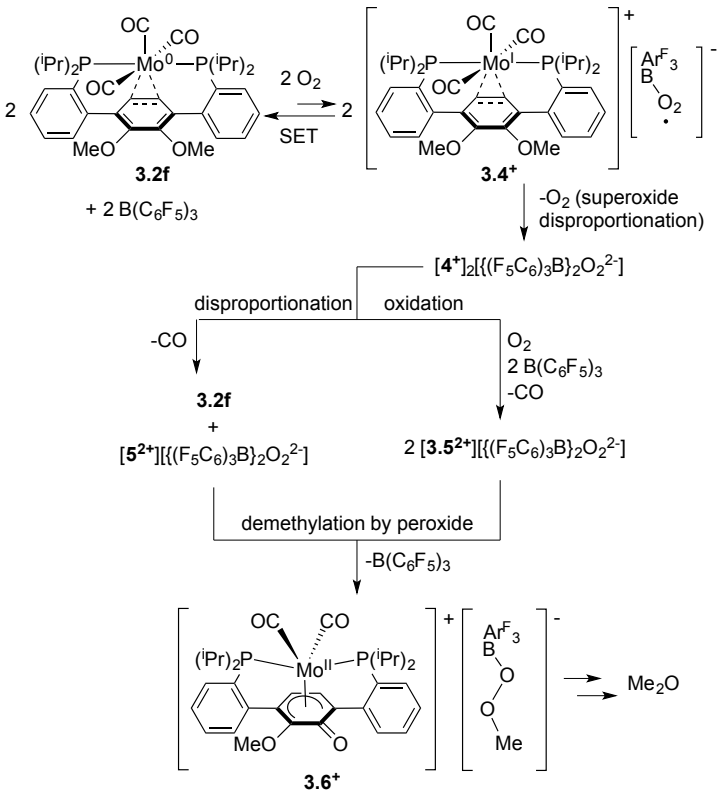


**Figure 3.3.** Proposed mechanism for intermolecular reactivity of **3.2f** and $B(C_6F_5)_3$ with $O_2$.

Extending these intermediates to the intramolecular system, the proposed mechanism for $O_2$ activation at the catechol and protected catecholate π-complexes initiates via an outer-sphere electron transfer (Figure 3.4A), with the protons (or Si, B) serving as intramolecular Lewis acidic moieties (as $B(C_6F_5)_3$ does with **3.2f** in intermolecular fashion) that facilitate the initial electron transfer and stabilize the resulting reduced $O_2$ species, $\bullet O_2^-$, as represented in **3.9**.[23a] Oxidation of the Mo complex through electron transfer to $O_2$ results in increased electrophilicity at E (E = H, $R_2Si$, ArB) as supported by structural analysis of $\mathbf{3.4}^+$, electrochemical analysis, and chemical oxidation of **3.2b**. Loss of carbonyl coupled with attack by $\bullet O_2^-$ on the electrophilic Lewis acid E results in scission of a catecholate-E bond, with subsequent steps leading to O–O bond cleavage (analogous to the formation of $\mathbf{3.6}^+$ and $Me_2O$). The intermediacy of a $Mo^{II}$ compound **3.10** accessed via further oxidation of **3.9** cannot be ruled out, with attack by a reduced oxygen species again resulting in formation of **3.11**. While it is unclear at which step the O–O bond is cleaved, one demonstrated possibility is that **3.2a** reduces $H_2O_2$ to yield $H_2O$ and **3.3**. Analogous $EO_2$ species (E = $R_2Si$, ArB) are anticipated to be even more reactive than $H_2O_2$, and therefore it is presumed if generated they will be consumed via further reaction with starting material **3.2**. A recently computed mechanism for $O_2$ reduction with hydroanthraquinones invokes H-atom abstraction,[26] and although the organo-quinonoid $\mathbf{3.1}^{\mathbf{Br}}$ does not react with $O_2$, it cannot be ruled out that **3.2a** follows a similar mechanism (Figure 3.4B), whereby the Mo center does not directly participate in the reactivity, but activates the catechol moiety.

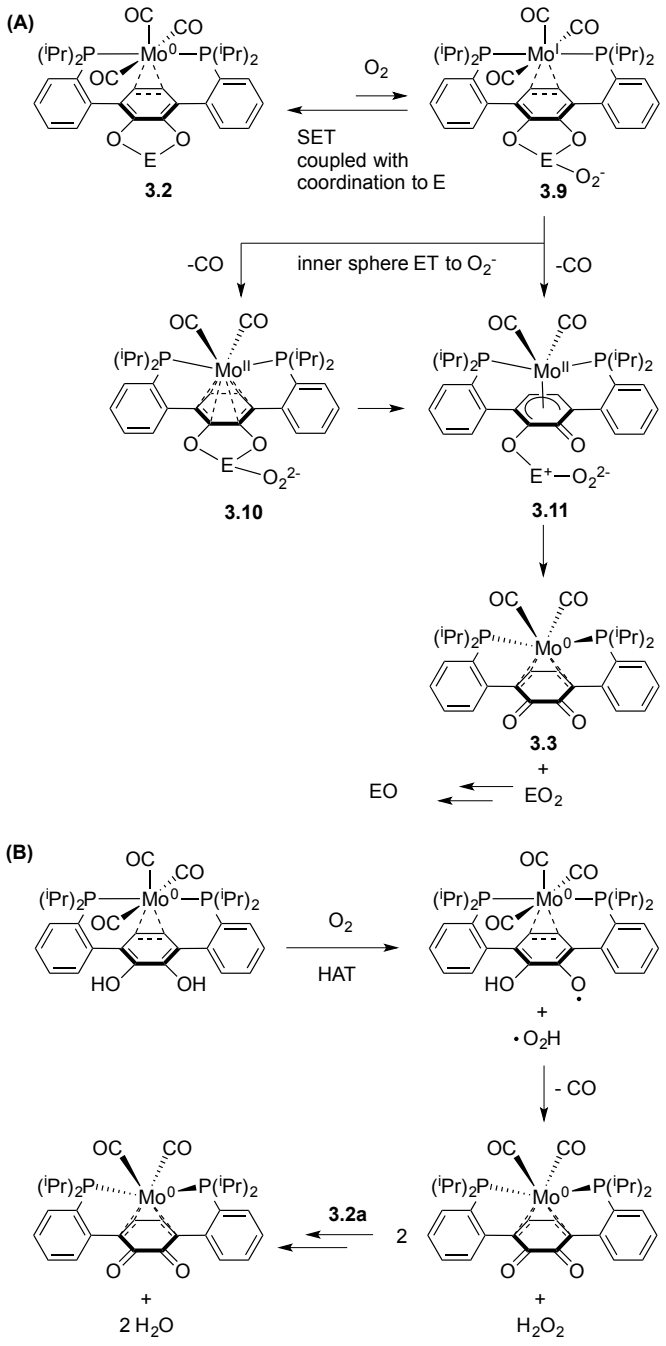


**Figure 3.4.** Proposed mechanism for intramolecular reactivity of **3.2a-e**,**h-i** with $O_2$ (A), and alternative mechanism for intramolecular reaction of **3.2a** with $O_2$ (B).

## CONCLUSIONS

In summary, π-bound Mo-catechol complexes were synthesized and their reactivity with dioxygen to yield a Mo-quinone product was investigated. Control experiments of Mo complexes in the absence of the catechol moiety or the catechol in the absence of Mo showed no reaction with $O_2$. Additionally, catechol added to solution, but not covalently connected to Mo (or tetramethylferrocene as an alternate single electron reductant), is oxidized only partially. Altering the substitution on the catechol oxygen centers from H to Si or B maintains reactivity with $O_2$, but at lower rates. The dimethyl-Mo quinonoid complex still reacts with $O_2$, but in the presence of $B(C_6F_5)_3$, to afford a bis-borane supported peroxide. Mechanistically, the $O_2$ activation is proposed to occur via intramolecular Lewis acid assisted electron transfer. The present studies demonstrate the ability of a π-bound metal-quinonoid complex to facilitate multi-electron and proton transfer (as well as silicon, boron, and carbon transfer) from the quinonoid moiety to a small molecule substrate, with coupling of the Mo and quinonoid fragments integral to the observed reactivity.

## EXPERIMENTAL SECTION

### General considerations:

Unless indicated otherwise, reactions performed under inert atmosphere were carried out in oven-dried glassware in a glovebox under a nitrogen atmosphere purified by circulation through RCI-DRI 13X-0408 Molecular Seives 13X, 4x8 Mesh Beads and BASF PuriStar® Catalyst R3-11G, 5x3 mm (Research Catalysts, Inc.). Solvents for all reactions were purified by Grubbs' method.[27] $C_6D_6$ was purchased from Cambridge Isotope Laboratories and vacuum distilled from sodium benzophenone ketyl. $CD_3CN$, $CD_2Cl_2$, and $CDCl_3$ were also purchased from Cambridge Isotope Laboratories and distilled from $CaH_2$ prior to use. Alumina and Celite were activated by heating under vacuum at 200 °C for 24 hours. $^1H$, $^{19}F$, and $^{31}P$ NMR spectra were recorded on Varian Mercury 300 MHz spectrometers at ambient temperature, unless denoted otherwise. $^{13}C$ NMR spectra were recorded on a Varian INOVA-500 MHz spectrometer. $^1H$ and $^{13}C$ NMR chemical shifts are reported with respect to internal solvent: 7.16 ppm and 128.06 ppm for $C_6D_6$, 1.94 ppm and 118.26 for $CD_3CN$, 5.32 ppm and 53.84 ppm for $CD_2Cl_2$, and 7.26 ppm and 77.16 ppm for $CDCl_3$, respectively. $^{19}F$ and $^{31}P$ NMR chemical shifts are reported with respect to an external standard of $C_6F_6$ (-164.9 ppm) and 85% $H_3PO_4$ (0.0 ppm).

Powder and thin film ATR-IR measurements were obtained by placing a powder or drop of solution of the complex on the surface of a Bruker APLHA ATR-IR spectrometer probe and allowing the solent to evaporate (Platinum Sampling Module, diamond, OPUS software package) at 2 $cm^{-1}$ resolution. Solution IR spectra were recorded on a Thermo-Fisher Scientific Nicolet 6700 FTIR spectrometer using a $CaF_2$

plate solution cell. Fast atom bombardment-mass spectrometry (FAB-MS) analysis was performed with a JEOL JMS-600H high resolution mass spectrometer. Gas chromatography-mass spectrometry (GC-MS) analysis was performed upon filtering the sample through a plug of silica gel. Electrochemical measurements were recorded with a Pine Instrument Company AFCBP1 bipotentiostat using the AfterMath software package. Cyclic voltammograms were recorded on ca. 2 mM solutions of the relevant complex in the glovebox at 20 °C with an auxiliary Pt-coil electrode, a $Ag/Ag^+$ reference electrode (0.01 M $AgNO_3$, 0.1 M [$^n$Bu4N$^+$][$PF_6^-$] in MeCN), and a 3.0 mm glassy carbon electrode disc (BASI). The electrolyte solution was 0.1 M [$^n$Bu4N$^+$][$PF_6^-$] in THF. All reported values are referenced to an internal ferrocene/ferrocenium couple. Elemental analysis was conducted by Robertson Microlit Labs (Ledgewood, NJ).

Unless otherwise noted all chemical reagents were purchased from commercial sources and used without further purification. Pinacol, 2-bromodiodobenzene, $HNpic_2$ ($HNpic_2$ = di(2-picolyl)amine), and *para*-trifluoromethylphenylboronic acid were purchased from Alfa Aesar. Veratrole and TMEDA were purchased from Alfa Aesar and distilled from $CaH_2$ prior to use. $B(OMe)_3$ was purchased from Alfa Aesar and distilled from sodium prior to use. Chlorodiisopropylphosphine and $Cu(MeCN)_4OTf$ were purchased from Sigma Aldrich. $Me_2SiCl_2$, $Et_2SiCl_2$, $^i Pr_2SiCl_2$, and $(ClMe_2Si)_2$ were purchased from Sigma Aldrich and distilled from $CaH_2$ prior to use. $(ClEt_2Si)_2O$ was prepared by hydrolysis of $Et_2SiCl_2$ followed by fractional distillation. Assignments of NMR spectra are given corresponding to the following numbering scheme:

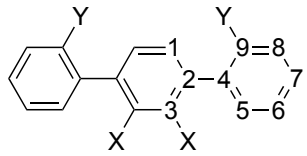


**Synthesis of 2,3-dimethoxyphenylene-1,4-bis(pinacolato)boronic ester**

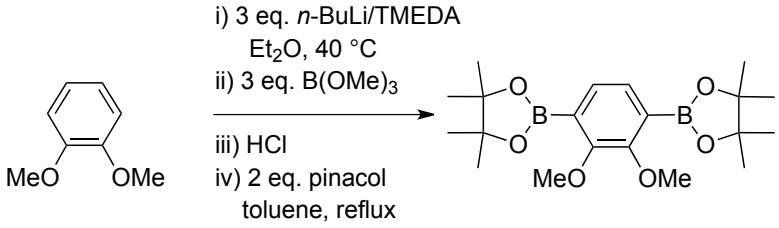


Adapted from the literature.[28] On the Schlenk line, veratrole (10.0 mL, 78.5 mmol) and TMEDA (20.0 mL, 133 mmol) were added via syringe under a counter-flow of $N_2$ to a 1000 mL Schlenk bomb charged with $Et_2O$ (500 mL) and a large stir bar and fitted with a rubber septum. The bomb was cooled toca. 4 °C using an ice bath, and under a counter-flow of $N_2$ *n*BuLi (100 mL, 2.5 M, 250 mmol) was added via Teflon cannula transfer. The ice bath was removed, the bomb was sealed with a screw-in Teflon stopper and heated to 40 °C (CAUTION: *Always* use a blast shield and all necessary personal protective equipment when heating/manipulating pyrophorics in a sealed vessel.) for 4 hours with *vigorous* stirring (Note: large amounts of precipitate form during this stage, and if adequate stirring is not maintained the final yield will be significantly diminished). The reaction was removed from heat and once again cooled to ca. 4 °C using an ice bath and the Teflon stopper replaced with a rubber septum. $B(OMe)_3$ (29.0 mL, 260 mmol) was then added via syring under counterflow of $N_2$ with vigorous stirring. After complete addition, the bomb was once again sealed with the screw-in Teflon stopper, and the reaction allowed to warm to room temperature over the course

of 12 hours with stirring. The bomb was again cooled to ca. 4 °C using an ice bath, opened to air, and the mixture quenched with the slow addition of HCl (6 M, 500 mL, 3 mol). All further manipulations were performed in air. Upon complete addition of HCl, the mixture was transferred to a 2L separatory funnel and the layers separated. The aqueous layer was washed with $Et_2O$ (2 x 200 mL), and the combined organic layers were dried over $MgSO_4$, filtered, and concentrated via rotary evaporation. The residue was combined with pinacol (19 g, 160 mmol) and Toluene (50 mL) in a 500 mL round bottom flask charged with a stir bar and equipped with a Dean-Stark trap. The mixture was then refluxed for 4 hours with stirring. After cooling to room temperature, all volatiles were removed by rotary evaporation and the residue was recrystallized from hot hexanes (ca. 200 mL) at -30 °C to afford approximately 10 g of the desired product as off-white powder/microcrystalline solid. Concentration of the filtrate followed by recrystallization from pentane can afford approximately another 5 g of desired product. Total isolated yield is 15.449 g (50.5%). The obtained product displayed a $^1$H NMR spectrum matching that previously reported in literature.[2] $^1$H NMR (300 MHz, $d_6$-acetone), δ(ppm): 7.31 (s, 2H, Ar-C*H*), 3.80 (s, 6H, OC$H_3$), 1.34 (s, 24H, C(C$H_3$)$_2$).

**Synthesis of 1,4-bis(2-bromophenyl)-2,3-dimethoxybenzene**

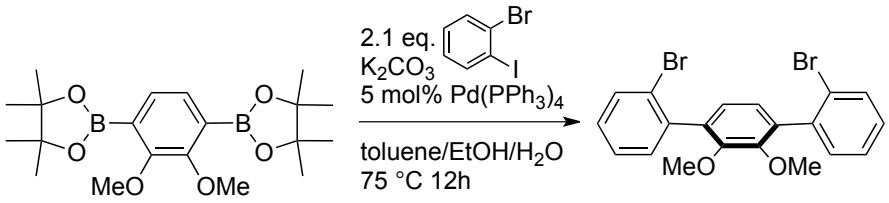


Suzuki coupling conditions were adapted from a previously published procedure.[29] 2,3-dimethoxyphenylene-1,4-bis(pinacolato)boronic ester (15.4993 g, 39.7 mmol), $K_2CO_3$ (26 g, 190 mmol), toluene (340 mL), $H_2O$ (185 mL), EtOH (185 mL) were combined in a 1000 mL Schlenk bomb with screw-in Teflon stopper. The mixture was degassed by three freeze-pump-thaw cycles, and 2-bromoiodobenzene (10.7 mL, 83.3 mmol) and $Pd(PPh_3)_4$ (1.744 g, 1.51 mmol) were added under a counter-flow of $N_2$. The mixture was again degassed by a freeze-pump-thaw cycle, and the Schlenk tube was placed in an oil bath and heated to 80°C. After stirring for 12 h, the mixture was allowed to cool to room temperature and the volatiles removed via rotary evaporation and further workup performed in air. $H_2O$ (250 mL) and DCM (250 mL) were added and the mixture transferred to a 1L separatory funnel with vigorous mixing. The layers were separated and the aqueous layer washed with DCM (2 x 100 mL). The combined organic fractions were dried over $MgSO_4$, filtered, and concentrated via rotary evaporation. The residue was dissolved in hot MeOH (100 mL), filtered, and cooled to -30 °C in a freezer. After 12 hours the resulting white precipitate was collected on a glass frit, rinsing with minimal cold MeOH and dried under vacuum to afford the desired product (10.3468 g, 58.1%). $^1$H NMR (300 MHz, $CDCl_3$), δ(ppm): 7.70 (d, 8.0 Hz, 2 H, Ar-C*H*), 7.39 (d, 5.5 Hz, 4 H, Ar-C*H*), 7.25 (m, 2 H, Ar-C*H*), 6.99 (s, 2 H, Ar-$C_1$*H*), 3.70 (s, 6 H, O$CH_3$). $^{13}$C

NMR (75 MHz, $CDCl_3$), δ(ppm): 150.58 (s, Ar-*C*H), 139.44 (s, Ar-C*H*), 135.88 (s, Ar-C*H*), 132.74 (s, Ar-C*H*), 131.56 (s, Ar-C*H*), 129.07 (s, Ar-C*H*), 127.10 (s, Ar-C*H*), 125.33 (s, Ar-C*H*), 123.92 (s, Ar-C*H*), 60.97 (s, OC$H_3$). MS (m/z): calcd, 447.9496 $[M]^+$; found, 447.9483 ($FAB^+$, $[M]^+$).

**Synthesis of 1,4-bis(2-bromophenyl)-2,3-dihydroxybenzene ($3.1^{Br}$)**

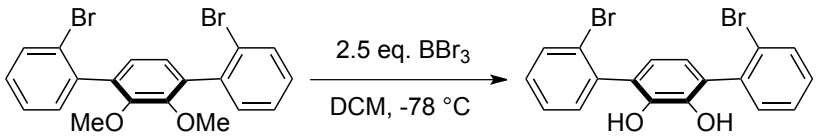


In a Schlenk flask under $N_2$ counterflow, 1,4-di(2-bromophenyl)-2,3-dimethoxybenzene (8.4322 g, 18.8 mmol) was dissolved in DCM (50 mL) with stirring. The flask was fitted with a septum and chilled to -78 °C in a dry ice/acetone bath. $BBr_3$ (4.5 mL neat, 1 mmol) was added to the flask drop-wise via syringe over 5 min. The reaction was allowed to warm to room temperature over 12 h. After cooling with an ice/water bath, the reaction was then quenched by *slow* dropwise addition of $H_2O$ until bubbling ceased. Further manipulations performed in air. The reaction mixture was further diluted with $H_2O$ (50 mL). The mixture was transferred to a separatory funnel, mixed well, and the layers separated. The aqueous layer was washed with DCM (2 x 25 mL). The combined organics were dried with $MgSO_4$, filtered, and concentrated via rotary evaporation to yield the desired product as a tan powder (7.389 g, 93.5%). $^1$H NMR (300 MHz, $CDCl_3$), δ(ppm): 7.75 (d, 2 H, Ar-C*H*), 7.46 (s, 2 H, Ar-C*H*), 7.44 (s, 2 H, Ar-C*H*), 7.34-7.27 (m, 2 H, Ar-C*H*), 6.84 (s, 2 H, Ar-$C_1H$), 5.34 (br, 2 H, O*H*).$^{13}$C{$^1$H} NMR (126 MHz, $CDCl_3$), δ(ppm): 140.9 (s, Ar-C*H*), 138.1 (s, Ar-C*H*), 133.2 (s, Ar-C*H*), 132.1 (s, Ar-

C*H*), 129.7 (s, Ar-C*H*), 127.9 (s, Ar-C*H*), 127.7 (s, Ar-C*H*), 124.0 (s, Ar-C*H*), 121.9 (s, Ar-C*H*). MS (m/z): calcd, 419.9184 $[M]^+$; found, 419.9180 ($FAB^+$, $[M]^+$).

**Synthesis of 1,4-bis(2-bromophenyl)-2,3-di(methoxymethylether)benzene**

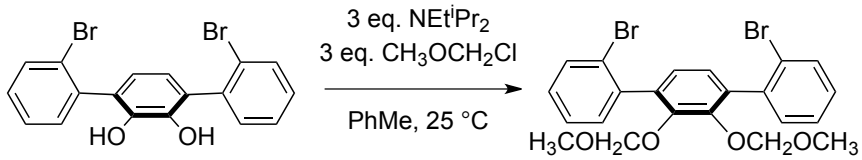


A Schlenk flask was charged with 1,4-di(2-bromophenyl)-2,3-dihydroxybenzene (6.0973 g, 14.5 mmol) dissolved in PhMe (100 mL). Under $N_2$ counter-flow, a 2.1 M solution of chloromethyl methyl ether in toluene (21.0 mL, 44.1 mmol)[30] was added to the stirred reaction mixture, followed by N,N-diisopropylethylamine (7.8 mL, 43.7 mmol). The reaction was allowed to stir for 12 hours at room temperature under $N_2$. The volatiles were removed under rotary evaporation, and further manipulations were performed in air. The residue was dissolved in $H_2O$ (150 mL) and DCM (150 mL) and transferred to a separatory funnel. The layers were separated and the aqueous layer washed with DCM (2 x 50 mL). The combined organic extracts were dried with $MgSO_4$, filtered and concentrated under rotary evaporation to yield the desired product as a white powder (6.9031 g, 93.6%). $^1$H NMR (300 MHz, $CDCl_3$), δ(ppm): 7.68 (d, 2 H, Ar-C*H*), 7.51-7.34 (m, 4 H, Ar-C*H*), 7.25-7.19 (m, 2 H, Ar-C*H*), 7.07 (s, 2 H, Ar-C$_1$*H*), 5.01-4.85 (br, 4 H, C*H*$_2$OCH$_3$), 2.93 (s, 6 H, CH$_2$OC*H*$_3$). $^{13}$C{$^1$H} NMR (75 MHz, $CDCl_3$), δ(ppm): 147.8 (s, Ar-C*H*), 139.4 (s, Ar-C*H*), 136.6 (s, Ar-C*H*), 132.6 (s, Ar-C*H*), 132.3 (s, Ar-C*H*),

129.0 (s, Ar-C*H*), 127.0 (s, Ar-C*H*), 126.0 (s, Ar-C*H*), 124.2 (s, Ar-C*H*), 99.2 (s, Ar-C*H*), 56.7 (s, Ar-C*H*). MS (m/z): calcd, 507.9708 $[M]^+$; found, 507.9713 ($FAB^+$, $[M]^+$).

**Synthesis of 1,4-bis(2-(diisopropylphosphino)phenyl)-2,3-catechol (3.1a)**

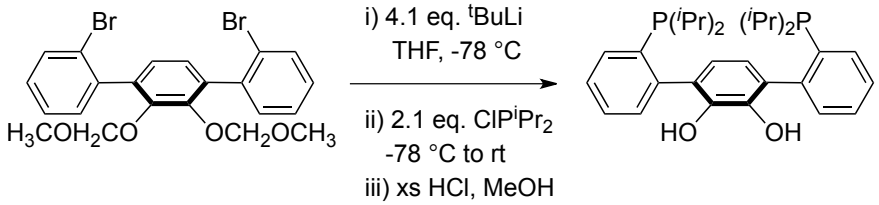


A Schlenk tube was charged with 1,4-di(2-bromophenyl)-2,3-di(methoxymethylether)benzene (6.9031 g, 13.6 mmol), THF (60 mL), and a stir bar. The reaction mixture was cooled to -78 °C with the use of a dry ice/acetone bath. Under a counter-flow of $N_2$, a 1.7 M solution of $^t$BuLi (33.0 mL, 56.1 mmol) in pentanes was added via syringe drop-wise. A light yellow color appeared in seconds, and as the reaction was allowed to stir for 30 minutes at -78 °C, a pale orange color evolved. After stirring for 1 hour at -78 °C, chlorodiisopropylphosphine (4.60 mL, 28.6 mmol) was added to the reaction mixture via syringe under a counter-flow of $N_2$, inducing a light yellow color. After stirring for 1 hour at -78 °C, the reaction was removed from the dry ice/acetone bath and allowed to warm to room temperature. After stirring for 2 hours at room temperature the volatiles were removed under reduced pressure. To the residue was added degassed MeOH (60 mL) and HCl (12 M, 10 mL). The mixture was then heated to 60 °C for 4 hours. After cooling to room temperature, the volatiles were again removed under reduced pressure. All further manipulations were performed under an $N_2$ atmosphere in a wet glove box. The residue was treated with DCM (100 mL) and

saturated aqueous $K_2CO_3$ (100 mL) and transferred to a separatory funnel with vigorous mixing. The layers were separated and the organics washed with saturated aqueous $NH_4Cl$ (100 mL). The layers were again separated and the aqueous layer washed with DCM (2 x 50 mL). The combined organics were dried with $MgSO_4$, filtered, and concentrated under vacuum to afford an off-white powder. Trituration with MeOH (25 mL) afforded a white precipitate that was collected on a glass frit. The solid was washed with $Et_2O$ (25 mL) and MeCN (25 mL), and then dried under vacuum to yield the desired product in 81.3% yield (5.4627 g). $^1$H NMR (300 MHz, $CDCl_3$), δ(ppm): 7.57 – 7.50 (m, 2 H, Ar-C*H*), 7.45 – 7.36 (m, 6 H, Ar-C*H*), 6.80 (s, 2 H, Ar-$C_1$*H*), 6.56, (br, 2 H, Ar-$C_3$O*H*), 2.24 (br, 2 H, PC*H*$(CH_3)_2$), 2.02 (br, 2 H, PC*H*(*C*$H_3)_2$), 1.20 – 0.80 (br, 24 H, PCH(*C*$H_3)_2$). $^{31}$P{$^1$H} (121 MHz, $CDCl_3$), δ(ppm): 3.06 (br), 2.17 (br), -1.56 (s), -29.16 (s). $^{13}$C{$^1$H} (126 MHz, $CDCl_3$) δ: 146.25 (d), 141.00 (s), 134.00 (d), 131.99 (s), 131.67 (s), 130.02 (s), 128.90 (s), 126.97 (s), 123.95 (s), 25.04 (br), 22.47 (br), 20.00 (br), 18.97 (br). MS (m/z): calcd, 493.2425 $[M-H]^+$; found, 493.2438 ($FAB^+$, $[M-H]^+$).

**Synthesis of dimethyl-(1,4-bis(2-(diisopropylphosphino)phenyl)-2,3-catechol)silane (3.1b)**

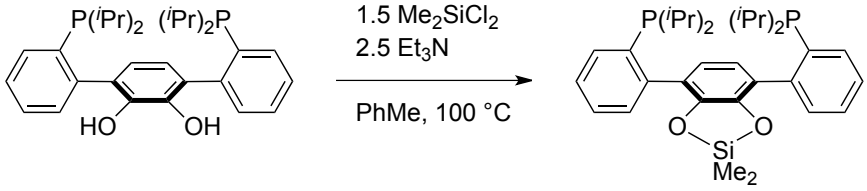


Diphosphine **3.1a** (2.5003 g, 5.06 mmol), $Me_2SiCl_2$ (0.835 g, 6.47 mmol), and $Et_3N$ (1.2033 g, 11.9 mmol) were combined with PhMe (20 mL) in a Schlenk bomb charged

with a stir bar and a screw-in Teflon stopper. The bomb was removed from the glove box and heated to 100 °C in an oil bath for 12 hours generating a white precipitate. After cooling to room temperature, the bomb was taken back into the glove box and the white precipitate filtered on celite, washing with additional PhMe. The filtrate was then concentrated *in vacuo* to yield the desired compound **3.1b** as a white powder in 97.5% yield (2.7152 g). $^{1}$H NMR (300 MHz, $C_6D_6$), δ(ppm): 7.40 (m, 4 H, Ar-C*H*), 7.14 (m, 4 H, Ar-C*H*), 6.94 (s, 2 H, Ar-$C_1$*H*), 1.90 (m, 4 H, PC*H*$(CH_3)_2$), 0.99 (m, 24 H, PCH(C*H*$_3)_2$), 0.17 (s, 6 H, SiC*H*$_3$). $^{31}$P{$^{1}$H} (121 MHz, $C_6D_6$), δ(ppm): -1.24 (s). $^{13}$C{$^{1}$H} NMR (126 MHz, $C_6D_6$), δ(ppm): 146.55 (s), 146.31 (s), 145.87 (s), 136.32 (d), 132.53 (d), 131.23 (d), 128.66 (s), 126.89 (s), 123.45 (d), 24.66 (br), 20.68 (s), 20.52 (s), 19.73 (br), -0.02 (s, Si*C*H$_3$). Compound hydrolyzed under FAB-MS conditions, only mass consistent with **3.1a** observed.

**Synthesis of diethyl-(1,4-bis(2-(diisopropylphosphino)phenyl)-2,3-catechol)silane (3.1c)**

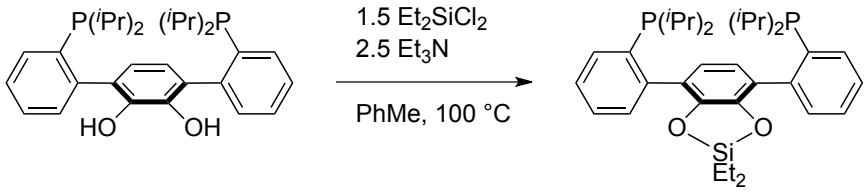


Compound **3.1c** was prepared analogously to above using diphosphine **3.1a** (0.1555 g, 0.314 mmol), $Et_2SiCl_2$ (0.0715 g, 0.455 mmol), and $Et_3N$ (0.1031 g, 1.02 mmol) in PhMe (10 mL). The desired compound **3.1c** was isolated as a white powder in 98.5% yield (0.1793 g). $^{1}$H NMR (300 MHz, $CDCl_3$), δ(ppm): 7.55 (m, 2 H, Ar-C*H*), 7.36 (m, 6 H,

Ar-C*H*), 6.75 (s, 2 H, Ar-$C_1$*H*), 2.03 (m, 4 H, PC*H*($CH_3$)$_2$), 0.97 (m, 4 H, PCH(C*H*$_3$)$_2$ and SiC*H*$_2$C*H*$_3$). $^{31}$P{$^1$H} (121 MHz, $CDCl_3$), δ(ppm): -2.06 (br), -2.73 (br). $^{13}$C{$^1$H} NMR (126 MHz, $CDCl_3$), δ(ppm): 146.15 (s), 145.85 (s), 145.61 (s), 135.77 (d), 132.41 (s), 131.14 (s), 123.22 (s), 126.73 (d), 123.15 (s), 24.36 (d, PC*H*($CH_3$)$_2$), 20.29 (s, PCH(C*H*$_3$)$_2$), 20.14 (s, PCH(C*H*$_3$)$_2$), 19.67 (d, PCH(C*H*$_3$)$_2$), 6.72 (s, SiCH$_2$C*H*$_3$), 5.49 (s, SiC*H*$_2$CH$_3$). MS (m/z): calcd, 579.2977 [M+H]$^+$; found, 579.2980 (FAB$^+$, [M+H]$^+$).

**Synthesis of diisopropyl-(1,4-bis(2-(diisopropylphosphino)phenyl)-2,3-catechol)silane (3.1d)**

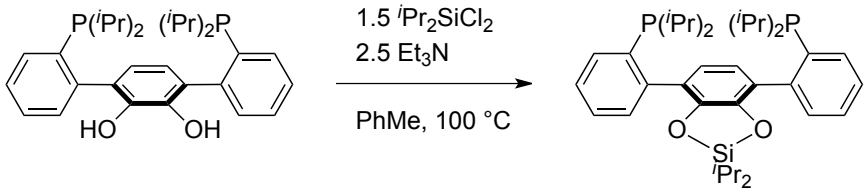


Compound **3.1d** was prepared analogously to above using diphosphine **3.1a** (0.1518 g, 0.307 mmol), $^i$Pr$_2$SiCl$_2$ (0.0976 g, 0.527 mmol), and Et$_3$N (0.0942 g, 0.931 mmol) in PhMe (10 mL). The desired compound **3.1d** was isolated as a white powder in 96.7% yield (0.1799 g). $^1$H NMR (300 MHz, $CDCl_3$), δ(ppm): 7.58 (m, 2 H, Ar-C*H*), 7.38 (m, 6 H, Ar-C*H*), 6.76 (s, 2 H, Ar-$C_1$*H*), 2.03 (m, 4 H, PC*H*($CH_3$)$_2$), 1.05 (m, 42 H, PCH(C*H*$_3$)$_2$ and SiC*H*(C*H*$_3$)$_2$). $^{31}$P{$^1$H} (121 MHz, $CDCl_3$), δ(ppm): -2.61 (br), -2.98 (br). $^{13}$C{$^1$H} NMR (126 MHz, $CDCl_3$), δ(ppm): 146.62 (s), 145.89 (s), 145.66 (s), 135.67 (d), 132.39 (s), 131.42 (s), 128.05 (s), 126.57 (m), 123.32 (s), 24.46 (d, PC*H*($CH_3$)$_2$), 20.31 (s, PCH(C*H*$_3$)$_2$), 20.17 (s, PCH(C*H*$_3$)$_2$), 19.78 (d, PCH(C*H*$_3$)$_2$), 16.04 (s, SiCH(C*H*$_3$)$_2$), 13.02 (s, SiC*H*($CH_3$)$_2$). MS (m/z): calcd, 607.3290 [M+H]$^+$; found, 607.3290 (FAB$^+$, [M+H]$^+$).

**Synthesis of 4-(trifluoromethyl)phenyl-(1,4-bis(2-(diisopropylphosphino)phenyl)-2,3-catechol)borane (3.1e)**

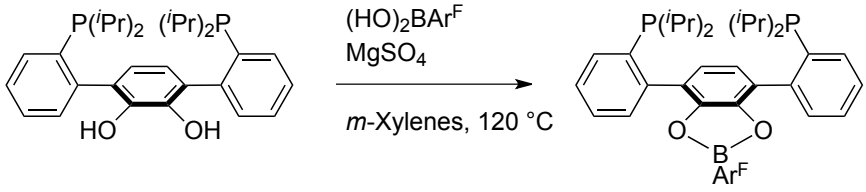


In the wet glove box under an atmosphere of $N_2$, **3.1a** (1.53 g, 3.09 mmol) and *p*$(F_3C)C_6H_4B(OH)_2$ (0.5876 g, 3.09 mmol), and $MgSO_4$ (0.4 g, 3.3 mmol) were combined in a Schlenk tube with *m*-xylenes (10 mL). The reaction was heated to 120 °C for 2.5 hours. The volatiles were removed under vacuum, the residue washed with $Et_2O$ (10 mL), and the product extracted with $C_6H_6$ (15 mL), filtered through Celite, and concentrated under vacuum to yield 0.9 g (44.8%) of the desired product as an off-white solid. $^1$H NMR (300 MHz, $C_6D_6$), δ(ppm): 7.80 (m, 2 H, Ar-C*H*), 7.52 (m, 2 H, Ar-C*H*), 7.37 (m, 2 H, Ar-C*H*), 7.24 (m, 2 H, Ar-C*H*), 7.20 (s, 2 H, Ar-$C_1$*H*), 1.92 (m, 4 H, PC*H*$(CH_3)_2$), 0.98 (m, 24 H, PCH(C*H*$_3)_2$). $^{31}$P{$^1$H} (121 MHz, $C_6D_6$), δ(ppm): -1.54 (s). $^{19}$F NMR (282 MHz, $C_6D_6$ , 25 °C), δ(ppm): -61.52 (s). $^{13}$C{$^1$H} NMR (126 MHz, $C_6D_6$), δ(ppm): 146.01 (s), 145.02 (s), 144.78 (s), 136.57 (s), 136.39 (s), 135.78 (s), 133.74 (q, *C*$F_3$), 132.79 (s), 131.12 (s), 128.88 (s), 127.62 (s), 125.40 (d), 124.85 (m), 24.70 (d, PC*H*$(CH_3)_2$), 20.45 (s, PCH(C*H*$_3)_2$), 20.29 (s, PCH(C*H*$_3)_2$), 19.75 (d, PCH(C*H*$_3)_2$). MS (m/z): calcd, 649.2784 $[M+H]^+$; found, 649.2794 (FAB$^+$, $[M+H]^+$).

**Synthesis of 1,4-bis(2-(diisopropylphosphino)phenyl)-2,3-dimethoxybenzene (3.1f)**

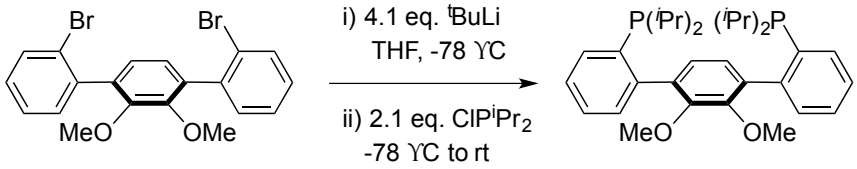


**3.1$^{Br}$f** **3.1f**

A Schlenk tube was charged with 1,4-di(2-bromophenyl)-2,3-di(methoxy)benzene (2.0449 g, 4.56 mmol), THF (30 mL), and a stir bar. The reaction mixture was cooled to -78 °C with the use of a dry ice/acetone bath. Under a counter-flow of $N_2$, a 1.7 M solution of $^t$BuLi (11.0 mL, 18.7 mmol) in pentanes was added via syringe dropwise. A light yellow color appeared in seconds, and as the reaction was allowed to stir for 30 min at -78 °C, an orange color evolved. After stirring for 1 hour at -78 °C, chlorodiisopropylphosphine (1.55 mL, 9.74 mmol) was added to the reaction mixture via syringe under a counter-flow of $N_2$, inducing a light yellow color. After stirring for 1h at -78 °C, the reaction was removed from the dry ice/acetone bath and allowed to warm to room temperature. After stirring for 2 hours at room temperature the volatiles were removed under reduced pressure. Further manipulations were performed under an $N_2$ atmosphere in a wet glove box. The residue was treated with DCM (50 mL) and $H_2O$ (50 mL) and transferred to a separatory funnel with vigorous mixing. The layers were separated and the aqueous washed with DCM (2 x 25 mL). The combined organics were dried with $MgSO_4$, filtered, and concentrated under vacuum to an off-white powder. Trituration with MeOH (20 mL) afforded a white precipitate that was collected on a glass frit, and then dried under vacuum to yield the desired product in 60.3% (1.4385 g).

$^{1}$H NMR (300 MHz, $CDCl_3$), δ(ppm): 7.42 (m, 2 H, Ar-C*H*), 7.12 (m, 6 H, Ar-C*H*), 7.00 (s, 2 H, Ar-$C_1$*H*), 3.56 (s, 6 H, O$CH_3$), 2.00 (m, 2 H, PC*H*($CH_3$)$_2$), 1.79 (m, 2 H, PC*H*($CH_3$)$_2$), 1.20 – 0.75 (m, 24H, PCH($CH_3$)$_2$). $^{31}$P{$^{1}$H} (121 MHz, $CDCl_3$), δ(ppm): -1.13 (s). $^{13}$C{$^{1}$H} (126 MHz, $CDCl_3$), δ(ppm): 150.43 (s), 146.83 (d), 136.44 (m), 132.32 (s), 130.77 (s), 127.97 (s), 126.55 (s), 125.77 (s), 60.12 (s), 25.22 (br), 24.41 (br), 20.0-19.0 (m). MS (m/z): calcd, 523.2895 $[M+H]^+$; found, 523.2891 ($FAB^+$, $[M+H]^+$).

**Synthesis of [1,4-bis(2-(diisopropylphosphino)phenyl)-2,3-catechol] tricarbonylmolybdenum(0) (3.2a)**

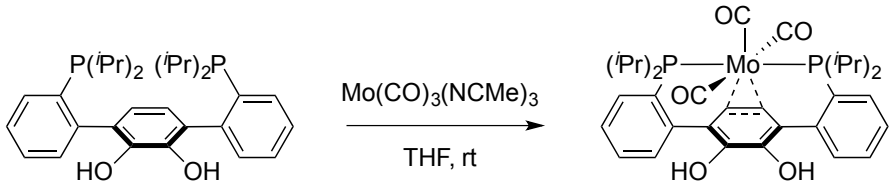


**3.1a** **3.2a**

From **3.1a**: $Mo(CO)_3(MeCN)_3$ (1.3010 g, 4.29 mmol) and **3.1a** (1.0494 g, 2.12 mmol) were combined with THF (20 mL) and stirred at room temperature for 72 hours, generating a dark brown solution. Upon completion of the reaction (a single major peak near 50 ppm by $^{31}$P NMR), the volatiles were removed under reduced pressure and the residue then triturated with MeCN (15 mL). The resulting orange precipitate was collected on a glass frit and washed with minimal MeCN until the brown filtrate had lightened to pale orange. The remaining solid was then dried under vacuum to yield 0.6192 g (43.3%) of the desired product (spectroscopic features reported below).


**3.2b** **3.2a**

From **3.2b**: In a water-tolerant glove box under $N_2$, NaOMe (0.3380 g, 6.25 mmol) was added to a stirred suspension of **3.2b** (1.5179 g, 2.08 mmol) in MeOH (15 mL) in a 100 mL round bottom flask, and the solution rapidly became homogeneous. After stirring for 1 hour at room temperature, the volatiles were removed under reduced pressure. The residue was then treated with a saturated aqueous $NH_4Cl$ solution (50 mL) and DCM (50 mL) and transferred to a separatory funnel and thoroughly mixed. The layers were separated and the aqueous layer washed with DCM (2 x 25 mL). The combine organics were dried over $MgSO_4$, filtered, and concentrated *in vacuo*. The resulting orange powder was transferred to a dry glove box and residual $H_2O$/MeOH removed by triturating the powder in dry MeCN, collecting the solid on a glass frit, washing with additional dry MeCN, and finally drying under vacuum to yield 1.3072 g (93.3%) of the desired product. Crystals suitable for X-ray diffraction were grown from slow evaporation of a saturated $C_6H_6$ solution. $^1$H NMR (300 MHz, $C_6D_6$ , 25 °C), δ(ppm): 7.55 (m, 4 H, Ar-C*H*), 7.12 (m, 4 H, Ar-C*H*), 5.73 (t, $J_{PH}$ = 4 Hz, 2 H, Ar-$C_1$*H*), 5.26 (s, 2 H, Ar-$C_1$O*H*), 2.66 (m, PC*H*$(CH_3)_2$), 2.54 (m, PC*H*$(CH_3)_2$). 1.62 (m, 6H, PCH(C*H*$_3)_2$), 1.20 (m, 12H, PCH(C*H*$_3)_2$), 0.92 (m, 6 H, PCH(C*H*$_3)_2$). $^{31}$P NMR (121 MHz, $C_6D_6$ , 25 °C), δ(ppm): 50.62 (s). $^{13}$C NMR (125 MHz, $C_6D_6$ , 75 °C), δ(ppm): 224.00 (t, Mo-*C*O), 214.23 (t, Mo-*C*O), 212.48 (t, Mo-*C*O), 144.34 (t, Ar-$C_4$), 141.67 (s, Ar-$C_3$), 132.77 (t,

Ar-$C_9$), 131.96 (s, Ar-$C_5$), 130.06 (s, Ar-$C_8$), 129.21 (s, Ar-$C_7$), 127.65 (s, Ar-$C_2$), 122.25 (t, Ar-$C_6$), 87.58 (s, Ar-$C_1$), 35.92 (t, P$C$H$(CH_3)_2$), 32.39 (t, P$C$H$(CH_3)_2$), 20.82 (m, PCH$(CH_3)_2$), 20.02 (s, PCH$(CH_3)_2$), 19.67 (m, PCH$(CH_3)_2$), 19.57 (m, PCH$(CH_3)_2$). IR (DCM), $\nu_{CO}$ ($cm^{-1}$): 1959.3, 1843.2 (br). $\lambda_{max}$ (THF, nm), $\varepsilon$ ($M^{-1}cm^{-1}$): 478, $3.9x10^3$; 355, $8.2x10^3$; 285, $3.3x10^4$. Anal. Calcd for [**3.2a**], $C_{33}H_{40}MoO_5P_2$: C, 58.76; H, 5.98. Found: C, 59.01; H, 5.72.

**Synthesis of [dimethyl-(1,4-bis(2-(diisopropylphosphino)phenyl)-2,3-catechol)silane]tricarbonylmolybdenum(0) (3.2b)**

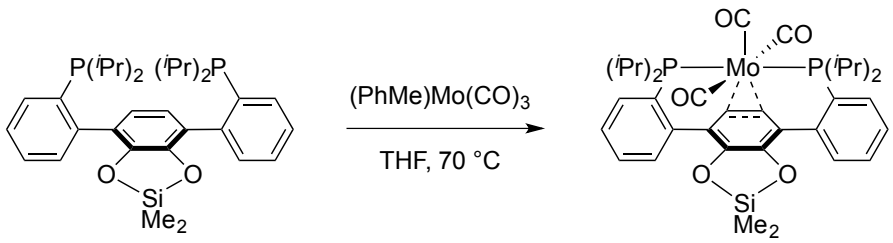


**3.1b** **3.2b**

Diphosphine **3.1b** (2.204 g, 4.00 mmol) and (PhMe)$Mo(CO)_3$ (1.314 g, 4.83 mmol) were combined in THF (10 mL) and added to a Schlenk tube charged with a stir bar and fitted with a screw-in Teflon stopper. The sealed vessel was removed from the glove box and heated to 70 °C with stirring in an oil bath for 3 hours. After complete conversion (a single peak at 52 ppm by $^{31}P$ NMR), the Schlenk tube was returned to the glove box and the volatiles were removed under reduced pressure. The residue was triturated with MeCN (10 mL), and the resulting orange precipitate was collected on a glass frit, washing with minimal additional MeCN until the filtrate was a pale orange. The orange powder was then dried under vacuum to yield 2.7561 g (94.2%) of the

desired product. Crystals suitable for X-ray diffraction were grown from cooling of a saturated MeCN solution at -35 °C. $^{1}$H NMR (300 MHz, $C_6D_6$ , 25 °C), δ(ppm): 7.92 (d, 2 H, Ar-C*H*), 7.55 (d, 2 H, Ar-C*H*), 7.25 (t, 2 H, Ar-C*H*), 7.10 (t, 2 H, Ar-C*H*), 5.69 (t, $J_{PH}$ = 4 Hz, 2 H, Ar-$C_1$*H*), 2.67 (m, PC*H*$(CH_3)_2$), 2.44 (m, PC*H*$(CH_3)_2$). 1.60 (m, 6H, PCH(C*H*$_3)_2$), 1.25 (m, 6H, PCH(C*H*$_3)_2$), 1.13 (m, 6H, PCH(C*H*$_3)_2$), 0.87 (m, 6 H, PCH(C*H*$_3)_2$), 0.58 (s, 3H, MeCN C*H*$_3$) 0.08 (s, 3 H, SiC*H*$_3$), -0.16 (s, 3 H, SiC*H*$_3$). $^{31}$P NMR (121 MHz, $C_6D_6$ , 25 °C), δ(ppm): 51.37 (s). $^{13}$C NMR (125 MHz, $C_6D_6$ , 25 °C), δ(ppm): 223.96 (t, Mo-*C*O), 214.11 (t, Mo-*C*O), 212.85 (t, Mo-*C*O), 146.48 (s, Ar-*C*$_3$), 144.58 (t, Ar-*C*$_4$), 131.45 (t, Ar-*C*$_9$), 131.27 (s, Ar-*C*$_5$), 131.17 (t, Ar-*C*$_8$), 128.73 (s, Ar-*C*$_7$), 127.31 (t, Ar-*C*$_2$), 120.99 (t Ar-*C*$_6$), 115.96 (s, MeCN N*C*CH$_3$), 85.12 (s, Ar-*C*$_1$), 35.66 (t, P*C*H$(CH_3)_2$), 32.39 (t, P*C*H$(CH_3)_2$), 20.57 (t, PCH(*C*H$_3)_2$), 19.67 (t, PCH(*C*H$_3)_2$), 19.60 (t, PCH(*C*H$_3)_2$), 19.40 (m, PCH(*C*H$_3)_2$), 0.16 (s, MeCN NC*C*H$_3$), -0.88 (s, Si*C*H$_3$), -1.04 (s, Si*C*H$_3$). IR (powder), $\nu_{CO}$ (cm$^{-1}$): 1956, 1838, 1800 (br). IR (DCM), $\nu_{CO}$ (cm$^{-1}$): 1959.3, 1843, 1835. Anal. Calcd for [**3.2b**•MeCN], $C_{37}H_{47}MoNO_5P_2$: C, 57.58; H, 6.24; N, 1.81. Found: C, 57.25; H, 5.87; N, 1.80.

**Synthesis of [diethyl-(1,4-bis(2-(diisopropylphosphino)phenyl)-2,3-catechol)silane]tricarbonylmolybdenum(0) (3.2c)**

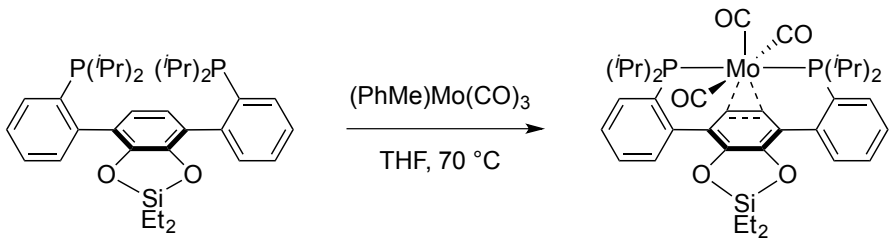


**3.1c** **3.2c**

Compound **3.2c** was prepared analogously to **3.2b** using diphosphine **3.1c** (0.1577 g, 0.272 mmol) and (PhMe)Mo(CO)$_3$ (0.1120 g, 0.412 mmol) in THF (8 mL). The desired compound **3.2c** was isolated as an orange powder in 79.2% yield (0.1638 g). $^1$H NMR (300 MHz, $C_6D_6$ , 25 °C), δ(ppm): 8.01 (d, 2 H, Ar-C*H*), 7.60 (d, 2 H, Ar-C*H*), 7.30 (t, 2 H, Ar-C*H*), 7.14 (t, 2 H, Ar-C*H*), 5.78 (t, $J_{PH}$ = 4 Hz, 2 H, Ar-$C_1$H), 2.72 (m, PC*H*$(CH_3)_2$), 2.49 (m, PC*H*$(CH_3)_2$). 1.66 (m, 6H, PCH(C*H*$_3)_2$), 1.30 (m, 6H, PCH(C*H*$_3)_2$), 1.21 (m, 6H, PCH(C*H*$_3)_2$), 0.94 (m, 9 H, PCH(C*H*$_3)_2$ and SiC*H*$_2$CH$_3$), 0.62 (m, 5 H, SiCH$_2$C*H*$_3$ and SiC*H*$_2$CH$_3$). $^{31}$P NMR (121 MHz, $C_6D_6$ , 25 °C), δ(ppm): 51.47 (s). $^{13}$C NMR (125 MHz, $C_6D_6$ , 25 °C), δ(ppm): 223.92 (t, Mo-*C*O), 214.07 (t, Mo-*C*O), 212.59 (t, Mo-*C*O), 146.84 (s, Ar-$C_3$), 144.67 (t, Ar-$C_4$), 131.56 (t, Ar-$C_9$), 131.32 (s, Ar-$C_5$), 131.14 (t, Ar-$C_8$), 128.76 (s, Ar-$C_7$), 127.28 (t, Ar-$C_2$), 120.97 (t, Ar-$C_6$), 85.14 (s, Ar-$C_1$), 35.65 (t, P*C*H$(CH_3)_2$), 31.38 (t, P*C*H$(CH_3)_2$), 20.59 (t, PCH(*C*H$_3)_2$), 19.68 (t, PCH(*C*H$_3)_2$), 19.56 (t, PCH(*C*H$_3)_2$), 19.39 (m, PCH(*C*H$_3)_2$), 6.21 (s, SiCH$_2$*C*H$_3$), 5.92 (s, SiCH$_2$*C*H$_3$), 5.64 (s, Si*C*H$_2$CH$_3$), 5.05 (s, Si*C*H$_2$CH$_3$). IR (film), $\nu_{CO}$ (cm$^{-1}$): 1957, 1840, 1819. Anal. Calcd for [**3.2c**], $C_{37}H_{47}MoO_5P_2Si$: C, 58.57; H, 6.38. Found: C, 59.02; H, 6.51.

**Synthesis of [diisopropyl-(1,4-bis(2-(diisopropylphosphino)phenyl)-2,3-catechol)silane]tricarbonylmolybdenum(0) (3.2d)**

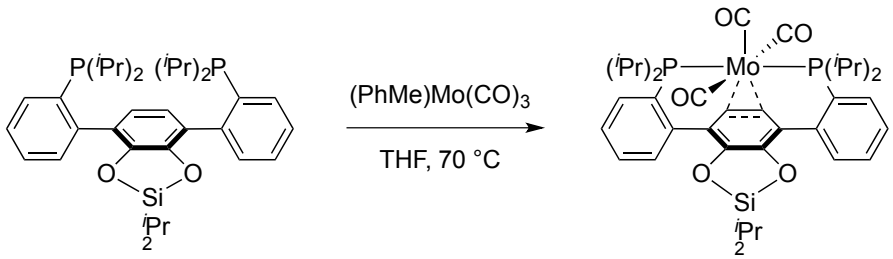


**3.1d** **3.2d**

Compound **3.2d** was prepared analogously to **3.2b** using diphosphine **3.1d** (0.1829 g, 0.301 mmol) and (PhMe)Mo(CO)$_3$ (0.1260 g, 0.463 mmol) in THF (8 mL). The desired compound **3.2d** was isolated as an orange powder in 78.5% yield (0.1862 g). $^1$H NMR (300 MHz, $C_6D_6$ , 25 °C), δ(ppm): 8.03 (d, 2 H, Ar-C*H*), 7.59 (d, 2 H, Ar-C*H*), 7.29 (t, 2 H, Ar-C*H*), 7.12 (t, 2 H, Ar-C*H*), 5.79 (t, $J_{PH}$ = 4 Hz, Ar-C$_1$*H*), 2.71 (m, PC*H*(CH$_3$)$_2$), 2.47 (m, PC*H*(CH$_3$)$_2$). 1.66 (m, 6H, PCH(C*H*$_3$)$_2$), 1.30 (m, 6H, PCH(C*H*$_3$)$_2$), 1.21 (m, 6H, PCH(C*H*$_3$)$_2$), 1.07 (m, 6 H, SiCH(C*H*$_3$)$_2$), 0.93 (m, 8 H, PCH(C*H*$_3$)$_2$ and SiC*H*(CH$_3$)$_2$), 0.79 (m, 6 H, SiCH(C*H*$_3$)$_2$. $^{31}$P NMR (121 MHz, $C_6D_6$ , 25 °C), δ(ppm): 51.69 (s). $^{13}$C NMR (125 MHz, $C_6D_6$ , 25 °C), δ(ppm): 223.84 (t, Mo-*C*O), 214.02 (t, Mo-*C*O), 212.30 (t, Mo-*C*O), 146.92 (s, Ar-*C*$_3$), 144.68 (t, Ar-*C*$_4$), 131.66 (t, Ar-*C*$_9$), 131.36 (s, Ar-*C*$_5$), 130.98 (t, Ar-*C*$_8$), 128.82 (s, Ar-*C*$_7$), 127.25 (t, Ar-*C*$_2$), 120.76 (t, Ar-*C*$_6$), 84.98 (s, Ar-*C*$_1$), 35.65 (t, P*C*H(CH$_3$)$_2$), 31.72 (t, P*C*H(CH$_3$)$_2$), 20.61 (t, PCH(*C*H$_3$)$_2$), 19.69 (t, PCH(*C*H$_3$)$_2$), 19.51 (t, PCH(*C*H$_3$)$_2$), 19.36 (m, PCH(*C*H$_3$)$_2$), 16.34 (s, SiCH(*C*H$_3$)$_2$), 15.85

(s, SiCH($CH_3$)$_2$), 13.45 (s, Si$C$H($CH_3$)$_2$), 12.76 (s, Si$C$H($CH_3$)$_2$). IR (powder), $\nu_{CO}$ (cm$^{-1}$): 1953, 1836, 1812. Anal. Calcd for [**3.2d**], $C_{39}H_{52}MoO_5P_2Si$: C, 59.53; H, 6.66. Found: C, 59.22; H, 6.51.

**Synthesis of [4-(trifluoromethyl)phenyl-(1,4-bis(2-(diisopropylphosphino)phenyl)-2,3-catechol)borane]tricarbonylmolybdenum(0) (3.2e)**

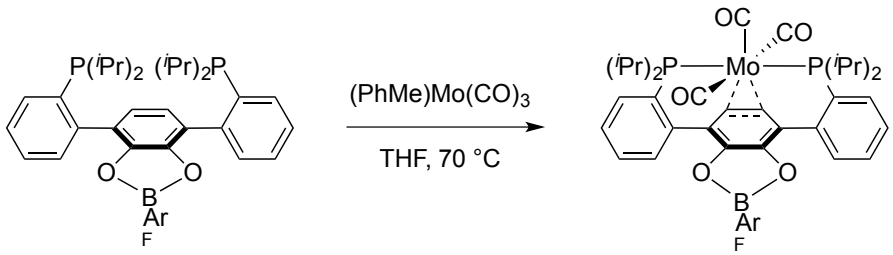


**3.1e** $Ar^F$ = $p(CF_3)C_6H_4$ **3.2e**

Compound **3.2e** was prepared analogously to **3.2b** using diphosphine **3.1e** (0.4090 g, 0.631 mmol) and (PhMe)Mo(CO)$_3$ (0.2345 g, 0.862 mmol) in THF (10 mL). The desired compound **3.2e** was isolated as a red powder in 76.6% yield (0.4010 g). $^1$H NMR (300 MHz, $C_6D_6$ , 25 °C), δ(ppm): 7.96 (m, 2 H, Ar-C$H$), 7.69 (d, 2 H, BAr-C$H$), 7.62 (d, 2 H, Ar-C$H$), 7.41 (t, 2 H, Ar-C$H$), 7.23 (m, 4 H, BAr-C$H$ and Ar-C$H$), 5.80 (t, $J_{PH}$ = 4 Hz, 2 H, quinonoid Ar-C$H$), 2.73 (m, 2 H, PC$H$($CH_3$)$_2$), 2.45 (m, 2 H, PC$H$($CH_3$)$_2$). 1.63 (m, 6H, PCH(C$H_3$)$_2$), 1.29 (m, 6 H, PCH(C$H_3$)$_2$), 1.10 (m, 6 H, PCH(C$H_3$)$_2$), 0.86 (m, 6 H, PCH(C$H_3$)$_2$). $^{31}$P NMR (121 MHz, $C_6D_6$ , 25 °C), δ(ppm): 51.49 (s). $^{19}$F NMR (282 MHz, $C_6D_6$ , 25 °C), δ(ppm): -61.68 (s). $^{13}$C NMR (125 MHz, $C_6D_6$ , 25 °C),

δ(ppm): 221.97 (t, Mo-*C*O), 213.90 (t, Mo-*C*O), 213.15 (t, Mo-*C*O), 146.13 (s, Ar-$C_3$), 143.08 (t, Ar-$C_4$), 135.89 (m, BAr-*C*), 134.00 (q, BAr-$CF_3$), 131.58 (m, BAr-*C*), 131.21 (t, Ar-$C_9$), 130.94 (m, Ar-$C_5$ and Ar-$C_8$), 129. 28 (br, Ar-$C_7$), 124.82 (t, Ar-$C_2$), 121.80 (t, Ar-$C_6$), 84.01 (s, Ar-$C_1$), 35.54 (t, P*C*H$(CH_3)_2$), 31.70 (t, P*C*H$(CH_3)_2$), 20.35 (br, CH$(CH_3)_2$), 19.53 (br, PCH$(CH_3)_2$), 19.37 (br, PCH$(CH_3)_2$). IR (powder), $\nu_{CO}$ ($cm^{-1}$): 1956, 1839 (br). Anal. Calcd for [**3.2e**] $C_{40}H_{42}BF_3MoO_5P_2$: C, 57.99; H, 5.11. Found: C, 57.50; H, 5.14.

**Synthesis of [1,4-bis(2-(diisopropylphosphino)phenyl)-2,3-dimethoxybenzene]tricarbonylmolybdenum(0) (3.2f)**

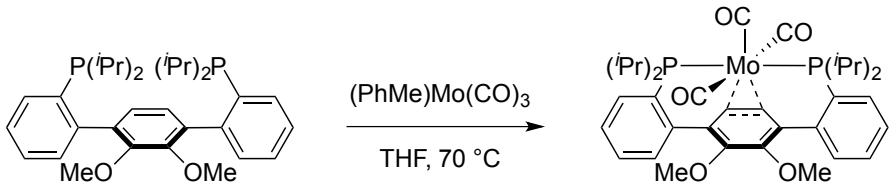


**3.1f** **3.2f**

Compound **3.2f** was prepared analogously to **3.2b** using diphosphine **3.1f** (0.6007 g, 1.15 mmol) and (PhMe)Mo$(CO)_3$ (0.3988 g, 1.47 mmol) in THF (15 mL). The desired compound **3.2f** was isolated as an orange powder in 78.7% yield (0.6354 g). $^1$H NMR (300 MHz, $C_6D_6$ , 25 °C), δ(ppm): 7.78 (m, 2 H, Ar-C*H*), 7.54 (d, 2 H, Ar-C*H*), 7.24 (t, 2 H, Ar-C*H*), 7.16 (t, 2 H, Ar-C*H*), 5.81 (t, $J_{PH}$ = 4 Hz, 2 H, Ar-$C_1H$), 2.64 (m, 2 H, PC*H*$(CH_3)_2$), 2.40 (m, 2 H, PC*H*$(CH_3)_2$). 1.68 (m, 6 H, PCH$(CH_3)_2$), 1.23 (m, 12 H, PCH$(CH_3)_2$), 0.91 (m, 6 H, PCH$(CH_3)_2$). $^{31}$P NMR (121 MHz, $C_6D_6$ , 25 °C), δ(ppm): 50.09 (s). $^{13}$C NMR (125 MHz, $C_6D_6$ , 25 °C), δ(ppm): 222.76 (t, Mo-*C*O), 213.66 (t,

Mo-*C*O), 213.62 (t, Mo-*C*O), 150.05 (s, Ar-$C_3$), 145.13 (t, Ar-$C_4$), 132.33 (t, Ar-$C_9$), 131.16 (s, Ar-$C_5$), 131.05 (t, Ar-$C_8$), 120.89 (t, Ar-$C_6$), 128.67 (s, Ar-$C_7$), 127.66 (t, Ar-$C_2$), 87.21 (s, Ar-$C_1$), 60.53 (s, quinonoid Ar-O*C*H$_3$), 36.42 (t, P*C*H(CH$_3$)$_2$), 33.08 (t, P*C*H(CH$_3$)$_2$), 21.26 (t, PCH(*C*H$_3$)$_2$), 20.04 (s, PCH(*C*H$_3$)$_2$), 19.59 (t, PCH(*C*H$_3$)$_2$), 19.47 (t, PCH(*C*H$_3$)$_2$). IR (powder), $\nu_{CO}$ (cm$^{-1}$): 1954, 1824 (br). Anal. Calcd for [**3.2f**], $C_{35}H_{44}MoO_5P_2$: C, 59.83; H, 6.31. Found: C, 60.12; H, 6.21.

**Synthesis of [tetramethyl-1,3-(1,4-bis(2-(diisopropylphosphino)phenyl)-2,3-catechol)disiloxane]tricarbonylmolybdenum(0) (3.2h)**

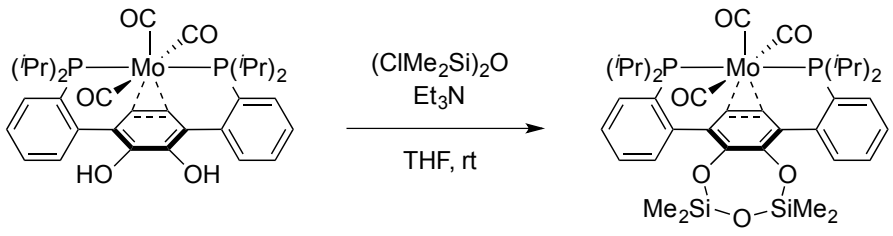


**3.2a** **3.2h**

Compound **3.2a** (0.0785 g, 0.116 mmol), $(ClMe_2Si)_2O$ (0.0404 g, 0.199 mmol), and $Et_3N$ (0.0643 g, 0.635 mmol) were combined in THF (5 mL) and stirred for 12 hours at room temperature, developing a precipitate over this time. The mixture was then filtered through a pad of celite, washing with additional THF. The filtrate was then concentrated *in vacuo* and triturated with MeCN (5 mL). The resulting orange precipitate was collected on a pad of celite, dissolved in $C_6H_6$, filtered through celite, and concentrated under reduced pressure. The resulting residue is a mixture of **3.2h** and **3.2b** in ca. 8:1 ratio, respectively. Recrystallization twice via vapor diffusion of pentane into a saturated $C_6H_6$ solution of the residue, collecting the filtrate, yields the desired

compound (0.0187g, 20.0%). $^{1}$H NMR (300 MHz, $C_6D_6$ , 25 °C), δ(ppm): 7.77 (d, 2 H, Ar-C*H*), 7.57 (d, 2 H, Ar-C*H*), 7.22 (t, 2 H, Ar-C*H*), 7.16 (m, 2 H, Ar-C*H*), 5.88 (t, $J_{PH}$ = 4 Hz, 2 H, Ar-$C_1$*H*), 2.67 (m, 2 H, PC*H*$(CH_3)_2$), 2.44 (m, 2 H, PC*H*$(CH_3)_2$). 1.66 (m, 6 H, PCH(C*H*$_3)_2$), 1.23 (m, 12 H, PCH(C*H*$_3)_2$), 0.93 (m, 6H, PCH(C*H*$_3)_2$), 0.30 (s, 3 H, SiC*H*$_3$), 0.05 (s, 3 H, SiC*H*$_3$). $^{31}$P NMR (121 MHz, $C_6D_6$ , 25 °C), δ(ppm): 50.05 (s). $^{13}$C NMR (121 MHz, $C_6D_6$ , 25 °C), δ(ppm): 223.83 (t, Mo-*C*O), 214.20 (t, Mo-*C*O), 213.02 (t, Mo-*C*O), 145.64 (t, Ar-$C_4$), 142.53 (s, Ar-$C_3$), 132.24 (t, Ar-$C_9$), 131.26 (s, Ar-$C_5$), 130.89 (t, Ar-$C_8$), 127.23 (t, Ar-$C_2$), 127.20 (t, Ar-$C_6$), 87.50 (s, Ar-$C_1$), 35.72 (t, P*C*H$(CH_3)_2$), 32.51 (t, P*C*H$(CH_3)_2$), 21.02 (t, PCH(*C*H$_3)_2$), 19.96 (s, PCH(*C*H$_3)_2$), 19.40 (t, PCH(*C*H$_3)_2$), -0.31 (s, Si*C*H$_3$), -0.47 (s, Si*C*H$_3$). IR (powder), $\nu_{CO}$ (cm$^{-1}$): 1956, 1838, 1800 (br).

**Synthesis of [tetraethyl-1,3-(1,4-bis(2-(diisopropylphosphino)phenyl)-2,3-catechol)disiloxane]tricarbonylmolybdenum(0) (3.2i)**

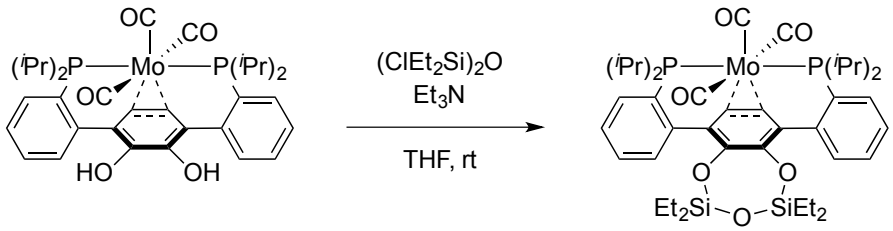


**3.2a** **3.2i**

Compound **3.2a** (0.1961 g, 0.291 mmol), $(ClEt_2Si)_2O$ (0.0768 g, 0.296 mmol), and $Et_3N$ (0.1414 g, 1.40 mmol) were combined in THF (5 mL) and stirred for 12 hours at room

temperature, developing a precipitate over this time. The mixture was then filtered through a pad of celite, washing with additional THF. The filtrate was then concentrated *in vacuo* and triturated with MeCN (5 mL). The resulting orange precipitate was collected on a pad of celite, dissolved in $C_6H_6$, filtered through celite, and concentrated under reduced pressure. The resulting residue is a mixture of **3.2i**, **3.2c**, and **3.2a** in ca. 7:2:1 ratio, respectively. Recrystallization four times from hot pentane yields the desired compound (0.0165 g, 6.7%). $^1$H NMR (300 MHz, $C_6D_6$ , 25 °C), δ(ppm): 7.77 (d, 2 H, Ar-C*H*), 7.57 (d, 2 H, Ar-C*H*), 7.24 (t, 2 H, Ar-C*H*), 7.16 (m, 2 H, Ar-C*H*), 5.88 (t, $J_{PH}$ = 4 Hz, 2 H, Ar-C$_1$*H*), 2.68 (m, 2 H, PC*H*(CH$_3$)$_2$), 2.45 (m, 2 H, PC*H*(CH$_3$)$_2$). 1.67 (m, 6 H, PCH(C*H*$_3$)$_2$), 1.24 (m, 12 H, PCH(C*H*$_3$)$_2$), 1.12 (t, $J^3$ = 8 Hz, 6 H, SiCH$_2$C*H*$_3$), 0.95 (m, 6H, PCH(C*H*$_3$)$_2$), 0.77 (m, 10 H, SiC*H*$_2$CH$_3$ and SiCH$_2$C*H*$_3$), 0.57 (m, 4 H, SiC*H*$_2$CH$_3$). $^{31}$P NMR (121 MHz, $C_6D_6$ , 25 °C), δ(ppm): 59.96 (s). $^{13}$C NMR (121 MHz, $C_6D_6$ , 25 °C), δ(ppm): 223.88 (t, Mo-*C*O), 214.28 (t, Mo-*C*O), 212.80 (t, Mo-*C*O), 145.68 (t, Ar-*C*$_4$), 142.74 (s, Ar-*C*$_3$), 132.30 (t, Ar-*C*$_9$), 131.28 (d, Ar-*C*$_5$), 131.13 (t, Ar-*C*$_8$), 127.27 (m, Ar-*C*$_2$), 127.21 (t, Ar-*C*$_6$), 88.15 (s, Ar-*C*$_1$), 35.73 (m, P*C*H(CH$_3$)$_2$), 32.52 (m, P*C*H(CH$_3$)$_2$), 21.07 (m, PCH(*C*H$_3$)$_2$), 19.95 (m, PCH(*C*H$_3$)$_2$), 19.59 (m, PCH(*C*H$_3$)$_2$), 19.41 (m, PCH(*C*H$_3$)$_2$), 6.64 (s, Si*C*H$_2$CH$_3$), 6.49 (s, SiCH$_2$*C*H$_3$), 6.42 (s, SiCH$_2$*C*H$_3$), 6.24 (s, Si*C*H$_2$CH$_3$). IR (film), $\nu_{CO}$ (cm$^{-1}$): 1956, 1840, 1816.

**Synthesis of [1,4-bis(2-(diisopropylphosphino)phenyl)-2,3-quinone]dicarbonylmolybdenum(0) (3.3)**

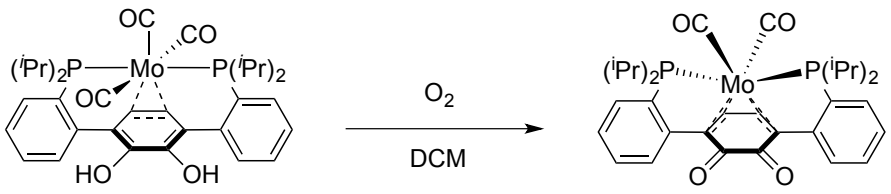


**3.2a** **3.3**

A solution of **3.2a** (0.0215 g, 0.0319 mmol) in THF (0.6 mL) was added to a J. Young style NMR tube and degassed via three freeze-pump-thaw cycles. An atmosphere of $O_2$ was then added to the headspace and the tube inverted for 60 seconds. $^{31}$P NMR spectroscopy revealed complete conversion to a new species at approximately 72 ppm. The volatiles were removed under vacuum, and the residue was dissolved in MeCN (2 mL) and then the volatiles removed under vacuum, repeating this multiple times to remove the $H_2O$ side product. Finally, the residue was triturated with Hexanes and the volatiles removed under vacuum to afford the desired product in 96.4% yield (0.0198 g, 0.0307 mmol). Refluxing the compound in PhMe for an hour and then allowing the solution to cool to room temperature formed crystals suitable for X-ray diffraction. $^{1}$H NMR (300 MHz, $CD_3CN$ , 25 °C), δ(ppm): 7.43-7.68 (m, 8 H, Ar-C*H*), 5.09 (s, 2 H, $C_1H$), 3.11 (m, 2 H, PC*H*$(CH_3)_2$). 2.93 (m, 2 H, PC*H*$(CH_3)_2$), 1.10-1.34 (m, 18 H, PCH(C$H_3)_2$), 0.82-0.92 (m, 6 H, PCH(C$H_3)_2$). $^{31}$P NMR (121 MHz, $CD_3CN$ , 25 °C), δ(ppm): 72.43 (s). $^{13}$C NMR (126 MHz, $CD_3CN$ , 25 °C), δ(ppm): 246.34 (t, 20 Hz, Mo-*C*O), 222.58 (t, 18 Hz, Mo-*C*O), 173.31 (s, quinonoid Ar-*C*O), 138.02 (m), 135.81 (m), 134.51 (s), 134.12 (s), 132.62 (t), 132.10 (t), 130.02 (t), 100.58 (s, quinonoid Ar-*C*H),

65.30 (s, O*C*H$_3$), 29.58 (m, P*C*H(CH$_3$)$_2$), 28.98 (s, P*C*H(CH$_3$)$_2$), 19.03 (s, PCH(*C*H$_3$)$_2$), 18.30 (t, PCH(*C*H$_3$)$_2$), 18.12 (s, PCH(*C*H$_3$)$_2$), 18.04 (s, PCH(*C*H$_3$)$_2$). IR (THF), $\nu_{CO}$ (cm$^{-1}$): 1875, 1605. Anal. Calcd for [**3.3**], $C_{32}H_{38}MoO_4P_2$: C, 59.63; H, 5.94. Found: C, 60.11; H, 6.04.

**Synthesis of [1,4-bis(2-(diisopropylphosphino)phenyl)-2,3-dimethoxybenzene]dicarbonylmolybdenum(II) trifluoromethanesulfonate ([3.5$^{2+}$][OTf]$_2$)**

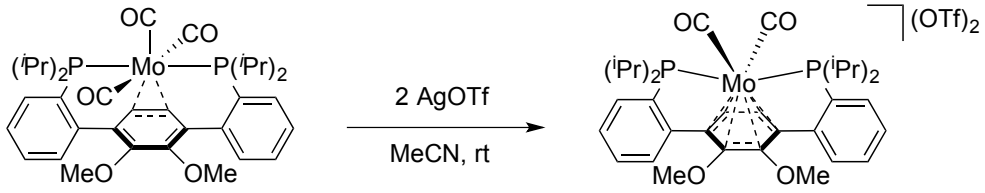


**3.2f** **[3.5$^{2+}$](OTf)$_2$**

To a stirred suspension of **3.2f** (0.0400 g, 0.0569 mmol) in MeCN (2 mL) was added a solution of AgOTf (0.0331 g, 0.129 mmol) in MeCN (2 mL). Upon addition the reaction became a purple heterogeneous mixture, which was stirred at room temperature until the purple color dissipated (approximately 20 min), resulting in a yellow/brown heterogeneous mixture. The solution was then filtered through celite, and the filtrate was evaporated under reduced pressure. The resulting residue was freed of excess MeCN by trituration with hexanes (3 mL), followed by evaporation under reduced pressure to yield the desired product as a tan solid (0.0505 g, 91.2%). $^1$H NMR (300 MHz, CD$_3$CN , 25 °C), δ(ppm): 7.70-8.00 (m, 8 H, Ar-C*H*), 6.80 (s, 2 H, Ar-C$_1$*H*), 3.42

(m, 2 H, PC*H*$(CH_3)_2$). 3.18 (m, 2 H, PC*H*$(CH_3)_2$), 1.35 (m, 18 H, PCH(C*H*$_3)_2$), 1.18 (m, 6 H, PCH(C*H*$_3)_2$). $^{31}$P NMR (121 MHz, $CD_3CN$ , 25 °C), δ(ppm): 72.43 (s). $^{19}$F NMR (282 MHz, $CD_3CN$ , 25 °C), δ(ppm): -79.19 (s). $^{13}$C NMR (126 MHz, $CD_3CN$ , 25 °C), δ(ppm): 222.65 (t, Mo-*C*O), 222.58 (t, Mo-*C*O), 141.31 (s, quinonoid Ar-*C*O), 138.02 (m), 135.81 (m), 134.51 (s), 134.12 (s), 132.62 (t), 132.10 (t), 130.02 (t), 100.58 (s, quinonoid Ar-*C*H), 65.30 (s, O*C*H$_3$), 29.58 (m, P*C*H$(CH_3)_2$), 28.98 (s, P*C*H$(CH_3)_2$), 19.03 (s, PCH(*C*H$_3)_2$), 18.30 (t, PCH(*C*H$_3)_2$), 18.12 (s, PCH(*C*H$_3)_2$), 18.04 (s, PCH(*C*H$_3)_2$). IR (MeCN), $\nu_{CO}$ (cm$^{-1}$): 2019, 1961. $\lambda_{max}$ (MeCN, nm), ε (M$^{-1}$cm$^{-1}$): 430, 5.0x10$^2$; 350, 2.0x10$^3$; 290, 6.4x10$^3$. Anal. Calcd for [**3.5**$^{2+}$][OTf]$_2$, $C_{36}H_{44}F_6MoO_{10}P_2S_2$: C, 44.45; H, 4.56. Found: C, 44.23; H, 4.39.

**Synthesis of [1,4-bis(2-(diisopropylphosphino)phenyl)-2,3-methylsemiquinonate]dicarbonylmolybdenum(II) trifluoromethanesulfonate ([3.6$^+$][OTf$^-$])**

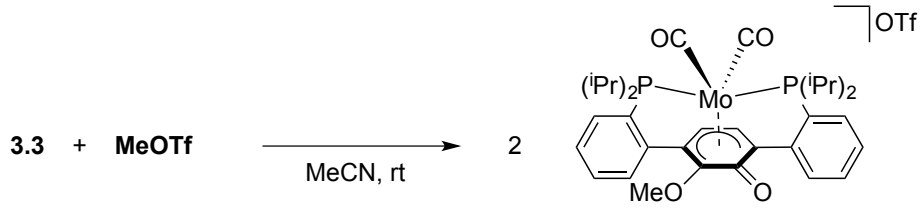


**[3.6$^+$][OTf$^-$]**

To a solution of **3.3** (0.0205 g, 0.0318 mmol) in MeCN (2 mL) was added MeOTf (5 μL, 0.0442 mmol). The mixture was stirred for 5 minutes and the volatiles were removed under vacuum. The residue was triturated with $C_6H_6$ and the precipitate collected on a

pad of celite, washing with additional $C_6H_6$. The solid was dissolved in MeCN, filtered through celite, and concentrated under reduced pressure. Excess MeCN was removed by triturating in hexanes followed by removal volatiles under vacuum. The desired compound was isolated as a pale yellow powder (0.0159 g, 0.0197 mmol, 61.8%). $^1$H NMR (300 MHz, $CD_3CN$ , 25 °C), δ(ppm): 7.60-7.80 (m, 8 H, Ar-C*H*), 5.89 (dd, $J_{HP}$ = 5.7 Hz, 1.2 Hz, 1 H, Ar-$C_1H$), 5.71 (dd, $J_{HP}$ = 5.7 Hz, 2.4 Hz, 1 H, Ar-$C_1H'$), 3.92 (s, 3 H, O$CH_3$), 3.41 (m, 2 H, PC*H*$(CH_3)_2$), 3.17 (m, 2 H, PC*H*$(CH_3)_2$), 1.20-1.45 (m, 18 H, PCH(C$H_3)_2$), 0.93-1.10 (m, 6 H, PCH(C$H_3)_2$). $^{31}$P NMR (121 MHz, $CD_3CN$ , 25 °C), δ(ppm): 78.19 (d, $J_{PP'}$ = 18 Hz), 65.44 (d, $J_{PP'}$ = 18 Hz). $^{19}$F NMR (282 MHz, $CD_3CN$ , 25 °C), δ(ppm): -77.09 (s). $^{13}$C NMR (126 MHz, $CD_3CN$ , 25 °C), δ(ppm): 233.60 (dd, $J_{CP}$ = 23.0 Hz, 21.5 Hz, Mo-*C*O), 228.62 (dd, $J_{CP}$ = 23.0 Hz, 21.5 Hz, Mo-*C*O), 163.51 (s, quinonoid Ar-*C*=O), 143.03 (d, Ar-*C),* 142.68 (d, Ar-*C*), 141.17 (d, Ar-*C*), 135.24 (m, $O_3S$-*C*$F_3$), 133.50 (m, Ar-*C*), 133.04 (m, Ar-*C*), 130.84 (m, Ar-*C*), 129.99 (m, Ar-*C*), 129.28 (m, Ar-*C*), 128.06 (m, Ar-*C*), 124.13 (m, Ar-*C*), 123.31 (s, Ar-*C*), 120.76 (s, Ar-*C*), 99.23 (m, quinonoid Ar-*C*H), 129.99 (m, Ar-*C*), 83.47 (m, quinonoid Ar-*C*H), 62.11 (m, O*C*$H_3$), 30.31 (s, P*C*H$(CH_3)_2$), 30.12 (s, P*C*H$(CH_3)_2$), 27.70 (m, P*C*H$(CH_3)_2$), 26.70 (m, P*C*H$(CH_3)_2$), 18.46 (m, PCH(*C*$H_3)_2$), 18.46 (m, PCH(*C*$H_3)_2$), 18.04 (m, PCH(*C*$H_3)_2$), 17.73 (m, PCH(*C*$H_3)_2$), 17.46 (m, PCH(*C*$H_3)_2$). IR (film), $\nu_{CO}$ ($cm^{-1}$): 1979, 1907, 1615.

**Synthesis of bis(1,3-dimethylcyclopentadienyl)iron(II) ($Me_4Fc$)**

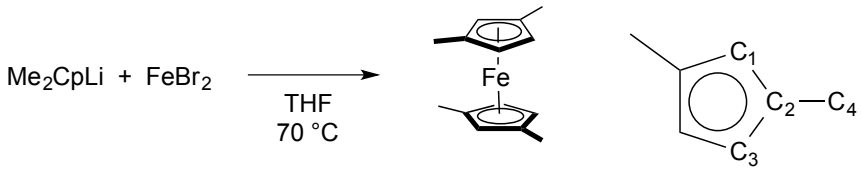


$Me_4Fc$

In a schlenk tube, $FeBr_2$ (1.0828 g, 5.02 mmol) and 1,3-dimethylcyclopentadienyl lithium (1.0438 g, 10.4 mmol) were combined in THF (30 mL) and heated to 70 °C for 3 hours, and the resulting brown/orange suspension was then concentrated under reduced pressure. The red-brown residue was extracted with $Et_2O$ (50 mL), filtered through alumina and concentrated under reduced pressure to yield the desired product as a red-orange oil (0.4038 g, 33.2%). $^1$H NMR (300 MHz, $C_6D_6$, 25 °C), δ(ppm): 3.73 (s, 4 H), 3.66 (s, 2 H), 1.86 (s, 12 H). $^{13}$C NMR (126 MHz, $C_6D_6$, 25 °C), δ(ppm): 83.17 (s, $C_2$), 71.86 (s, $C_1$), 70.03 (s, $C_3$), 14.34 (s, $C_4$). ESI-MS (m/z, relative abundance): 242.2 $[M]^+$, 100%; 227.2 $[M\text{-}CH_3]^+$, 12%. MS (m/z): calcd, 242.0785 $[M]^+$; found, 242.0764 ($FAB^+$, $[M]^+$).

**Control Reactions with $O_2$**

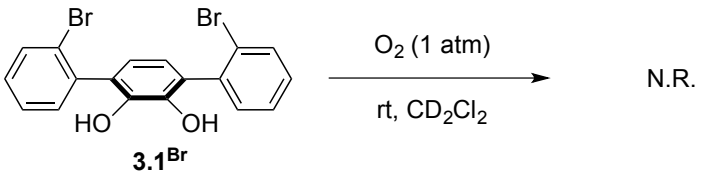


**3.1**$^{Br}$

**3.1**$^{Br}$: An NMR solution of **3.1**$^{Br}$ (0.0214 g, mmol) in $CD_2Cl_2$ (0.5 mL) prepared on the bench top was added to a J. Young style NMR tube and degassed via three freeze-pump-thaw cycles. An atmosphere of $O_2$ was added to the headspace and the reaction monitored by $^1$H NMR spectroscopy. There was no observed reaction over the course of 24 hours.

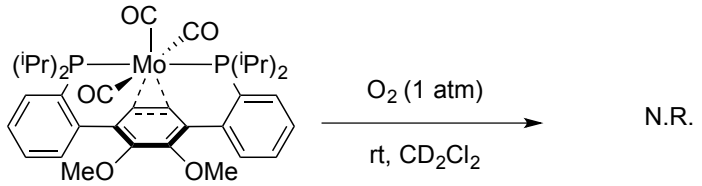


**3.2f**

**3.2f**: In the glove box, a solution of **3.2f** (0.0198 g, mmol) in $CD_2Cl_2$ (0.6 mL) was added to a J. Young style NMR tube. On the Schlenk line, the solution was degassed via three freeze-pump-thaw cycles and an atmosphere of $O_2$ was added to the headspace. The reaction was then monitored by $^1$H and $^{31}$P NMR spectroscopy. There was no observed reaction over the course of 24 hours.

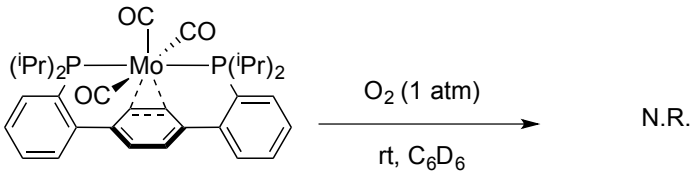


**3.2g**

**3.2g**: In the glove box, a solution of **3.2g** (0.0225 g, mmol) in $C_6D_6$ (0.6 mL) was added to a J. Young style NMR tube. On the Schlenk line, the solution was degassed via three freeze-pump-thaw cycles and an atmosphere of $O_2$ was added to the headspace. The reaction was then monitored by $^1H$ and $^{31}P$ NMR spectroscopy. There was no observed reaction over the course of 24 hours.

**Reactions with $O_2$**

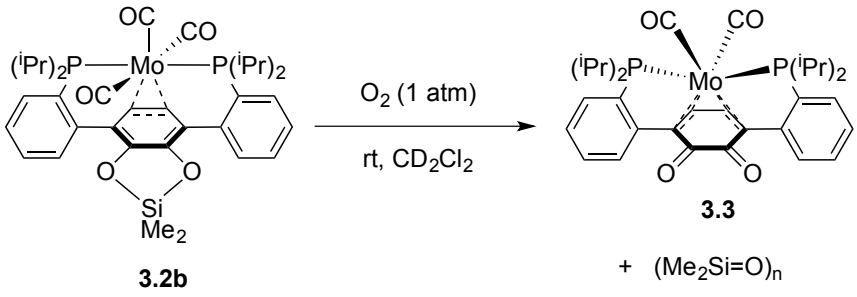


**3.2b** **3.3**

**3.2b**: A solution of **3.2b** (0.0232 g, 0.0317 mmol) in $CD_2Cl_2$ (0.6 mL) in a J. Young style NMR tube was degassed via three freeze-pump-thaw cycles. An atmosphere of $O_2$ was then added to the headspace, and the tube continuously inverted, monitoring the reaction over time by $^1H$ and $^{31}P$ NMR spectroscopy. After 1.5 hours at room temperature, the reaction exhibited a roughly 1:1:1 mixture of unconverted **3.2b**, product **3.3**, as well as an intermediate species identified as **3.2h** (confirmed by independent synthesis, *vida supra*). After 3 hours the reaction had gone to completion

with **3.2b** fully converted to **3.3** and a mixture of $Me_2Si$-containing products. An aliquant of the reaction mixture diluted in DCM was filtered through silica gel and submitted to gas chromatography-mass spectrometry (GC-MS) analysis, which revealed the $Me_2Si$-containing products to be cyclooligomers of dimethylsiloxane (i.e. $(Me_2SiO)_n$ where n = 3, 4, 5, 6).

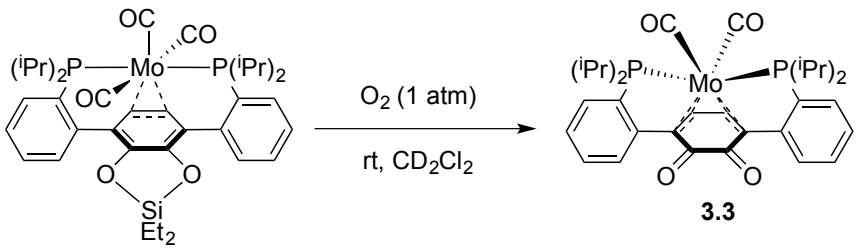


**3.2c** **3.3**

+ $(Et_2Si{=}O)_n$

**3.2c**: The above procedure was repeated with **3.2c** (0.0211 g, mmol) in $CD_2Cl_2$ (0.6 mL). After 8 hours at room temperature, **3.2c** had converted to a 1:1 mixture of **3.3** and **3.2i**. After 48 hours at room temperature, **3.2i** had fully converted to **3.3**.

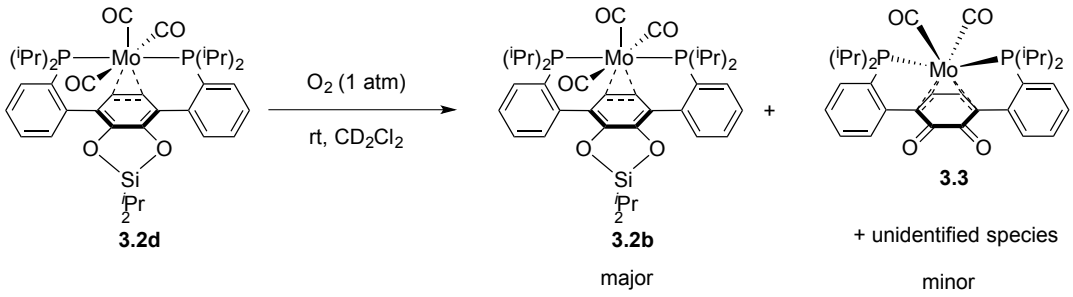


**3.2d**: The above procedure was repeated with **3.2d** (0.0241 g, mmol) in $CD_2Cl_2$ (0.6 mL) and monitored by $^{1}H$ and $^{31}P$ NMR spectroscopy. After 5 days at room temperature, **3.3** had formed in ca. 15% along with ca. 35% unidentified species.

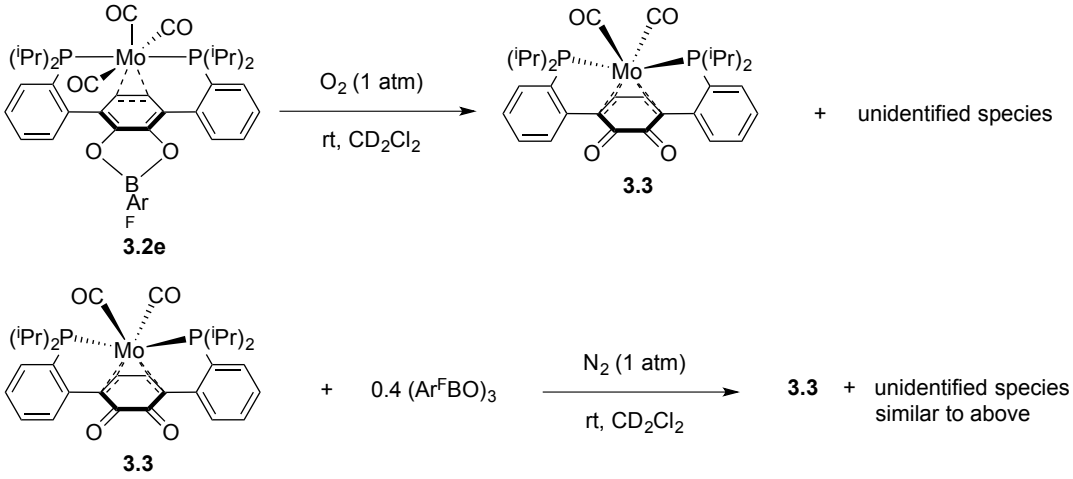


**3.2e**: The above procedure was repeated with **3.2e** (0.0201 g, 0.0243 mmol) in $CD_2Cl_2$ (0.6 mL) and monitored by $^{1}H$, $^{19}F$, and $^{31}P$ NMR spectroscopy. After 36 hours, **3.2e** had converted to a mixture of species comprised mainly of **3.3** (ca. 80% relative integration by $^{31}P$ NMR) and other unidentified products. Additionally, the $^{19}F$ NMR revealed two clusters of broad peaks grouped around -59.5 ppm and -61.5 ppm.

To better understand the unidentified mixture of species, a solution of **3.3** (0.0202 g, 0.0313 mmol) and $(Ar^FBO)_3$ (0.0063 g, 0.0122 mmol, independently synthesized, $Ar^F$ = *p*-$CF_3C_6H_4$)[31] in $CD_2Cl_2$ (0.6 mL) was monitored by $^1H$, $^{19}F$, and $^{31}P$ NMR spectroscopy. After one hour at room temperature, the mixture exhibited spectra that were qualitatively similar to the product of **3.2e** with $O_2$. Notably, by $^{31}P$ NMR spectroscopy, broad peaks were observed ca. 1.5 ppm upfield of **3.3**, with a relative ratio of 1:4 (unknown species : **3.3**), and by $^{19}F$ NMR, two sets of broad peaks were observed, grouped around -59.5 ppm and -61.5 ppm. Based on these results, it is plausible that in the reaction of **3.2e** with $O_2$ "$Ar^FB$=O" or some other reactive B-O species may be transiently generated (analogous to $Me_2Si$=O in reaction of **3.2b** with $O_2$), which could then react further by cyclization or oligomerization. The reaction of **3.3** with $(Ar^FBO)_3$ suggests that **3.3** may form a Lewis acid-base adduct with $(Ar^FBO)_3$, possibly prohibiting cyclization of "$Ar^FBO$" into the otherwise thermodynamic sink $(Ar^FBO)_3$ and instead favoring higher oligomers.

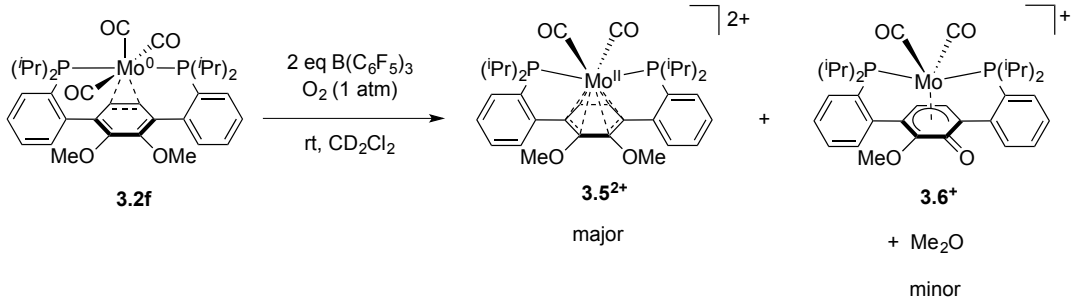


**3.2f** with $B(C_6F_5)_3$: A solution of **3.2f** (0.0210 g, 0.0299 mmol) and $B(C_6F_5)_3$ (0.0301 g, 0.0588 mmol) were combined in $CD_2Cl_2$ (0.6 mL) and added to a J. Young style NMR tube. The solution was degassed via three freeze-pump-thaw cycles and an atmosphere

of $O_2$ was added to the headspace. The reaction was followed by $^{1}H$, $^{19}F$, and $^{31}P$ NMR spectroscopy. After 30 minutes the color of the solution had changed from orange to dark brown to deep purple with no signals observable by $^{31}P$ NMR spectroscopy and only broad resonances observable by $^{1}H$ NMR spectroscopy. After ca. 2 hours a large number of purple crystals had formed in the tube suitable for x-ray diffraction. If unperturbed, over the course of another 4-5 hours the purple color faded to yield a pale yellow solution with non-crystalline yellow precipitate. $^{31}P$ and $^{1}H$ NMR spectroscopy revealed two new diamagnetic products, a major symmetric species assigned as **3.5**$^{2+}$ and a minor asymmetric species assigned as **3.6**$^{+}$. These assignments were confirmed by removal of the volatiles under vacuum and reconstituting the residue in $CD_3CN$ (0.6 mL) and comparing the NMR spectra to those of the independently synthesized [**3.5**$^{2+}$][OTf]$_2$ and [**3.6**$^{+}$][OTf].

The above reaction with $O_2$ was repeated with **3.2f** (0.0221g, 0.0315 mmol) and $B(C_6F_5)_3$ (0.0332 g, 0.0648 mmol) in $CD_2Cl_2$ (0.6 mL). After approximately 24 hours, the volatiles were vacuum transferred to a second J. Young style NMR tube and the formation of $Me_2O$ was confirmed ($\delta$ = 3.27 ppm)[32] in addition to small amounts of MeOH and $H_2O$. The solution was then submitted to GC-MS and the $Me_2O$ eluted at 1.45 min with two major peaks at 45.1 and 46.1 m/z.

The reaction was repeated as above with **3.2f** (0.0197 g, 0.0280 mmol) and $B(C_6F_5)_3$ (0.0302 g, 0.0590) in $CD_2Cl_2$ (0.6 mL). Instead of natural abundance $O_2$, 98% $^{18}O_2$. After 3 days, the volatiles were vacuum transferred to a second J. Young style NMR tube and

the formation of $Me_2O$ confirmed. The solution was submitted to GC-MS, and the $Me_2O$ observed at 1.45 min with major peaks at 47.1 and 48.2 m/z consistent with $Me_2{}^{18}O$, as well as minor peaks at 45.1 and 46.1 m/z consistent with $Me_2{}^{16}O$. Relative ratio of $^{18}O/^{16}O$ estimated at 3:1.

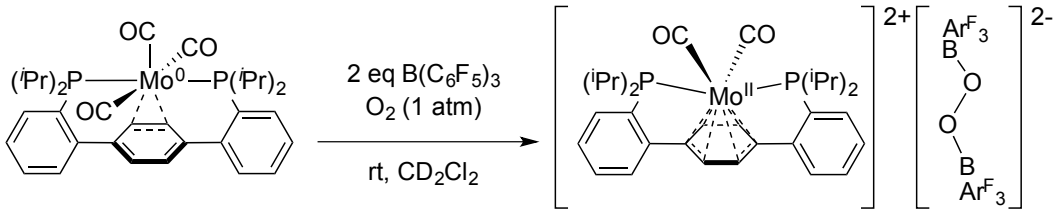


**3.2g** [P2Mo(CO)2 2+][{(F5C6)3B}2O2 2-]

**3.2g** with $B(C_6F_5)_3$: A solution of **3.2g** (0.0186 g, 0.0289 mmol) and $B(C_6F_5)_3$ (0.0329 g, 0.0643 mmol) were combined in $CD_2Cl_2$ (0.6 mL) and added to a J. Young style NMR tube. The solution was degassed via three freeze-pump-thaw cycles and an atmosphere of $O_2$ was added to the headspace. The reaction was followed by $^1H$, $^{19}F$, and $^{31}P$ NMR spectroscopy. After 45 minutes the color of the solution had changed from orange to dark brown to purple with loss of signal by $^{31}P$ NMR spectroscopy and broadening of resonances by $^1H$ NMR spectroscopy. By $^{19}F$ NMR spectroscopy, generation of $[((F_5C_6)_3B)_2O_2{}^{2-}]$ can be observed. After 36 hours at room temperature, $^{31}P$ and $^1H$ NMR spectroscopy reveal formation of $[P_2Mo(CO)_2]^{2+}$.

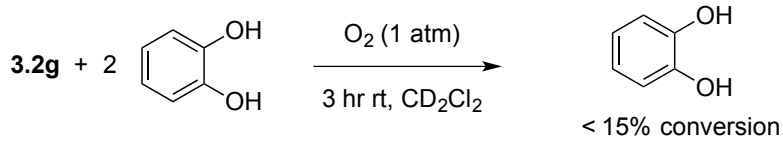


**3.2g** with catechol: A solution of **3.2g** (0.0203 g, 0.0315 mmol) and catechol (0.0073 g, 0.0663 mmol) in $CD_2Cl_2$ (0.6 mL) in a J. Young style NMR tube was degassed via three freeze-pump-thaw cycles. An atmosphere of $O_2$ was then added to the headspace, and the tube continuously inverted, monitoring the reaction over time by $^1H$ and $^{31}P$ NMR spectroscopy. Conversion of catechol was determined via $^1H$ NMR integration using the residual PhMe from synthesis of **3.2g** as internal standard.

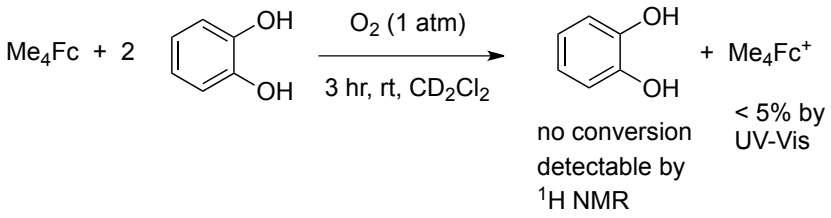


$Me_4Fc$ with catechol: A solution of $Me_4Fc$ (0.0106 g, 0.0438 mmol) and catechol (0.0107 g, 0.0972 mmol) with diglyme (0.0022g, 0.0164 mmol) used as internal standard in $CD_2Cl_2$ (0.6 mL) in a J. Young style NMR tube was degassed via three freeze-pump-thaw cycles. An atmosphere of $O_2$ was then added to the headspace, and the tube continuously inverted, monitoring the reaction over time by $^1H$ and $^{31}P$ NMR spectroscopy. After 3 hours, the volatiles were removed under vacuum. The residue was diluted in THF (3 mL), and an aliquot (0.15 mL) was then further diluted with additional THF (2.85 mL, total volume 3.0 mL). Quantification of $Me_4Fc$ oxidation was determined by UV-vis analysis of this diluted solution and comparison to a similarly

diluted solution of $Me_4Fc$ (0.0106 g, 0.0438 mmol) after oxidation with Ag(OTf) (0.0118 g, 0.0459 mmol) and filtering to remove the $Ag^0$ precipitates.

**Reactions with $H_2O_2$**

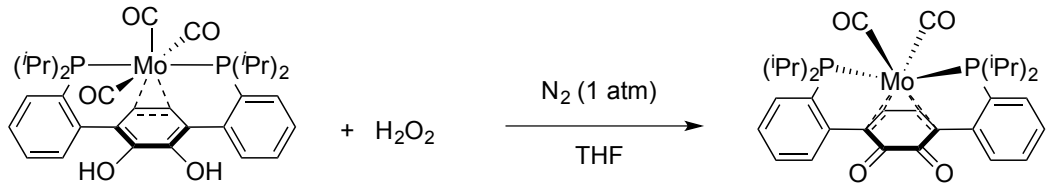


**3.2a** **3.3**

**3.2a**: In a water-tolerant glove box under an $N_2$ atmosphere, **3.2a** (0.0213 g, 0.0316 mmol) in THF (2 mL) was stirred in a 20 mL vial. An aqueous solution of $H_2O_2$ (3.3 M, 12 μL, 0.0396 mmol) was added to the solution and the mixture stirred for 1 hour at room temperature. The volatiles were then removed under reduced pressure, and the residue was taken up in $CD_2Cl_2$ (0.6 mL) to reveal quantitative conversion from **3.2a** to **3.3**.

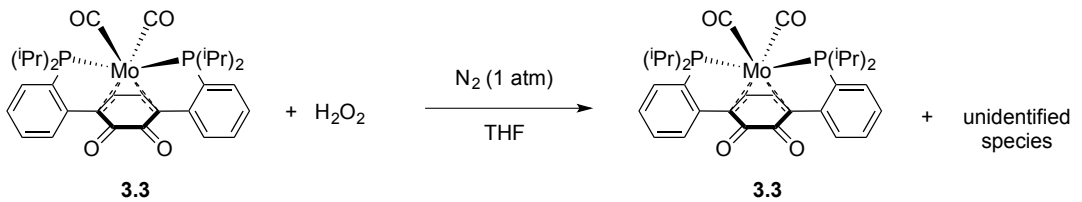


**3.3** **3.3**

major minor

**3.3**: As above, to a stirred solution of **3.3** (0.0198 g, 0.0307 mmol) and 1,3,5-trimethoxybenzene (0.0039 g, 0.0315 mmol) in THF (2 mL) in a 20 mL vial was added

an aqueous solution of $H_2O_2$ (3.3 M, 12 μL, 0.0396 mmol). The mixture was stirred for 1 hour at room temperature. The volatiles were then removed under reduced pressure, and the residue was taken up in $CD_2Cl_2$ (0.6 mL) to reveal approximately 80% of **3.3** remained, along with approximately 20% conversion to unidentified species by $^1H$ (relative integration of central arene C-H to internal standard trimethoxybenzene aryl C-H) and $^{31}P$ (relative integration of peak at 71 ppm corresponding to **3.3** to group of signals at ca. 58 ppm corresponding to unidentified species) NMR spectroscopy.

**Quantification of $O_2$ consumed and CO released in conversion of 3.2a to 3.3**

In a Schlenk flask charged with a stir bar, 0.0504 g (0.0747 mmol) of **3.2a** was dissolved in $CHCl_3$ (12 mL). The solution was degassed by three freeze-pump-thaw cycles. The reaction vessel was then exposed to 5.01 eq of $O_2$ (0.377 mmol) via calibrated gas bulb and stirred *vigorously* for 5 hours at room temperature. After 5 hours the solution was frozen and the gas in the Schlenk flask was pumped through a liquid nitrogen cooled trap and collected in a calibrated volume (31.2 mL) using a Toepler pump. After 20 minutes (ca. 25 cycles of the Toepler pump) the Schlenk flask was sealed and thawed. Upon thawing the solution was re-frozen and the aforementioned Toepler pump process was repeated. After three of the described freeze-Toepler pump-thaw cycles, the pressure of gas collected was found to be 246.6 mm Hg (0.414 mmol, 5.51 eq after confirming quantitative conversion of **3.2a** to **3.3** by $^1H$ and $^{31}P$ NMR spectroscopy). The gas was then exposed to a degassed solution of NaOH (0.75 g, 18.8 mmol) and pyrogallol (0.5 g, 3.96 mmol) in $H_2O$ (20 mL) in a second Schlenk flask, and the

solution was stirred *vigorously* for 4 hours to consume the excess $O_2$. After 4 hours, the aqueous solution was frozen and the gas in the Schlenk flask was pumped through a liquid nitrogen cooled trap and collected in a calibrated bulb (31.2 mL) using three of the aforementioned freeze-Toepler pump-thaw cycles and the pressure of gas measured. Using the Toepler pump, the gas was then pumped through a CuO filled tube. The tube was heated and kept between 300 and 350 °C. After 1 hour of pumping the gas through the CuO tube, the pressure of gas was again measured. By subtracting the two measurements, the total pressure of gas consumed in the CuO tube was found to be 47.5 mm Hg (0.0797 mmol, 1.06 eq). Performing the experiment described above in triplicate, it was found that reaction of **3.3** with approximately 5 equivalents of $O_2$ generated 0.048 ± 0.02 equivalents of gas, and the amount of non-$O_2$ gas consumed in the CuO tube was found to be 1.05 ± 0.05. This data is consistent with a stoichiometry of **3.2a** consuming 0.5 equivalents of $O_2$ and releasing 1 equivalent of CO.

To further support this stoichiometry and confirm the identity of the gas being released in the reaction as CO, the Toepler pump experiment was repeated as mentioned above using 0.0492 g (0.0729 mmol) of **3.2a** with the following modification: after consuming the excess $O_2$ in the NaOH/pyrogallol solution (rather than burning the gas in the CuO tube) the remaining gas was exposed to a solution of $HN(pic)_2$ (0.0524 g, 0.263 mmol) and $Cu(MeCN)_4OTf$ (0.0954 g, 0.253 mmol) in MeCN (12 mL) and the mixture stirred *vigorously* for 4 hours. After 4 hours the gas remaining was measured, and the total gas consumed by the $Cu^I$ solution was found to be 0.98 eq. IR data of the resulting $Cu^I$ solution revealed a band at 2091 $cm^{-1}$ consistent with formation of the previously

reported $HNpic_2Cu(CO)BArF_{20}$,[33] and identical to the band observed by independently exposing a mixture of $Cu(MeCN)_4OTf$ and $HN(pic)_2$ to excess CO in MeCN.

**Ultraviolet-Visible Spectroscopy**

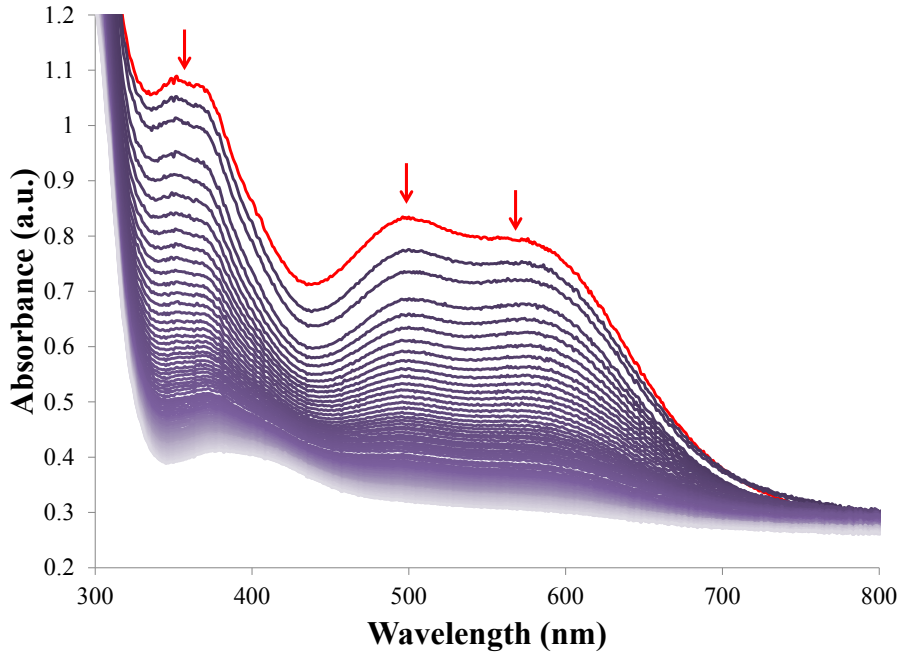


**Figure 3.5.** Reaction of **3.2e** with 2 AgOTf in THF. The red trace represents the first data point after mixing. New band with $\lambda_{max}$ = 575 nm assigned to intermediate [**3.4**$^+$][OTf]. Traces taken every 30 seconds. After 20 minutes all of the major bands have diminished, consistent with formation of [**3.5**$^{2+}$][OTf]$_2$. (Note: traces shifted up ca. 0.3 a.u. with respect to baseline due to formation of $Ag^0$ precipitate).

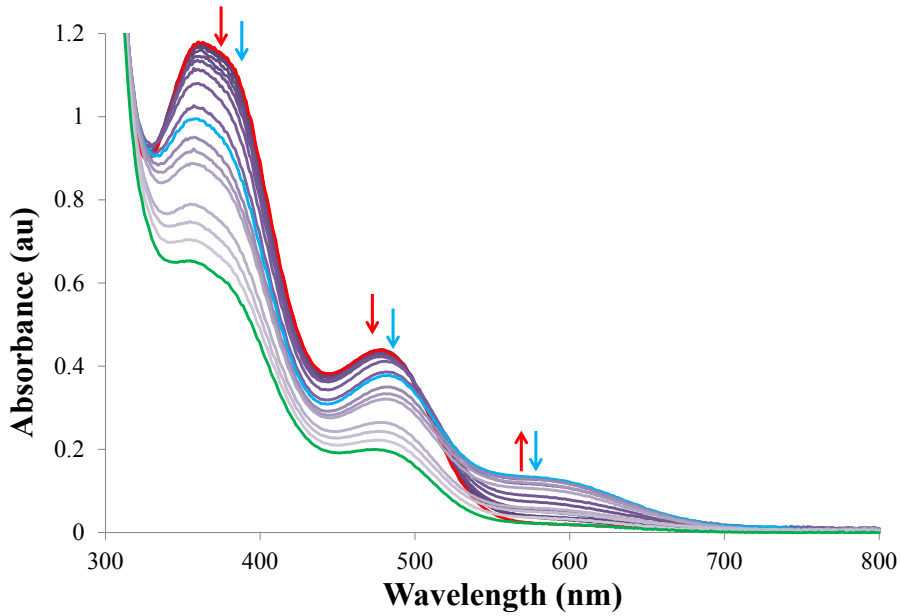


**Figure 3.6.** Reaction of **3.2e** and $B(C_6F_5)_3$ with $O_2$ in DCM. The red trace represents the first data point 30 seconds after mixing. Over time (red arrow), a new band with $\lambda_{max}$ = 575 nm assigned to $[\mathbf{3.4}^+]_2[\{(F_5C_6)_3B\}_2O_2^{2-}]_2$ increases to a maximum at approximately 60 minutes (blue trace), and diminishes again (blue arrow) over the course of another 600 minutes (green trace). Over the course of the reaction, the bands with $\lambda_{max}$ = 390 nm and 480 nm corresponding to **3.2e** have been halved, consistent with a **3.2e**:$B(C_6F_5)_3$ stoichiometry of 1:2. (Note: time between traces varies)

**Cyclic Voltammetry**

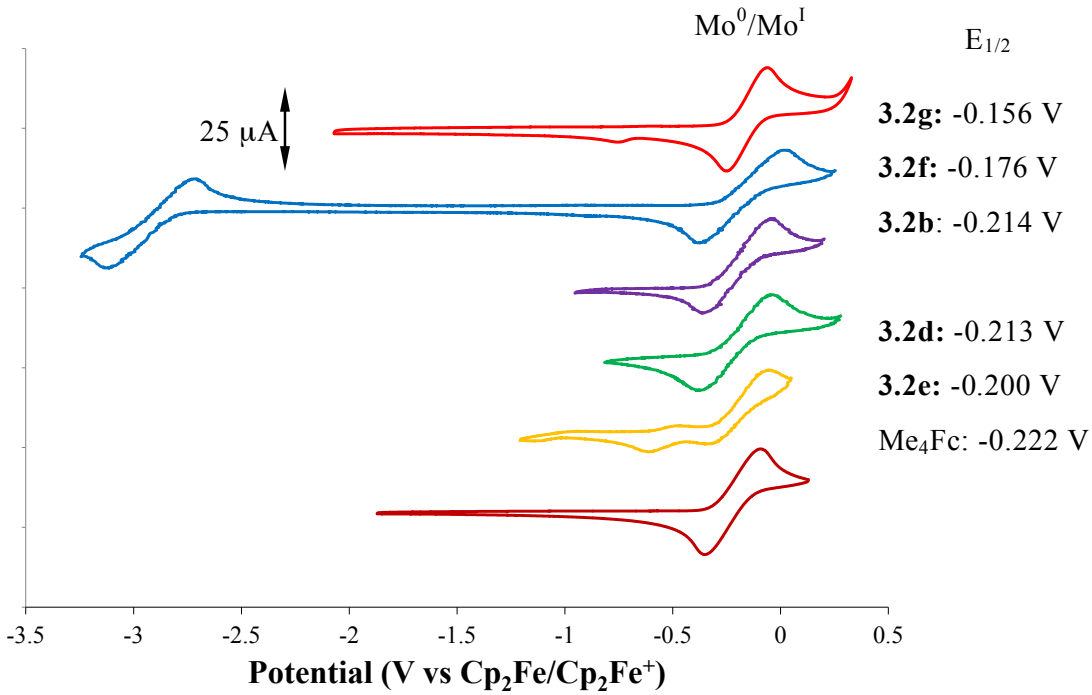


**Figure 3.7.** Cyclic voltammograms of compounds **3.2b**, **3.2d**, **3.2e**, **3.2f** , **3.2g**, and $Me_4Fc$ taken in 0.1 M [$^n$Bu$_4$N$^+$][$PF_6^-$] in THF with a glassy carbon working electrode at 250 mV/s. Potentials reported with respect to the $Cp_2Fe/Cp_2Fe^+$ couple.

## Crystallographic Information

CCDC 1026539-1026542 contain the supplementary crystallographic data for this paper. These data can be obtained free of charge from The Cambridge Crystallographic Data Centre via www.ccdc.cam.ac.uk/data_request/cif.

## Refinement Details

In each case, crystals were mounted on a glass fiber or nylon loop using Paratone oil, then placed on the diffractometer under a nitrogen stream. Low temperature (100 K) X-ray data were obtained on a Bruker APEXII CCD based diffractometer (Mo sealed X-ray tube, $K_\alpha$ = 0.71073 Å) or a Bruker PHOTON100 CMOS based diffractometer (Mo micro-focus sealed X-ray tube, $K_\alpha$ = 0.71073 Å). All diffractometer manipulations, including data collection, integration, and scaling were carried out using the Bruker APEXII software.[34] Absorption corrections were applied using SADABS.[35] Space groups were determined on the basis of systematic absences and intensity statistics and the structures were solved by direct methods using XS[36], by intrinsic phasing using XT (incorporated into SHELXTL), or by charge flipping using Olex2[37] and refined by full-matrix least squares on $F^2$. All non-hydrogen atoms were refined using anisotropic displacement parameters. Hydrogen atoms were placed in the idealized positions and refined using a riding model. The structure was refined (weighed least squares refinement on $F^2$) to convergence. Graphical representation of structures with 50% probability thermal ellipsoids was generated using Diamond visualization software.[38]

**Table 3.1.** Crystal and refinement data for complexes **3.2a**•2.25$C_6H_6$ and **3.2b**•NCMe.

| | **3.2a**•2.25$C_6H_6$ | **3.2b**•NCMe |
|---|---|---|
| CCDC Number | 1026539 | 1026540 |
| Empirical formula | $C_{93}H_{107}Mo_2O_{10}P_4$ | $C_{37}H_{47}MoNO_5P_2Si$ |
| Formula weight | 1700.55 | 771.73 |
| T (K) | 100 | 100 |
| *a*, Å | 11.9691(7) | 11.4020(4) |
| *b*, Å | 16.935(1) | 17.1733(7) |
| *c*, Å | 22.841(1) | 19.0484(7) |
| α, deg | 106.621(3) | 90 |
| β, deg | 91.522(3) | 102.399(1) |
| γ, deg | 109.707(3) | 90 |
| Volume, Å$^3$ | 4137.5(4) | 3642.9(2) |
| Z | 2 | 4 |
| Crystal system | Triclinic | Monoclinic |
| Space group | P-1 | $P2_1/c$ |
| $d_{calc}$, g/cm$^3$ | 1.365 | 1.407 |
| θ range, deg | 1.84-30.00 | 2.18-33.14 |
| $\mu$, mm$^{-1}$ | 0.440 | 0.523 |
| Abs. Correction | Semi-empirical | Semi-empirical |
| GOF | 1.633 | 0.990 |
| $R_1$,[a] $wR_2$ [b] [I>2 σ(I)] | 0.0506, 0.2015 | 0.0486, 0.1523 |

[a] $R_1 = \sum||F_o| - |F_c||/\sum|F_o|$. [b] $wR_2 = [\sum[w(F_o^2-F_c^2)^2]/\sum[w(F_o^2)^2]]^{1/2}$.

**Table 3.2.** Crystal and refinement data for complexes **3.3** and $[\mathbf{3.4}^+]_2[[(F_5C_6)_3B]_2O_2^{2-}]\bullet 2CH_2Cl_2$.

| | **3.3** | $[\mathbf{3.4}^+]_2[[(F_5C_6)_3B]_2O_2^{2-}]\bullet 2CH_2Cl_2$ |
|---|---|---|
| CCDC Number | 1026541 | 1026542 |
| Empirical formula | $C_{32}H_{38}MoO_4P_2$ | $C_{108}H_{92}B_2Cl_4F_{30}Mo_2O_{12}P_4$ |
| Formula weight | 644.50 g/mol | 2631.00 g/mol |
| T (K) | 100 | 100 |
| *a*, Å | 11.6649(8) | 12.511(1) |
| *b*, Å | 16.1870(8) | 15.145(1) |
| *c*, Å | 16.4201(8) | 15.613(1) |
| α, deg | 90 | 64.704(3) |
| β, deg | 108.193(3) | 81.599(3) |
| γ, deg | 90 | 85.342(3) |
| Volume, Å$^3$ | 2945.4(3) | 2645.5(4) |
| Z | 4 | 1 |
| Crystal system | Monoclinic | Triclinic |
| Space group | $P2_1/c$ | P-1 |
| $d_{calc}$, g/cm$^3$ | 1.453 | 1.651 |
| θ range, deg | 2.27-37.78 | 1.45-27.48 |
| $\mu$, mm$^{-1}$ | 0.590 | 0.514 |
| Abs. Correction | Semi-empirical | Semi-empirical |
| GOF | 0.830 | 0.901 |
| $R_1$,[a] $wR_2$ [b] [I>2 σ(I)] | 0.0356, 0.1189 | 0.0576, 0.1453 |

[a] $R_1 = \sum||F_o| - |F_c||/\sum|F_o|$. [b] $wR_2 = [\sum[w(F_o^2-F_c^2)^2]/\sum[w(F_o^2)^2]]^{1/2}$.

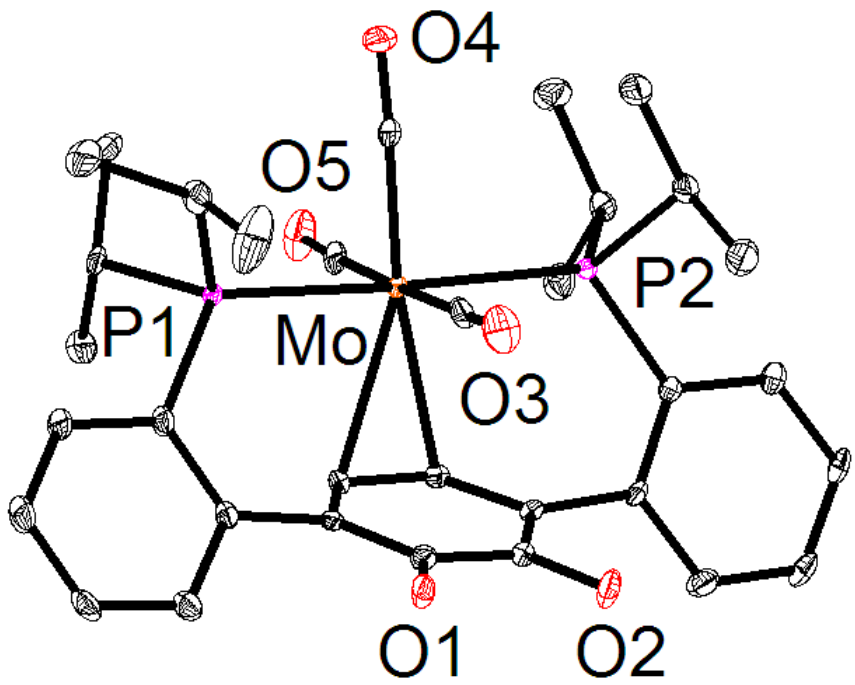


**Figure 3.8.** Structural drawing of **3.2a** with 50% probability ellipsoids. Hydrogen atoms and solvent molecules are omitted for clarity. Carbon atoms are shown in black.

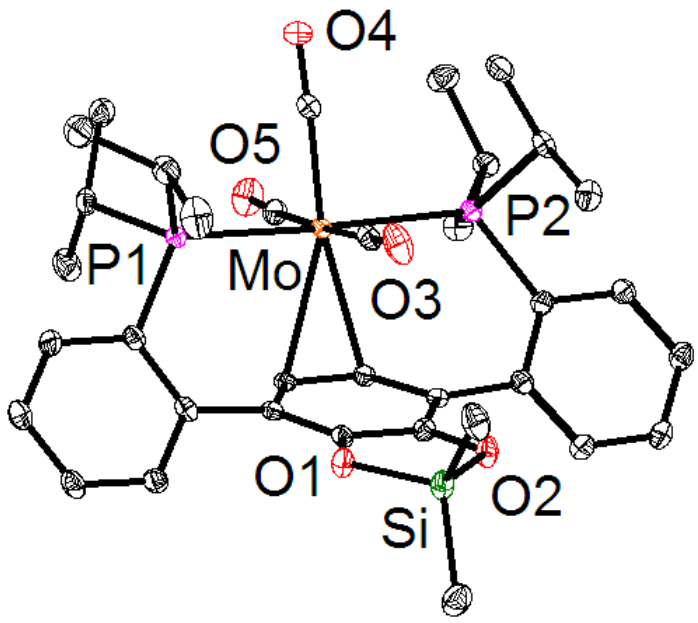


**Figure 3.9.** Structural drawing of **3.2b** with 50% probability ellipsoids. Hydrogen atoms and solvent molecules are omitted for clarity. Carbon atoms are shown in black.

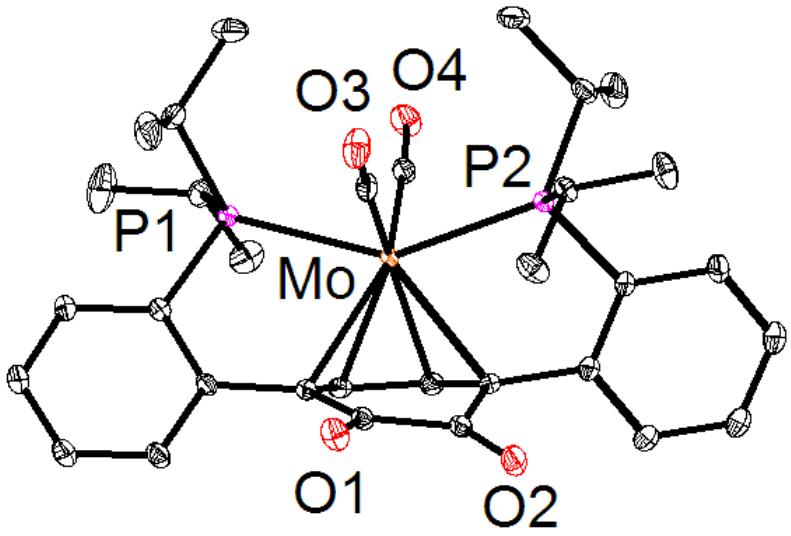


**Figure 3.10.** Structural drawing of **3.3** with 50% probability ellipsoids. Hydrogen atoms and solvent molecules are omitted for clarity. Carbon atoms are shown in black.

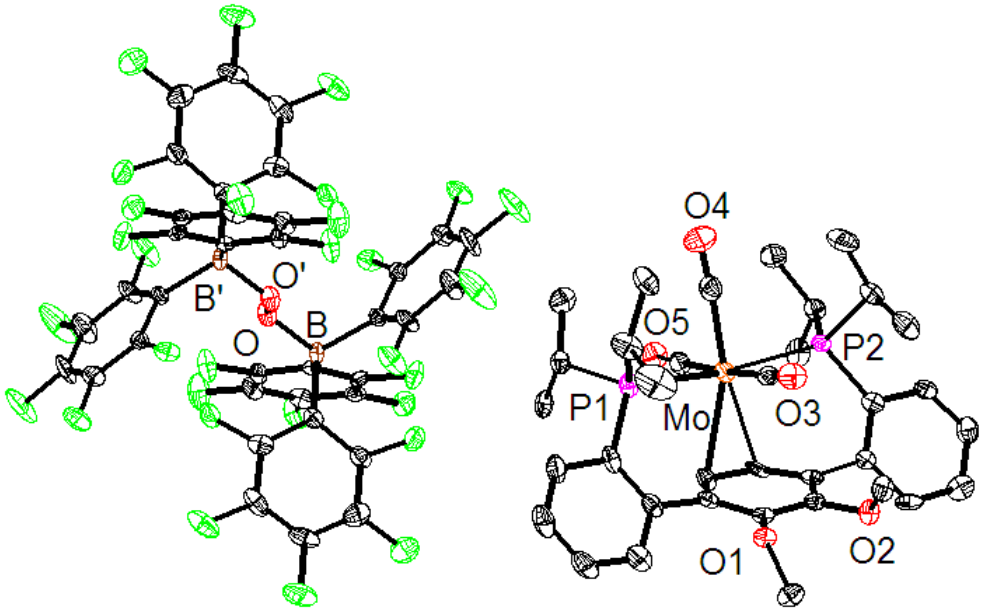


**Figure 3.11.** Structural drawing of $[\mathbf{3.4}^{+}]_2[[(F_5C_6)_3B]_2O_2^{2-}]$ with 50% probability ellipsoids. Hydrogen atoms, solvent molecules, and second Mo compound are omitted for clarity. Carbon and fluorine atoms are shown in black and green, respectively.

**Special Refinement Details for $\mathbf{3.4}^{+}$:** A ligand isopropyl group and the DCM solvent molecule were positionally disordered. Both were satisfactorily modeled as approximately 50:50 mixtures using "PART" cards in SHELX

## REFERENCES


[1] a) M. Costas, M. P. Mehn, M. P. Jensen, L. Que, *Chem. Rev.* **2004**, *104*, 939-986; b) J. W. Whittaker, *Chem. Rev.* **2003**, *103*, 2347-2364; c) M. Sono, M. P. Roach, E. D. Coulter, J. H. Dawson, *Chem. Rev.* **1996**, *96*, 2841-2888.

[2] a) O. R. Luca, R. H. Crabtree, *Chem. Soc. Rev.* **2013**, *42*, 1440-1459; b) V. Lyaskovskyy, B. de Bruin, *ACS Cat.* **2012**, *2*, 270-279; c) V. K. K. Praneeth, M. R. Ringenberg, T. R. Ward, *Angew. Chem., Int. Ed.* **2012**, *51*, 10228-10234; d) R. Eisenberg, H. B. Gray, *Inorg. Chem.* **2011**, *50*, 9741-9751; e) P. J. Chirik, K. Wieghardt, *Science* **2010**, *327*, 794-795; f) M. R. Haneline, A. F. Heyduk, *J. Am. Chem. Soc.* **2006**, *128*, 8410-8411; g) C. G. Pierpont, *Coord. Chem. Rev.* **2001**, *216–217*, 99-125.

[3] a) K. Umehara, S. Kuwata, T. Ikariya, *J. Am. Chem. Soc.* **2013**, *135*, 6754-6757; b) C. T. Carver, B. D. Matson, J. M. Mayer, *J. Am. Chem. Soc.* **2012**, *134*, 5444-5447; c) J. F. Hull, Y. Himeda, W.-H. Wang, B. Hashiguchi, R. Periana, D. J. Szalda, J. T. Muckerman, E. Fujita, *Nat. Chem.* **2012**, *4*, 383-388; d) C. Costentin, S. Drouet, M. Robert, J.-M. Savéant, *Science* **2012**, *338*, 90-94; e) C. Gunanathan, D. Milstein, *Acc. Chem. Res.* **2011**, *44*, 588-602; f) M. Rakowski DuBois, D. L. DuBois, *Chem. Soc. Rev.* **2009**, *38*, 62-72; g) S. W. Kohl, L. Weiner, L. Schwartsburd, L. Konstantinovski, L. J. W. Shimon, Y. Ben-David, M. A. Iron, D. Milstein, *Science* **2009**, *324*, 74-77.

[4] a) J. J. Warren, T. A. Tronic, J. M. Mayer, *Chemical Reviews* **2010**, *110*, 6961-7001; b) B. W. Purse, L.-H. Tran, J. Piera, B. Åkermark, J.-E. Bäckvall, *Chem. Eur. J.* **2008**, *14*, 7500-7503; c) C. J. Chang, L. L. Chng, D. G. Nocera, *J. Am. Chem. Soc.* **2003**, *125*, 1866-1876; d) P. Chaudhuri, M. Hess, J. Müller, K. Hildenbrand, E. Bill, T. Weyhermüller, K. Wieghardt, *J. Am. Chem. Soc.* **1999**, *121*, 9599-9610; e) J. P. Collman, N. K. Devaraj, R. A. Decréau, Y. Yang, Y.-L. Yan, W. Ebina, T. A. Eberspacher, C. E. D. Chidsey, *Science* **2007**, *315*, 1565-1568.

[5] a) S. B. Kim, R. D. Pike, D. A. Sweigart, *Acc. Chem. Res.* **2013**, *46*, 2485-2497; b) J. A. Reingold, S. Uk Son, S. Bok Kim, C. A. Dullaghan, M. Oh, P. C. Frake, G. B. Carpenter, D. A. Sweigart, *Dalton Trans.* **2006**, 2385-2398.

[6] S. U. Son, S. B. Kim, J. A. Reingold, G. B. Carpenter, D. A. Sweigart, *J. Am. Chem. Soc.* **2005**, *127*, 12238-12239.

[7] a) K. T. Horak, A. Velian, M. W. Day, T. Agapie, *Chem. Comm.* **2014**, *50*, 4427-4429; b) D. E. Herbert, N. C. Lara, T. Agapie, *Chem. Eur. J.* **2013**, *19*, 16453-16460; c) S. Suseno, T. Agapie, *Organometallics* **2013**, *32*, 3161-3164; d) P. Kelley, S. Lin, G. Edouard, M. W. Day, T. Agapie, *J. Am. Chem. Soc.* **2012**, *134*, 5480-5483; e) A. Velian, S. Lin, A. J. M. Miller, M. W. Day, T. Agapie, *J. Am. Chem. Soc.* **2010**, *132*, 6296-6297.

[8] S. Lin, M. W. Day, T. Agapie, *J. Am. Chem. Soc.* **2011**, *133*, 3828-3831.

[9] J. A. Buss, G. A. Edouard, C. Cheng, J. Shi, T. Agapie, *J. Am. Chem. Soc.* **2014**, *136*, 11272-11275.

[10] a) C. A. Lippert, S. A. Arnstein, C. D. Sherrill, J. D. Soper, *J. Am. Chem. Soc.* **2010**, *132*, 3879-3892; b) A. M. Morris, C. G. Pierpont, R. G. Finke, *J. Mol. Cat. A: Chem.* **2009**, *309*, 137-145; c) F. H. Vaillancourt, J. T. Bolin, L. D. Eltis, *Crit. Rev. Biochem. Mol. Biol.* **2006**, *41*, 241-267; d) C.-X. Yin, R. G. Finke, *J. Am. Chem. Soc.* **2005**, *127*, 9003-9013.

[11] a) A. H. Randolph, N. J. Seewald, K. Rickert, Brown, N. Seth, *Inorg. Chem.* **2013**, *52*, 12587-12598; b) C. G. P. a. E. Nordlander, in *Molybdenum: Its Biological and*

*Coordination Chemistry* (Ed.: A. Holder), Nova Science Publishers, New York, **2012**, pp. 161-174.
[12] J. L. Campos, W. F. De Giovani, J. R. Romero, *Synthesis* **1990**, *1990*, 597-599.
[13] R. M. Kretzer, R. A. Ghiladi, E. L. Lebeau, H.-C. Liang, K. D. Karlin, *Inorg. Chem.* **2003**, *42*, 3016-3025.
[14] a) R. Keyrouz, V. Jouikov, *New J. Chem.* **2003**, *27*, 902-904; b) D. S. Fattakhova, V. V. Jouikov, M. G. Voronkov, *J. Organomet. Chem.* **2000**, *613*, 170-176.
[15] a) G. Hussman, W. D. Wulff, T. J. Barton, *J. Am. Chem. Soc.* **1983**, *105*, 1263-1269; b) M. G. Voronkov, S. V. Basenko, *J. Organomet. Chem.* **1995**, *500*, 325-329.
[16] C. J. Harlan, T. Hascall, E. Fujita, J. R. Norton, *J. Am. Chem. Soc.* **1999**, *121*, 7274-7275.
[17] J. T. Henthorn, T. Agapie, *Angew. Chem., Int. Ed.* **2014**, *53*, 12893-12896.
[18] a) A. J. M. Miller, W. Kaminsky, K. I. Goldberg, *Organometallics* **2014**, *33*, 1245-1252; b) H. Amouri, J. Vaissermann, M. N. Rager, Y. Besace, *Inorg. Chem.* **1999**, *38*, 1211-1215.
[19] A. Falceto, E. Carmona, S. Alvarez, *Organometallics* **2014**.
[20] W. E. Geiger, *Coord. Chem. Rev.* **2013**, *257*, 1459-1471.
[21] a) N. J. Stone, D. A. Sweigart, A. M. Bond, *Organometallics* **1986**, *5*, 2553-2555; b) C. G. Zoski, D. A. Sweigart, N. J. Stone, P. H. Rieger, E. Mocellin, T. F. Mann, D. R. Mann, D. K. Gosser, M. M. Doeff, A. M. Bond, *J. Am. Chem. Soc.* **1988**, *110*, 2109-2116.
[22] D. L. Maricle, W. G. Hodgson, *Anal. Chem.* **1965**, *37*, 1562-1565.
[23] a) S. Fukuzumi, K. Ohkubo, *Coord. Chem. Rev.* **2010**, *254*, 372-385; b) S. Fukuzumi, Y. Morimoto, H. Kotani, P. Naumov, Y.-M. Lee, W. Nam, *Nat. Chem.* **2010**, *2*, 756-759; c) Y. Morimoto, H. Kotani, J. Park, Y.-M. Lee, W. Nam, S. Fukuzumi, *J. Am. Chem. Soc.* **2010**, *133*, 403-405; d) K. T. Tarantino, P. Liu, R. R. Knowles, *J. Am. Chem. Soc.* **2013**, *135*, 10022-10025.
[24] D. Zheng, Q. Wang, H.-S. Lee, X.-Q. Yang, D. Qu, *Chem. Eur. J.* **2013**, *19*, 8679-8683.
[25] A. Wu, E. R. Biehl, P. C. Reeves, *J. Chem. Soc., Perkin Trans. 2* **1972**, 449-451.
[26] T. Nishimi, T. Kamachi, K. Kato, T. Kato, K. Yoshizawa, *Eur. J. Org. Chem.* **2011**, *2011*, 4113-4120.

[27] Pangborn, A.B.; Giardell, M.A.; Grubbs, R.H.; Rosen, R.K.; Timmers, F.J. *Organometallics*, **1996**, *15*, 1518.
[28] Ikeda, C.; Sakamoto, N.; Nabeshima, T. *Org. Lett.* **2008**, *10*, 4601-4604.
[29] Albrecht, M.; Schneider, M. *Synthesis*, **2000**, *11*, 1557-1560.
[30] Berliner, M.A.; Belecki, K. *J. Org. Chem.*, **2005**, *70*, 9618-9621.
[31] Hayashi, T.; Senda, T.; Takaya, Y.; Ogasawara, M. *J. Am. Chem. Soc.*, **1999**, *121*, 11591-11592.
[32] Leszcynska, K.; Mix, A.; Berger, R.J.F.; Rummel, B.; Neumann, B.; Stammler H-G.; Jutzi, P. *Angew. Chem., Int. Ed.* **2011**, *50*, 6843-6846.
[33] Kretzer, R.M.; Ghiladi, R.A.; Lebeau, E.L.; Liang, H.-C.; Karlin, K.D. *Inorg. Chem.*, **2003**, *42*, 3016-3025.
[34] APEX2, Version 2 User Manual, M86-E01078, Bruker Analytical X-ray Systems, Madison, WI, June 2006.
[35] Sheldrick, G.M. "SADABS (version 2008/1): Program for Absorption

Correction for Data from Area Detector Frames", University of Göttingen, 2008.
[36] Sheldrick, G.M. (2008). Acta Cryst. A64, 112-122.
[37] Dolomanov, O.V. (2009). OLEX2. J. Appl. Cryst. **42**, 339-341.
[38] Brandenburg, K. (1999). DIAMOND. Crystal Impact GbR, Bonn, Germany.

# CHAPTER 4

PROTON-COUPLED ELECTRON TRANSFER

## Modulation of Proton-Coupled Electron Transfer Through Molybdenum-quinonoid Interactions

Published in part as:

*Inorg. Chem.* **2016**, *55*, 5337−5442

**ABSTRACT**

A series of π-bound molybdenum quinonoid complexes supported by pendant phosphines has been synthesized. These compounds formally span three protonation-oxidation states of the quinonoid fragment (catechol, semiquinone, quinone) and two different oxidation states of the metal ($Mo^0$, $Mo^{II}$), notably demonstrating a total of two protons and four electrons accessible in the system. Transfer of multiple equivalents of protons and electrons from the $Mo^0$ and $Mo^{II}$ catechol complexes, **4.1** and **4.2**, to H-atom acceptors azobenzene and TEMPO suggest the presence of weak O–H bonds. Thermochemical analysis reveals bond dissociation free energies (BDFEs) for the first O–H of 72.6 kcal/mol in the $Mo^0$ complex **4.1** and 66.3 kcal/mol in the $Mo^{II}$ complex **4.2**, compared to 76.4 kcal/mol for a metal-free catechol **4.8**, demonstrating that proton-coupled electron transfer can be facilitated significantly by the π-bound metal center.

## INTRODUCTION

Proton-coupled electron transfer (PCET) reactions encompass some of the most complex and challenging transformations in synthetic chemistry, including multi-proton multi-electron processes such as $O_2$ reduction.[1] In biology, tyrosine[2] and quinone[3] moieties have been implicated in multi-electron processes, and as such the PCET of phenols[4] and hydroquinones[5] have been extensively studied in water, and to a lesser extent in non-aqueous solvents. Interest in the effects of non-covalent interactions such as hydrogen bonding[6] and cation-π interactions[7] on structure and reactivity has grown over the last few decades with wide-ranging applications across many disciplines of chemistry. Hydrogen bonding has been shown to modulate the PCET of simple phenolic small molecule systems,[8] while cation-π interactions (specifically π-bound transition metals) have been shown to facilitate activation of C–H[9] and C–heteroatom[10] bonds in aromatic systems. Though π-bound transition metal quinonoid complexes have previously been reported, their study has largely focused on incorporation into metal-organometallic frameworks[11] and thus their potential for PCET chemistry remains underexplored.

Transition metal complexes with pendant acid/base moieties have been demonstrated to facilitate small molecule reactivity through cooperative metal-ligand proton transfer,[12] and redox-noninnocent ligands supporting transition metals have been shown to facilitate storage of multiple redox equivalents;[13] however systems involving a single metal that can access multiple equivalents of protons and electrons are quite rare.[14] π-bound transition metal quinonoid complexes have the potential to access two protons and two electrons from the quinonoid moiety, as well as any electrons

accessible through redox states at the metal center. Not only could these systems be envisioned to facilitate multi-proton, multi-electron transformations, but also changes in the oxidation state at the metal center could be envisioned as a method to affect the PCET chemistry of the quinonoid fragment. We have recently reported the synthesis of a series of π-bound $Mo^0$-quinonoid complexes and demonstrated their ability to transfer two $H^+$ (as well as $R_2Si^{2+}$, $ArB^{2+}$, and $Me^+$) and two electrons to $O_2$.[15] Herein we report an expanded series of Mo-quinonoid complexes in varying protonation and oxidation states spanning a total of two protons and four electrons, and investigate the impact of the metal-arene interaction on the PCET chemistry of the quinonoid fragment.

## RESULTS AND DISCUSSION

**Scheme 4.1.** Synthesis and reactivity of Mo-quinonoid complexes.

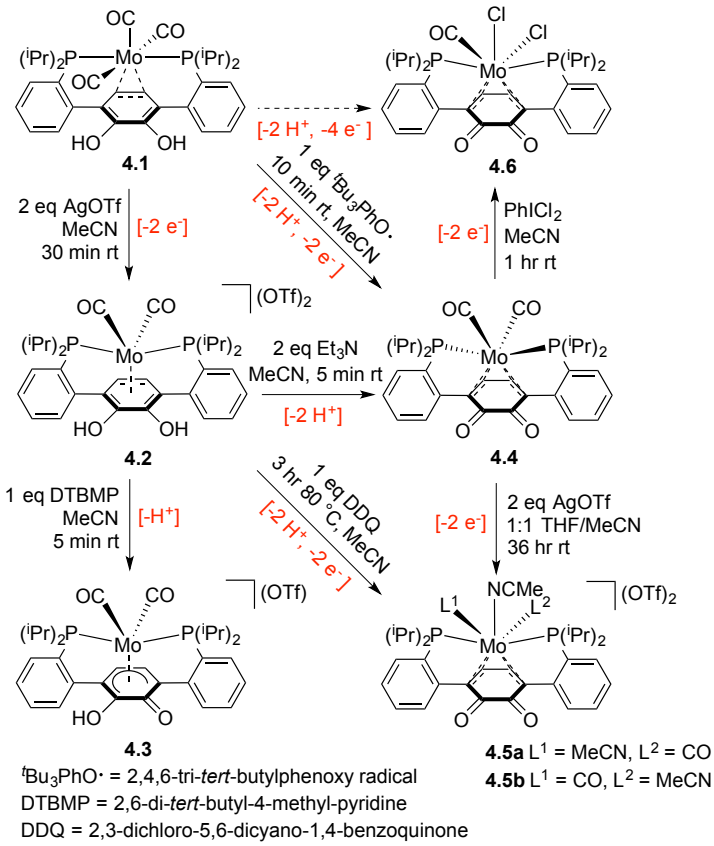


Treatment of **4.1** with two equivalents of AgOTf in MeCN results in oxidation of the metal center by two electrons to yield the $Mo^{II}$ complex **4.2** (Scheme 4.1). Oxidation of the metal center results in loss of a CO ligand and a haptotropic shift of the metal-arene interaction from $\eta^2$ to $\eta^6$. Solution IR data for **4.2** in MeCN reveals strong bands assigned to carbonyl C–O stretches at 2010 and 1955 $cm^{-1}$ (ca. 150 $cm^{-1}$ higher in energy compared to **4.1**), consistent with a more oxidized metal center. A single crystal X-ray diffraction (XRD) study of **4.2** confirms the presence of the $Mo(CO)_2$ unit, but the structure is highly disordered with respect to the position of the catechol oxygen atoms

and thus hinders detailed discussion of the metal-arene interaction through bond metrics.

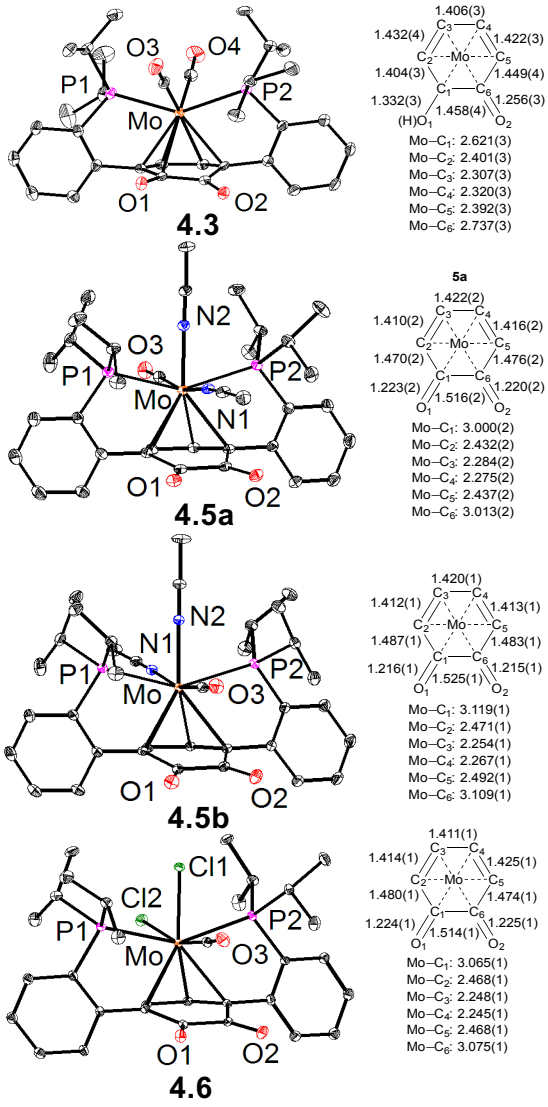


**Figure 4.1.** Solid-state structures of **4.3**, **4.5a**, **4.5b** and **4.6** with 50% probability thermal ellipsoids. Solvent molecules, hydrogen atoms, and outer-sphere anions are omitted for clarity. Carbon atoms are depicted in black. Select bond distances (average values of four molecules in asymmetric unit for **4.3**) are given in Å.

Treatment of **4.2** with one equivalent of 2,6-di-*tert*-butyl-4-methylpyridine (DTBMP) in MeCN results in quantitative mono-deprotonation to yield **4.3**. The appearance of a band in the IR at 1608 $cm^{-1}$ and a carbon resonance in the $^{13}C$ NMR spectrum at ca. 156 ppm are consistent with the formation of the semiquinone C=O moiety upon deprotonation. Additionally, a shift to lower energy of the IR bands assigned to Mo-bound carbon monoxide C–O stretches (1904 and 1880 $cm^{-1}$ in **4.3**) is consistent with a more electron rich metal center, as has also been previously observed in cationic $Mn(CO)_3$ quinonoid complexes.[16] An XRD study of **4.3** (Figure 4.1) confirms these spectroscopic findings, revealing one long quinonoid C–O bond (avg 1.33 Å) and one short quinonoid C–O bond (avg 1.26 Å), consistent with the semiquinone assignment. Compound **4.3** can be further deprotonated with $Et_3N$ to yield the previously reported compound **4.4**.

Reaction of **4.4** with two equivalents of AgOTf in a 1:1 mixture of THF/MeCN results in the formation of two isomers, as determined by $^{31}P$ NMR spectroscopy and crystallography (Figure 4.1), differing in the position of the CO ligand relative to the quinone moiety. The major species **4.5a**, which resonates as a singlet at ca. 75 ppm in $CD_3CN$ ($^{31}P$), can be enriched to approximately 80% via successive recrystallizations, albeit in low yield (~20%). XRD studies of **4.5a** and **4.5b** reveal $Mo^{II}$-quinone complexes with two outer-sphere counter anions. Oxidation of the metal center from (formally) $Mo^0$ to $Mo^{II}$ results in loss of a carbonyl ligand and coordination of two MeCN molecules, yielding a *pseudo*-pentagonal bipyramidal geometry about the metal center with the remaining carbonyl *anti* with respect to the quinone. Upon oxidation the quinone fragment retains the short C–O bonds (avg 1.22 Å in **4.5a** and **4.5b** compared to 1.23 Å in **4.4**), while the diene fragment reveals a slight contraction of the C=C

bonds (avg 1.41 Å in **4.5a** and **4.5b** compared to 1.44 Å in **4.4**) consistent with less π-backbonding in the more oxidized complex. The syntheses of compounds **4.4** and **4.5a**/**4.5b** described above involve sequential steps involving the separate transfer of $2e^-$ and $2H^+$. These compounds can also be prepared in single synthetic steps from **4.1** via reaction with 2 equivalents of 2,4,6-tri-*tert*-butylphenoxy radical and from **4.2** via reaction with 2,3-dichloro-5,6-dicyano-1,4-benzoquinone (DDQ), respectively, in combined $2e^-/2H^+$ transformations.

Oxidation of **4.4** with $PhICl_2$ results in formation of a third $Mo^{II}$-quinone complex **4.6**. Here again a CO ligand is lost upon oxidation and binding of two chloride ligands and a single isomer is generated (NMR and IR spectroscopy). An XRD study (Figure 4.1) shows the CO ligand *syn* with respect to the quinone CO moieties (analogous to **4.5b**) and bond metrics similar to those of **4.5a** and **4.5b**. Compounds **4.5a**, **4.5b**, and **4.6** represent rare examples of accessing redox equivalents beyond the two stored in the catechol moiety, and allow two different oxidation state entries into the study of PCET chemistry of Mo-quinonoid complexes.

**Scheme 4.2. R**eactivity of quinonoid complexes with azobenzene and TEMPO.

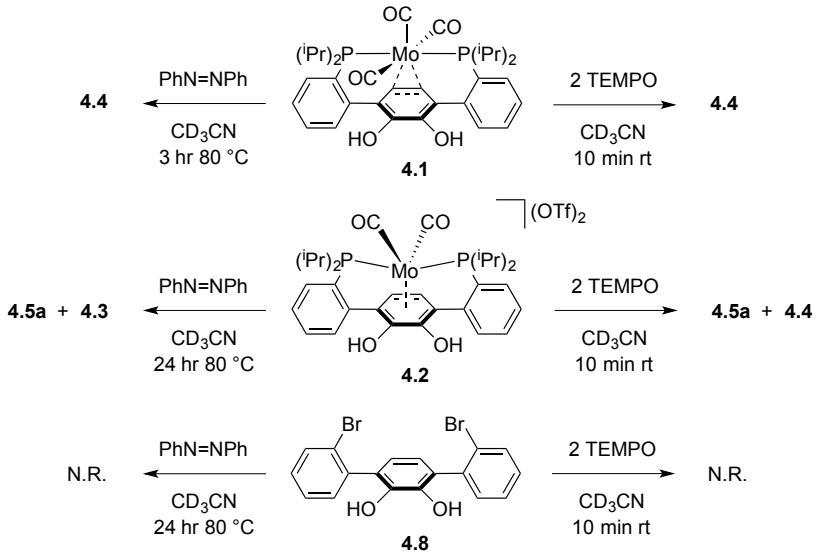


Reactions of compounds **4.1** and **4.2** with azobenzene and (2,2,6,6-tetramethylpiperidyl)oxyl (TEMPO) were performed in MeCN (Scheme 4.2). Compound **4.1** reacts with azobenzene quantitatively to yield **4.4**, while **4.2** generates a mixture of **4.5** and **4.3** in ca. 1:2 ratio (NMR spectroscopy). Similar to the reaction with azobenzene, **4.1** reacts with TEMPO to quantitatively yield **4.4**, while **4.2** yields a mixture of **4.5a** and **4.4** in ca. 1:1 ratio ($^1$H NMR spectroscopy). The formation of both oxidized (compound **4.5a**) and deprotonated (compounds **4.3** and **4.4**) products from the reactions of compound **4.2** with azobenzene and TEMPO can be rationalized via competing acid-base side reactions between **4.2** and the by-products TEMPOH and 1,2-diphenylhydrazine. As a control, under identical conditions it was found that the metal-free quinonoid compound 2,6-bis(orthobromophenyl)catechol (**4.8**) exhibited no reaction with azobenzene or TEMPO.

These results suggest that the O–H bonds in compounds **4.1** and **4.2** are relatively weak, as they react with azobenzene to generate 1,2-diphenylhydrazine, with a reported

N–H bond dissociation free energy (BDFE) of 67 kcal/mol (in DMSO) and TEMPO to generate TEMPOH, with a reported O–H BDFE of 66.5 kcal/mol (in MeCN). Furthermore, the metal-quinonoid complexes are activated with respect to (overall) H-atom transfer when compared to the metal-free compound **4.8**, which shows no reactivity with TEMPO or azobenzene under similar conditions. Based on these reactions alone, thermodynamic assumptions cannot be made about the Mo complexes, as CO is irreversibly lost upon oxidation; however, by measuring the $pK_a$'s of compounds **4.1**, **4.2**, and **4.3** as well as the oxidation potentials of the respective conjugate bases, BDFE's for the first O–H in MeCN can be calculated using equation (1)[14b] to determine the effect of the metal-quinonoid interaction in varying protonation and oxidation states on the PCET chemistry.

$$BDFE_{MeCN}(X–H) = 54.9 + 1.37pK_a(X–H/X^-) + 23.06E°(X^-/X\cdot) \quad (1)$$

The $pK_a$'s for compounds **4.1**, **4.2**, and **4.3** were determined in MeCN using acids/bases of known strength, measuring the equilibrium constants by $^1$H NMR spectroscopy (see experimental section for further details) and combining the equilibrium constant with the $pK_a$ of the known acid/base using Hess's Law to determine the $pK_a$ of the desired compounds as previously reported.[17] The conjugate bases of compounds **4.2** and **4.3** are compounds **4.3** and **4.4**, respectively, and their preparations found above and elsewhere,[15] while the conjugate bases of **4.1** and **4.8** were prepared via deprotonation with benzyl potassium in the presence of crown ether (see experimental details). Oxidation potentials were determined via electrochemical experiments (Figure 4.2). In all cases, two oxidation events[18] were observed via cyclic and square-wave voltammetries, with the first event used to calculate the BDFEs. All

observed events were irreversible, with the exception of the first event for the conjugate base of **4.8** (purple traces, Figure 4.2). While BDFE values have previously been calculated using irreversible oxidation events measured via cyclic voltammetry,[14b, 19] square-wave measurements were employed to minimize error associated with irreversible events. The $pK_a$ and oxidation potential values are collected in Table 1, along with the resulting BDFE values calculated using equation (1).

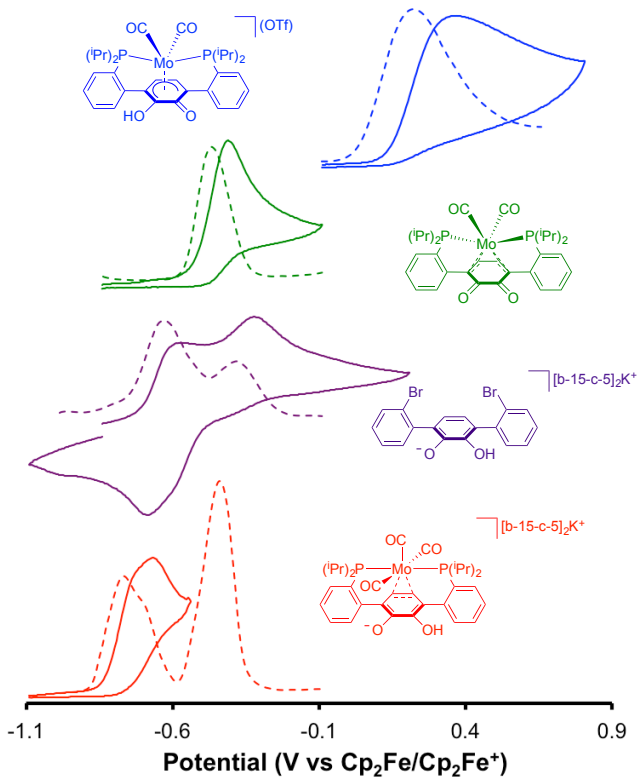


**Figure 4.2.** Cyclic voltammograms (solid lines) and square-wave voltammograms (dashed lines) of conjugate bases of compounds **4.1** (red), **4.2** (blue), **4.3** (green), and **4.8** (purple) in 0.1 M [$^n$Bu$_4$N$^+$][PF$_6^+$] in MeCN recorded with a glassy carbon electrode. Scan rate of 50 mV/s for cyclic voltammograms. (b-15-c-5) = benzo-15-crown-5.

**Table 4.1.** Thermochemical data for selected quinonoid compounds

| | $pK_{a(O–H)}$[a] | $E°_{(O^-/O\cdot)}$[b] | $BDFE_{O–H}$[c] |
|---|---|---|---|
| **4.1** | 25.89(9) | -0.770 V | 72.6 kcal/mol |
| **4.2** | 4.74(9) | 0.220 V | 66.3 kcal/mol |
| **4.3** | 17.1(4) | -0.470 V | 67.5 kcal/mol |
| **4.8** | 26.3(1) | -0.630 V | 76.4 kcal/mol |

[a] $pK_a$ for first O–H determined via solution equilibria (see SI). [b] Oxidation potential for conjugate base determined via square-wave voltammetry. [c] Calculated using equation (1).

Comparing first compound **4.1** to compound **4.8**, the effect of $\eta^2$ coordination of the $Mo^0(CO)_3$ moiety to the quinonoid fragment on the PCET chemistry can be assessed. Compounds **4.1** and **4.8** exhibit similar $pK_a$ values (25.89(9) and 26.3(1)), while the presence of the $Mo^0(CO)_3$ unit in **1** results in a more reducing species, shifting the oxidation potential 140 mV more negative. Overall the presence of the metal-quinonoid interaction in **4.1** results in a lower first O–H BDFE of 72.6 kcal/mol compared to 76.4 kcal/mol for the metal-free quinonoid **4.8**.

Next, comparing compound **4.1** to compound **4.2**, the effect of changing the oxidation state of the metal center on the PCET chemistry can be analyzed. Oxidation of **4.1** from $Mo^0$ to $Mo^{II}$ accompanied by loss of a CO ligand and a shift of the metal-quinonoid interaction from $\eta^2$ to $\eta^6$ results in >20 orders of magnitude increase in acidity, with a measured $pK_a$ of 4.74(9) for **4.2** compared to 25.89(9) for **4.1**. This increase in acidity is greater than the calculated increase in acidity for phenol upon one-electron oxidation.[20] The oxidation from **4.1** to **4.2** also results in a large positive shift in the oxidation potential of the conjugate base (+0.220 V for conjugate base of **4.2** compared to -0.770 V for conjugate base of **4.1**), consistent with a more electron deficient species. The increased acidity in **4.2** thermodynamically outweighs the positive shift in oxidation potential, resulting in a weaker calculated BDFE for the first O–H of 66.3 kcal/mol.

Finally, the effect of protonation state while maintaining the same overall oxidation state on the metal-quinonoid interaction and the resulting PCET chemistry can be analyzed by comparing compounds **4.2** and **4.3**. Deprotonation of **4.2** to yield **4.3** results in a shift of the metal-quinonoid interaction from $\eta^6$ to $\eta^5$, as well as a decrease in the overall charge from di-cation to mono-cation. The acidity of the remaining O–H moiety ($pK_a$ = 17.1(4)) of **4.3**, is lower than in **4.2**. A more negative oxidation potential of the conjugate base (-0.470 V) is observed for **4.3**. The negative shift of the oxidation potential nearly counter-balances the decrease in acidity, resulting in a modest increase in the BDFE to 67.5 kcal/mol for compound **4.3**.

These results demonstrate that metal-quinonoid interactions can be used to modulate the PCET of the quinonoid fragment, with the first O–H BDFE shifting over a notable 10 kcal/mol from 76.4 kcal/mol for metal-free compound **4.8** to 66.3 kcal/mol in compound **4.2**. Not only does the strength of the O–H bond weaken with increasing metal-quinonoid interaction, but changes in the acidity and oxidation potentials could result in access to different PCET pathways. For example, compound **4.1** exhibits relatively low acidity ($pK_a$ = 25.89) and mild reducing power (E° = -0.285 V), with a significant shift in the oxidation potential upon proton transfer (E° = -0.770 V for the conjugate base). These thermodynamic parameters suggest that compound **4.1** is likely to proceed through either a concerted proton-electron transfer (CPET) pathway or a stepwise electron transfer-proton transfer (ET-PT) pathway, and disfavors the stepwise PT-ET pathway. Alternatively, compound **4.2** exhibits significantly greater acidity ($pK_a$ = 4.74) and low reducing power (E° = +0.94 V), with a large shift in oxidation potential upon proton transfer (E° = +0.220 V for conjugate base **4.3**). These thermodynamic parameters suggest compound **4.2** is likely to

proceed through a CPET pathway or a stepwise PT-ET pathway, and disfavors a stepwise ET-PT pathway.

**Scheme 4.3.** Thermochemical analysis of stepwise vs. concerted pathways in reactions of **4.1** and **4.2** with TEMPO.

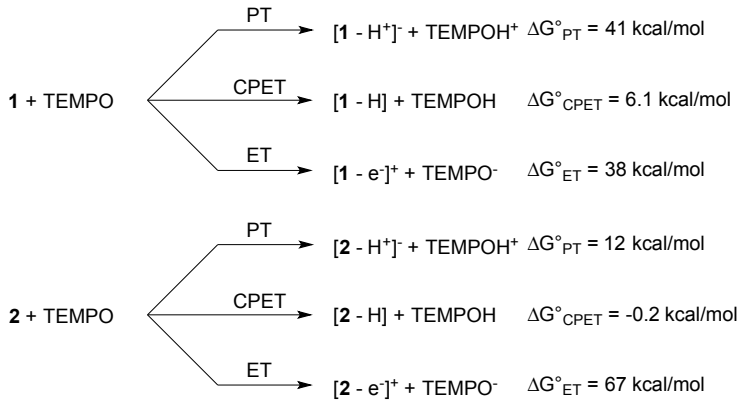


For example, the thermodynamics of the reactions of **4.1** and **4.2** with TEMPO can be analyzed to differentiate the three potential pathways: proton transfer (PT), electron transfer (ET), and CPET (Scheme 4.3). For compound **4.1**, comparing the $pK_a$ of **4.1** (25.89(9)) to the estimated $pK_a$ of $TEMPOH^+$ (ca. -4),[14b] an initial proton transfer from **4.1** to TEMPO would involve an equilibrium constant of $10^{-30}$, giving $\Delta G°_{PT}$ = 41 kcal/mol (Scheme 3). The electron transfer pathway is similarly uphill, with oxidation potential E° = -0.285 V for compound **4.1** and E° = -1.95 V for the TEMPO/$TEMPO^-$ couple[21] resulting in a $\Delta G°_{ET}$ = 38 kcal/mol. The concerted pathway instead is more thermodynamically accessible with $\Delta G°_{CPET}$ = 6.1 kcal/mol. Through the same analysis with compound **4.2**, we can calculate the proton transfer pathway to be uphill with $\Delta G°_{PT}$ = 12 kcal/mol, while the electron transfer pathway is significantly uphill with $\Delta G°_{ET}$ = 67 kcal/mol, and the concerted pathway is nearly thermo-neutral with $\Delta G°_{CPET}$ = -0.2 kcal/mol. While it should be

emphasized that this analysis is purely thermodynamic, these result indicate that in the reaction of **4.1** and **4.2** with TEMPO the CPET pathway is favored in both cases, but with **4.2** the stepwise PT-ET pathway may also be accessible.

**Scheme 4.4.** Thermochemical analysis of ET vs. CPET pathways in reactions of **4.1** with $O_2$.

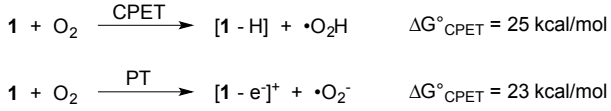


Finally, this thermochemical data can be used to analyze the reaction of **4.1** with $O_2$. The previously proposed mechanism initiated through outer-sphere electron transfer to generate a $Mo^{I}$ species and $•O_2^-$, though the CPET pathway could not be ruled out.[15] Using E° = -1.28 V for the $•O_2^-/O_2$ couple in MeCN[22] and 47.8 kcal/mol as the BDFE of $•O_2H$,[23] the thermodynamic values of $\Delta G°_{CPET}$ = 25 kcal/mol and $\Delta G°_{ET}$ = 23 kcal/mol can be calculated (Scheme 4.4). While it should again be emphasized that these analyses are purely thermodynamic, these calculations suggest that the outer-sphere electron transfer pathway is thermodynamically accessible when compared to the CPET pathway.

## CONCLUSIONS

In summary, the synthesis of an expanded series of Mo-quinonoid complexes has been reported, demonstrating a total of two protons and four electrons accessible to the system. The $Mo^0$-catechol and $Mo^{II}$-catechol complexes both exhibit PCET reactivity with azobenzene and TEMPO. Thermochemical analysis reveals that $\eta^2$ interaction of the $Mo^0(CO)_3$ moiety with the catechol in **4.1** results in a 3.8 kcal/mol decrease in the BDFE of the first O–H as compared to the metal-free catechol **4.8**, while oxidation of the metal center from $Mo^0$ to $Mo^{II}$ (along with loss of a CO ligand and shift of the metal-quinonoid interaction from $\eta^2$ to $\eta^6$) results in a further decrease in the first O–H BDFE by 6.3 kcal/mol for compound **4.2**, an overall decrease of 10.1 kcal/mol. Furthermore, changing the oxidation state of the metal center from $Mo^0$ to $Mo^{II}$ may allow access to alternate PCET pathways based on changes in acidities and oxidation potentials. These results prompt further investigation into the use of π-bound transition metal fragments to modulate the PCET chemistry of hydroquinone and other similar moieties within the context of multi-proton multi-electron small molecule transformations.

## EXPERIMENTAL SECTION

### General considerations:

Unless indicated otherwise, reactions performed under inert atmosphere were carried out in oven-dried glassware in a glovebox under a nitrogen atmosphere purified by circulation through RCI-DRI 13X-0408 Molecular Seives 13X, 4x8 Mesh Beads and BASF PuriStar® Catalyst R3-11G, 5x3 mm (Research Catalysts, Inc.). Solvents for all reactions were purified by Grubbs' method.[24] $CD_3CN$ and $CD_2Cl_2$ were purchased from Cambridge Isotope Laboratories and distilled from $CaH_2$ prior to use. Alumina and Celite were activated by heating under vacuum at 200 °C for 24 hours. $^{1}H$, $^{19}F$, and $^{31}P$ NMR spectra were recorded on Varian Mercury 300 MHz spectrometers at ambient temperature, unless denoted otherwise. $^{13}C$ NMR spectra were recorded on a Varian INOVA-500 MHz spectrometer. $^{1}H$ and $^{13}C$ NMR chemical shifts are reported with respect to internal solvent: 1.94 ppm and 118.26 for $CD_3CN$, and 5.32 ppm and 53.84 ppm for $CD_2Cl_2$, respectively. $^{19}F$ and $^{31}P$ NMR chemical shifts are reported with respect to an external standard of $C_6F_6$ (-164.9 ppm) and 85% $H_3PO_4$ (0.0 ppm).

Powder and thin film ATR-IR measurements were obtained by placing a powder or drop of solution of the complex on the surface of a Bruker APLHA ATR-IR spectrometer probe and allowing the solvent to evaporate (Platinum Sampling Module, diamond, OPUS software package) at 2 $cm^{-1}$ resolution. Solution IR spectra were recorded on a Thermo-Fisher Scientific Nicolet 6700 FTIR spectrometer using a $CaF_2$ plate solution cell. Fast atom bombardment-mass spectrometry (FAB-MS) analysis was performed with a JEOL JMS-600H high-resolution mass spectrometer. Gas chromatography-mass spectrometry (GC-MS) analysis was performed upon filtering the

sample through a plug of silica gel. Electrochemical measurements were recorded with a Pine Instrument Company AFCBP1 bipotentiostat using the AfterMath software package. Cyclic voltammograms and square-wave voltammograms were recorded on ca. 2 mM solutions of the relevant complex in the glovebox at 20 °C with an auxiliary Pt-coil electrode, a $Ag/Ag^+$ reference electrode (0.01 M $AgNO_3$, 0.1 M [$^n$Bu4N$^+$][$PF_6^-$] in MeCN), and a 3.0 mm glassy carbon electrode disc (BASI). The electrolyte solution was 0.1 M [$^n$Bu4N$^+$][$PF_6^-$] in MeCN. All reported values are referenced to an internal ferrocene/ferrocenium couple. Elemental analysis was conducted by Robertson Microlit Labs (Ledgewood, NJ).

Unless otherwise noted all chemical reagents were purchased from commercial sources and used without further purification. AgOTf, 2,3-dichloro-5,6-dicyano-1,4-benzoquinone and benzo-15-crown-5 were purchased from Sigma Aldrich and used as received. 2,6-di-*tert*-butyl-4-methylpyridine, 4-*tert*-butylphenol, 2-nitroaniline, and [2,2,2]-diazobicyclooctane were purchased from Sigma Aldrich and sublimed prior to use. $PhICl_2$,[25] BnK,[26] **4.1**,[15] **4.4**,[15] and **4.8**[15] were prepared using literature procedures. Assignments of NMR spectra are given corresponding to the following numbering scheme:

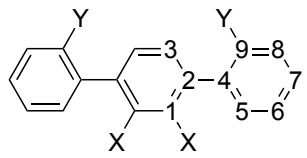

**Synthesis of [1,4-bis(2-(diisopropylphosphino)phenyl)-2,3-catechol] dicarbonylmolybdenum(II) bis(trifluoromethanesulfonate) (4.2)**

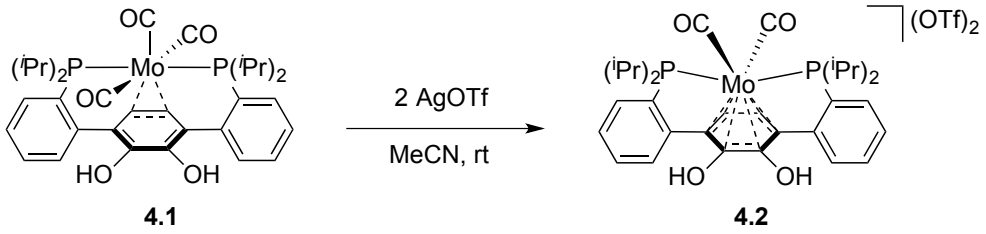


**4.1** **4.2**

Compound **4.1** (0.0833 g, 0.123 mmol) was stirred as a suspension in MeCN (2 mL). AgOTf (0.0617 g, 0.240 mmol) was added as a solution in MeCN (2 mL) to the stirring suspension. Upon addition the reaction became a purple heterogeneous mixture, which was stirred at room temperature until the purple color dissipated (approximately 20 min), resulting in a yellow/brown heterogeneous mixture. The solution was then filtered through celite and the filtrate evaporated under reduced pressure. The resulting residue was freed of excess MeCN by trituration with hexanes (3 mL), followed by evaporation under reduced pressure to yield a tan solid (0.1089 g, 93%). $^{1}$H NMR (500 MHz, $CD_3CN$, 25 °C): δ 10.07 (s, 2 H, Ar-O*H*), 7.87 (m, 4 H), 7.80 (t, 7.5 Hz, 2 H), 7.77 (t, 7 Hz, 2 H), 6.46 (s, 2H, Ar-$C_3$*H*), 3.32 (m, 2 H, C*H*($CH_3$)$_2$). 3.20 (m, 2 H, C*H*($CH_3$)$_2$), 1.37 (m, 6 H, C*H*($CH_3$)$_2$), 1.31 (m, 6 H, CH(C*H*$_3$)$_2$), 1.21 (m, 6 H, CH(C*H*$_3$)$_2$), 1.18 (m, 6 H, CH(C*H*$_3$)$_2$). $^{31}$P NMR (121 MHz, $CD_3CN$, 25 °C): 72.38 (s). $^{19}$F NMR (282 MHz, $CD_3CN$, 25 °C): -79.33 (s). $^{13}$C NMR (150 MHz, $CD_3CN$ , 25 °C): 226.99 (t, Mo-*C*O), 224.17 (t, Mo-*C*O), 140.34 (s, Ar-*C*$_1$), 137.96 (m, Ar-*C*$_2$), 136.49 (m, Ar-C$_9$), 134.62 (s, Ar-*C*$_5$), 134.28 (s, Ar-*C*$_6$), 131.94 (t, Ar-*C*), 129.89 (t, Ar-*C*), 124.87 (t, Ar-*C*), 95.74 (s, Ar-*C*$_3$), 28.83 (m, *C*H($CH_3$)$_2$), 18.58 (s, *C*H($CH_3$)$_2$), 18.00 (s, *C*H($CH_3$)$_2$), 17.92 (s,

*C*H(CH$_3$)$_2$). IR (MeCN), $\nu_{CO}$ (cm$^{-1}$): 2010, 1955. Anal. Calcd for [**4.2**], $C_{34}H_{40}F_6MoO_{10}P_2S_2$: C, 43.23; H, 4.27. Found: C, 43.16; H, 4.38.

**Synthesis of [1,4-bis(2-(diisopropylphosphino)phenyl)-2,3-semiquinonate]dicarbonylmolybdenum(II) trifluoromethanesulfonate (4.3)**

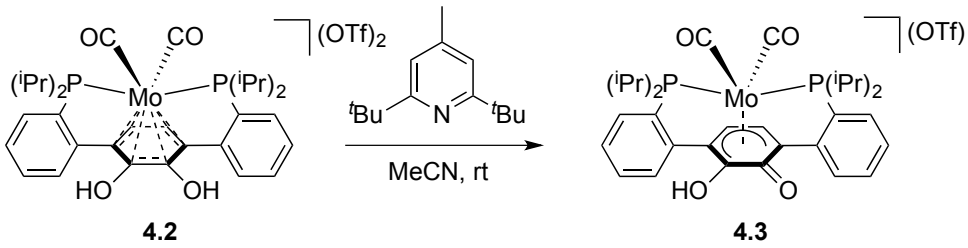


To a solution of **4.2** (0.0427 g, 0.0452 mmol) in MeCN (2 mL) was added 2,6-di-*tert*-butyl-4-methylpyridine (0.0049 g, 0.0437 mmol) as a solution in MeCN (2 mL). The mixture was stirred at room temperature for 30 minutes, at which point the volatiles were removed under vacuum. The resulting residue was taken up in a minimal amount of MeCN and added to a stirred solution of $Et_2O$ (15 mL) drop-wise. Upon complete addition, the resulting suspension was cooled to -35 °C for 20 minutes and then filtered cold on a pad of celite. The solid was dissolved in MeCN, filtered, and concentrated under vacuum to afford the desired product (0.0258 g, 72%). Crystals suitable for X-ray diffraction were grown via vapor diffusion of $Et_2O$ into a saturated solution of **3** in DMF. $^1$H NMR (300 MHz, $CD_3CN$, 25 °C): δ 9.09 (s, br), 7.77 (m, 4 H), 7.68 (m, 4H), 5.90 (s, 2 H), 3.17 (m, 4 H), 1.28 (m, 18 H), 1.06 (m, 6 H). $^{31}$P NMR (121 MHz, $CD_3CN$, 25 °C): 72.02 (s). $^{19}$F NMR (282 MHz, $CD_3CN$, 25 °C): -79.19 (s). $^{13}$C NMR (150 MHz, $CD_3CN$, 25 °C): 236.68 (t, Mo-*C*O), 229.21 (t, Mo-*C*O), 156.00 (s, Ar-$C_1$), 142.65 (t, Ar-

$C_2$), 136.55 (m, Ar-$C_9$), 133.38 (s, Ar-$C_5$), 133.10 (s, Ar-$C_6$), 130.10 (s, Ar-*C*), 129.88 (s, Ar-*C*), 116.70 (s, Ar-*C*), 88.92 (s, Ar-$C_3$), 28.89 (t, *C*H($CH_3$)$_2$), 27.33 (t, *C*H($CH_3$)$_2$), 18.43 (s, *C*H($CH_3$)$_2$), 18.24 (s, *C*H($CH_3$)$_2$), 18.04 (s, *C*H($CH_3$)$_2$). IR (THF, $cm^{-1}$), $\nu_{CO}$: 1904, 1880, 1608. Anal. Calcd for [**4.3**], $C_{33}H_{39}F_3MoO_7P_2S$: C, 49.88; H, 4.95. Found: C, 49.56; H, 5.02.

**Synthesis of [1,4-bis(2-(diisopropylphosphino)phenyl)-2,3-benzoquinone]bis(acetonitrile)carbonylmolybdenum(II) trifluoromethanesulfonate (4.5a and 4.5b)**

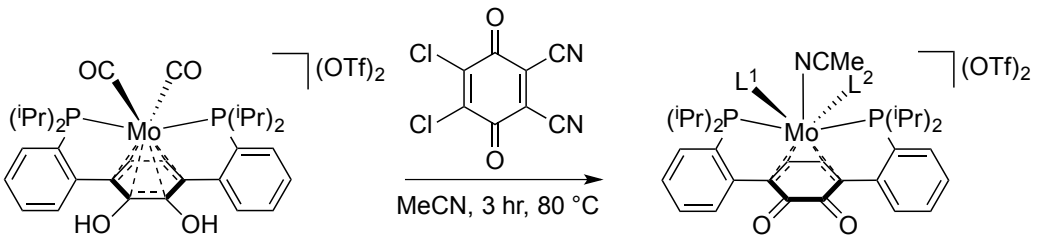


**4.2**

**4.5a** + **4.5b**

**4.5a** $L^1$ = MeCN, $L^2$ = CO
**4.5b** $L^1$ = CO, $L^2$ = MeCN

Compound **4.2** (3.0274 g, 3.20 mmol) and 2,3-dichloro-5,6-dicyano-1,4-benzoquinone (0.7187 g, 3.17 mmol) were combined in a schlenk tube charged with a stir bar and MeCN (15 mL). The schlenk tube was sealed and heated to 80 °C for 3 hours. Completion of the reaction was determined via $^{31}$P NMR analysis of an aliquot of the reaction mixture, revealing loss of the starting material at ~72 ppm, and presence of two new signals at ca. 74 ppm and ca. 70 ppm. After cooling to room temperature, all volatiles were removed under vacuum. The residue was then vigorously triturated with THF (8 mL) to precipitate a brick red powder, and the solid collected on a glass frit.

The solid was then redissolved in a minimal amount of MeCN and recrystallized via vapor diffusion of $Et_2O$. Crystals grown from this mixture after 48 hours at room temperature were then collected and dried under vacuum to afford a mixture of **4.5a** and **4.5b** in ca. 3:2 ratio (2.6323 g, 82%). These crystals were found suitable for X-ray diffraction. Note: the $NCCH_3$ ligands exchange slowly with the $CD_3CN$ NMR solvent for compound **4.5b**, such that the bound acetonitrile can be easily observed by both $^1H$ and $^{13}C$ NMR spectroscopies. Compound **4.5a** exhibits faster ligand exchange, such that signals for the bound acetonitrile ligands could only be observed by $^1H$ NMR spectroscopy.

**4.5a**: $^1H$ NMR (300 MHz, $CD_3CN$, 25 °C), δ(ppm): 7.6 – 7.8 (m, 8 H, Ar-C*H*), 6.22 (t, $J_{PH}$ = 1.4 Hz, 2 H, Ar-$C_1$H), 3.49 (m, 2 H, PC*H*$(CH_3)_2$), 3.14 (m, 2 H, PC*H*$(CH_3)_2$), 3.10 (t, 3.6 Hz, 3 H, equatorial NCC*H*$_3$), 2.48 (s, 3 H, axial NCC*H*$_3$), 1.2 – 1.5 (m, 18 H, PCH(C*H*$_3)_2$), 0.70 (m, 6 H, $PCH_2$(C*H*$_3)_2$). $^{31}P$ NMR (121 MHz, $CD_3CN$, 25 °C), δ(ppm): 74.63 (s). $^{19}F$ NMR (282 MHz, $CD_3CN$, 25 °C): -79.22 (s). $^{13}C$ NMR (125 MHz, $CD_3CN$, 25 °C), δ(ppm): 213.38 (t, Mo-*C*O), 178.73 (s, Ar-$C_3$), 147.06 (t, Ar-$C_4$), 143.00 (t, Ar-$C_9$), 135.31 (s, Ar-$C_5$), 133.36 (t, Ar-$C_8$), 132.15 (s, Ar-$C_7$), 131.92 (t, Ar-$C_2$), 130.91 (t, Ar-$C_6$), 88.79 (s, Ar-$C_1$), 29.54 (m, P*C*H$(CH_3)_2$), 27.53 (t, P*C*H$(CH_3)_2$), 20.82 (s, PCH(*C*H$_3)_2$), 20.27 (s, PCH(*C*H$_3)_2$), 19.71 (t, PCH(*C*H$_3)_2$), 18.75 (t, PCH(*C*H$_3)_2$). IR (powder), $\nu_{CO}$ ($cm^{-1}$): 2020, 1680.

**4.5b**: $^1H$ NMR (300 MHz, $CD_3CN$, 25 °C), δ(ppm): 7.6 – 7.8 (m, 8 H, Ar-C*H*), 6.27 (t, $J_{PH}$ = 1.2 Hz, 2 H, Ar-$C_1$H), 3.49 (m, 2 H, PC*H*$(CH_3)_2$), 3.32 (m, 2 H, PC*H*$(CH_3)_2$), 2.98 (t, 3.6 Hz, 3 H, equatorial NCC*H*$_3$), 2.57 (s, 3 H, axial NCC*H*$_3$), 1.2 – 1.5 (m, 12 H, PCH(C*H*$_3)_2$), 1.09 (m, 6 H, $PCH_2$(C*H*$_3)_2$), 1.04 (m, 6 H, $PCH_2$(C*H*$_3)_2$). $^{31}P$ NMR (121

MHz, $CD_3CN$, 25 °C), δ(ppm): 70.25 (s). $^{19}F$ NMR (282 MHz, $CD_3CN$, 25 °C): -79.22 (s). $^{13}C$ NMR (125 MHz, $CD_3CN$, 25 °C), δ(ppm): 219.05 (t, Mo-*C*O), 175.53 (s, Ar-$C_3$), 144.34 (t, Ar-$C_4$), 142.26 (t, Ar-$C_9$), 136.01 (s, Ar-$C_5$), 133.03 (t, Ar-$C_8$), 132.57 (s, Ar-$C_7$), 132.32 (t, Ar-$C_2$), 130.91 (t, Ar-$C_6$), 92.96 (s, Ar-$C_1$), 30.61 (m, P*C*H$(CH_3)_2$), 27.87 (t, P*C*H$(CH_3)_2$), 20.37 (s, PCH$(CH_3)_2$), 20.27 (s, PCH$(CH_3)_2$), 19.74 (s, PCH$(CH_3)_2$), 18.65 (t, PCH$(CH_3)_2$). IR (powder), $\nu_{CO}$ ($cm^{-1}$): 1990, 1680.

Anal. Calcd for [**4.5a/4.5b**]•MeCN, $C_{39}H_{47}F_6MoN_3O_9P_2S_2$: C, 45.14; H, 4.56; N, 4.05. Found: C, 45.34; H, 4.61; N, 4.04.

**Synthesis of [1,4-bis(2-(diisopropylphosphino)phenyl)-2,3-benzoquinone]dichlorocarbonylmolybdenum(II) (4.6)**

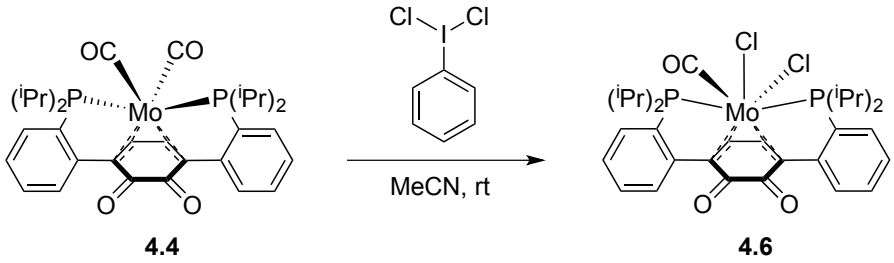


**4.4** **4.6**

From **4.4**: In the glovebox, a schlenk flask was charged with compound **4.4** (0.1712 g, 0.234 mmol), MeCN (10 mL), and a stir bar, and the flask was brought out to the schlenk line. Under a counterflow of $N_2$, $PhICl_2$ (0.1505 g, 0.547 mmol) was added all at once as a solid. The reaction became a dark red homogeneous solution with evolution of gas. The reaction was stirred under $N_2$ for 1 hour at room temperature, during which a large amount of brick-red material had precipitated from solution. The volatiles were then removed under reduced pressure and the schlenk flask then returned to the

glovebox. The residue was triturated with THF (20 mL) and the precipitate collected on a glass frit, washing with additional THF (10 mL). The solid was then dried under vacuum to afford the desired product as a brick-red powder in 87.5% yield (0.6621 g). Spectroscopic data can be found below.

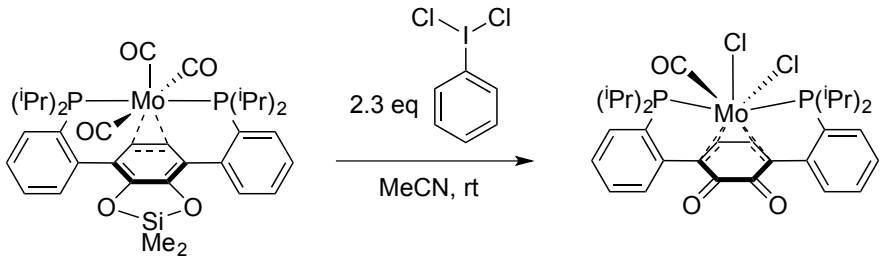


**4.1-SiMe$_2$** **4.6**

From **4.1-SiMe$_2$**: In the glovebox, a schlenk flask was charged with compound **4.1-SiMe$_2$** (0.1712 g, 0.234 mmol), MeCN (10 mL), and a stir bar, and the flask was brought out to the schlenk line. Under a counterflow of $N_2$, $PhICl_2$ (0.1505 g, 0.547 mmol) was added all at once as a solid. The reaction became a dark red homogeneous solution with evolution of gas. The reaction was stirred under $N_2$ for 1 hour at room temperature, during which a large amount of brick-red material had precipitated from solution. The volatiles were then removed under reduced pressure and the schlenk flask then returned to the glovebox. The residue was triturated with THF (20 mL) and the precipitate collected on a glass frit, washing with additional THF (10 mL). The solid was then dried under vacuum to afford the desired product as a brick-red powder in 87.5% yield (0.6621 g). Crystals suitable for X-ray diffraction were grown via layering of pentane onto a saturated solution of the compound in DCM. $^1$H NMR (300 MHz, $CD_2Cl_2$ , 25 °C), δ(ppm): 7.62 (m, 4 H, Ar-C*H*), 7.55 (m, 2 H, Ar-C*H*), 7.47 (m, 2 H, Ar-C*H*), 7.45 (m, 2 H, Ar-C*H*), 5.93 (s, Ar-C$_1$*H*), 3.57 (m, 2 H, PC*H*$(CH_3)_2$), 3.13 (m, 2 H,

PC*H*$(CH_3)_2$), 1.57 (m, 6H, PCH(C$H_3$)$_2$), 1.48 (m, 6H, PCH(C$H_3$)$_2$), 1.27 (m, 6H, PCH(C$H_3$)$_2$), 0.55 (m, 6 H, PCH(C$H_3$)$_2$). $^{31}$P NMR (121 MHz, $CD_2Cl_2$ , 25 °C), δ(ppm): 53.48 (s). $^{13}$C NMR (125 MHz, $C_6D_6$ , 25 °C), δ(ppm): 220.88 (t, Mo-*C*O), 174.96 (s, Ar-$C_3$), 143.58 (t, Ar-$C_4$), 133.90 (t, Ar-$C_9$), 130.98 (s, Ar-$C_5$), 130.91 (t, Ar-$C_8$), 129.97 (s, Ar-$C_7$), 129.74 (t, Ar-$C_2$), 115.29 (t, Ar-$C_6$), 94.67 (s, Ar-$C_1$), 29.78 (t, P*C*H$(CH_3)_2$), 27.10 (t, P*C*H$(CH_3)_2$), 20.60 (t, PCH(*C*H$_3$)$_2$), 20.26 (t, PCH(*C*H$_3$)$_2$), 19.83 (t, PCH(*C*H$_3$)$_2$), 18.84 (m, PCH(*C*H$_3$)$_2$), 16.34. IR (powder), $\nu_{CO}$ (cm$^{-1}$): 1965, 1652. Anal. Calcd for [**4.6**], $C_{31}H_{38}MoO_3P_2$: C, 54.16; H, 5.57. Found: C, 53.40; H, 5.54.

**Synthesis of bis(benzo-15-crown-5)potassium [1,4-bis(2-(diisopropylphosphino)phenyl)-2,3-semicatecholate]tricarbonylmolybdenum(0) (4.9)**

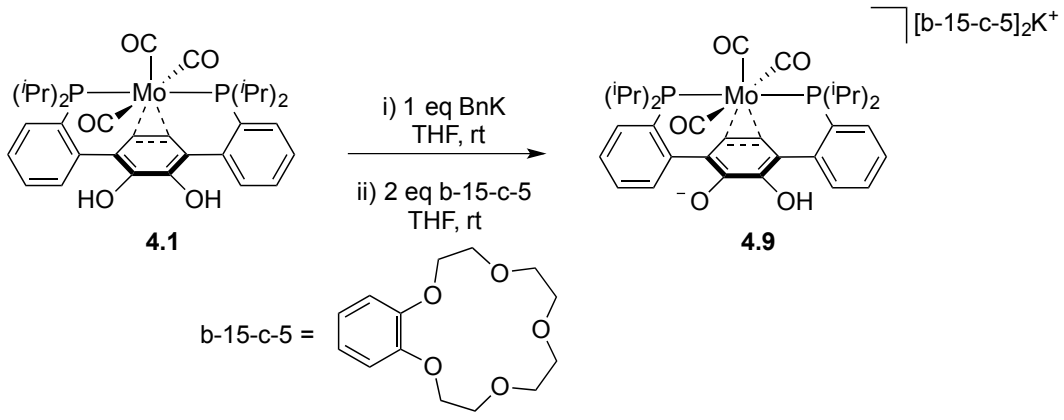


To a solution of **4.1** (0.0623 g, 0.0924 mmol) in THF (2 mL) was added dropwise a solution of BnK (0.0118 g, 0.0906 mmol) in THF (2 mL). Upon complete addition, a solution of benzo-15-crown-5 (0.0507 g, 0.189 mmol) in THF (2 mL) and the mixture was stirred at room temperature for 30 minutes. The volatiles were then removed under

reduced pressure, and the resulting residue was triturated with $Et_2O$ (5 mL) and the solid collected on a pad of celite. The solid was then dissolved in benzene (5 mL), filtered through celite, and concentrated in vacuo to afford the desired product as an orange powder (0.0756 g, 66%). $^1$H NMR (300 MHz, $CD_3CN$ , 25 °C), δ(ppm): 9.22 (s, br, 1 H, O–*H*), 8.04 (d, 8 Hz, 2 H, Ar-C*H*), 7.91 (d, 8 Hz, 2 H, Ar-C*H*), 7.38 (t, 8 Hz, 2 H, Ar-C*H*), 7.25 (t, 8 Hz, 2 H, Ar-C*H*), 6.91 (m, 2 H, crown Ar-C*H*), 6.81 (m, 2 H, crown Ar-C*H*), 5.38 (t, 4.9 Hz, 2 H, quinonoid Ar-$C_3H$), 3.91 (m, 4 H, crown O–C$H_2$), 3.66 (m, 8 H, crown O–C$H_2$), 3.66 (m, 8 H, crown O–C$H_2$), 3.57 (m, 4 H, crown O–C$H_2$), 2.93 (m, 2 H, PC*H*$(CH_3)_2$), 2.48 (m, 2 H, PC*H*$(CH_3)_2$), 1.42 (m, 6 H, PCH(C$H_3)_2$), 1.31 (m, 6 H, PCH(C$H_3)_2$), 0.96 (m, 6 H, PCH(C$H_3)_2$), 0.90 (m, 6 H, PCH(C$H_3)_2$). $^{31}$P NMR (121 MHz, $CD_3CN$ , 25 °C), δ(ppm): 51.42 (s). $^{13}$C NMR (126 MHz, $CD_3CN$ , 25 °C), δ(ppm): 229.15 (t, 10 Hz, Mo-*C*O), 216.66 (t, 10 Hz, Mo-*C*O), 211.78 (t, 10 Hz, Mo-*C*O), 149.80 (s, Ar-$C_1$), 148.65 (s, crown Ar-*C*–O), 133.03 (s, Ar-C*H*), 132.29 (s, Ar-C*H*), 131.73 (s, Ar-C*H*), 130.73 (s, Ar-C*H*), 128.59 (s, Ar-C*H*), 126.62 (s, Ar-C*H*), 124.95 (s, Ar-C*H*), 122.43 (s, crown Ar-*C*H), 120.19 (s, Ar-*C*), 114.32 (s, crown Ar-*C*H), 86.58 (s, $C_3$), 69.49 (s, crown O–*C*$H_2$), 68.75 (s, crown O–*C*$H_2$), 68.26 (s, crown O–*C*$H_2$), 67.91 (s, crown O–*C*$H_2$), 34.65 (t, P*C*H$(CH_3)_2$), 31.16 (t, P*C*H$(CH_3)_2$), 20.31 (t, PCH(*C*$H_3)_2$), 19.92 (t, PCH(*C*$H_3)_2$), 19.53 (s, PCH(*C*$H_3)_2$), 19.52 (s, PCH(*C*$H_3)_2$). IR (THF), $\nu_{CO}$ ($cm^{-1}$): 1875, 1605. Anal. Calcd for [**4.9**], $C_{61}H_{79}KMoO_{15}P_2$: C, 58.65; H, 6.37. Found: C, 57.33; H, 6.10.

**Synthesis of bis(benzo-15-crown-5)potassium [1,4-bis(2-bromophenyl)-2,3-semicatecholate] (4.10)**

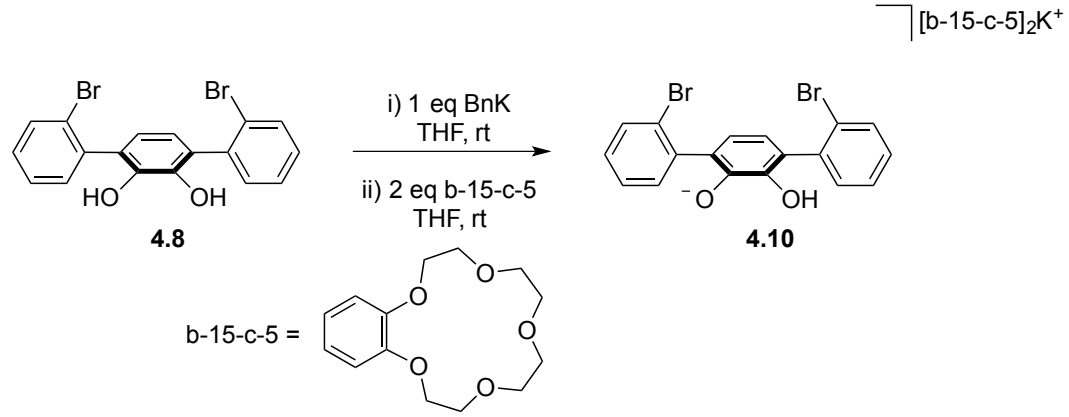


To a solution of **4.8** (0.0998 g, 0.238 mmol) in THF (2 mL) was added dropwise a solution of BnK (0.0309 g, 0.237 mmol) in THF (2 mL). Upon complete addition, a solution of benzo-15-crown-5 (0.1351 g, 0.504 mmol) in THF (2 mL) and the mixture was stirred at room temperature for 30 minutes. The volatiles were then removed under reduced pressure, and the resulting residue was triturated with $Et_2O$ (5 mL) and the solid collected on a pad of celite. The solid was then dissolved in benzene (5 mL), filtered through celite, and concentrated in vacuo to afford the desired product as an orange powder (0.1213, 51%). $^1$H NMR (300 MHz, $CD_3CN$ , 25 °C), δ(ppm): 9.22 (s, br, 1 H, O–*H*), 8.04 (d, 8 Hz, 2 H, Ar-C*H*), 7.91 (d, 8 Hz, 2 H, Ar-C*H*), 7.38 (t, 8 Hz, 2 H, Ar-C*H*), 7.25 (t, 8 Hz, 2 H, Ar-C*H*), 6.91 (m, 2 H, crown Ar-C*H*), 6.81 (m, 2 H, crown Ar-C*H*), 5.38 (t, 4.9 Hz, 2 H, quinonoid Ar-$C_3H$), 3.91 (m, 4 H, crown O–$CH_2$), 3.66 (m, 8 H, crown O–$CH_2$), 3.66 (m, 8 H, crown O–$CH_2$), 3.57 (m, 4 H, crown O–$CH_2$), 2.93 (m, 2 H, PC*H*$(CH_3)_2$), 2.48 (m, 2 H, PC*H*$(CH_3)_2$), 1.42 (m, 6 H, PCH$(CH_3)_2$), 1.31 (m, 6 H, PCH$(CH_3)_2$), 0.96 (m, 6 H, PCH$(CH_3)_2$), 0.90 (m, 6 H, PCH$(CH_3)_2$). $^{31}$P NMR

(121 MHz, $CD_3CN$ , 25 °C), δ(ppm): 51.42 (s). $^{13}C$ NMR (126 MHz, $CD_3CN$ , 25 °C), δ(ppm): 228.21 (t, 10 Hz, Mo-*C*O), 215.71 (t, 10 Hz, Mo-*C*O), 210.83 (t, 10 Hz, Mo-*C*O), 148.86 (s, Ar-$C_1$), 147.70 (s, crown Ar-*C*–O), 132.09 (m), 131.35 (s, Ar-C*H*), 130.79 (s, Ar-C*H*), 129.78 (s, Ar-C*H*), 127.64 (s, Ar-C*H*), 125.68 (s, Ar-C*H*), 124.00 (s, Ar-C*H*), 121.48 (s, crown Ar-*C*H), 113.37 (s, crown Ar-*C*H), 85.63 (s, $C_3$), 68.55 (s, crown O–$CH_2$), 67.81 (s, crown O–$CH_2$), 67.32 (s, crown O–$CH_2$), 66.96 (s, crown O–$CH_2$), 33.70 (t, P*C*H$(CH_3)_2$), 30.22 (t, P*C*H$(CH_3)_2$), 19.37 (t, PCH(*C*$H_3)_2$), 18.98 (t, PCH(*C*$H_3)_2$), 18.58 (s, PCH(*C*$H_3)_2$), 18.57 (s, PCH(*C*$H_3)_2$). Anal. Calcd for [**4.3**], $C_{46}H_{51}Br_2KO_{12}$: C, 55.54; H, 5.17. Found: C, 54.15; H, 5.33.

**General procedure for determining the p$K_a$ of compounds 4.1, 4.2, 4.3 and 4.8**

The $pK_a$ values for compounds **4.1**, **4.2**, **4.3**, and **4.8** were determined via $^1H$ NMR spectroscopy and are the average of triplicate self-consistent trials, as has been described previously.[17] The compound of interest was combined with an acid or base of known $pK_a$ and the equilibrium populations were determined via $^1H$ NMR spectroscopy. All compounds exhibit rapid proton exchange on the NMR time-scale, such that the chemical shift can be used to determine the mole fraction of the species in solution via the equation $\chi_A = (\delta_{eq} - \delta_A)/(\delta_A - \delta_B)$, where $\chi_A$ is mole fraction of the acid, $\delta_e$ is the equilibrium chemical shift and $\delta_A$ and $\delta_B$ are the chemical shifts of the pure acid and the pure conjugate base, respectively. The value of $\chi_A$ was determined using well-resolved $^1H$ NMR signals, with good agreement observed between the independent calculations. The value used to determine the equilibrium concentration was the average of the independent caluclations. Once the equilibrium concentrations were determined, the equilibrium constant between the compound of interest and the acid/base of known $pK_a$ was determined, and by using Hess's law the $pK_a$ of the Mo complex (or **4.8**) was determined. The following acids/bases were used to determine the unknown $pK_a$'s: 4-*tert*-butylphenol ($pK_a$ = 27.45) for compound **4.1** and **4.8**; [2,2,2]-diazobicyclooctane ($pK_a$ = 18.60) for compound **4.3**; 2-nitroaniline ($pK_a$ = 4.80) for compound **4.2**.

**Reactions of 4.1, 4.2 and 4.8 with azobenzene and TEMPO**

**4.1** and TEMPO: Compound **4.1** (0.0295 g, 0.0437 mmol) and TEMPO (0.0147 g, 0.0941 mmol) were combined in $CD_3CN$ (0.6 mL) in a 1 dram vial and thoroughly mixed for 30 seconds until all of **4.1** had solubilized and the color had darkened from pale orange to red-orange. The solution was then transferred to an NMR tube and the $^{1}H$ and $^{31}P$ NMR spectra were recorded (Figure **C4.21**).

**2** and TEMPO: Compound **2** (0.0225 g, 0.0238 mmol) and TEMPO (0.0082 g, 0.0525 mmol) were combined in $CD_3CN$ (0.6 mL) in a 1 dram vial and thoroughly mixed for 30 seconds until all of **2** had solubilized and the color had darkened from pale orange to red-orange. The solution was then transferred to an NMR tube and the $^{1}H$ and $^{31}P$ NMR spectra were recorded (Figure **C4.22**).

**4.8** and TEMPO: Compound **4.8** (0.0412 g, 0.0981 mmol) and TEMPO (0.0299 g, 0.191 mmol) were combined in $CD_3CN$ (0.6 mL) in a 1 dram vial and thoroughly mixed for 30 seconds until all of **4.8** had solubilized. No color change was observed. The solution was then transferred to an NMR tube and the $^{1}H$ and $^{31}P$ NMR spectra were recorded (Figure **C4.23**).

**4.1** and azobenzene: Compound **4.1** (0.0226 g, 0.0335 mmol) and azobenzene (0.0070 g, 0.0384 mmol) were combined in $CD_3CN$ (0.6 mL) and the resulting suspension was

transferred to a J-young style NMR tube. The tube was then heated to 80 °C, monitoring by $^{1}H$ and $^{31}P$ NMR spectra over time (Figure **C4.24**).

**4.2** and azobenzene: Compound **4.2** (0.0199 g, 0.0211 mmol) and azobenzene (0.0046 g, 0.0252 mmol) were combined in $CD_3CN$ (0.6 mL) and the resulting solution was transferred to a J-young style NMR tube. The tube was then heated to 80 °C, monitoring by $^{1}H$ and $^{31}P$ NMR spectra over time (Figure **C4.25**).

**4.8** and azobenzene: Compound **4.8** (0.0367 g, 0.0874 mmol) and azobenzene (0.0167 g, 0.0916 mmol) were combined in $CD_3CN$ (0.6 mL) and the resulting solution was transferred to a J-young style NMR tube. The tube was then heated to 80 °C, monitoring by $^{1}H$ and $^{31}P$ NMR spectra over time.

**Refinement Details**

In each case, crystals were mounted on a glass fiber or nylon loop using Paratone oil, then placed on the diffractometer under a nitrogen stream. Low temperature (100 K) X-ray data were obtained on a Bruker APEXII CCD based diffractometer (Mo sealed X-ray tube, $K_\alpha$ = 0.71073 Å) or a Bruker PHOTON100 CMOS based diffractometer (Mo micro-focus sealed X-ray tube, $K_\alpha$ = 0.71073 Å). All diffractometer manipulations, including data collection, integration, and scaling were carried out using the Bruker APEXII software.[27] Absorption corrections were applied using SADABS.[28] Space groups were determined on the basis of systematic absences and intensity statistics and the structures were solved by direct methods using XS[29], by intrinsic phasing using XT (incorporated into SHELXTL), or by charge flipping using Olex2[30] and refined by full-matrix least squares on $F^2$. All non-hydrogen atoms were refined using anisotropic displacement parameters. Hydrogen atoms were placed in the idealized positions and refined using a riding model. The structures were refined (weighed least squares refinement on $F^2$) to convergence. Graphical representation of structures with 50% probability thermal ellipsoids was generated using Diamond visualization software.[31]

**Table 4.2.** Crystal and refinement data for complexes **4.3•0.5DMF** and **4.5a•2NCMe**.

| | **4.3•0.5DMF** | **4.5a•2NCMe** |
|---|---|---|
| Empirical formula | $C_{34.5}H_{42.5}F_3MoN_{0.5}O_{7.5}P_2S$ | $C_{39}H_{50}F_{12}MoN_4O_3P_2Sb_2$ |
| Formula weight | 831.18 g/mol | 1252.23 g/mol |
| T (K) | 100 | 100 |
| *a*, Å | 30.285(3) | 10.005(1) |
| *b*, Å | 26.445(2) | 27.668(2) |
| *c*, Å | 17.945(1) | 19.306(1) |
| α, deg | 90 | 90 |
| β, deg | 93.729(2) | 94.925(3) |
| γ, deg | 90 | 90 |
| Volume, Å$^3$ | 14341(2) | 5324.3(5) |
| Z | 4 | 4 |
| Crystal system | Monoclinic | Monoclinic |
| Space group | $P2_1/c$ | $P2_1/n$ |
| $d_{calc}$, g/cm$^3$ | 1.407 | 1.562 |
| θ range, deg | 2.18-33.14 | 1.29-38.57 |
| $\mu$, mm$^{-1}$ | 0.573 | 1.377 |
| Abs. Correction | Semi-empirical | Semi-empirical |
| GOF | 1.057 | 1.132 |
| $R_1$,[a] $wR_2$ [b] [I>2 σ(I)] | 0.0872, 0.1294 | 0.0409, 0.1502 |

[a] $R_1 = \sum||F_o| - |F_c||/\sum|F_o|$. [b] $wR_2 = [\sum[w(F_o^2-F_c^2)^2]/\sum[w(F_o^2)^2]^{1/2}$.

**Table 4.3.** Crystal and refinement data for complexes **4.5b** and **4.6**.

| | **4.5b** | **4.6** |
|---|---|---|
| Empirical formula | $C_{37}H_{44}F_6MoN_2O_9P_2S_2$ | $C_{31}H_{38}Cl_2MoO_3P_2$ |
| Formula weight | 996.74 g/mol | 687.39 g/mol |
| T (K) | 100 | 100 |
| *a*, Å | 11.3464(4) | 16.255(1) |
| *b*, Å | 21.2519(8) | 16.255(1) |
| *c*, Å | 17.4117(7) | 22.205(2) |
| α, deg | 90 | 90 |
| β, deg | 94.171(1) | 90 |
| γ, deg | 90 | 90 |
| Volume, Å$^3$ | 4187.4(3) | 5866.9(5) |
| Z | 4 | 8 |
| Crystal system | Monoclinic | Orthorhombic |
| Space group | $P2_1/n$ | Pbca |
| $d_{calc}$, g/cm$^3$ | 1.581 | 1.556 |
| θ range, deg | 2.629-43.71 | 1.83-45.29 |
| $\mu$, mm$^{-1}$ | 0.571 | 0.771 |
| Abs. Correction | Semi-empirical | Semi-empirical |
| GOF | 1.025 | 0.954 |
| $R_1$,[a] $wR_2$ [b] [I>2 σ(I)] | 0.0496, 0.0741 | 0.0338, 0.0868 |

[a] $R_1 = \sum||F_o| - |F_c||/\sum|F_o|$. [b] $wR_2 = [\sum[w(F_o^2-F_c^2)^2]/\sum[w(F_o^2)^2]]^{1/2}$.

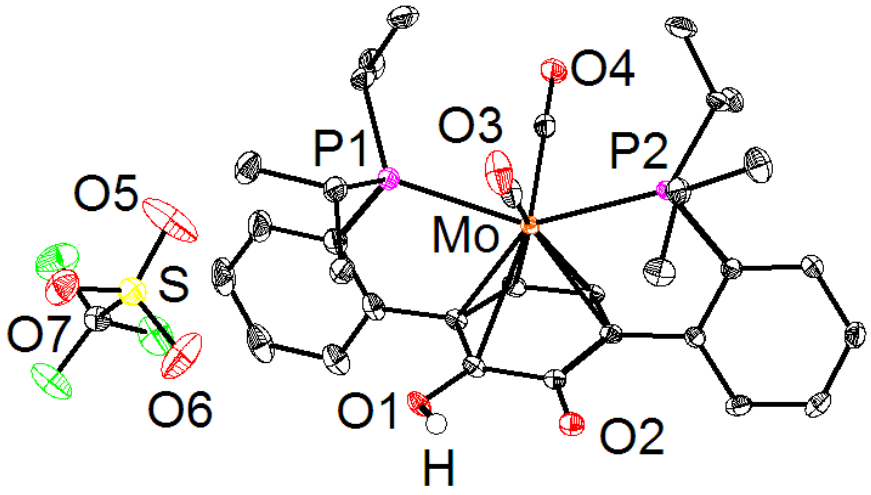


**Figure 4.3.** Structural drawing of **4.3•0.5DMF** with 50% probability ellipsoids. Hydrogen atoms, solvent molecules, and additional three Mo complexes and three triflate anions of the asymmetric unit are omitted for clarity. Carbon and fluorine atoms are shown in black and green, respectively.

**Special Refinement Details for 4.3:** A triflate anion and a DMF solvent molecule were positionally disordered. Both were satisfactorily modeled as approximately 50:50 mixtures using "PART", "SAME", and "EADP" cards in SHELX.

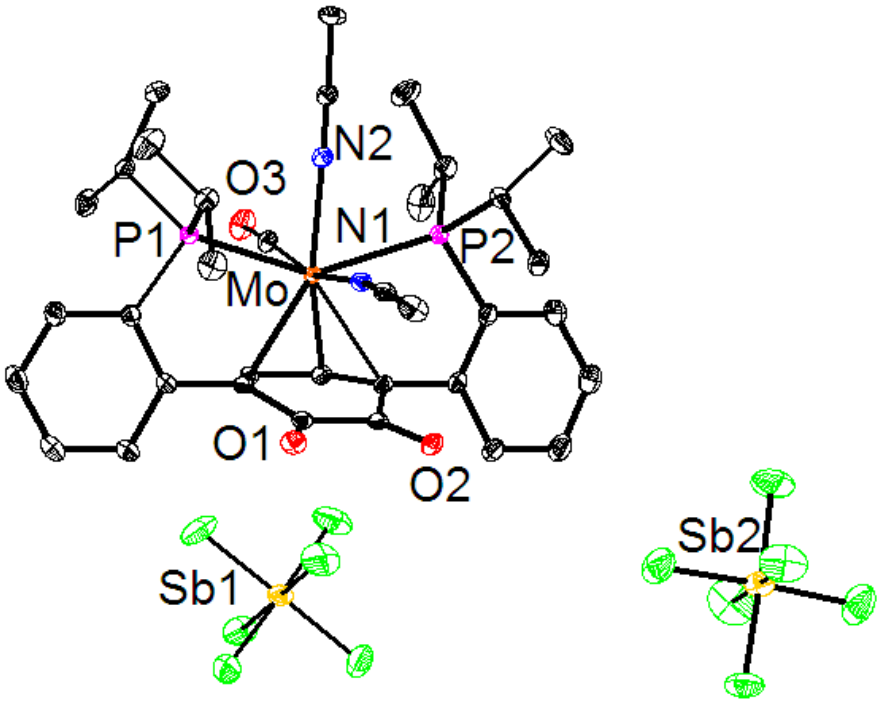


**Figure 4.4.** Structural drawing of **4.5a•2NCMe** with 50% probability ellipsoids. Hydrogen atoms and solvent molecules are omitted for clarity. Carbon and fluorine atoms are shown in black and green, respectively.

**Special Refinement Details for 4.5a:** Two acetonitrile solvent molecules were highly disordered and could not be adequately modeled even with constraints. The electron density of these molecules was removed using the "solvent mask" function in Olex2.

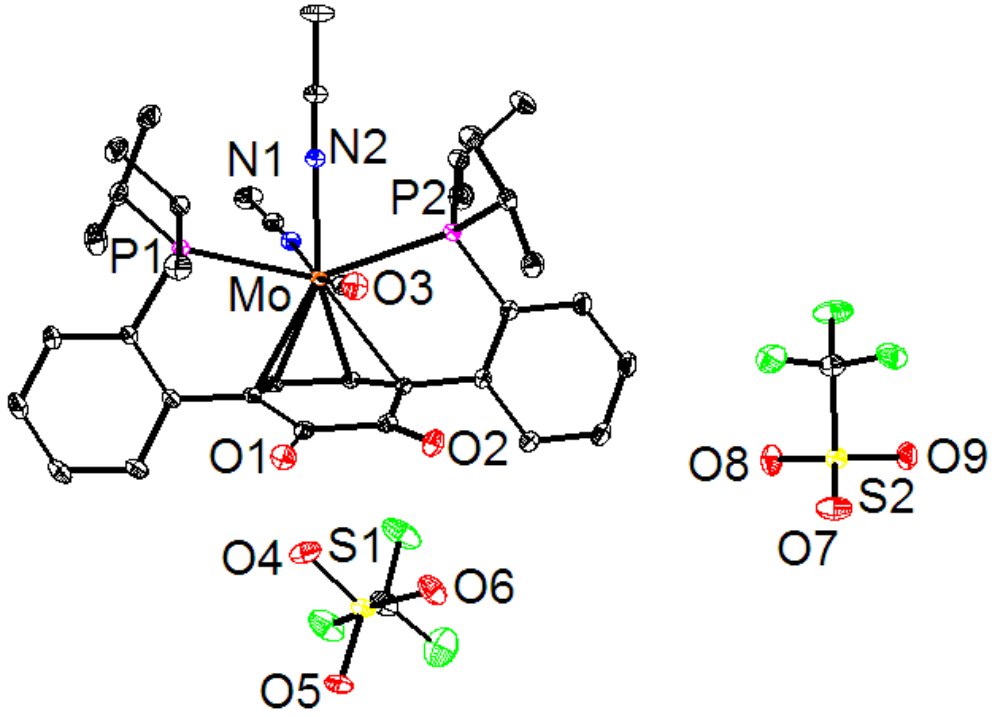


**Figure 4.5.** Structural drawing of **4.5b** with 50% probability ellipsoids. Hydrogen atoms are omitted for clarity. Carbon and fluorine atoms are shown in black and green, respectively.

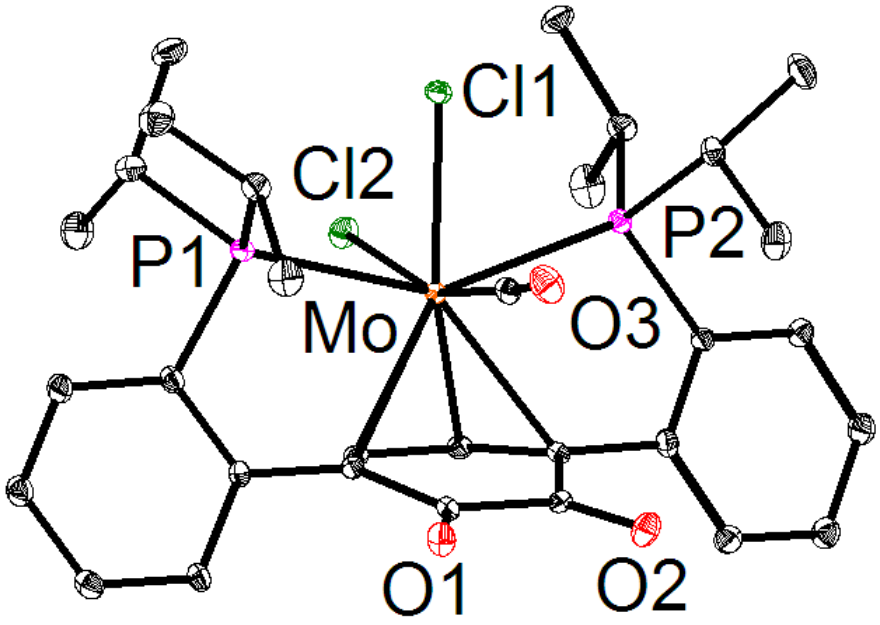


**Figure 4.6.** Structural drawing of **4.6** with 50% probability ellipsoids. Hydrogen atoms are omitted for clarity. Carbon atoms are shown in black.

## REFERENCES


[1] a) J. A. Cracknell, K. A. Vincent, F. A. Armstrong, *Chem. Rev.* **2008**, *108*, 2439-2461; b) R. Borup, J. Meyers, B. Pivovar, Y. S. Kim, R. Mukundan, N. Garland, D. Myers, M. Wilson, F. Garzon, D. Wood, P. Zelenay, K. More, K. Stroh, T. Zawodzinski, J. Boncella, J. E. McGrath, M. Inaba, K. Miyatake, M. Hori, K. Ota, Z. Ogumi, S. Miyata, A. Nishikata, Z. Siroma, Y. Uchimoto, K. Yasuda, K.-i. Kimijima, N. Iwashita, *Chem. Rev.* **2007**, *107*, 3904-3951; c) S. B. Adler, *Chem. Rev.* **2004**, *104*, 4791-4844; d) M. Costas, M. P. Mehn, M. P. Jensen, L. Que, *Chem. Rev.* **2004**, *104*, 939-986; e) B. E. Schultz, S. I. Chan, *Annu. Rev. Biophys. Biomol. Struct.* **2001**, *30*, 23-65; f) D. A. Proshlyakov, M. A. Pressler, C. DeMaso, J. F. Leykam, D. L. DeWitt, G. T. Babcock, *Science* **2000**, *290*, 1588-1591; g) I. Schlichting, J. Berendzen, K. Chu, A. M. Stock, S. A. Maves, D. E. Benson, R. M. Sweet, D. Ringe, G. A. Petsko, S. G. Sligar, *Science* **2000**, *287*, 1615-1622; h) S. Ferguson-Miller, G. T. Babcock, *Chem. Rev.* **1996**, *96*, 2889-2908; i) M. Sono, M. P. Roach, E. D. Coulter, J. H. Dawson, *Chem. Rev.* **1996**, *96*, 2841-2888; j) G. T. Babcock, M. Wikstrom, *Nature* **1992**, *356*, 301-309.

[2] a) J. Stubbe, D. G. Nocera, C. S. Yee, M. C. Y. Chang, *Chem. Rev.* **2003**, *103*, 2167-2202; b) J. W. Whittaker, *Chem. Rev.* **2003**, *103*, 2347-2364.

[3] a) J. Barber, *Inorg. Chem.* **2008**, *47*, 1700-1710; b) T. J. Meyer, M. H. V. Huynh, H. H. Thorp, *Angew. Chem. Int. Ed.* **2007**, *46*, 5284-5304; c) A. Osyczka, C. C. Moser, P. L. Dutton, *Trends Biochem. Sci.* **2005**, *30*, 176-182; d) E. A. Berry, M. Guergova-Kuras, L.-s. Huang, A. R. Crofts, *Annu. Rev. Biochem.* **2000**, *69*, 1005-1075; e) M. Y. Okamura, M. L. Paddock, M. S. Graige, G. Feher, *Biochimica et Biophysica Acta (BBA) - Bioenergetics* **2000**, *1458*, 148-163; f) G. Feher, J. P. Allen, M. Y. Okamura, D. C. Rees, *Nature* **1989**, *339*, 111-116.

[4] a) M. R. DeFelippis, C. P. Murthy, F. Broitman, D. Weinraub, M. Faraggi, M. H. Klapper, *J. Phys. Chem.* **1991**, *95*, 3416-3419; b) A. Harriman, *J. Phys. Chem.* **1987**, *91*, 6102-6104; c) S. V. Jovanovic, A. Harriman, M. G. Simic, *J. Phys. Chem.* **1986**, *90*, 1935-1939.

[5] a) Y. Hui, E. L. K. Chng, C. Y. L. Chng, H. L. Poh, R. D. Webster, *J. Am. Chem. Soc.* **2009**, *131*, 1523-1534; b) M. Quan, D. Sanchez, M. F. Wasylkiw, D. K. Smith, *J. Am. Chem. Soc.* **2007**, *129*, 12847-12856.

[6] a) L. Vogt, D. J. Vinyard, S. Khan, G. W. Brudvig, *Curr. Opin. Chem. Biol.* **2015**, *25*, 152-158; b) T. J. Auvil, A. G. Schafer, A. E. Mattson, *Eur. J. Org. Chem.* **2014**, *2014*, 2633-2646; c) A. G. Slater, L. M. A. Perdigão, P. H. Beton, N. R. Champness, *Acc. Chem. Res.* **2014**, *47*, 3417-3427.

[7] a) J. M. Maier, P. Li, J. Hwang, M. D. Smith, K. D. Shimizu, *Journal of the American Chemical Society* **2015**, *137*, 8014-8017; b) A. S. Mahadevi, G. N. Sastry, *Chemical Reviews* **2013**, *113*, 2100-2138.

[8] a) R. Amorati, S. Menichetti, C. Viglianisi, M. C. Foti, *Chem. Commun.* **2012**, *48*, 11904-11906; b) R. Amorati, L. Valgimigli, *Org. Biomol. Chem.* **2012**, *10*, 4147-4158.

[9] a) E. M. D'Amato, C. N. Neumann, T. Ritter, *Organometallics* **2015**; b) P. Ricci, K. Krämer, I. Larrosa, *Journal of the American Chemical Society* **2014**, *136*, 18082-18086; c) P. Ricci, K. Krämer, X. C. Cambeiro, I. Larrosa, *Journal of the American Chemical*

*Society* **2013**, *135*, 13258-13261; d) A. R. Pape, K. P. Kaliappan, E. P. Kündig, *Chemical Reviews* **2000**, *100*, 2917-2940.

[10] a) J. W. Walton, J. M. J. Williams, *Chemical Communications* **2015**, *51*, 2786-2789; b) M. Rosillo, G. Dominguez, J. Perez-Castells, *Chemical Society Reviews* **2007**, *36*, 1589-1604; c) K. Kamikawa, M. Uemura, *Synlett* **2000**, *2000*, 0938-0949; d) H. Amouri, J. Vaissermann, M. N. Rager, Y. Besace, *Inorg. Chem.* **1999**, *38*, 1211-1215; e) A. J. M. Miller, W. Kaminsky, K. I. Goldberg, *Organometallics* **2014**, *33*, 1245-1252.

[11] a) S. B. Kim, R. D. Pike, D. A. Sweigart, *Acc. Chem. Res.* **2013**, *46*, 2485-2497; b) J. Moussa, H. Amouri, *Angew. Chem. Int. Ed.* **2008**, *47*, 1372-1380; c) J. A. Reingold, S. Uk Son, S. Bok Kim, C. A. Dullaghan, M. Oh, P. C. Frake, G. B. Carpenter, D. A. Sweigart, *Dalton Trans.* **2006**, 2385-2398.

[12] a) K. Umehara, S. Kuwata, T. Ikariya, *J. Am. Chem. Soc.* **2013**, *135*, 6754-6757; b) C. T. Carver, B. D. Matson, J. M. Mayer, *J. Am. Chem. Soc.* **2012**, *134*, 5444-5447; c) C. Costentin, S. Drouet, M. Robert, J.-M. Savéant, *Science* **2012**, *338*, 90-94; d) J. F. Hull, Y. Himeda, W.-H. Wang, B. Hashiguchi, R. Periana, D. J. Szalda, J. T. Muckerman, E. Fujita, *Nat Chem* **2012**, *4*, 383-388; e) C. Gunanathan, D. Milstein, *Acc. Chem. Res.* **2011**, *44*, 588-602; f) S. W. Kohl, L. Weiner, L. Schwartsburd, L. Konstantinovski, L. J. W. Shimon, Y. Ben-David, M. A. Iron, D. Milstein, *Science* **2009**, *324*, 74-77; g) M. Rakowski DuBois, D. L. DuBois, *Chem. Soc. Rev.* **2009**, *38*, 62-72.

[13] a) M. Wang, J. England, T. Weyhermüller, K. Wieghardt, *Inorg. Chem.* **2014**, *53*, 2276-2287; b) O. R. Luca, R. H. Crabtree, *Chem. Soc. Rev.* **2013**, *42*, 1440-1459; c) J. England, C. C. Scarborough, T. Weyhermüller, S. Sproules, K. Wieghardt, *Eur. J. Inorg. Chem.* **2012**, *2012*, 4605-4621; d) V. Lyaskovskyy, B. de Bruin, *ACS Catalysis* **2012**, *2*, 270-279; e) V. K. K. Praneeth, M. R. Ringenberg, T. R. Ward, *Angew. Chem. Int. Ed.* **2012**, *51*, 10228-10234; f) C. C. Scarborough, K. M. Lancaster, S. DeBeer, T. Weyhermüller, S. Sproules, K. Wieghardt, *Inorg. Chem.* **2012**, *51*, 3718-3732; g) R. Eisenberg, H. B. Gray, *Inorg. Chem.* **2011**, *50*, 9741-9751; h) P. J. Chirik, K. Wieghardt, *Science* **2010**, *327*, 794-795; i) M. R. Haneline, A. F. Heyduk, *J. Am. Chem. Soc.* **2006**, *128*, 8410-8411; j) C. Stanciu, M. E. Jones, P. E. Fanwick, M. M. Abu-Omar, *J. Am. Chem. Soc.* **2007**, *129*, 12400-12401; k) C. G. Pierpont, *Coord. Chem. Rev.* **2001**, *216–217*, 99-125.

[14] a) F. Lu, R. A. Zarkesh, A. F. Heyduk, *Eur. J. Inorg. Chem.* **2012**, *2012*, 467-470; b) J. J. Warren, T. A. Tronic, J. M. Mayer, *Chemical Reviews* **2010**, *110*, 6961-7001; c) B. W. Purse, L.-H. Tran, J. Piera, B. Åkermark, J.-E. Bäckvall, *Chemistry – A European Journal* **2008**, *14*, 7500-7503; d) J. P. Collman, N. K. Devaraj, R. A. Decréau, Y. Yang, Y.-L. Yan, W. Ebina, T. A. Eberspacher, C. E. D. Chidsey, *Science* **2007**, *315*, 1565-1568; e) C. J. Chang, L. L. Chng, D. G. Nocera, *J. Am. Chem. Soc.* **2003**, *125*, 1866-1876; f) P. Chaudhuri, M. Hess, J. Müller, K. Hildenbrand, E. Bill, T. Weyhermüller, K. Wieghardt, *J. Am. Chem. Soc.* **1999**, *121*, 9599-9610.

[15] J. T. Henthorn, S. Lin, T. Agapie, *J. Am. Chem. Soc.* **2015**, *137*, 1458-1464.

[16] M. Oh, G. B. Carpenter, D. A. Sweigart, *Organometallics* **2002**, *21*, 1290-1295.

[17] T. S. Teets, J. A. Labinger, J. E. Bercaw, *Organometallics* **2013**, *32*, 5530-5545.

[18] Both oxidation events are shown for the purple and red traces in Figure 2. In the blue and green traces, the second event was further removed from the first, and thus have been omitted for clarity.
[19] F. G. Bordwell, J. Cheng, *J. Am. Chem. Soc.* **1991**, *113*, 1736-1743.
[20] B. J. Koo, M. Huynh, R. L. Halbach, J. Stubbe, D. G. Nocera, *J. Am. Chem. Soc.* **2015**, *137*, 11860-11863.
[21] Y. Mori, Y. Sakaguchi, H. Hayashi, *The Journal of Physical Chemistry A* **2000**, *104*, 4896-4905.
[22] P. S. Singh, D. H. Evans, *The Journal of Physical Chemistry B* **2006**, *110*, 637-644.
[23] Calculated using gas phase BDFE of 42.7 kcal/mol and $\Delta G_{solv}^{\circ}(H\bullet) = \Delta G_{solv}^{\circ}(H_2) = 5.12$ kcal/mol. This calculation assumes $\Delta G_{solv}^{\circ}(O_2) = \Delta G_{solv}^{\circ}(\bullet OOH)$, which may not be valid. For further discussion of converting gas phase BDFE into solution phase values, see [14b].
[24] Pangborn, A.B.; Giardell, M.A.; Grubbs, R.H.; Rosen, R.K.; Timmers, F.J. *Organometallics* **1996**, *15*, 1518.
[25] Podgorsek, A.; Iskra, J. *Molecules* **2010**, *15*, 2857–2871.
[26] Schlosser, M.; Hartman, R. *Angew. Chem., Int. Ed.* **1973**, *12*, 508−509.
[27] APEX2, Version 2 User Manual, M86-E01078, Bruker Analytical X-ray Systems, Madison, WI, June 2006.
[28] Sheldrick, G.M. "SADABS (version 2008/1): Program for Absorption Correction for Data from Area Detector Frames", University of Göttingen, 2008.
[29] Sheldrick, G.M. (2008). Acta Cryst. A64, 112-122.
[30] Dolomanov, O.V. (2009). OLEX2. J. Appl. Cryst. **42**, 339-341.
[31] Brandenburg, K. (1999). DIAMOND. Crystal Impact GbR, Bonn, Germany.

# CHAPTER 5

E–X Bond Activation and Other Reactivity

E–X Bond Activation and Small Molecule Reactivity Facilitated by Molybdenum Quinonoid Complexes

## ABSTRACT

Mo-quinonoid complexes with coordinatively unsaturated or substitutionally labile ligands were targeted for inner-sphere small molecule reactivity. $Mo^0$-quinone compound **5.6a** demonstrated a labile MeCN ligand that could be displaced by nucleophiles such as azide. Compound **5.6a** was also found to react with $Me_3SiCl$, $H_2$, and $PhSiH_3$ to yield Mo–Cl and Mo–H products. Compound **5.6a** proved effective as a hydrosilylation pre-catalyst for various aldehydes. Initial investigations suggest a Lewis-base catalyzed mechanism.

## INTRODUCTION

Metal-ligand cooperativity can lead to interesting and diverse reactivity,[1] with activation of small molecules such as $H_2$ or silane across metal-ligand bonds well documented.[2] Shvo's catalyst is an unusual subset of such complexes in that the small molecule activation occurs across a ligand that is bound orthogonal to the metal.[3] A similar class of transition metal complexes are the quinonoid complexes.[4] While π-bound transition metal quinonoid complexes have been previously studied, they typically are coordinatively saturated by cyclopentadienyl or carbonyl ligands, thus prohibiting inner-sphere bond activation. We have recently reported the synthesis of a series of π-bound $Mo^0$-quinonoid complexes and demonstrated their ability to transfer two $H^+$ (as well as $R_2Si^{2+}$, $ArB^{2+}$, and $Me^+$) and two electrons to $O_2$. Herein we report the activation of E–X bonds across a Mo-quinonoid fragment and demonstrate catalytic hydrosilylation of aldehydes.

## RESULTS AND DISCUSSION

**Scheme 5.1.** Synthesis of $Mo^0$-catecholate compounds **5.2** and **5.4a,b**.

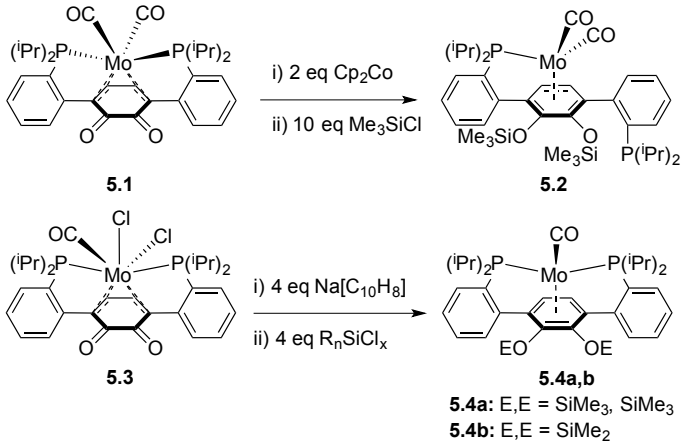


In an effort to access reduced Mo-quinonoid complexes with coordinately unsaturated metal centers or substitutionally labile metal-bound ligands, chemical reduction of oxidized compounds **5.1** and **5.3** were pursued (Scheme 5.1). Treatment of **5.1** with 2 equivalents of $Cp_2Co$ followed by quenching with excess $Me_3SiCl$ results in reduction of the quinonoid moiety from (formally) quinone to catecholate. Reduction results in a haptotropic shift of the metal-quinonoid interaction from $\eta^4$ to $\eta^6$ concomitant with dissociation of a phosphine ligand, as evidenced by the asymmetric $^1H$ and $^{31}P$ NMR spectra, suggestive of a $C_1$ symmetric product. The $^{31}P$ NMR spectrum reveals two singlets, the downfield peak at ca. 95 ppm assigned as Mo-bound phosphine, and the upfield peak at ca. -1 ppm consistent with unbound phosphine. Additionally, the $^1H$ NMR spectrum reveals a doublet and a doublet of doublets in the quinonoid C–*H* region each integrating to 1 H, assigned as coupling between two chemically distinct protons ($^3J_{HaHb}$ = 5.6 Hz), as well as coupling to phosphine ($^3J_{PH}$ = 1.8 Hz), consistent

with the assigned asymmetric product. The $^{1}H$ and $^{31}P$ NMR spectra are also consistent with the analogous parent compound recently reported.

Starting from the more oxidized $Mo^{II}$-quinone compound **5.3**, four-electron reduction to $Mo^{0}$-catecholate can be achieved using four equivalents of sodium naphthalenide in THF, followed by quenching with excess $Me_3SiCl$ or $Me_2SiCl_2$ to afford the $C_s$ symmetric products **5.4a** and **5.4b**, respectively. As in **5.2**, reduction results in a haptotropic shift of the metal-quinonoid interaction from $\eta^4$ to $\eta^6$, while loss of chloride rather than phosphine yields the coordinatively satured mono-carbonyl compounds **5.4a** and **5.4b**. The $^{1}H$ and $^{31}P$ NMR spectra of **5.4a** and **5.4b** are also consistent with the analogous parent compound previously reported. These results suggest that for the reduced quinonoid fragment (catechol/catecholate), the $\eta^6$ metal-quinonoid interaction is favored over $\eta^4$ or $\eta^2$, and in the resulting Mo-carbonyl products (**5.2**, **5.4a,b**) the metal remains coordinatively saturated. Thus, it is postulated that maintaining the $\eta^4$ Mo-quinonoid interaction may facilitate access to a coordinatively unsaturated metal center.

**Scheme 5.2.** Synthesis of $Mo^{0}$-quinone complex **5.6a**.

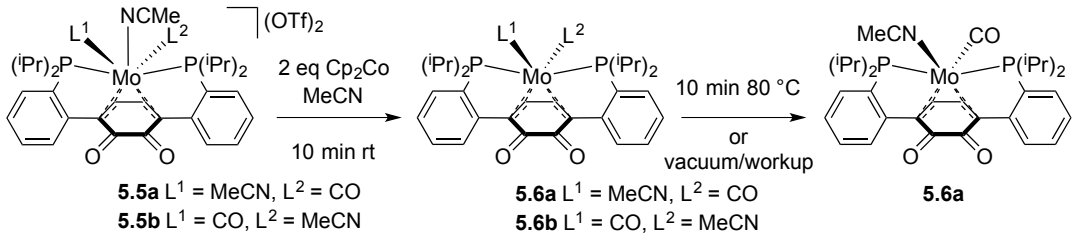


Two-electron reduction of the $Mo^{II}$-quinone species **5.5a,b** can be achieved with two equivalents of $Cp_2Co$ to yield the formally $Mo^{0}$-quinone products **5.6a,b** (Scheme 5.2). The reduction initially yields a mixture of two products as determined by $^{31}P$ NMR

spectroscopy, analogous to the two isomers of starting material **5.5a,b**. This mixture can be thermally converted to a single isomer over the course of several minutes at 80 °C, or alternatively after pumping down the solution and workup, with compound **5.6a** isolated as the single product. An XRD study of compound **5.6a** is presented in Figure 5.1. Upon two-electron reduction, the quinonoid C–O bond lengths increase only slightly from 1.22 Å in **5.5a** to 1.24 Å in **5.6a**, consistent with C–O double bonds and formal assignment as $Mo^0$-quinone.

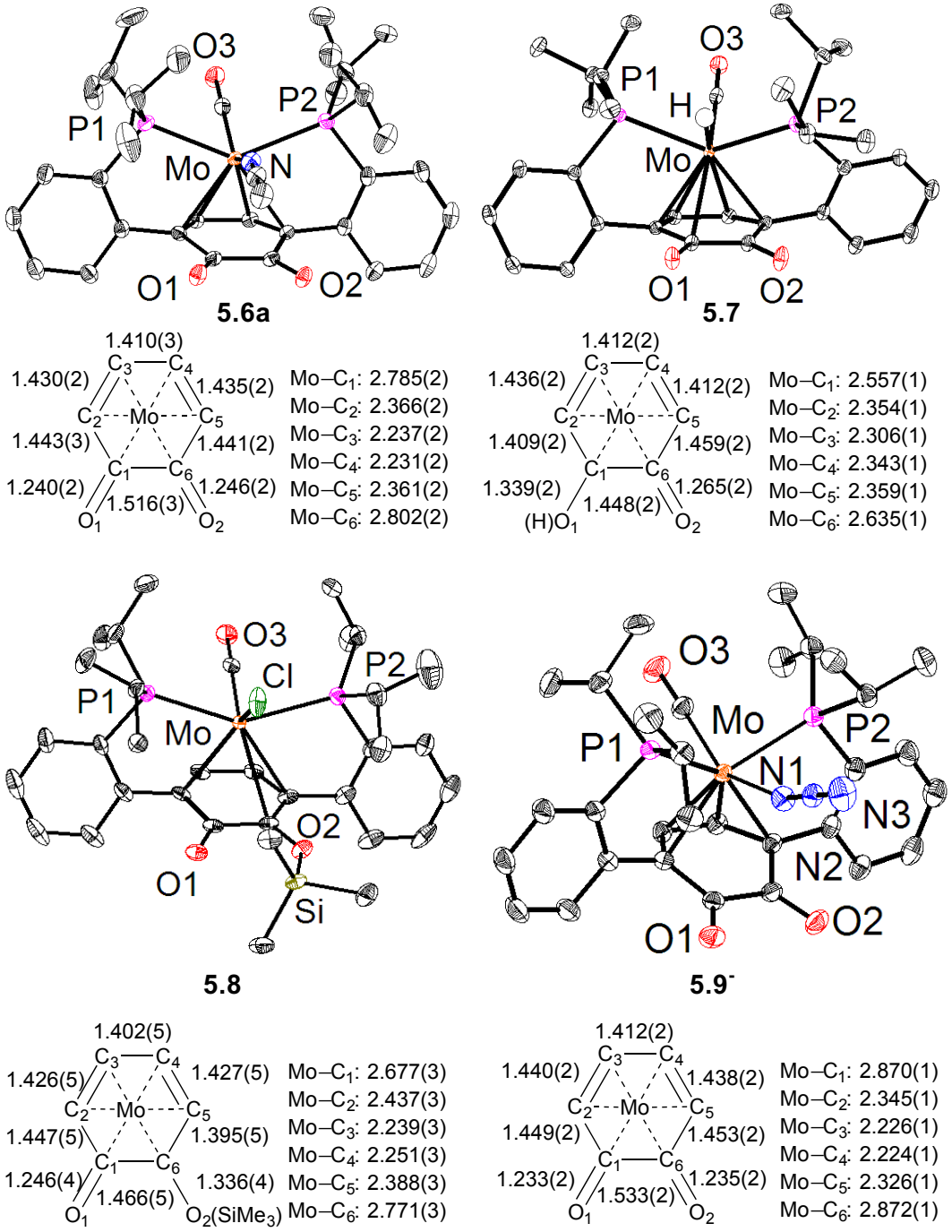


**Figure 5.1.** Solid-state structures of **5.6a**, **5.7**, **5.8** and **5.9**$^{-}$ with 50% probability thermal ellipsoids. Solvent molecules, hydrogen atoms (except hydride in **5.7**), and outer-sphere

cations are omitted for clarity. Carbon atoms are depicted in black. Select bond distances are given in Å.

**Scheme 5.3.** Reactivity of **5.6** with $N_3^-$, $Me_3SiCl$, and $H_2$.

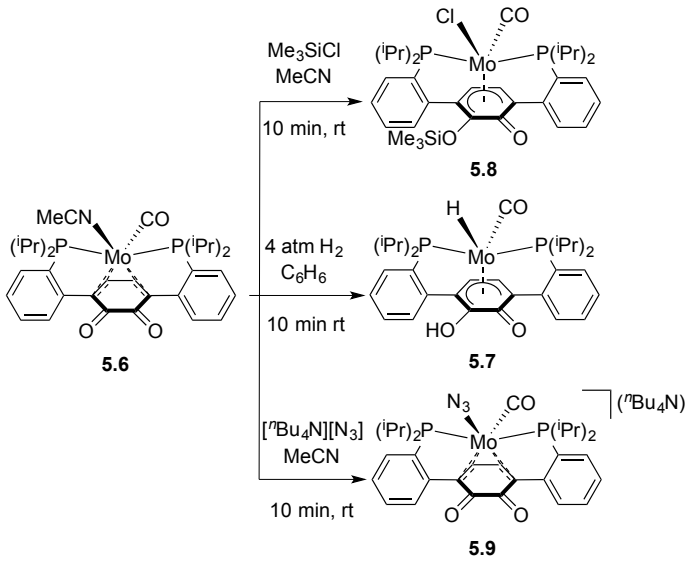


The MeCN ligand in compound **5.6a** was found to be labile and readily substituted with azide upon reaction with $[^nBu_4N^+][N_3^-]$ to yield **5.9**. Reactivity of compound **5.6a** was expanded to neutral small molecules, with $Me_3SiCl$ yielding the Mo-Cl compound **5.8**. Next, reactivity with $H_2$ was investigated. It was found that in $C_6D_6$ **5.6a** reacts with excess $H_2$ in minutes to yield a single new species **5.7**, resonating as a singlet at ca. 96 ppm in the $^{31}P$ NMR spectrum. The $^1H$ NMR spectrum of **5.7** exhibits an upfield triplet ($^2J_{HP}$ = 72 Hz) at ca. -2.4 ppm, as well as a broad downfield singlet at ca. 8.8 ppm, each integrating as 1 H, assigned to Mo-hydride and quinonoid O–H moieties, respectively. The solid state structure confirms the spectroscopic assignments, revealing one short quinonoid C–O bond (1.26 Å) and one long quinonoid C–O bond (1.33 Å), consistent with the hydride semiquinone assignment. Reaction of **5.6a** with $H_2$ to yield

**5.7** formally involves intramolecular reduction of the quinonoid moiety by the metal center and heterolytic cleavage of $H_2$ across the Mo-quinonoid fragment. This type of $H_2$ reactivity is reminiscent of Shvo's catalyst and the pyridine diphosphine systems studied by Milstein and coworkers, in that the (formally) proton resulting from $H_2$ heterolysis is accepted by an atom of the ligand not directly bound to the metal center facilitated by electron movement through the ligand framework.

**Scheme 5.4.** Proposed reactivity of **5.6a** with $PhSiH_3$ in $C_6H_6$.

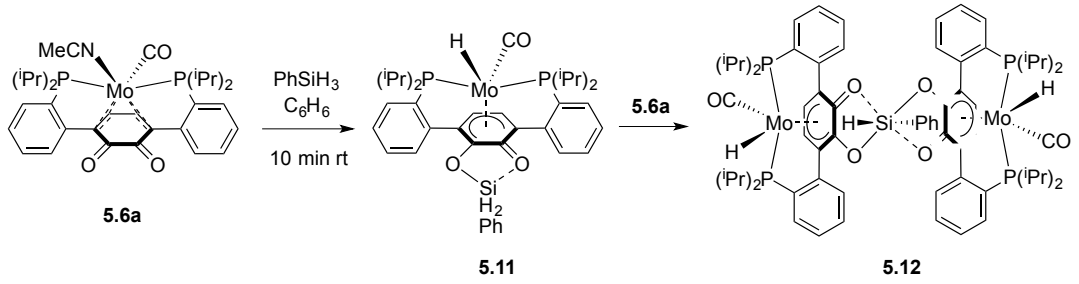


Compound **5.7** was found unreactive toward (de)hydrogenation chemistry, thus reactivity of **5.6a** with other E–X bonds was investigated. It was found that **5.6a** reacts with $PhSiH_3$ in $C_6H_6$ at room temperature to yield a major new species spectroscopically similar to **5.7**. This new compound exhibits a singlet by $^{31}P$ NMR spectroscopy at ca. 94 ppm and a triplet ($^2J_{HP}$ = 70 Hz) in the $^1H$ NMR spectrum at ca. -2.6 ppm, consistent with formation of a hydride-semiquinone product. In analogy to **5.7**, initial Si–H activation is assumed to yield **5.11** (Scheme 5.4). In the case of **5.11**, coordination of the semiquinone C=O moiety to give a 5-coordinate hypervalent silicon center is anticipated to activate the remaining Si–H bonds for further reactivity. Reaction of **5.11** with a second equivalent of **5.6a** is postulated to yield the 6-coordinate hypervalent silicon di-Mo complex **5.12**. The remaining Si–H bond in **5.12** is anticipated to be even more activated compared to **5.11**, and in the absence of other suitable electrophiles may

react with Mo species in solution resulting in decomposition. After 2 hours at room temperature, a new singlet appears in the $^{31}P$ NMR spectrum at ca. -2.5 ppm consistent with unbound phosphine, corresponding to ca. 25% of material, with further growth of this peak over longer periods of time.

**Table 5.1.** Summary of benzaldehyde hydrosilylation reactivity.

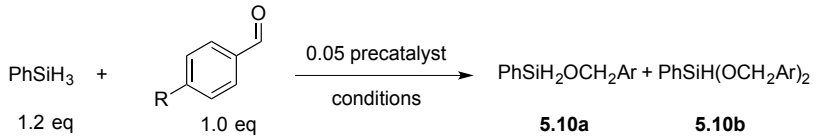


| Entry | R | Precatalyst | Solvent | Temperature (°C) | Time (hr) | Conversion (%)[a] | Ratio **5.10a/5.10b**[a] |
|---|---|---|---|---|---|---|---|
| 1 | H | **5.6a** | $C_6D_6$ | 20 | 48 | <5 | - |
| 2 | H | **5.6a** | $C_6D_6$ | 80 | 24 | 100 | 12 |
| 3 | $CF_3$ | **5.6a** | $C_6D_6$ | 80 | 12 | 100 | 14 |
| 4 | $CF_3$ | **5.6a** | 9:1 | 20 | 12 | 54 | 3.2 |
| 5 | $CF_3$ | **5.6a** | 3:1 | 20 | 12 | 65 | 3.0 |
| 6 | $CF_3$ | **5.6a** | 1:1 | 20 | 12 | 80 | 4.1 |
| 7 | $CF_3$ | **5.6a** | 1:3 | 20 | 12 | 94 | 7.8 |
| 8 | $CF_3$ | **5.6a** | $CD_3CN$ | 20 | 0.5 | 100 | 26 |
| 9 | H | **5.6a** | $CD_3CN$ | 20 | 5 | >95 | 17 |
| 10 | $NMe_2$ | **5.6a** | $CD_3CN$ | 20 | 26 | 92 | 13 |
| 11 | $CF_3$ | **5.5a/b** | $CD_3CN$ | 80 | 12 | 0 | - |
| 12 | $CF_3$ | **5.1** | $CD_3CN$ | 20 | 24 | 0 | - |
| 12 | $CF_3$ | **2.2g** | $CD_3CN$ | 20 | 24 | 0 | - |
| 13 | $CF_3$ | **LiO$^t$Bu** | $CD_3CN$ | 20 | 0.25 | 100 | >50 |

General conditions: 7.5 $\mu$mol of precatalyst, 150 $\mu$mol of substrate, and 280 $\mu$mol of $PhSiH_3$ were combined with 0.5 mL of solvent in J. Young NMR tube, monitoring by $^1H$ NMR spectroscopy over time. [a]Determined via NMR integration.

Based on these results, compound **5.6a** was investigated for catalytic hydrosilylation reactivity with substituted benzaldehydes (see Table 5.1). Initial reactions in $C_6D_6$ revealed negligible conversion at room temperature (Entry 1), but full conversion at 80 °C over the course of hours (Entry 2 and 3). Next, it was found that switching the

solvent to MeCN resulted in complete conversion within 30 minutes at room temperature (Entry 8). It was observed that modest conversion at room temperature could be achieved in $C_6D_6$ with the addition of MeCN (Entry 4), while increasing the ratio of MeCN to benzene results in increasing conversion (Entries 4–8). Electron withdrawing substituents were found to accelerate reactivity, while electron donating groups were found to slow reactivity (Entries 8–10). Finally, compounds **5.5a/b**, **5.1**, and **2.2g** were found to be ineffectual precatalysts under these conditions (Entries 11–13), while the strong Lewis base LiO$^t$Bu demonstrated catalytic competency (Entry 14). Additionally, while **5.6a** demonstrates Si–H activation in $C_6D_6$ to yield a Mo–H species as evidenced by $^1$H NMR spectroscopy, no Mo–H resonance is observed in $CD_3CN$.

**Scheme 5.5.** Proposed reactivity of **5.12** with aldehyde.

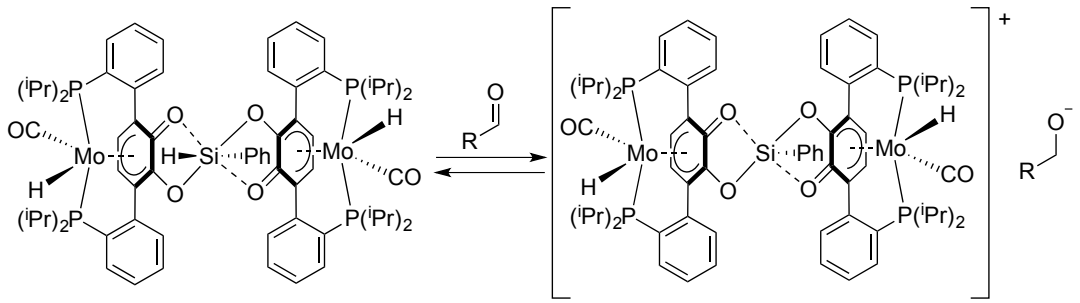


**5.12** **5.13**

Based on these results, two different Lewis base-catalyzed mechanisms for hydrosilylation are proposed for compound **5.6a**. The first mechanism which is operative in the absence of acetonitrile involves sequential Si–H bond activations to yield putative compound **5.12**, which contains an activated Si–H bond (Scheme 5.4). Compound **5.12** is proposed to react with aldehyde to generate the cation **5.13** (Scheme 5.5) and an alkoxide, the latter facilitating Lews base-catalyzed hydrosilylation. Indeed, small crystals grown from the catalytic mixture of **5.6a**/$PhSiH_3$/PhC(O)H (Table 5.1,

Entry 2) were found to be suitable for x-ray diffraction. The XRD study revealed the cationic structure of **5.13** (Figure 5.2), suggesting the loss of hydride from the proposed **5.12**. This proposed mechanism would also be consistent with the observation that addition of MeCN increases conversion, as increasing the polarity of the reaction medium would favor the formation of the charged **5.13** and alkoxide species.

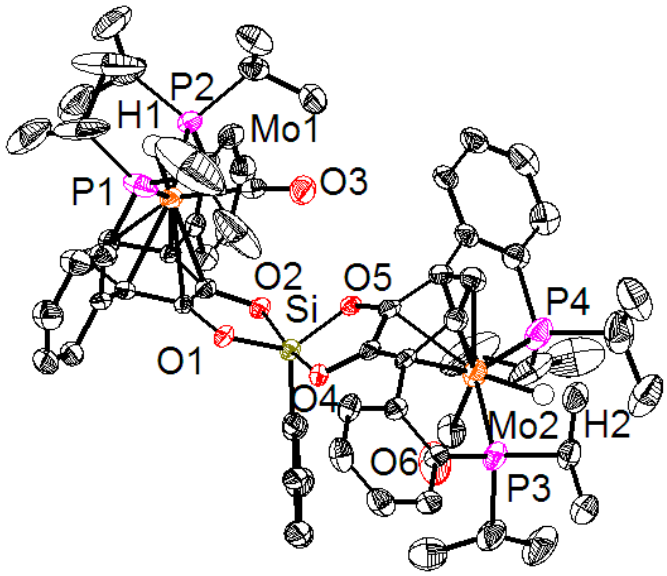


**5.13**$^{+}$

**Figure 5.2.** Solid-state structure of cation **5.13** with 50% probability thermal ellipsoids. Solvent molecules, hydrogen atoms (except hydrides), and outer-sphere anion omitted for clarity. Carbon atoms are depicted in black.

**Scheme 5.6.** Proposed reactivity of **5.6a** with $PhSiH_3$ in MeCN.

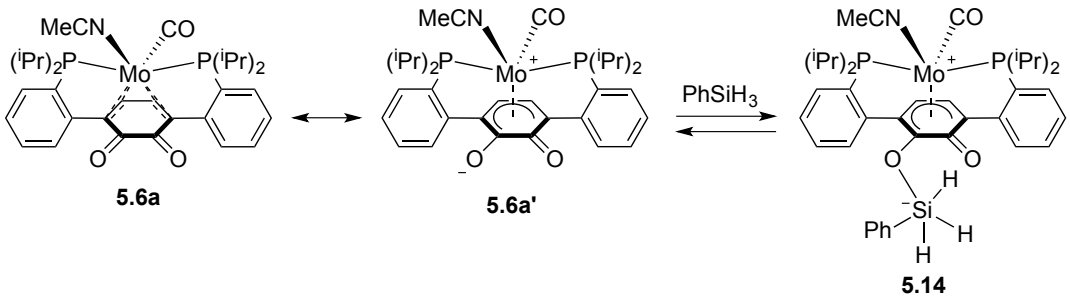


Alternatively, no evidence has been observed to suggest that Si–H bond activation occurs in MeCN, thus it is proposed that **5.6a** acts as nucleophile directly through redox tautomer **5.6a'** (Scheme 5.7). Nucleophilic attack of **5.6a'** on $PhSiH_3$ would generate the zwitter-ion **5.13**, which is proposed to be the active hydrosilylation species. In either case, it is proposed that the active catalyst is generated through coordination of the quinonoid oxygen atoms to the Si center of the silane, which generates more hydridic Si–H bonds. In the absence of MeCN, it is proposed that the activated Si–H bond transfers the hydride to Mo to yield first **5.11** then **5.12**. While in the presence of MeCN the activated Si–H bond may still react with the metal center (as unidentified species are generated over time as observed by $^{31}P$ NMR spectroscopy), it is proposed that direct reactivity with substrate occurs due to lack of MeCN dissociation from the metal center.

## CONCLUSIONS

In summary, $Mo^0$- and $Mo^{II}$-quinone compounds were successfully reduced by two- and four-electrons, respectively, to yield coordinatively saturated $Mo^0$-catecholate species. Selective two-electron reduction of a $Mo^{II}$-quinone complex was found to afford a $Mo^0$-quinone complex with a substitutionally labile MeCN ligand. Compound **5.6a** was shown to react with $Me_3SiCl$, $PhSiH_3$, and $H_2$ to yield Mo–Cl and Mo–H products, demonstrating the first examples of E–X bond activation in π-bound Mo-quinonoid complexes. Compound **5.6a** was also shown to be an active pre-catalyst for the hydrosilylation of aldehydes, with initial studies suggesting a Lewis base-catalyzed mechanism.

## EXPERIMENTAL SECTION

### General Considerations

Unless indicated otherwise, reactions performed under inert atmosphere were carried out in oven-dried glassware in a glovebox under a nitrogen atmosphere purified by circulation through RCI-DRI 13X-0408 Molecular Seives 13X, 4x8 Mesh Beads and BASF PuriStar® Catalyst R3-11G, 5x3 mm (Research Catalysts, Inc.). Solvents for all reactions were purified by Grubbs' method.[6] $C_6D_6$ was purchased from Cambridge Isotope Laboratories and vacuum distilled from sodium benzophenone ketyl. $CD_3CN$, was also purchased from Cambridge Isotope Laboratories and distilled from $CaH_2$ prior to use. Alumina and Celite were activated by heating under vacuum at 200 °C for 24 hours. $^1H$ and $^{31}P$ NMR spectra were recorded on Varian Mercury 300 MHz spectrometers at ambient temperature, unless denoted otherwise. $^1H$ NMR chemical shifts are reported with respect to internal solvent: 7.16 ppm for $C_6D_6$, and 1.94 ppm for $CD_3CN$, respectively. $^{31}P$ NMR chemical shifts are reported with respect to an external standard of 85% $H_3PO_4$ (0.0 ppm).

Unless otherwise noted all chemical reagents were purchased from commercial sources and used without further purification.

**Synthesis of [(1,4-bis(2-(diisopropylphosphino)phenyl)-2,3-bis(trimethylsilyl)catechol)]dicarbonylmolybdenum(0) (5.2)**

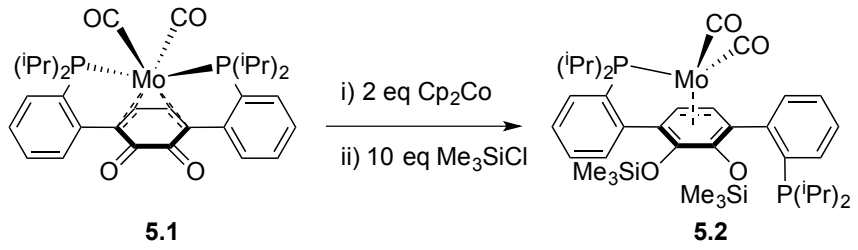


**5.1** **5.2**

A solution of $Cp_2Co$ (0.0309 g, 0.163 mmol) in THF (ca. 2 mL) was added to a stirred suspension of **5.1** (0.0503 g, 0.0780 mmol) in THF (ca. 3 mL). The mixture was stirred for 5 minutes at room temperature, generating a homogeneous solution. $Me_3SiCl$ (0.100 mL, 0.788 mmol) was added neat, immediately generating a light precipitate. After stirring for 30 minutes at room temperature, the heterogeneous mixture was filtered through celite and the filtrate concentrated under vacuum. The residue was reconstituted in $C_6H_6$ (ca. 4 mL) , filtered through celite, and again concentrated under vacuum to yield 0.0542 g (88%) of the desired product. $^1$H NMR (300 MHz, $C_6D_6$, 25 °C), δ(ppm): 7.92 (m, 1 H, Ar-C*H*), 7.27 (m, 2 H, Ar-C*H*), 6.94-7.11 (m, 5 H, Ar-C*H*), 4.89 (d, $J_{HH'}$ = 5.6 Hz, 1 H, Ar-$C_1H$), 4.02 (dd, $J_{HH'}$ = 5.6 Hz , $J_{HP}$ = 1.8 Hz, 1 H, Ar-$C_1$'*H*), 2.57 (m, 1 H, PC*H*$(CH_3)_2$), 2.32 (m, 1 H, PC*H*$(CH_3)_2$), 2.10 (m, 1 H, PC*H*$(CH_3)_2$), 1.75 (m, 1 H, PC*H*$(CH_3)_2$), 1.32 (m, 6 H, PCH(C$H_3)_2$), 1.14 (m, 9 H, PCH(C$H_3)_2$), 0.97 (m, 3 H, PCH(C$H_3)_2$), 0.86 (m, 3 H, PCH(C$H_3)_2$), 0.28 (m, 9 H, Si(C$H_3)_3$), 0.12 (m, 9 H, Si(C$H_3)_3$). $^{31}$P NMR (121 MHz, $C_6D_6$, 25 °C), δ(ppm): 94.70 (s, Mo-*P*), -1.26 (s, unbound *P*).

**Synthesis of [(1,4-bis(2-(diisopropylphosphino)phenyl)-2,3-dimethylsilylene)catechol)]carbonylmolybdenum(0) (5.4a)**

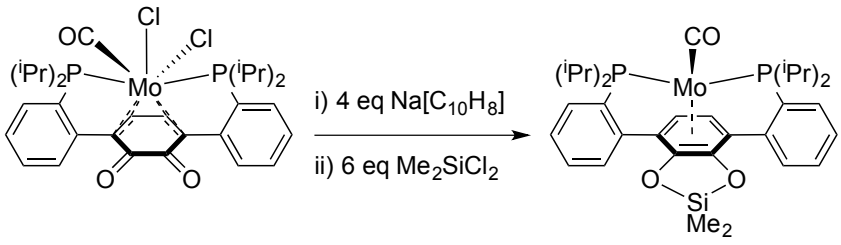


**5.3** **5.4b**

A dark green solution of $Na[C_{10}H_8]$ was generated by stirring naphthalene (0.0203 g, 0.158 mmol) in THF (ca. 2 mL) over Na mirror for 30 minutes. The $Na[C_{10}H_8]$ solution was then added to a stirred suspension of **5.3** (0.0199 g, 0.0309 mmol) in THF (ca. 3 mL). The mixture was stirred for 60 minutes at room temperature, generating a homogeneous solution. $Me_2SiCl_2$ (0.0260 g, 0.201 mmol) was then added neat, immediately generating a light precipitate. After stirring for 30 minutes at room temperature, the heterogeneous mixture was filtered through celite and the filtrate concentrated under vacuum. The residue was reconstituted in $C_6H_6$ (ca. 4 mL) , filtered through celite, and again concentrated under vacuum to yield 0.0445 g of the desired product with naphthalene as an orange solid. $^1$H NMR (300 MHz, $C_6D_6$, 25 °C), δ(ppm): 7.4 (d, 7 Hz, 2 H, Ar-C*H*), 7.28 (m, 2 H, Ar-C*H*), 7.0-7.15 (m, 4 H, Ar-C*H*), 4.34 (t, $J_{HP}$ = 1.8 Hz, 2 H, Ar-$C_1H$), 2.53 (m, 2 H, PC*H*$(CH_3)_2$), 2.18 (m, 2 H, PC*H*$(CH_3)_2$), 1.41 (m, 6 H, PCH(C*H*$_3)_2$), 1.10 (m, 12 H, PCH(C*H*$_3)_2$), 0.97 (m, 6 H, PCH(C*H*$_3)_2$), 0.50 (m, 3 H, Si(C*H*$_3$)), 0.14 (m, 3 H, Si(C*H*$_3$)). $^{31}$P NMR (121 MHz, $C_6D_6$, 25 °C), δ(ppm): 82.60 (s).

**Synthesis of [(1,4-bis(2-(diisopropylphosphino)phenyl)-2,3-bis(trimethylsilyl)catechol)]carbonylmolybdenum(0) (5.4b)**

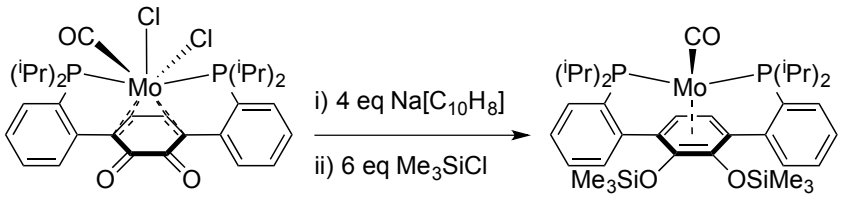


**5.3** **5.4b**

A dark green solution of $Na[C_{10}H_8]$ was generated by stirring naphthalene (0.0203 g, 0.158 mmol) in THF (ca. 2 mL) over Na mirror for 30 minutes. The $Na[C_{10}H_8]$ solution was then added to a stirred suspension of **5.3** (0.0190 g, 0.0295 mmol) in THF (ca. 3 mL). The mixture was stirred for 60 minutes at room temperature, generating a homogeneous solution. $Me_3SiCl$ (0.0210 g, 0.193 mmol) was then added neat, immediately generating a light precipitate. After stirring for 30 minutes at room temperature, the heterogeneous mixture was filtered through celite and the filtrate concentrated under vacuum. The residue was reconstituted in $C_6H_6$ (ca. 4 mL) , filtered through celite, and again concentrated under vacuum to yield 0.0479 g of the desired product with naphthalene as an orange solid. $^1$H NMR (300 MHz, $C_6D_6$, 25 °C), δ(ppm): 7.4 (d, 7 Hz, 2 H, Ar-C*H*), 7.28 (m, 2 H, Ar-C*H*), 7.0-7.15 (m, 4 H, Ar-C*H*), 4.34 (t, $J_{HP}$ = 1.8 Hz, 2 H, Ar-$C_1$*H*), 2.53 (m, 2 H, PC*H*$(CH_3)_2$), 2.18 (m, 2 H, PC*H*$(CH_3)_2$), 1.41 (m, 6 H, PCH(C*H*$_3)_2$), 1.10 (m, 12 H, PCH(C*H*$_3)_2$), 0.97 (m, 6 H, PCH(C*H*$_3)_2$), 0.50 (m, 3 H, Si(C*H*$_3$)), 0.14 (m, 3 H, Si(C*H*$_3$)). $^{31}$P NMR (121 MHz, $C_6D_6$, 25 °C), δ(ppm): 80.77 (s).

**Synthesis of [(1,4-bis(2-(diisopropylphosphino)phenyl)-2,3-quinone)]molybdenum(0)carbonyl(acetonitrile) (5.6)**

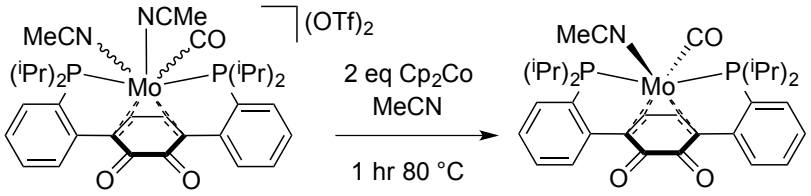


**5.5a/b** **5.6a**

Compound **5.5** (0.2321 g, 0.233 mmol) and $Cp_2Co$ (0.0867 g, 0.458 mmol) were combined in MeCN (ca. 10 mL) in a Schlenk tube charged with a stir bar and fitted with a Teflon valve. The tube was sealed and heated to 80 °C for 1 hour. After cooling to room temperature, the volatiles were removed under vacuum. The residue was triturated with $Et_2O$ (ca. 5 mL), and the precipitate filtered over celite. The precipitate was then extracted with $C_6H_6$ (ca. 10 mL), filtered through celite, and the filtrate concentrated under vacuum to yield 0.1101 g (70%) of the desired product as a dark red powder. Crystals suitable for x-ray diffraction were grown via vapor diffusion of $Et_2O$ into a concentrated MeCN solution of a 1:1 mixture of **5.6a** and PhNHNHPh. $^1$H NMR (300 MHz, $C_6D_6$, 25 °C), δ(ppm): 7.92 (m, 2 H, Ar-C*H*), 7.22 (m, 2 H, Ar-C*H*), 7.05-7.12 (m, 4 H, Ar-C*H*), 4.29 (s, 2 H, Ar-$C_1$*H*), 2.63 (m, 2 H, PC*H*$(CH_3)_2$), 2.13 (m, 2 H, PC*H*$(CH_3)_2$), 1.74 (s, 3 H, NCC*H*$_3$), 1.52 (m, 6 H, PCH(C*H*$_3)_2$), 0.90-1.10 (m, 18 H, PCH(C*H*$_3)_2$). $^{31}$P NMR (121 MHz, $C_6D_6$, 25 °C), δ(ppm): 80.55 (s).

**Synthesis of [(1,4-bis(2-(diisopropylphosphino)phenyl)-2,3-semiquinonate)]molybdenum(II)carbonyl(hydride) (5.7)**

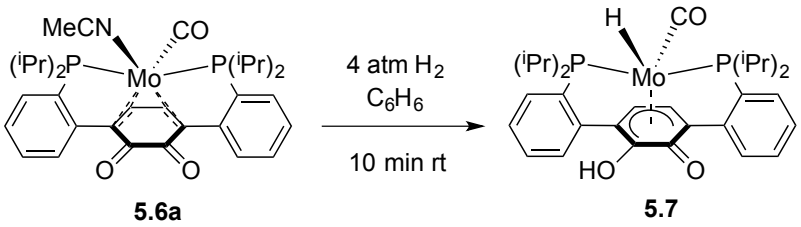


**5.6a** **5.7**

Compound **5.6** (0.0212 g, 0.0322 mmol) was solubilized in $C_6D_6$ (ca. 0.5 mL) and added to a J. Young style NMR tube. The solution was then degassed via three freeze-pump-thaw cycles, and the headspace was replaced with 4 atmospheres of $H_2$. After inverting for 10 minutes at room temperature, quantitative conversion was observed by NMR spectroscopy. Crystals suitable for x-ray diffraction were grown upon standing in a concentrated MeCN solution. $^1$H NMR (300 MHz, $C_6D_6$, 25 °C), δ(ppm): 8.84 (s, 1 H, O–*H*), 7.30 (m, 2 H, Ar-C*H*), 7.00-7.10 (m, 6 H, Ar-C*H*), 5.16 (s, 2 H, Ar-$C_1$*H*), 2.51 (m, 4 H, PC*H*$(CH_3)_2$), 1.00-1.30 (m, 24 H, PCH(C*H*$_3)_2$), -2.36 (t, $^2J_{HP}$ = 72 Hz, 1 H, Mo-*H*). $^{31}$P NMR (121 MHz, $C_6D_6$, 25 °C), δ(ppm): 96.02 (s).

**Synthesis of [(1,4-bis(2-(diisopropylphosphino)phenyl)-2,3-(trimethylsilyl)semiquinonate)]molybdenum(II)carbonyl(chloride) (5.8)**

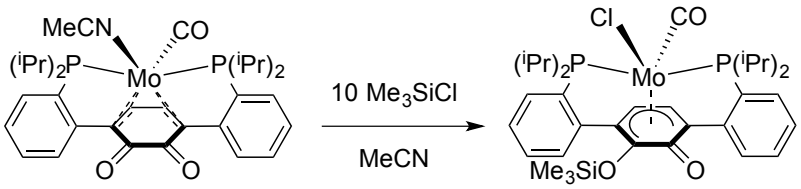


**5.6a** **5.8**

To a solution of compound **5.6** (0.1976 g, 0.301 mmol) in MeCN (ca. 5 mL) was added neat $Me_3SiCl$ (0.30 mL, 2.36 mmol). The mixture was stirred at room temperature for 30 minutes, over which time a precipitate had formed. The volatiles were then removed under reduced pressure. The residue was then triturated with MeCN (ca. 3 mL), and the precipitate filtered over a pad of celite washing with additional MeCN (ca. 1 mL). The remaining purple solid was then solubilized with $Et_2O$ (ca. 5 mL), filtered, and concentrated under vacuum to afford 0.1988 g (91%) of the desired compound. Crystals suitable for x-ray diffraction were grown via vapor diffusion of pentane into a concentrated benzene solution. $^1$H NMR (300 MHz, $C_6D_6$, 25 °C), δ(ppm): 8.84 (d, 7.7 Hz, 2 H, Ar-C*H*), 7.07 (m, 2 H, Ar-C*H*), 6.98 (m, 4 H, Ar-C*H*), 4.31 (s, 2 H, Ar-$C_1$*H*), 3.42 (m, 2 H, PC*H*$(CH_3)_2$), 2.57 (m, 2 H, PC*H*$(CH_3)_2$), 1.49 (m, 6 H, PCH(C*H*$_3)_2$), 1.19 (m, 6 H, PCH(C*H*$_3)_2$), 0.98 (m, 6 H, PCH(C*H*$_3)_2$), 0.39 (s, 9 H, Si(C*H*$_3)_3$). $^{31}$P NMR (121 MHz, $C_6D_6$, 25 °C), δ(ppm): 65.57 (s).

**Refinement Details**

In each case, crystals were mounted on a glass fiber or nylon loop using Paratone oil, then placed on the diffractometer under a nitrogen stream. Low temperature (100 K) X-ray data were obtained on a Bruker APEXII CCD based diffractometer (Mo sealed X-ray tube, $K_\alpha$ = 0.71073 Å) or a Bruker PHOTON100 CMOS based diffractometer (Mo micro-focus sealed X-ray tube, $K_\alpha$ = 0.71073 Å). All diffractometer manipulations, including data collection, integration, and scaling were carried out using the Bruker APEXII software.[7] Absorption corrections were applied using SADABS.[8] Space groups were determined on the basis of systematic absences and intensity statistics and the structures were solved by direct methods using XS[9], by intrinsic phasing using XT (incorporated into SHELXTL), or by charge flipping using Olex2[10] and refined by full-matrix least squares on $F^2$. All non-hydrogen atoms were refined using anisotropic displacement parameters. Hydrogen atoms were placed in the idealized positions and refined using a riding model. The structures were refined (weighed least squares refinement on $F^2$) to convergence. Graphical representation of structures with 50% probability thermal ellipsoids was generated using Diamond visualization software.[11]

**Table 5.2.** Crystal and refinement data for complexes **5.6•2(PhNH)$_2$**, **5.7•NCMe**, and **[5.9$^-$][Cp$_2$Co$^+$]•3C$_6$H$_6$**.

| | **5.6•2(PhNH)$_2$** | **5.7•NCMe** | **[5.9$^-$][Cp$_2$Co$^+$]•3C$_6$H$_6$** |
|---|---|---|---|
| Empirical formula | $C_{57}H_{65}MoN_5O_3P_2$ | $C_{33}H_{43}MoNO_3P_2$ | $C_{58}H_{66}CoMoN_4O_3P_2$ |
| Formula weight | 1026.06 | 659.56 | 1083.96 |
| T (K) | 100(2) | 100(2) | 100(2) |
| *a*, Å | 10.9476(6) | 9.0297(6) | 16.122(2) |
| *b*, Å | 13.9763(7) | 13.0226(8) | 9.744(1) |
| *c*, Å | 19.100(1) | 14.8559(9) | 33.850(3) |
| α, deg | 78.051(2) | 110.083(2) | 90 |
| β, deg | 81.673(2) | 94.570(3) | 94.425(8) |
| γ, deg | 67.189(2) | 101.936(3) | 90 |
| Volume, Å$^3$ | 2628.8(2) | 1583.5(2) | 5301.9(1) |
| Z | 2 | 2 | 4 |
| Crystal system | Triclinic | Triclinic | Monoclinic |
| Space group | P-1 | P-1 | $P2_1/c$ |
| $d_{calc}$, g/cm$^3$ | 1.2962 | 1.383 | 1.358 |
| θ range, deg | 2.23–33.14 | 1.72–37.78 | 1.21–38.20 |
| $\mu$, mm$^{-1}$ | 0.358 | 0.549 | 0.657 |
| Abs. Correction | Multiscan | Multiscan | Multiscan |
| GOF | 1.0441 | 1.146 | 0.980 |
| $R_1$,[a] $wR_2$ [b] [I>2 σ(I)] | 0.0521, 0.0738 | 0.0371, 0.0526 | 0.0418, 0.1139 |

[a] $R_1 = \sum||F_o| - |F_c||/\sum|F_o|$. [b] $wR_2 = [\sum[w(F_o^2-F_c^2)^2]/\sum[w(F_o^2)^2]]^{1/2}$.

**Table 5.4.** Crystal and refinement data for complexes **5.8•2C$_6$H$_6$**, and [**5.13**][**TfO$^-$**].

| | **5.8•2C$_6$H$_6$** | [**5.13**][**TfO$^-$**]•**3.5C$_6$H$_6$** |
|---|---|---|
| Empirical formula | $C_{37}H_{50}ClMoO_3P_2Si$ | $C_{90}H_{104}F_3Mo_2O_9P_4SSi$ |
| Formula weight | 764.19 | 659.56 |
| T (K) | 100(2) | 100(2) |
| *a*, Å | 19.539(1) | 9.0297(6) |
| *b*, Å | 10.4416(7) | 13.0226(8) |
| *c*, Å | 37.210(2) | 14.8559(9) |
| α, deg | 90.022(4) | 110.083(2) |
| β, deg | 102.173(3) | 94.570(3) |
| γ, deg | 89.970(3) | 101.936(3) |
| Volume, Å$^3$ | 7420.6(8) | 1583.5(2) |
| Z | 8 | 2 |
| Crystal system | Triclinic | Triclinic |
| Space group | P-1 | P-1 |
| $d_{calc}$, g/cm$^3$ | 1.368 | 1.383 |
| θ range, deg | 1.06–30.99 | 1.72–37.78 |
| $\mu$, mm$^{-1}$ | 0.578 | 0.549 |
| Abs. Correction | Multiscan | Multiscan |
| GOF | 1.016 | 1.146 |
| $R_1$,[a] $wR_2$[b] [I>2 σ(I)] | 0.0572, 0.1611 | 0.0371, 0.0526 |

[a] $R_1 = \sum||F_o| - |F_c||/\sum|F_o|$. [b] $wR_2 = [\sum[w(F_o^2-F_c^2)^2]/\sum[w(F_o^2)^2]^{1/2}$.

## REFERENCES


[1] a) G. A. Filonenko, M. P. Conley, C. Copéret, M. Lutz, E. J. M. Hensen, E. A. Pidko, *ACS Catal.* **2013**, *3*, 2522-2526; b) J. R. Khusnutdinova, D. Milstein, *Angew. Chem., Int. Ed.* **2015**, *54*, 12236-12273.

[2] a) V. K. K. Praneeth, M. R. Ringenberg and T. R. Ward, *Angew. Chem., Int. Ed.*, **2012**, *51*, 10228; b) O. R. Luca and R. H. Crabtree, *Chem. Soc. Rev.*, **2013**, *42*, 1440; c) H. Gru¨tzmacher, *Angew. Chem., Int. Ed.*, **2008**, *47*, 1814; d) J. I. van der Vlugt and J. N. H. Reek, *Angew. Chem., Int. Ed.*, **2009**, *48*, 8832; e) S. Schneider, J. Meiners and B. Askevold, *Chem. – Eur. J.*, **2012**, 412; f ) V. Lyaskovskyy and B. de Bruin, *ACS Catal.*, **2012**, *2*, 270.

[3] B. L. Conley, M. K. Pennington-Boggio, E. Boz, T. J. Williams, *Chem. Revs.* **2010**, *110*, 2294-2312.

[4] a) S. B. Kim, R. D. Pike, D. A. Sweigart, *Acc. Chem. Res.* **2013**, *46*, 2485-2497; b) J. Moussa, H. Amouri, *Angew. Chem. Int. Ed.* **2008**, *47*, 1372-1380; c) J. A. Reingold, S. Uk Son, S. Bok Kim, C. A. Dullaghan, M. Oh, P. C. Frake, G. B. Carpenter, D. A. Sweigart, *Dalton Trans.* **2006**, 2385-2398.

[5] J. T. Henthorn, S. Lin, T. Agapie, *J. Am. Chem. Soc.* **2015**, *137*, 1458-1464.

[6] Pangborn, A.B.; Giardell, M.A.; Grubbs, R.H.; Rosen, R.K.; Timmers, F.J. *Organometallics* **1996**, *15*, 1518.

[7] APEX2, Version 2 User Manual, M86-E01078, Bruker Analytical X-ray Systems, Madison, WI, June 2006.

[8] Sheldrick, G.M. "SADABS (version 2008/1): Program for Absorption Correction for Data from Area Detector Frames", University of Göttingen, 2008.

[9] Sheldrick, G.M. (2008). Acta Cryst. A64, 112-122.

[10] Dolomanov, O.V. (2009). OLEX2. J. Appl. Cryst. **42**, 339-341.

[11] Brandenburg, K. (1999). DIAMOND. Crystal Impact GbR, Bonn, Germany.

# APPENDIX A

## Multimetallic Mo-Cu and Mo-Mo Complexes Supported By A Catechol-Diphosphine Ligand

## ABSTRACT

Multimetallic complexes inspired by the carbon monoxide dehydrogenase biological active site were designed and synthesized. Supported by the catechol-diphosphine ligand, Mo-Cu complexes with 1:1 and 1:2 Mo:Cu ratio were synthesized and structurally characterized. The complexes demonstrated no reactivity with CO, but did exhibit some reactivity with isocyanide. Initial attempts at reducing the complexes, as well as chemically modifying the Mo=O moieties have shown some potential.

## INTRODUCTION

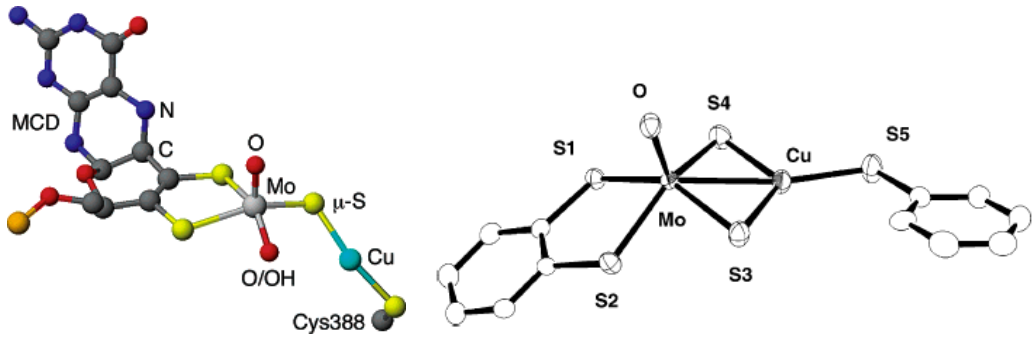


**Figure A.1**. Active site of Mo-Cu CODH[3] (left) and model complex of CODH with bridging sulfides[4] (right).

Carbon Monoxide Dehydrogenase (CODH) is a metalloenzyme that reversibly oxidizes CO to generate $CO_2$ in bacteria and archaea. There are two forms of CODH, the Ni-Fe CODH isolated from *Carboxydothermus hydrogenoformans*[1] and the Mo-Cu CODH isolated from *Oligotropha carboxidovorans*[2]. The active site of Mo-Cu CODH contains a five-coordinate pterin-bound Mo-dioxo (oxo-hydroxo) center bound to a Cu-cysteinate center through a bridging sulfide (see Figure 1). Several synthetic mimics[3,4] of this active site have successfully incorporated Mo-oxo centers with $Cu^{I}$ moieties through bridging sulfides, though reactivity with CO or isocyanide has yet to be demonstrated. Model systems of similar Mo and W metalloenzyme active sites incorporating oxo and dithiolate ligands have demonstrated catalytically accessible $Mo^{IV}/Mo^{VI}$ couples through oxo-transfer reagents such as phosphines and thioethers, though there has been no reported reactivity with $CO/CO_2$ or isocyanides/isocyanates in these systems[5,6]. Recently, cyclopentadienyl-diamidate supported Mo- and W-oxo

complexes demonstrated degenerate and non-degenerate oxo-transfer with $CO/CO_2$ and isocyanide/isocyanate substrates via the more reduced $M^{II}/M^{IV}$ couple[7].

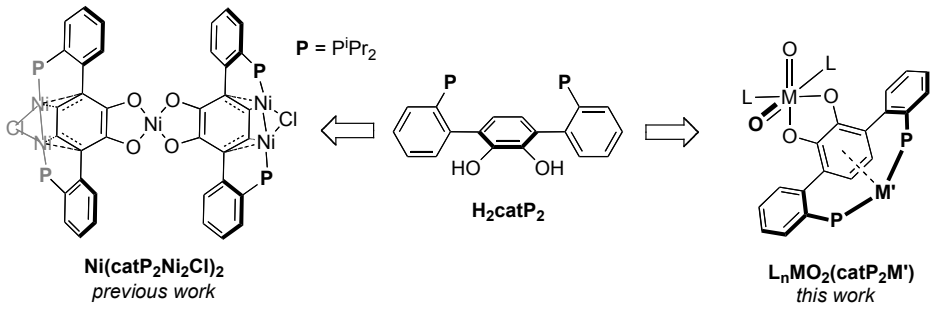


**Figure A.2**. Targeted multimetallic CODH model complexes (right) inspired by previous catechol-diphosphine complex (left).

Previously, Lin (Sibo Lin, Quarterly Report January, 2012) demonstrated the synthesis of a penta-Ni complex, $Ni(catP_2Ni_2Cl)_2$, via the catechol-diphosphine ligand $H_2catP_2$ (see Figure 2), where one square-planar $Ni^{II}$ center is bound between the oxygen atoms of 2 catecholate ligands, and two $Ni_2Cl$ moieties are bound by the phosphine donors and exhibit interaction with the π-system of the central arene rings. Inspired by this multimetallic complex with a hard, high valent $Ni^{II}$ bound by the catecholate moiety and softer, lower-valent $Ni^{I}_2$ centers bound by the phoshpines, synthesis of multimetallic complexes of relevance to the active site of Mo-Cu CODH were envisioned via the bis-chelating ligand precursor $H_2catP_2$ (Figure 2).

In the case of Mo-Cu systems (M=Mo and M'=Cu in Figure 2) in which $Cu^{I}$ is bound by the phosphines, interaction between Cu and the π-system of the central arene are not strongly anticipated as previous terphenyl-diphosphine $Cu^{I}$ complexes synthesized in the group have not demonstrated such interactions in solid-state structures.

Alternatively, mono- and multi-metallic systems in which a low-valent metal interacts with the π-system of the central arene (such as Mo) could potentially access the redox-non-innocence of the catechol ligand[8,9] with the oxygen atoms also serving as potential proton relays. This could allow access to chemistry related to proton[10] and dinitrogen[11] reduction.

## RESULTS

The synthesis and characterization of catechol-diphosphine ligand $H_2catP_2$ has been reported previously (Sibo Lin, Quarterly Report January, 2012). Reaction of a suspension of $H_2catP_2$ in MeCN with 1 equivalent of $Cu(MeCN)_4OTf$ resulted in a homogeneous, pale yellow solution after stirring for 2 hours at room temperature (Figure 3). The product, $H_2catP_2CuOTf$, was characterized by $^{31}P$ nuclear magnetic resonance (NMR) spectroscopy, revealing a broad singlet at ca. 9 ppm. This chemical shift is consistent with other $Cu^I$-para-terphenyl-diphosphine complexes synthesized previously in the Agapie group. In the $^1H$ NMR spectrum, a sharp singlet observed at 6.77 ppm, integrating as two relative to the rest of the spectrum, was assigned as the central arene protons. A broad resonance centered at 5.8 ppm was observed and assigned as the hydroxyl protons. The remaining aromatic and aliphatic resonances are consistent with a $C_{2v}$ symmetric product. Electron Spray Ionization Mass Spectrometry (ESI-MS) data from a solution of $H_2catP_2CuOTf$ in MeCN reveals a major peak at 557.3 m/z, consistent with the $[H_2catP_2Cu]^+$ fragment.

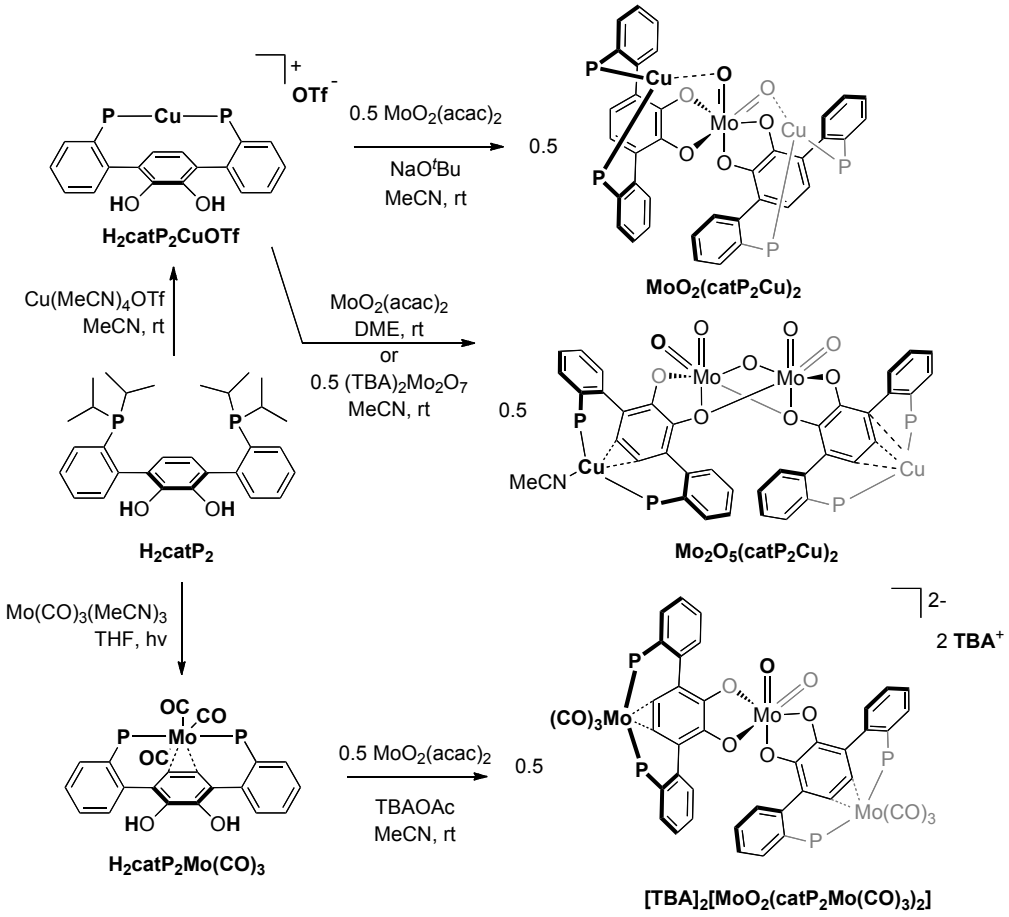


**Figure A.3**. Synthesis of various metal complexes of $H_2catP_2$. $TBA^+ = {}^n Bu_4N^+$.

Reaction of $H_2catP_2CuOTf$ with half an equivalent of $MoO_2(acac)_2$ and one equivalent of $NaO^tBu$ in MeCN at room temperature over the course of 30 minutes yields a dark red/purple solution (Figure 3). The resulting product, $MoO_2(catP_2Cu)_2$, was characterized by $^{31}P$ NMR, revealing a broad singlet at 10 ppm. While the $^1H$ NMR spectrum is consistent with an overall $C_2$ symmetric molecule, symmetry across the catechol-diphosphine ligand has been broken, as evidenced by the two doublets at 6.53 and 6.28 ppm (J = 7.5 Hz). These resonances, integrating as two relative to the rest of

the spectrum, were assigned as the central arene protons. The fact that the $^{31}P$ NMR does not reveal this break in symmetry can be ascribed to the very broad nature of the $^{31}P$ resonance bound to Cu. ESI-MS data of a solution of $MoO_2(catP_2Cu)_2$ in either THF or MeCN reveals a major peak at 1241.2 m/z and a minor peak at 1263.2 m/z, consistent with the $[MoO_2(catP_2Cu)_2 + H]^+$ and $[MoO_2(catP_2Cu)_2 + Na]^+$ fragments, respectively. Purple crystals grown from vapor diffusion of pentane into THF were studied by XRD, revealing a six-coordinate cis-dioxo Molybdenum center bound by two catechol-diphosphine ligands via the catechol oxygen atoms (Figure 4). Each catechol-diphosphine ligand is also bound to a three-coordinate $Cu^I$ center through the phosphine atoms, with the coordination sphere of Cu being completed by an interaction with the proximal Molybdenum-bound oxo. Bond length anaylsis of the Mo-O and Cu-O distances is more consistent with an assignment of a Molybdenum-oxo coordinating to $Cu^I$ than a bridging oxo.

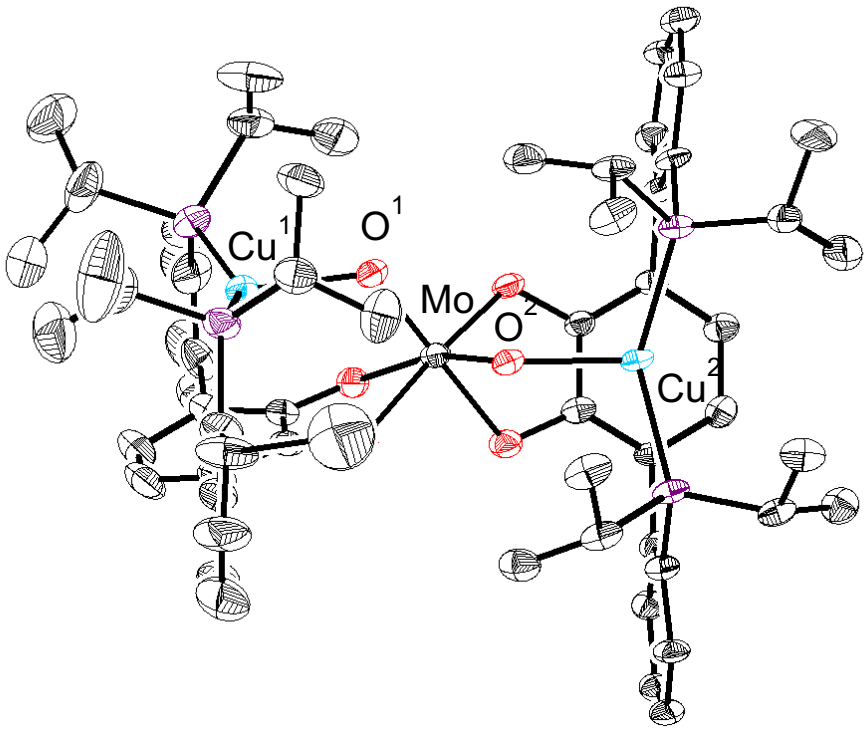


**Figure A.4**. Solid-state structure of $MoO_2(catP_2Cu)_2$. Hydrogen atoms and solvent molecules omitted for clarity. Phosphorus, oxygen and carbon atoms depicted in purple, red, and grey, respectively. Select bond distances (Å): $Cu^1$–$O^1$ = 2.11; $Cu^2$–$O^2$ = 2.13; $Mo^1$–$O^1$ = 1.73; $Cu^1$–$O^1$ = 1.75.

Altering the ratio of $H_2catP_2CuOTf$ and $MoO_2(acac)_2$ in the absence of base, a new product containing a one-to-one Mo/Cu ratio was isolated. Reaction of $H_2catP_2CuOTf$ with one equivalent of $MoO_2(acac)_2$ in neat DME at room temperature over the course of several hours yields a dark green/black solution. After removing the volatiles in vacuo, $^{31}P$ and $^1H$ NMR of the MeCN soluble material reveal multiple broad resonances assigned as a mixture of species. Yellow plates were crystallized out of a solution of this mixture overnight and analyzed by XRD to reveal a dimeric product, $Mo_2O_5(catP_2Cu)_2$

(Figure 5). This product contains a $Mo_2O_5$ core in which two cis-dioxo molybdenum centers are joined by a bridging oxo. Each Molybdenum atom is bound by a cathecol-diphosphine ligand through the catechol moiety, with one catechol oxygen atom bridging to the secondary molybdenum atom. In this complex, the phosphine-bound Cu atoms exhibit an interaction with the π-system of the central arene of the catechol-diphosphine ligand rather than the proximal oxo. A more rational synthesis (Figure 3) of $Mo_2O_5(catP_2Cu)_2$ was pursued through reaction of $(TBA)_2Mo_2O_7$ with two equivalents of $H_2catP_2CuOTf$ in MeCN, initially generating a dark green/black solution. Over the course of a day, a light colored precipitate formed. This precipitate was filtered, washed with MeCN, and then dissolved in benzene. The $^{31}P$ NMR of the isolated yellow product reveals a pair of broad doublets at 10.2 and 12.2 ppm, consistent with the structure of $Mo_2O_5(catP_2Cu)_2$. The $^{1}H$ NMR reveals a pair of broad resonances at 6.43 and 6.63 ppm, each integrating as two against the rest of the spectrum, assigned to the central arene ring. The remaining aromatic resonances are consistent with a $C_2$ symmetric molecule in which the two halves of the catechol-diphosphine ligand are chemically distinct. ESI-MS data from a THF solution of $Mo_2O_5(catP_2Cu)_2$ reveals major peaks at 1384.9, 1407.0, and 1625.7 m/z, which can be assigned as the $[Mo_2O_5(catP_2Cu)_2]^+$, $[Na + Mo_2O_5(catP_2Cu)_2]^+$, and $[TBA + Mo_2O_5(catP_2Cu)_2]^+$ fragments, respectively.

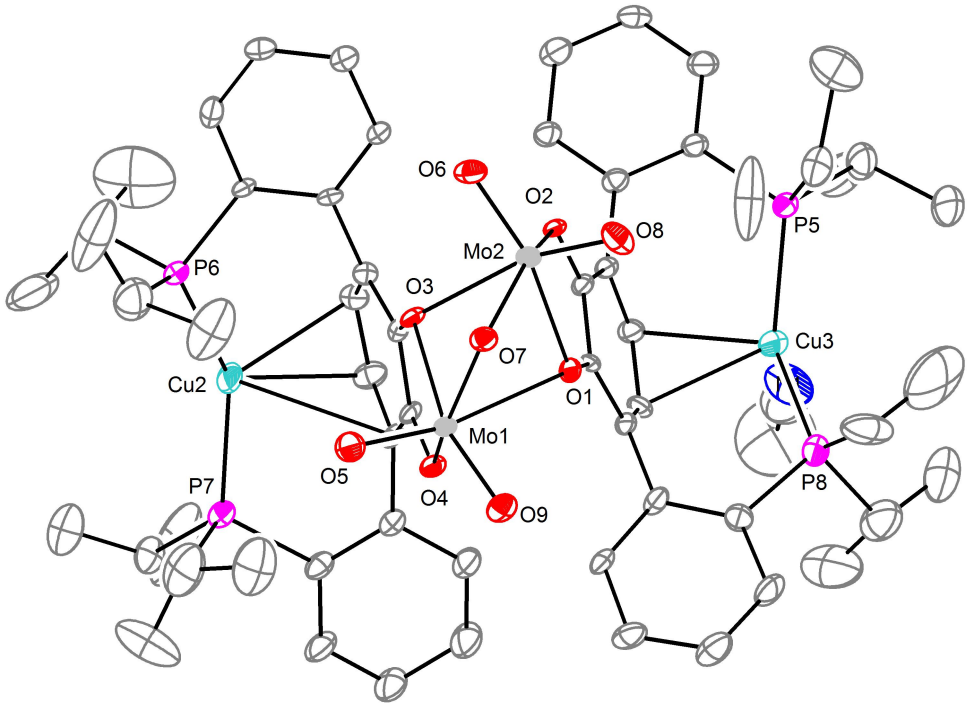


**Figure A.5**. Preliminary XRD structure of $Mo_2O_5(catP_2Cu)_2$. Hydrogen atoms omitted for clarity. Carbon atoms depicted in grey.

**Scheme A.1.** Synthesis of [TEA][$MoO_3(catP_2Cu)$].

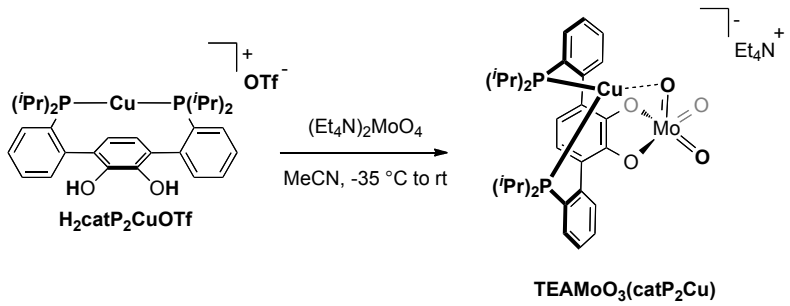


An alternative Mo-Cu complex demonstrating a 1:1 Mo:Cu ratio can accessed via reaction of $H_2catP_2CuOTf$ with $(Et_4N)_2MoO_4$ in MeCN (see Scheme A.1). Care must be

given to introduce $H_2catP_2CuOTf$ slowly to the molybdate solution and at low temperature, otherwise $MoO_2(catP_2Cu)_2$ is generated as a significant side product. While the $^{31}P$ NMR spectrum of the new product $[Et_4N][MoO_3(catP_2Cu)]$ is not significantly shifted from starting material $H_2catP_2CuOTf$, the signal is significantly sharper, suggestive of a Cu-oxo interaction present in solution. In the $^{1}H$ NMR spectrum, the resonance assigned to the catechol C–H protons has shifted upfield ca. 0.5 ppm in $[Et_4N][MoO_3(catP_2Cu)]$, consistent with formation of the Mo-catecholate moiety. Single crystals of $TEAMoO_3(catP_2Cu)$ suitable for XRD were grown via diffusion of $Et_2O$ into a saturated MeCN solution. In the solid state, the complex exists as a coordination polymer (Figure A.6).

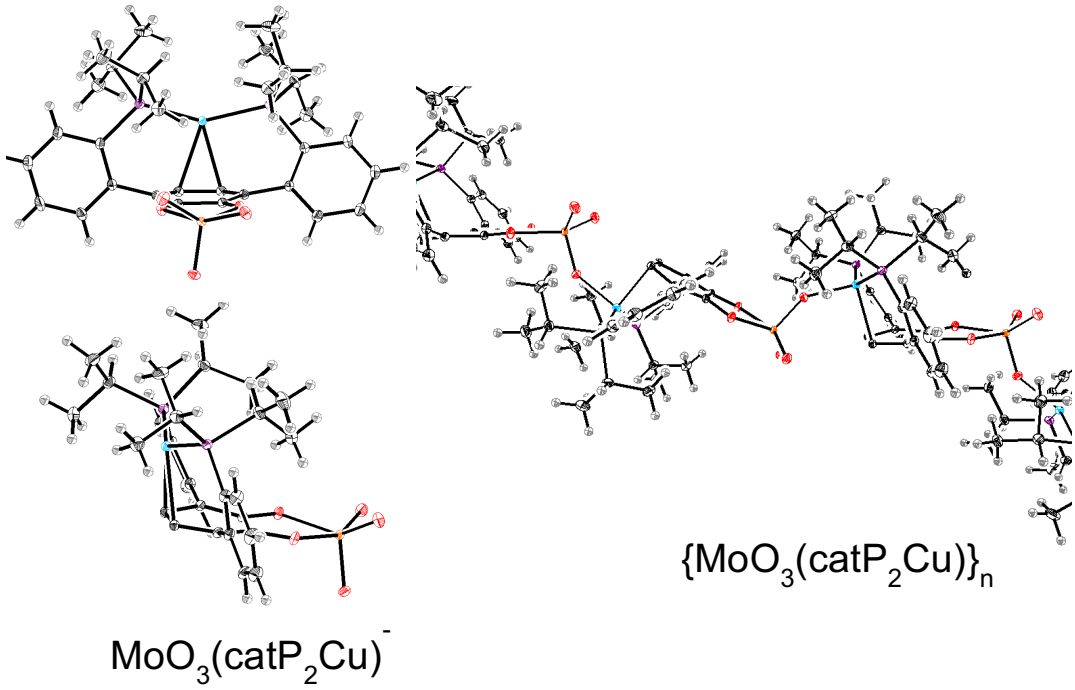


**Figure A.6**. Solid-state structure of $TEAMoO_3(catP_2Cu)$. Cations omitted for clarity. Molybdenum, copper, phosphorus, oxygen, carbon and hydrogen atoms depicted in

orange, teal, purple, red, black and grey, respectively. Depiction of single $MoO_3(catP_2Cu)^-$ unit (left top and bottom); coordination polymer of $\{MoO_3(catP_2Cu)\}_n$ (right).

Reaction of $H_2catP_2Mo(CO)_3$ with half an equivalent of $MoO_2(acac)_2$ and one equivalent of TBAOAc in MeCN over the course of one hour yields a dark orange solution. After removal of the solvent, precipitation from an ethereal solution with pentane results in isolation of an orange product, $[TBA]_2[MoO_2(catP_2Mo(CO)_3)_2]$. The $^{31}P$ NMR of $[TBA]_2[MoO_2(catP_2Mo(CO)_3)_2]$ reveals a pair of doublets at 49.3 and 52.8 ppm ($J_{PP}$ = 95.6 Hz), consistent with coupling of chemically distinct phosphines through the Mo center. The $^1H$ NMR reveals a pair of doublet-of-triplets at 5.97 and 6.06 ppm, integrating as two against the rest of the spectrum, assigned to the central arene. The complex splitting is assigned as coupling between the two distinct protons, as well as proton-phosphine coupling through the Mo center. The remaining aromatic resonances are consistent with a $C_2$ symmetric molecule in which the two sides of the catechol-diphosphine ligand are chemically distinct. Negative polarity ESI-MS data for a solution of $TBA_2MoO_2(catP_2Mo(CO)_3)_2$ in MeCN exhibits a major peak at 802.9 m/z, which could be assigned as the $[MoO_2(catP_2Mo(CO)_3)]^-$ fragment. IR (KBr) of $[TBA]_2[MoO_2(catP_2Mo(CO)_3)_2]$ reveals a sharp stretch in the carbonyl region at 1835 $cm^{-1}$ and a less intense, more broad stretch at 1785 $cm^{-1}$ consistent with the $Mo(CO)_3$ unit remaining intact.

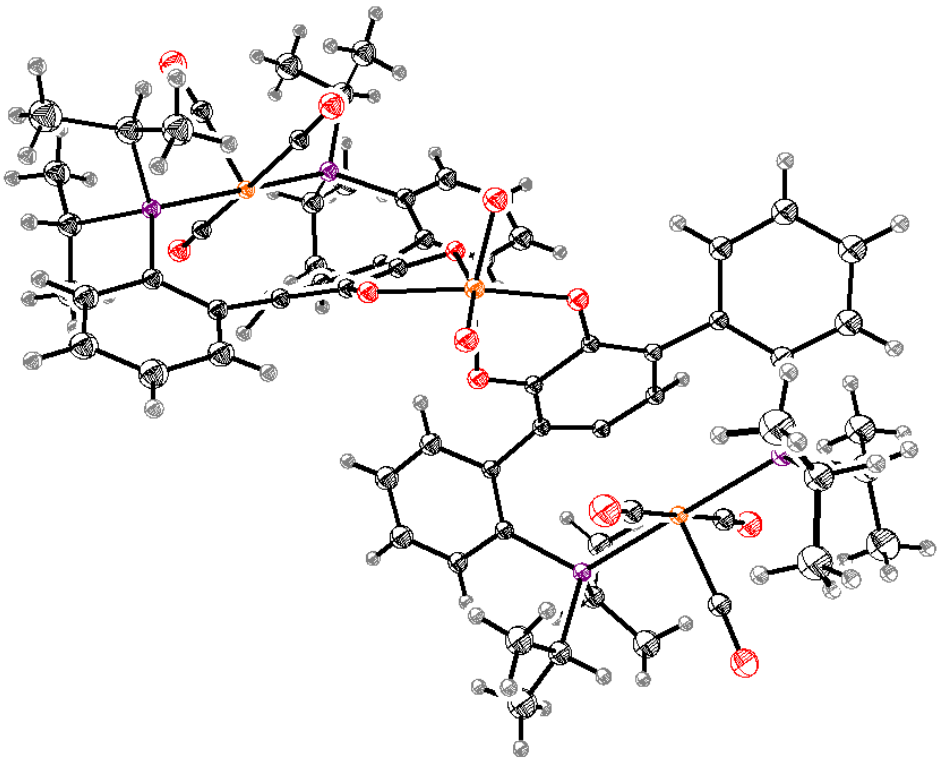

**Figure A.7**. Preliminary XRD structure of $[TBA]_2[MoO_2(catP_2Mo(CO)_3)_2]$. TBA cations omitted for clarity. Molybdenum, phosphorus, oxygen, carbon, and hydrogen atoms depicted in orange, purple, red, black, and grey, respectively.

With metal complex $MoO_2(catP_2Cu)_2$ in hand, preliminary reactivity of this complex was investigated toward small molecule activation. Exposure of a solution of $MoO_2(catP_2Cu)_2$ to an atmosphere of CO showed no reaction by $^{31}P$ and $^{1}H$ NMR, either in $CD_3CN$ or $C_6D_6$. When a solution of $MoO_2(catP_2Cu)_2$ in $C_6D_6$ was treated with one equivalent of $^{t}$BuNC a new set of resonances appears in both the $^{31}P$ and $^{1}H$ NMR, and by adding in additional equivalents of $^{t}$BuNC (up to 6: see Figure A.S11 for $^{31}P$ NMR of titration), resonances corresponding to starting material $MoO_2(catP_2Cu)_2$ diminish as the new resonances grow.

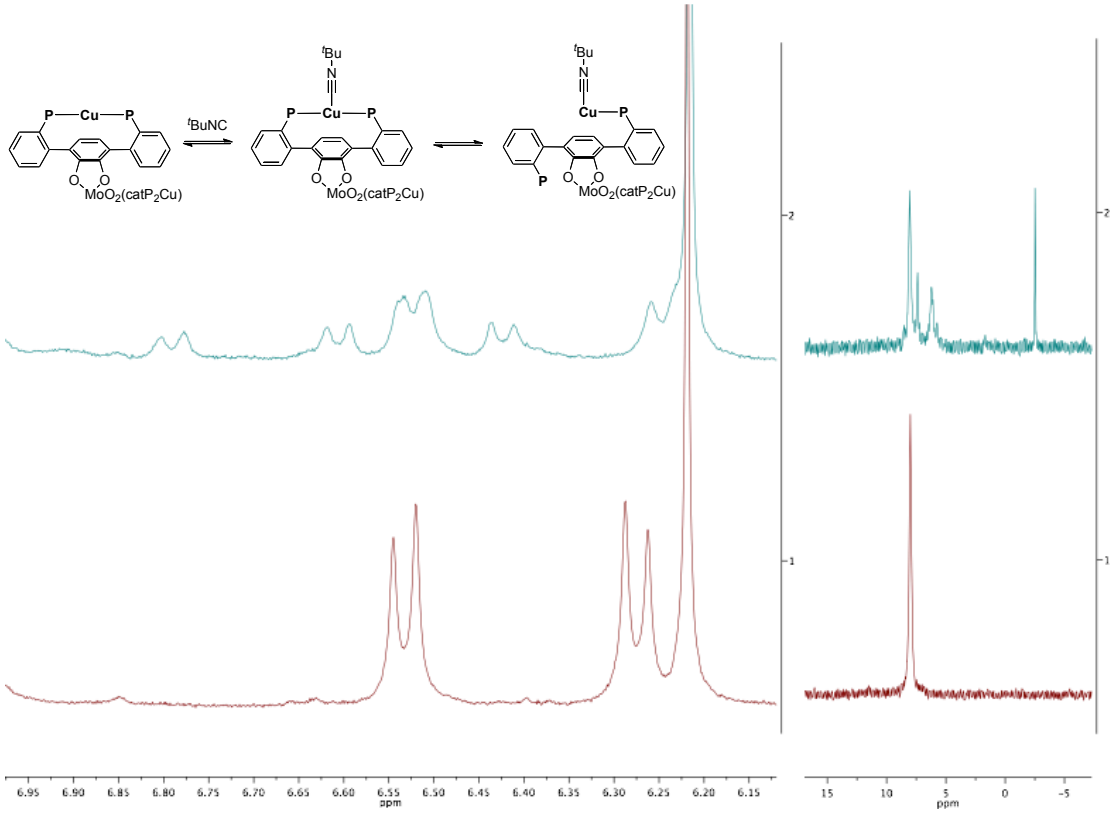


**Figure A.8**. $^{31}$P (right) and $^{1}$H NMR (left) of reaction of $MoO_2(catP_2Cu)_2$ (maroon) with one equivalent $^{t}$BuNC in $C_6D_6$ with 1,3,5-trimethoxybenzene as internal standard (green). Above: Proposed equilibrium for $^{t}$BuNC binding to Cu.

The $^{31}$P NMR reveals three new peaks that appear upon addition of one equivalent of $^{t}$BuNC at 2.5, 6.2, and 7.4 ppm, which integrate approximately as 1 : 2 : 1. In the $^{1}$H NMR, three new doublets appear in the central arene region from 6-7 ppm in addition to those of the starting material at 6.25 and 6.52 ppm. The new doublets appear at 6.80, 6.61, and 6.43 ppm and integrate as 1 : 1 : 1. It is presumed that a fourth doublet lies buried under the 6.52 ppm resonance of $MoO_2(catP_2Cu)_2$, which no longer integrates 1 : 1 against the 6.25 ppm resonance. Two-dimensional NMR studies have yet to be performed to confirm this

hypothesis. Based on the integrations of these new resonances in both the $^{31}P$ and $^{1}H$ NMR, it is proposed that $^{t}$BuNC binds to $Cu^{I}$ and an equilibrium exists between a species with both phosphine arms of the catechol-diphosphine ligand bound to Cu and another species with one phosphine bound and the second phosphine dissociated (see Figure A.8).

Reduction of $MoO_2(catP_2Cu)_2$ was investigated toward the goal of accessing either a more nucleophilic Mo-oxo moiety or a $Mo^{IV}$ species capable of reducing $CO_2$ to yield a $Mo^{VI}$-oxo species with concurrent loss of CO. The cyclic voltammogram (CV) of $MoO_2(catP_2Cu)_2$ presented in (Figure A.9) reveals only irreversible reduction events that have been assigned as reduction of Cu and reduction of corresponding ligand oxidation products. $MoO_2(catP_2Cu)_2$ showed no reactivity with Na[naphthalenide] or $Ph_3P$, and reaction with $Me_3P$ appears to only yield Cu-bound $Me_3P$ products with no $Me_3PO$ detectable by $^{31}P$ NMR. Reaction of $MoO_2(catP_2Cu)_2$ with $Me_3SiOTf$ in MeCN results in a brown/grey solution exhibiting broad $^{31}P$ and $^{1}H$ NMR spectra. ESI-MS data of the resulting brown/grey product in THF revelas a major peak at 1224.2 m/z and a minor peak at 1241.0 m/z. While the latter is assigned as the $[MoO_2(catP_2Cu)_2 + H]^+$ fragment and is consistent with $MoO_2(catP_2Cu)_2$, the major 1224.2 m/z peak corresponds to a mono-oxo $[MoO(catP_2Cu)_2]^+$ fragment. This fragment could suggest that the desired $MoO(OSiMe_3)(catP_2Cu)_2OTf$ species was formed and under the ESI conditions the $^{-}OSiMe_3$ group is lost, yielding the 1224.2 m/z fragment. Similar oxo-abstraction was attempted by reaction of $MoO_2(catP_2Cu)_2$ with two equivalents of $Ph_3SiSH$, which has been shown in literature[12,13] to substitute sulfido for oxo ligands. Heating at 50 °C over four hours resulted in a color change from dark red to brown. $^{31}P$ and $^{1}H$ NMR of the resulting brown solution revealed loss of resonances corresponding to $MoO_2(catP_2Cu)_2$ and displayed only broad features. ESI-MS analysis of this brown product in THF reveals a dominant peak at 1224.3 m/z corresponding to the mono-oxo

fragment $[MoO(catP_2Cu)_2]^+$, as well as minor peaks at 1241.2, 1256.2, and 1273.2 m/z. The former corresponds to the parent $[MoO_2(catP_2Cu)_2 + H]^+$ fragment, while the latter two peaks can be assigned as the sulfide-incorporating $[MoOS(catP_2Cu)_2]^+$ and $[MoS_2(catP_2Cu)_2 + H]^+$ fragments, respectively, suggesting the substitution of either one or both oxo's for sulfides (see Scheme A.2). Attempts at crystallographically isolating these products were unsuccessful.

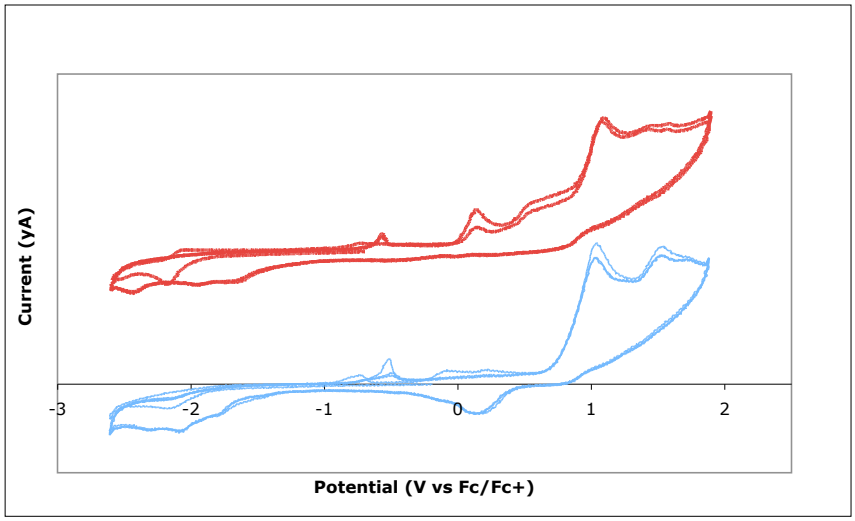


**Figure A.9**. Cyclic voltammogram (250 mV/s, falling) of 3 mM $H_2catP_2CuOTf$ (blue) and 3 mM $MoO_2(catP_2Cu)_2$ (red) with 0.1 M $Bu_4NPF_6$ in MeCN.

**Scheme A.2**. Possible oxo-substitution products from reaction with $Ph_3SiSH$.

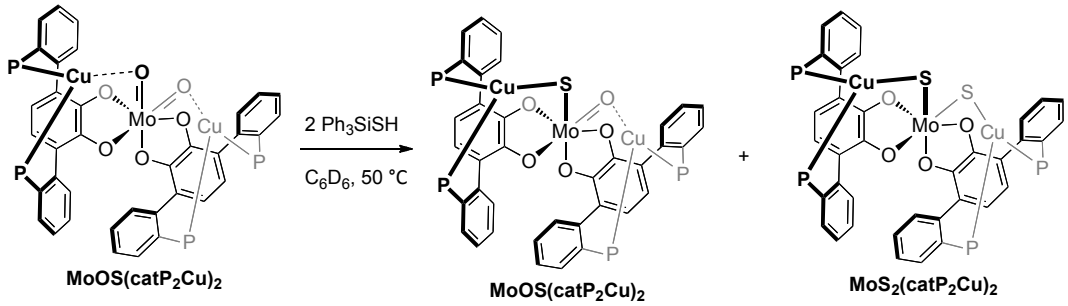


Electrochemical investigation of the Mo complexes $H_2catP_2Mo(CO)_3$ and

$TBA_2MoO_2(catP_2Mo(CO)_3)_2$ reveal accessible oxidation events for both compounds (see Figure 10). The parent compound, para-$P_2Mo(CO)_3$ has been oxidized by two electrons with AgOTf to yield the $Mo^{II}$ complex para-$P_2Mo(CO)_2(OTf)_2$. The CV in Figure 9 suggests a similar oxidation may be accessible for $H_2catP_2Mo(CO)_3$. The CV for $TBA_2MoO_2(catP_2Mo(CO)_3)_2$ reveals several closely overlapping oxidative waves which could be indicative of multiple oxidative events or the result of weak electrochemical communication between the two $Mo(CO)_3$ units through the $MoO_2$ center. These oxidations reveal corresponding reductions that are shifted more than 1 V negative from the oxidations, suggesting some sort of rearrangement or chemical reaction that takes place upon oxidation.

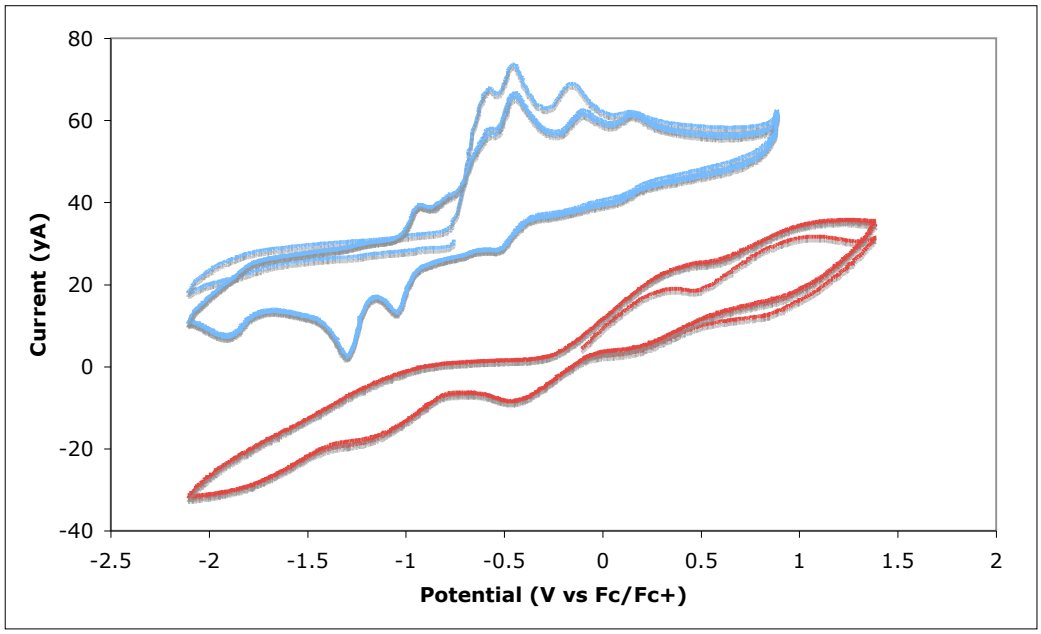


**Figure A.10**. Cyclic voltammogram of 3 mM $TBA_2MoO_2(catP_2Mo(CO)_3)_2$ (blue, 250 mV/s, falling) with 0.1 M $Bu_4NPF_6$ in MeCN and 3 mM $H_2catP_2Mo(CO)_3$ (red, 250 mV/s, rising) with 0.1 M $Bu_4NPF_6$ in THF.

## DISCUSSION

The structurally characterized compounds $MoO_2(catP_2Cu)_2$ and $Mo_2O_5(catP_2Cu)_2$ both demonstrate the successful introduction of a $Cu^I$-diphosphine moiety into a Mo-dioxo core via bis-chelating catechol-diphosphine ligand precursor $H_2catP_2$. In $MoO_2(catP_2Cu)_2$, there is a direct interaction between each Cu center and each Mo-oxo in the solid state, while $Mo_2O_5(catP_2Cu)_2$ demonstrates an interaction between Cu and the π-system of the central arene of $catP_2$. This π-system interaction is likely the result of geometric inflexibility enforced by the $Mo_2O_5$ core, as well as the overall neutral charge on the compound (i.e. the lack of counter-anions capable of coordinating to Cu). While the presence of the bridging oxo enforces a 1 : 1 Cu/Mo ratio, it lowers the coordination number around each Mo to 5 donor atoms, resulting in the $\mu^2\kappa^1\kappa^2$ binding of the catecholates to generate pseuodo-octohedral Mo's, restricting the angle of the central arene relative to the Mo center, and preventing the Cu atom from reaching the oxo. In $MoO_2(catP_2Cu)_2$, the more flexible central arene can bend upward toward the oxo, closing the distance between the Cu and oxygen atoms, resulting in an interaction.

As there has only been one structurally characterized CO bound Cu phosphine complex reported in the literature[14], a complex in which the phosphine-bound metal contained bound CO ligands was desired, and the successful installation of the $Mo(CO)_3$ unit on the parent ligand resulted in pursuing $H_2catP_2Mo(CO)_3$ not only for incorporation into a CODH model, but also for investigation of its possible redox properties and proton/electron transfer abilities. The cyclic voltammograms for both $H_2catP_2Mo(CO)_3$ and $TBA_2MoO_2(catP_2Mo(CO)_3)_2$ suggest there are accessible oxidized products for both systems that could demonstrate interesting chemistry. Aside from CO, the reaction of

$MoO_2(catP_2Cu)_2$ with $^t$BuNC is encouraging, though structural confirmation of coordinated $^t$BuNC was never achieved.

The lack of observable reactivity for $MoO_2(catP_2Cu)_2$ with CO is likely due to the complex's relatively electrophilic oxo's and inaccessibility of lower oxidation states of the Mo center. The nucleophilicty of the oxo's could be increased through reduction of the Mo center, however the hard Mo center does not appear susceptible to reduction due to the strong sigma-donating catecholate and oxo ligands. Synthesis of the thiol variant of $H_2catP_2$ is currently being pursued via the Newman-Kwart[15] rearrangement, in an effort to "soften" these supporting ligands on Mo. Alternatively, substitution for one of the oxo's has been attempted via reaction with $Ph_3SiSH$, and ESI data suggests the desired sulfide containing products were accessed. Incorporation of a sulfide bridging between Mo and Cu would not only help to soften the Mo center, but also may demonstrate insertion of CO or isocyanide into the Cu-S bond, as insertion of CO into the Cu-S bond in CODH has been proposed in the mechanism of CO oxidation[2]. Holm[16] has synthesized a number of $W^{VI}$ complexes with various oxo, sulfido, and dithiolate ligands as models for the Xanthine Oxidoreductase family active sites, and similar synthetic routes are being investigated using $H_2catP_2$ toward accessing $MoO_2SCu$ systems.

## CONCLUSIONS

The catechol-diphosphine ligand $H_2catP_2$ has demonstrated itself to be a versatile bis-chelate in synthesizing multimetallic complexes $MoO_2(catP_2Cu)_2$, $Mo_2O_5(catP_2Cu)_2$ and $TBA_2MoO_2(catP_2Mo(CO)_3)_2$. The structurally characterized complexes $MoO_2(catP_2Cu)_2$ and $Mo_2O_5(catP_2Cu)_2$ exhibit key structural elements desired of a CODH mimic, notably proximity of the Cu center to the Mo-dioxo unit in $MoO_2(catP_2Cu)_2$ and the 1:1 Mo/Cu ratio in $Mo_2O_5(catP_2Cu)_2$. Reactivity of $MoO_2(catP_2Cu)_2$ with $^t$BuNC is encouraging and could be pursued further, while lack of reactivity with CO was not unexpected. To further probe desired reactivity of these systems, related complexes that incorporate bridging sulfides and dithiolate supporting ligands should be synthetically targeted, as well as the thio-catechol variant of the $H_2catP_2$ ligand. Similarly, the dimeric $TBA_2Mo_2O_5(catP_2Cu)_2$ could be investigated as a precursor toward accessing a heterobimetallic MoCu complex with a secondary dithiolate supporting ligand.

.

## EXPERIMENTAL SECTION

**Synthesis of $H_2catP_2CuOTf$**. A solution of $Cu(MeCN)_4OTf$ (156.0 mg, 00.414 mmol) in MeCN (4 mL) was added to $H_2catP_2$ (201.6 mg, 0.408 mmol). The suspension was stirred at room temperature until a homogeneous solution formed. Volatiles were removed under vacuum. The remaining crude was washed with benzene, and the precipitate dissolved in THF, filtered and concentrated in vacuo to yield an off-white solid (277.3 mg, 96% yield). See Figures A.S1 and A.S2 for NMR spectra of this compound.

**Synthesis of $MoO_2(catP_2Cu)_2$**. A solution of $H_2catP_2CuOTf$ (117.5 mg, 0.166 mmol) in minimal MeCN was added to a solution of $MoO_2(acac)_2$ (29.5 mg, 0.0904 mmol) in MeCN (2 mL) with stirring. To this solution was added $NaO^tBu$ (16.4 mg, 0.171 mmol) with the aid of minimal MeCN. Upon addition, a dark red color developed. The reaction solution was left to stir for 2 hours. The volatiles were removed in vacuo, and the crude solid was washed with $Et_2O$ and the precipitate dissolved in benzene, filtered, and lyophilized to yield a dark red powder (95.3 mg, 92.5%). XRD quality crystals were grown from vapor diffusion of pentane into a THF solution of $MoO_2(catP_2Cu)_2$. See Figures A.S5 and A.S6 for NMR spectra of this compound.

**Synthesis of $Mo_2O_5(catP_2Cu)_2$**. $H_2catP_2CuOTf$ (42.0 mg, 0.0594 mmol) and $TBA_2Mo_2O_7$ (22.0 mg, 0.0279 mmol) were combined in MeCN (5 mL), immediately generating a dark green/black solution. This reaction mixture was left stirring, and over the course of several hours a light colored precipitate formed. After stirring for a day, the volatiles were removed in vacuo. The crude residue was washed with MeCN, and the resulting precipitate dissolved

in benzene, filtered, and lyophilized to yield a yellow powder (10.2 mg, 25% yield). See Figures A.S7 and A.S8 for NMR spectra of this compound.

**Synthesis of $TBA_2MoO_2(catP_2Mo(CO)_3)_2$.** To a suspension of $H_2catP_2Mo(CO)_3$ (22.1 mg, 0.0328 mmol) in MeCN (2 mL) was added sequentially a solution of $MoO_2(acac)_2$ (5.3 mg, 0.0162 mmol) in MeCN (1 mL) and TBAOAc (20.3 mg, 0.0673 mmol) also in MeCN (1 mL). The resulting orange solution was stirred for 2 hours and then the volatiles were removed in vacuo. The crude residue was dissolved in a minimal amount of $Et_2O$ and pentane was added to precipitate a bright orange solid. This solid was dissolved in benzene, filtered, and lyophilized to yield a bright orange powder (19.7 mg, 61% yield). See Figures A.S9 and A.S10 for NMR spectra of this compound.

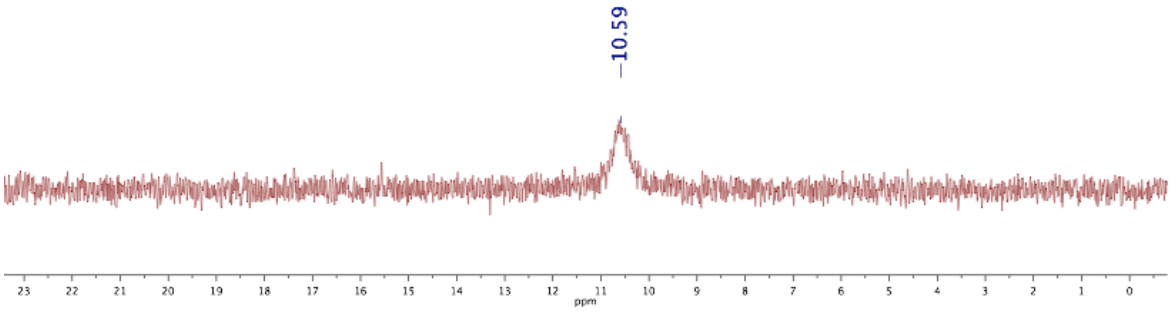


**Figure AS.1.** $^{31}P$ NMR(121 MHz, $CD_3CN$) spectrum of $H_2catP_2CuOTf$

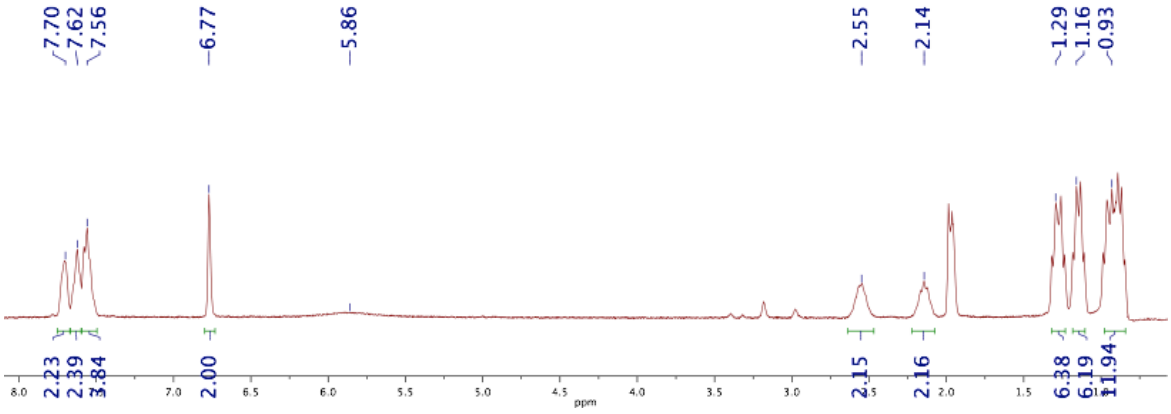


**Figure A.S2.** $^{1}$H NMR(300 MHz, $CD_3CN$) spectrum of $H_2catP_2CuOTf$

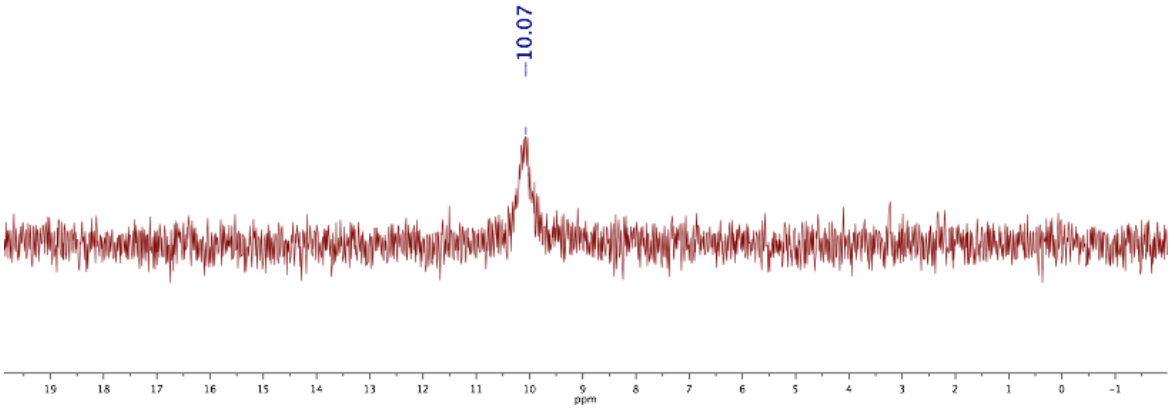


**Figure A.S3.** $^{31}$P NMR(121 MHz, $CD_3CN$) spectrum of $MoO_2(catP_2Cu)_2$

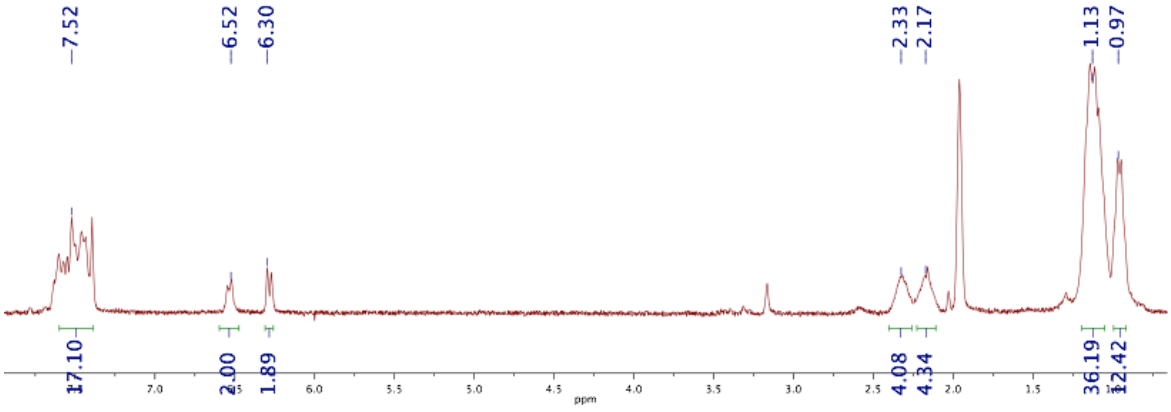


**Figure A.S4.** $^{1}$H NMR(300 MHz, $CD_3CN$) spectrum of $MoO_2(catP_2Cu)_2$

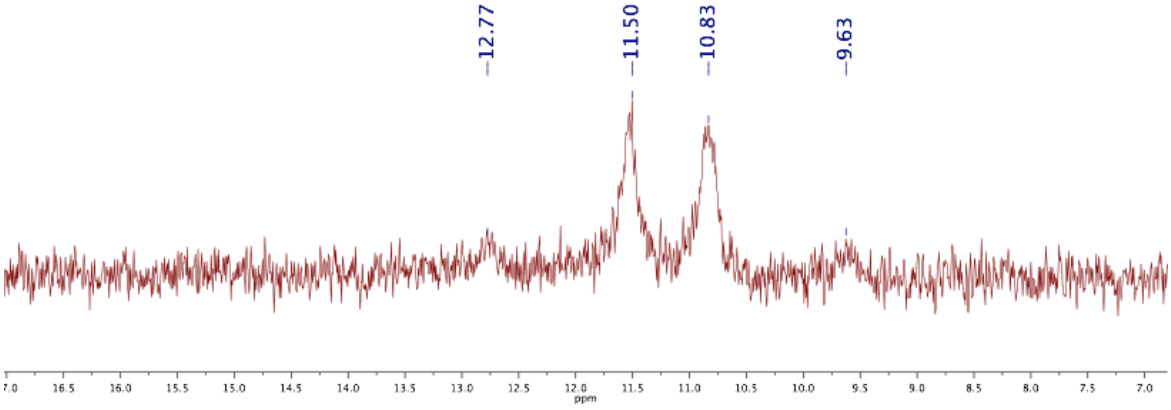


**Figure AS.5.** $^{31}P$ NMR(121 MHz, $C_6D_6$) spectrum of $Mo_2O_5(catP_2Cu)_2$

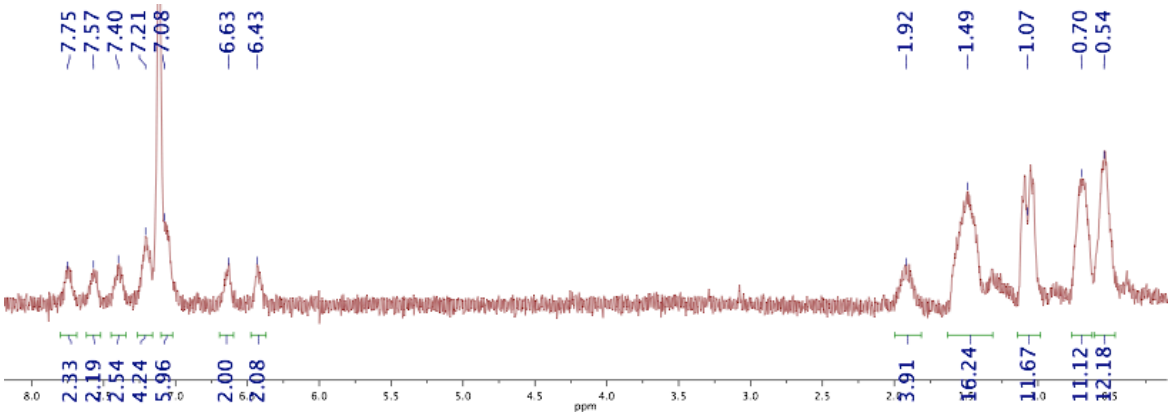


**Figure A.S6.** $^{1}H$ NMR(300 MHz, $C_6D_6$) spectrum of $Mo_2O_5(catP_2Cu)_2$

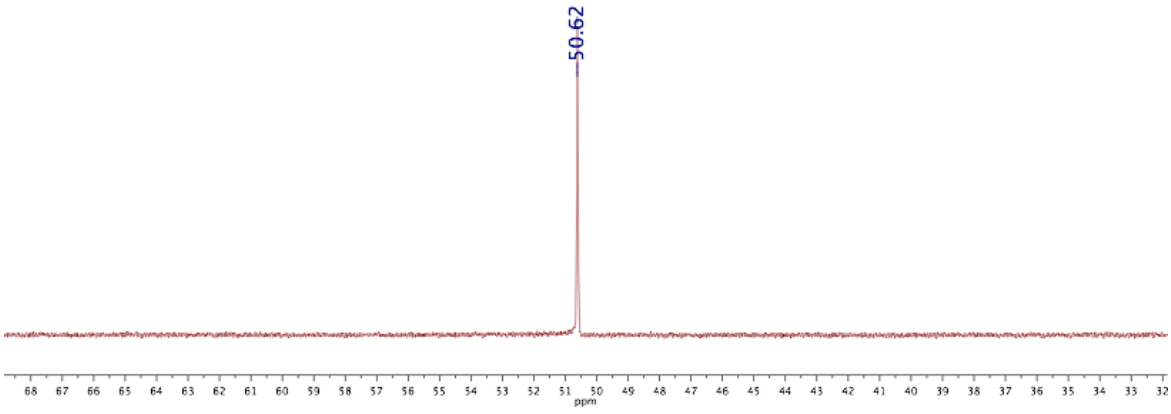


**Figure A.S7.** $^{31}P$ NMR(121 MHz, $C_6D_6$) spectrum of $H_2catP_2Mo(CO)_3$

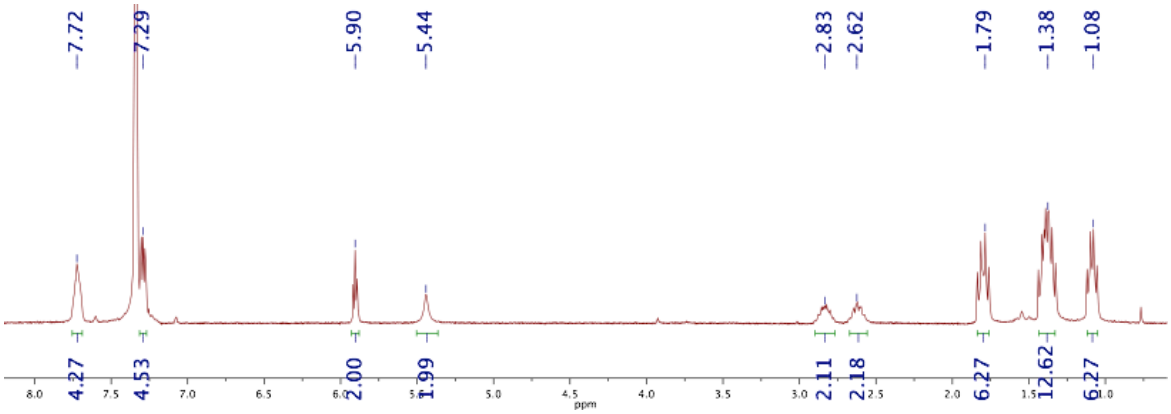


**Figure A.S8**. $^{1}$H NMR(300 MHz, $C_6D_6$) spectrum of $H_2catP_2Mo(CO)_3$

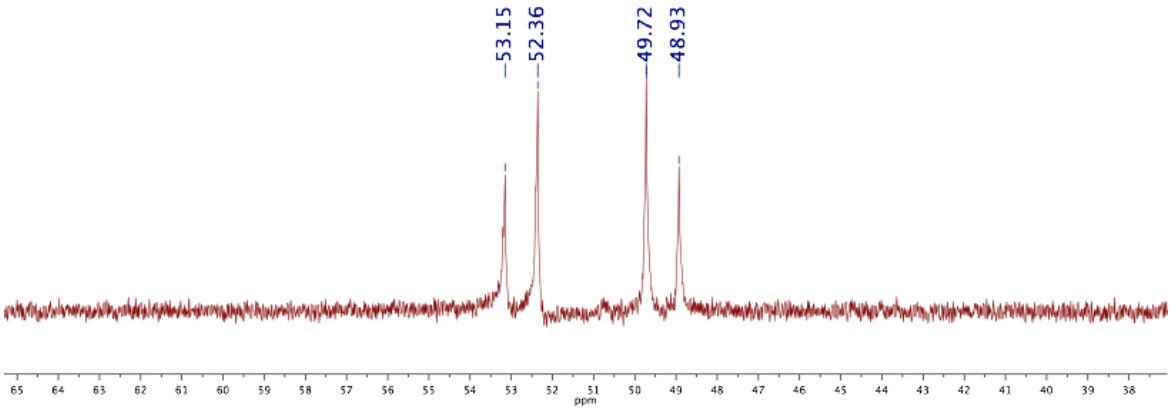


**Figure A.S9.** $^{31}$P NMR(121 MHz, $C_6D_6$) spectrum of $TBA_2MoO_2(catP_2Mo(CO)_3)_2$

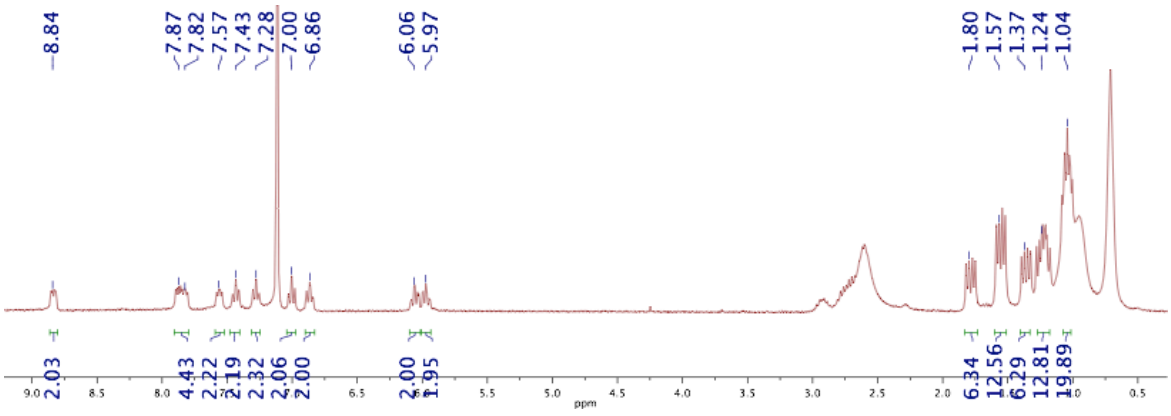


**Figure A.S10**. $^{1}$H NMR(300 MHz, $C_6D_6$) spectrum of $TBA_2MoO_2(catP_2Mo(CO)_3)_2$

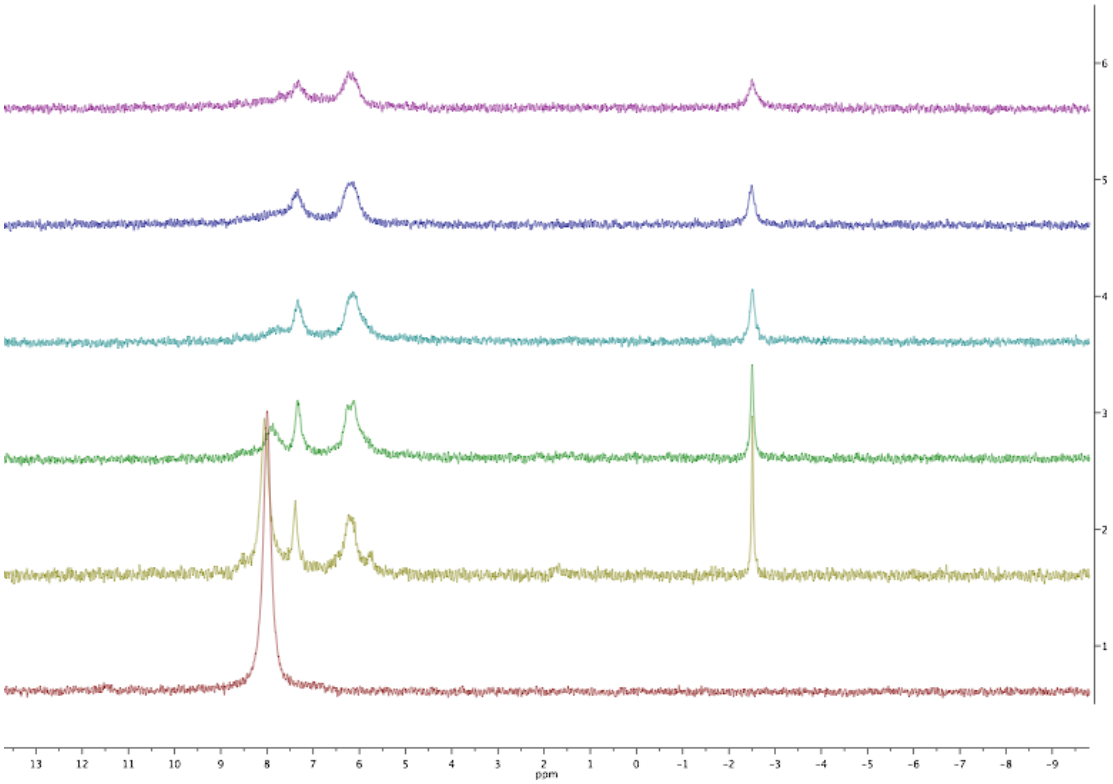


**Figure A.S11**. $^{31}P$ NMR(121 MHz, $C_6D_6$) spectrum of addition of $^{t}$BuNC to $MoO_2(catP_2Cu)_2$. Equivalents by panel: 1) 0 eq, 2) 1 eq, 3) 2 eq, 4) 3 eq, 5) 4 eq, 6) 6 eq.

## REFERENCES


[1] Jeoung, J-H.; Dobbek, H. *Science*, **2007**, *318*, 1461-1464.

[2] Dobbek, H.; Gremer, L.; Kiefersauer, R.; Huber, R.; Meyer, O. *Proc. Natl. Acad. Sci.*, **2002**, *99*, 15971-15976.

[3] Gourlay, C.; Nielsen, D.J.; White, J.M.; Knottenbelt, S.Z.; Kirk, M.L.; Young, C.G. *J. Am. Chem. Soc.*, **2006**, *128*, 2164-2165.

[4] Takuma, M.; Ohki, Y.; Tatsumi, K. *Inorg. Chem.*, **2005**, *44*, 6034-6043.

[5] Enermark, J.H.; Cooney, J.J.A.; Wang, J-J.; Holm, R.H. *Chem. Rev.*, **2004**, *104*, 1175-1200.

[6] Holm, R.H.; Solomon, E.I.; Majumdar, A.; Tenderholt, A. *Coord. Chem. Rev.*, **2011**, *255*, 993-1015.

[7] Yonke, B.L.; Reeds, J.P.; Zavalij, P.Y.; Sita, L.R. *Angew. Chem. Int. Ed.*, **2011**, *50*, 12342-12346.

[8] Pierpont, C.G. *Coord. Chem. Rev.*, **2001**, *216-217*, 99-125.

[9] Dei, A.; Gatteschi, D.; Sangregorio, C.; Sorace, L. *Acc. Chem. Res.*, **2004**, *37*, 827-835.

[10] Karunadasa, H.I.; Montalvo, E.; Sun, Y.; Majda, M.; Long, J.R.; Chang, C.J. *Science*, **2012**, *335*, 698-702.

[11] Arashiba, K.; Miyake, Y.; Nishibayashi, Y. *Nature Chem.*, **2011**, *3*, 120-125.

[12] Partyka, D.V.; Holm, R.H. *Inorg. Chem.*, **2004**, *43*, 8609-8616.

[13] Donahue, J.P. *Chem. Rev.*, **2006**, *106*, 4747-4783.

[14] Nakajima, Y.; Shiraishi, Y.; Tsuchimoto, T.; Ozawa, F. *Chem. Comm.*, **2011**, *47*, 6332-6334.

[15] Lloyd-Jones, G.C.; Moseley, J.D.; Renny, J.S. *Synthesis*, **2008**, *5*, 0661-0689.

[16] Groysman, S.; Wang, J-J.; Tagore, R.; Lee, S.C.; Holm, R.H. *J. Am. Chem. Soc.*, **2008**, *130*, 12794-12807.

# APPENDIX A

## Biologically Inspired Multimetallic Complexes

## ABSTRACT

Metalloproteins such as Acetyl Coenzyme A Synthase and Carbon Monoxide Dehydrogenase catalyze reactions involving $CO_2$ and CO to generate organic products useful in biological systems. Inspired by these active sites, a series of mulidentate ligands incorporating various sulfur and nitrogen donors into a bipyridine-bisphenol framework were synthesized. First row transition metal complexes supported by these ligands were pursued and both mono- and multi-metallic complexes characterized structurally and spectroscopically. Multi-metallic Copper complexes are shown to react with dioxygen, yet structural modification of the supporting ligand may prove beneficial in facilitating cooperative intramolecular reactivity. Future investigations of multi-metallic complexes with Nickel and Molybdenum are also discussed.

## INTRODUCTION

In nature, metalloproteins catalyze a multitude of reactions of interest to the modern chemist, ranging from C-H bond functionalization to small molecule activation ($H_2$[1], $N_2$[2], $O_2$[3], $CO/CO_2$[4,5], etc.). Many of these transformations are chemically complex, requiring transfer of multiple electron/proton equivalents, and in some cases

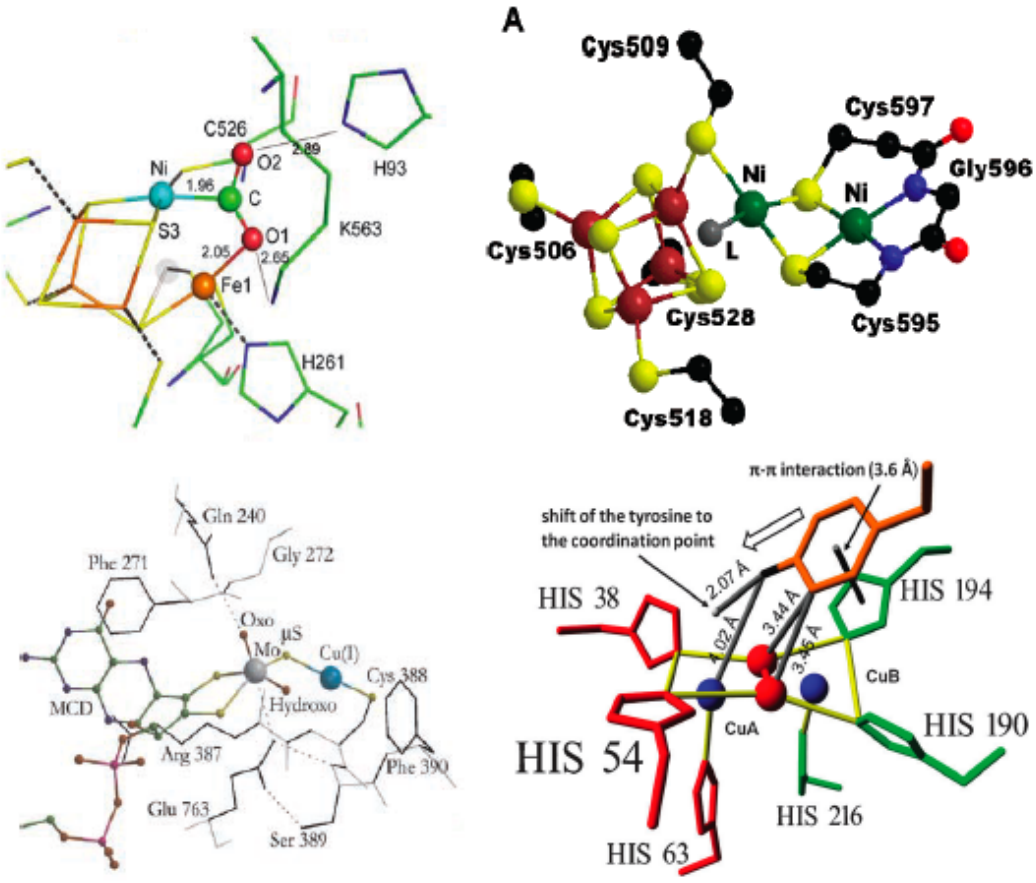


**Figure B.1:** Active site structures of Ni-Fe CODH showing $CO_2$ bridging between Ni and Fe (top left)[6], Acetyl-Coenzyme A Synthase in the oxidized $Ni^{II}Ni^{II}$ state (top right)[7], Mo-Cu CODH (bottom left)[8], and Tyrosinase showing substrate orientation (bottom right)[9].

they involve the interaction of multiple substrates with the metalloprotein active site. A prime example is the bifunctional enzyme Carbon Monoxide Dehydrogenase/Acetyl Coenzyme-A Synthase (CODH/ACS) from Moorella Thermoacetica[7]. The ~300 kDa $\alpha_2\beta_2$ dimer reversibly catalyzes the two electron reduction of $CO_2$ to CO at the C-cluster (Ni-Fe CODH), while the A-cluster (ACS) reversibly catalyzes the assembly of acetyl coenzyme-A from CO, the methyl group of a corrinoid Iron-Sulfur protein (CoFeSP), and coenzyme-A, as given by the reactions below.

$$CO_2 + 2e^- + 2H^+ \rightleftarrows CO + H_2O$$

$$CO + \text{Me-Co}^{III}\text{FeSP} + CoA \rightleftarrows \text{Co}^{I}\text{FeSP} + \text{Acetyl-CoA}$$

Inspection of the two active sites of CODH/ACS reveals hetero-multi-metallic centers primarily composed of Nickel, Iron, and Sulfur (Figure B.1). There are a number of metallo-proteins with active sites composed from these elements, for example the Hydrogenases ([NiFe] $H_2$ase[10,11], [FeFe] $H_2$ase[12-14], [Fe] $H_2$ase[15,16]), as well as those which incorporate metals other than Nickel and Iron, with examples including the Molybdenum and Copper containing CODH[8] and the Copper containing Tyrosinase[9] (see Figure B.1). These examples are by no means exhaustive. In the majority of these systems, substrate reactivity often occurs at multiple earth-abundant metal centers held in close proximity to one another by Sulfur and Nitrogen-containing ligands. Inspired by these active sites, synthesis of a class of multinucleating ligands based on a bipyridine- bisphenol backbone (Figure B.2) was pursued that could allow access to multi-metallic complexes relevant to biological systems.

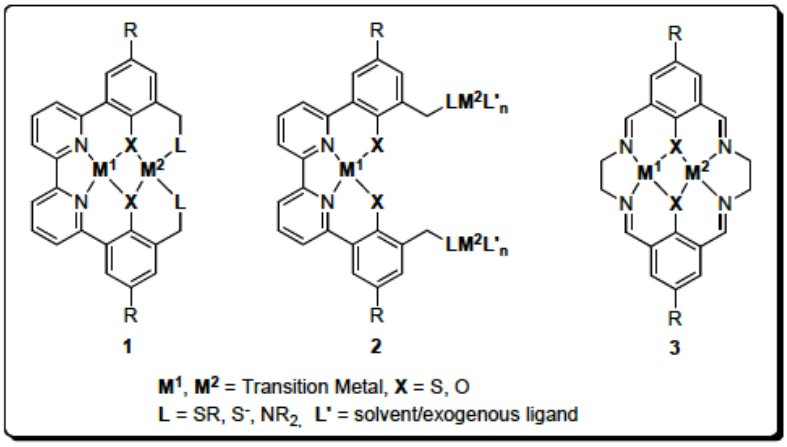


**Figure B.2:** Multimetallic compounds pursued in this report (center and left), and their structural similarity to Schiff-base macrocylces (right).

Macrocyclic systems structurally similar to **1** and **2** proposed in Figure B.2, namely Schiff-base compounds **3** and their variants, are well documented in the literature[17,18]. Though some of these systems have demonstrated interesting electrochemical[19,20] and magnetic properties[21] of the coupled metal centers, they have demonstrated little substrate-based reactivity[22], possibly due to the coordinatively saturated nature of these compounds. It is believed that by employing hemi-labile terminal donors in an acyclic system, the terminal metal centers will have flexible coordination geometries to stabilize multiple oxidation states (i.e. tetrahedral $Ni^{I/0}$ vs square planar $Ni^{II}$) and accessible coordination sites at which to bind substrate and potentially access further chemistry.

## Results and Discussion

**Scheme B.1.** Synthesis of bis-thioether proligand **10**.

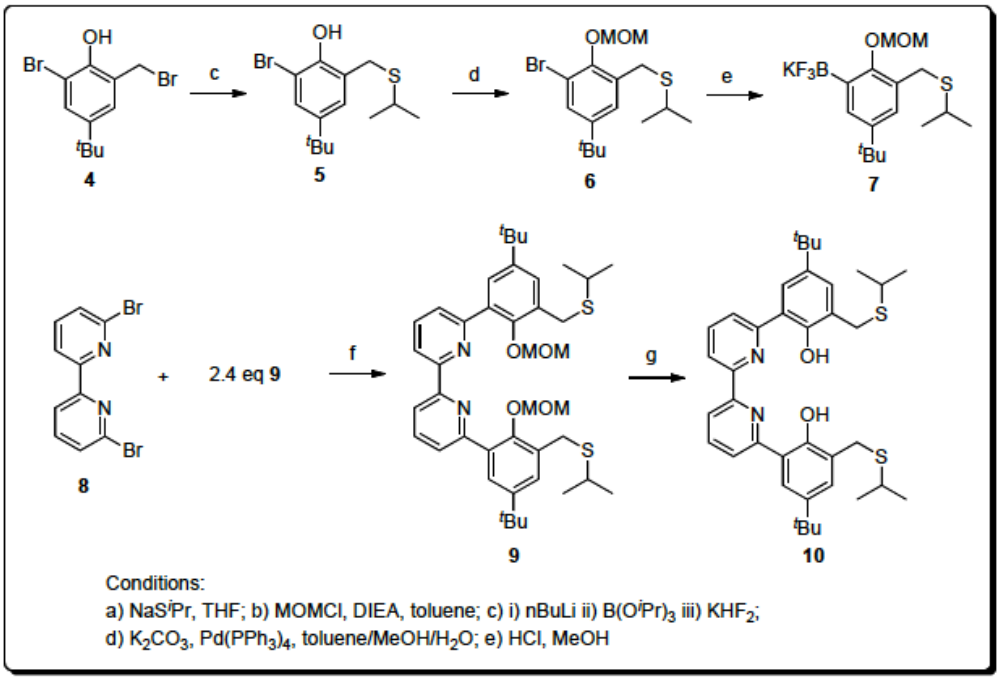


In pursuit of metal complexes of the type 1 in Figure B.2, the initial synthetic route chosen was that outlined in Scheme B.1, wherein the key step involves a Suzuki-Miyaura coupling between 6,6'-dibromo-2,2'-bipyridine (8) and the aryltrifluoroborate potassium salt 7. In attempting to access compound 9 via other cross-coupling methods, it was discerned that the Suzuki route gave higher, more reproducible yields than the corresponding Negishi coupling and that the aryltrifluoroborate salts were more easily isolated and purified than the corresponding boronic acids and esters. A simple SN2 reaction between sodium isopropylthiolate and bromide 4 easily yields thioether 5, while MOM protection of the phenol followed by halogen-lithium exchange, quenching with B(OiPr)3 and work-up with KHF2 afforded the

trifluoroborate salt 7 in moderate yield.

**Scheme B.2.** Attempted metalations of **10** with $Ni^{II}$ and $Ni^{0}$ precursors.

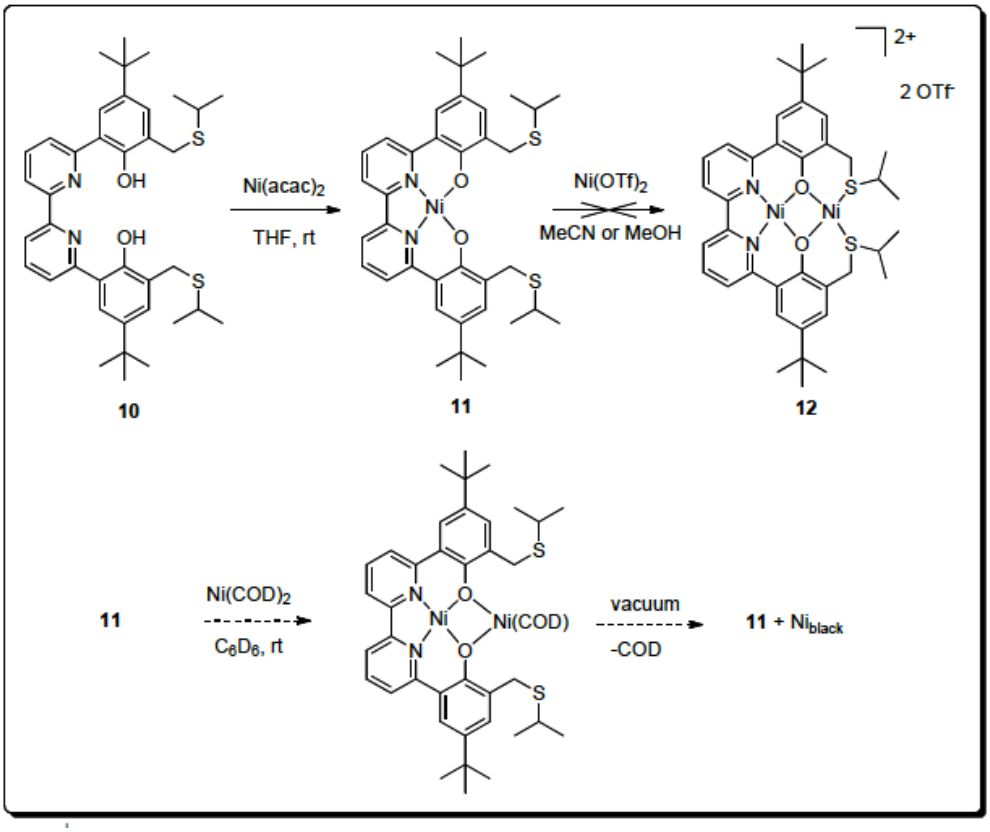


Suzuki cross-coupling of **7** with 6,6'-dibromo-2,2'-bipyridine afforded the desired coupled product **9** in good yield, and the MOM protecting group could easily be cleaved with methanolic HCl, yielding the desired **10**. Treatment of a solution of **10** in THF with one equivalent of $Ni(acac)_2$ also as a solution in THF at room temperature produced a color change from pale yellow to dark red over the course of 1 hour. Removal of the volatiles in vacuo resulted in isolation of a salmon-orange solid. Upon work-up, the diamagnetic $^1H$ NMR spectrum of the resulting product revealed resonances consistent with a $C_{2v}$ symmetric molecule. The absence of a phenol signal and the lack of a shift in

the benzylic methylene and the isopropyl methyne resonances compared to the starting material suggest that Ni is bound in the bpy-phenol pocket as indicated in Scheme B.2. Electrospray Ionization Mass Spectrometry (ESI-MS) data from a solution of the salmon-orange product in $CH_2Cl_2$ revealed peaks at 793, 1477, and 685. These masses are assigned as $[M + CH_2Cl_2 + Na]^+$, $[2M + CH_2Cl_2 + Na]^+$, and $[M + H]^+$, where M corresponds to structure **11**.

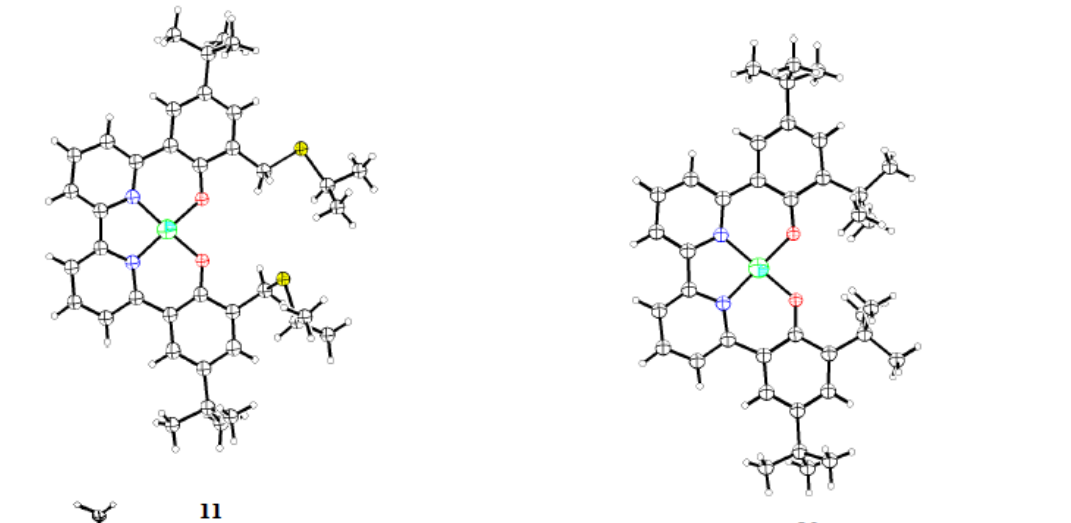


| Selected Distances (Å) | 11 | 13 |
|---|---|---|
| Ni-O | 1.8186 | 1.8369 |
| Ni-N | 1.8562 | 1.8802 |
| Bond Angles (°) | | |
| O-Ni-O | 82.877 | 85.895 |
| O-Ni-N | 95.397 | 94.07 |
| N-Ni-N | 86.666 | 86.392 |

**Figure B.3:** Crystal structures of compound 11 (top left) and literature23 compound 13 (top right). Colors and atoms correspond to Nitrogen (blue), Oxygen (red), Sulfur (yellow), and Nickel (green). Comparison of selected bond lengths and angles (table).

Crystals grown by slow evaporation of a solution of this orange solid in $CH_2Cl_2$ at room temperature were analyzed by XRD and revealed the structure given in Figure B.3. The Ni atom is coordinated in a square-planar geometry slightly distorted toward tetrahedral. This structure and its metrical parameters correspond well to the similar tert-butyl-substituted literature[23] compound **13**. The Ni-N and Ni-O bond distances are slightly shorter in **11** than in **13**, which is likely due to a steric interaction between the ortho-tert-butyl groups in **13**. This interaction would result in expansion of the O-Ni-O angle and contractions of the N-Ni-O and N-Ni-N angles, which is consistent with the observed values.

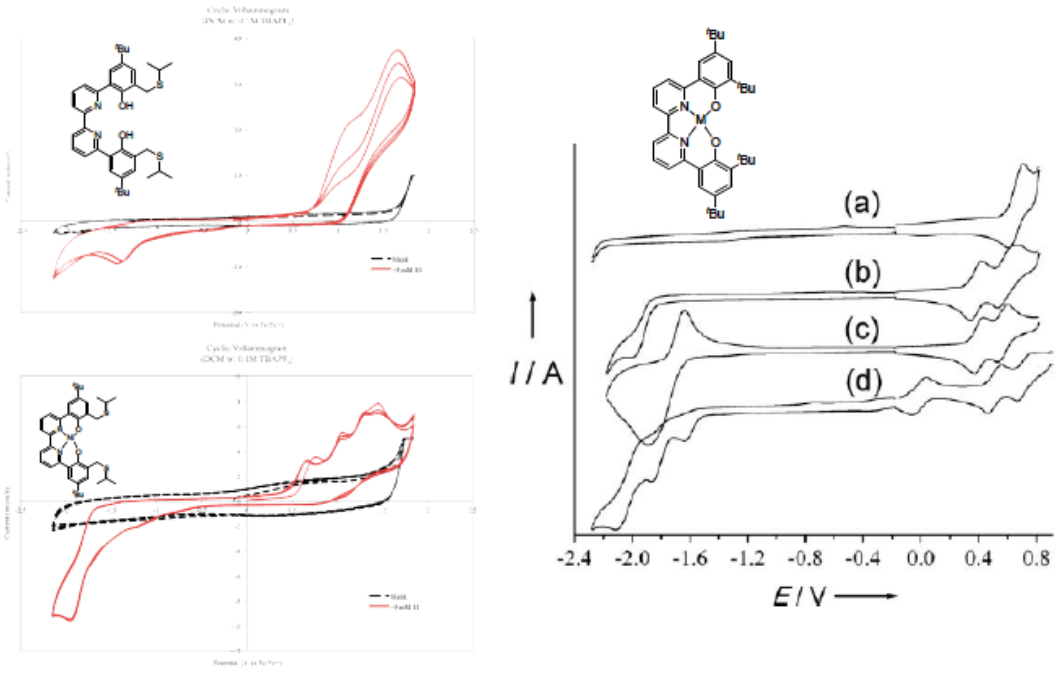


**Figure B.4:** Cyclic voltammograms of compound **10** (top left), compound **11** (bottom left), and a series of $LM^{II}$ literature compounds23 with similar structure (right). For the $LM^{II}$ compounds, M = Zn (a), Ni (b), Cu (c), and Co (d). All voltammograms were

taken in $CH_2Cl_2$ with 0.1 M $TBAPF_6$ (compounds 10 and 11) or 0.1 M TBAClO4 (LMII) supporting electrolyte. Potentials are referenced to $Fc/Fc^+$.

Electrochemical investigation of compound **11** in $CH_2Cl_2$ revealed 4 irreversible oxidations and an irreversible reduction (see Figure B.4), while the electrochemistry of compound **10** exhibits 2 irreversible oxidations and an irreversible reduction. Comparing **10** and **11** with literature compound **13**, the first two oxidations of **11** at 0.7 and 1.0 V (vs Fc/Fc+) are assigned as ligand-based oxidation of the phenoxides that have been split by electrochemical communication through the Ni center, and the second two oxidations at 1.3 and 1.5 V are assigned as oxidation of the benzylic thioethers that have also been split by interaction with the Ni center, while the event at -1.9 V is assigned as ligand-based reduction of the bipyridine backbone. These assignments are consistent with the CV observed for compound **13** (also Figure B.4), which demonstrates 2 reversible oxidations assigned to the phenoxides, and an irreversible reduction assigned to reduction of the bipyridine ligand.

Pursuing di-Ni compounds of relevance to the active site of ACS (see Figure B.1), reaction of **11** with $Ni(OTf)_2$ was attempted for extended time periods both at room temperature and refluxing in MeCN or MeOH, however only the unreacted starting materials were isolated upon workup. Access to the desired di-cationic compound **12** via other $Ni^{II}$ sources such as $NiI_2$ or $Ni(ClO_4)_2$-$6H_2O$ have not yet been investigated. Alternatively, addition of one equivalent of $Ni(COD)_2$ to a solution of **11** in $C_6D_6$ led to a color change from dark red to brown over the course of 12 hours at room temperature. The $^1H$ NMR spectrum of this brown solution showed only resonances assignable to $Ni(COD)_2$ and free COD, with no resonances assignable to diamagnetic

starting material **11**. Removal of the volatiles in vacuo resulted in isolation of a brown solid; however, dissolving of this brown solid in either $C_6H_6$ or THF followed by filtering and concentrating in vacuo resulted in isolation of a salmon-orange solid with diamagnetic $^1$H NMR resonances assignable to **11**, corresponding to the bulk of the starting material by mass. It is postulated that in solution a di-Nickel compound is formed that is unstable to loss of COD, as indicated in Scheme B.2, and upon work-up this compound decomposes to the mono-Ni compound **11** and Ni black.

The results of these initial attempts at forming a di-Ni compound suggest that under these conditions the terminal thioether sulfurs may be too poor of sigma donors to stabilize a $Ni^{II}$ cation and too poor of pi-acids to stabilize $Ni^0$. There are surprisingly few di-cationic, square-planar, bis-thioether, acyclic $Ni^{II}$ compounds that have been crystallographically characterized in the literature, which have been accessed either via bis-thioether ligands[24-28] or alkylation of neutral bis-thiolate Ni compounds[29-31]. A structurally related Schiff-base Cu compound employing thioether ligands has been reported in the literature[32], and in this report the authors found that reaction of the neutral $Cu^{II}$ compound with $AgBF_4$ results in the formation of a hetero-bimetallic cationic complex in which the phenoxides bridge to a $Ag^+$ ion terminally bound by the two thioether sulfur atoms. Through bond-length analysis of the solid-state structure, the authors propose only weak interactions between $Ag^+$ and the phenoxide oxygens and stronger interactions between $Ag^+$ and S (though this is to be expected based on Hard-Soft Acid-Base theory). Extending this to compound **11**, it is possible that the similarly covalent Ni-O bonds would result in only weakly donating M-O interactions to a second metal center.

Based on this analysis, it was speculated that the bridging phenoxides/bis-thioethers

present in compound **11** could not suitably stabilize a di-Ni complex capable of participating in substrate-based reactivity.

**Scheme B.3.** Access to mixed thiolate/thioether compounds via alkylation of bis-thiolates.

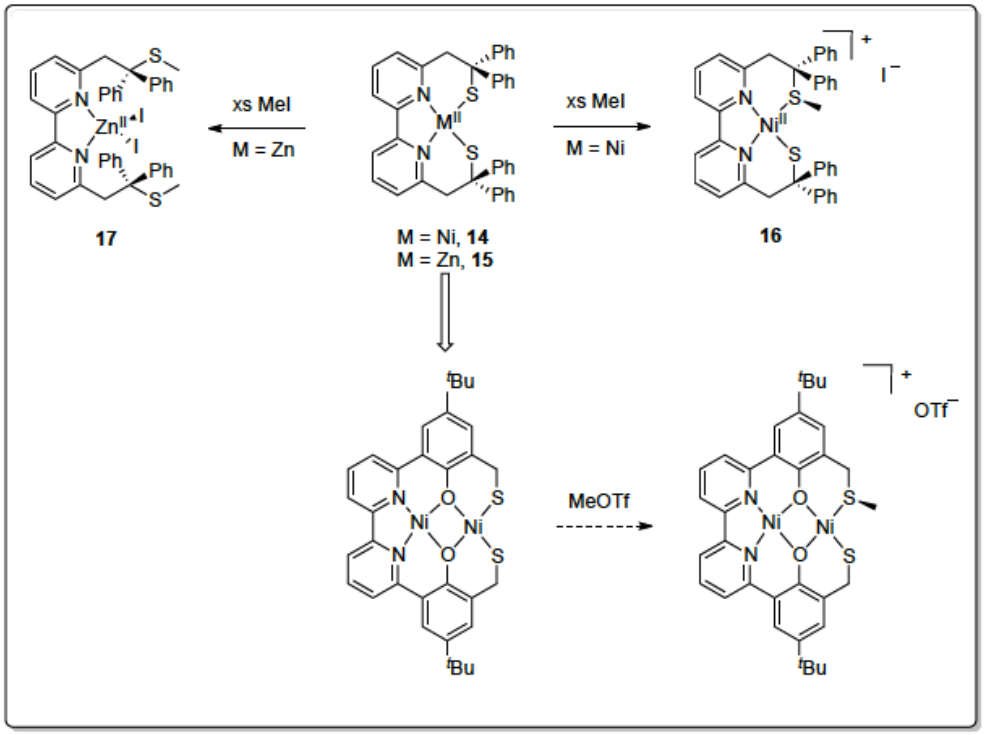


Focus was shifted toward pursuing a mixed thiolate/thioether ligand that could bind a second $Ni^{II}$ atom through an anionic thiolate, but also retain hemi-lability through a thioether moiety. It was believed that a mixed thiolate/thioether di-Ni compound could be accessed via mono-alkylation of a di-thiolate di-Ni compound as shown in Scheme B.3. Duboc[33] recently demonstrated that starting from neutral MII bipyridine-bis-thiolate compounds **14** and **15**, the identity of the metal determined the thiolate alkylation product with $CH_3^+$ sources such as MeI. Thus when M is Zn, exposure of **15** to an excess of MeI results in the isolation of a bis-thioether product **17** in which the

sulfur atoms are no longer bound to the metal center. Alternatively, when M is Ni exposure of compound **14** to an excess of MeI results in the formation of the mono-alkylated cationic mixed thiolate/thioether product **16** in which the thioether sulfur remains bound to the metal, while the corresponding bis-alkylated product is not observed. The authors suggest this is due to the electronics of the more covalent Ni-S interaction in contrast to the more ionic Zn-S interaction, which they support this hypothesis with DFT calculations, in addition to sterics.

Focusing on accessing a mixed thiolate/thioether system similar to that of Duboc, an alternate synthetic route was devised that would allow installation of the terminal donor atoms later in the synthesis, giving access to a more diverse set of ligands. This more direct, modular synthesis is outlined in Scheme B.4. Starting from para-tertbutylphenol, reaction with MOMCl in the presence of Hunig's base yielded the desired MOM protected product 18. Ortho directed lithiation followed by quenching with $B(OiPr)_3$ and workup with $KHF_2$ afforded the desired aryltrifluoroborate salt 19 in high yield. The Suzuki coupling of this compound with 6,6'-dichloro-2,2'-bipyridine led to the desired product **21**. It should be noted that Suzuki couplings of 6,6'-dibromo-2,2'-bipyridine34,35 and various chloropyridines[36,37] with arylboronic acid derivatives are well documented in the literature, yet this is the first reported Suzuki coupling employing 6,6'-dichloro-2,2'-bipyridine. A one-pot MOM deprotection/ortho bromomethylation with HBr in acetic acid yielded the desired dibromide **22** in near quantitative yield. From here, several functional groups were successfully installed at the benzylic position via $S_N2$ reactions, namely acetylthioester (**23**), di-(2-picolyl)-amine (**24**), N-methyl-(2-picolyl)- amine (**25**), and methylimidazolium bromide (**26**).

**Scheme B.4.** Alternate synthetic route to multinucleating, acyclic ligands.

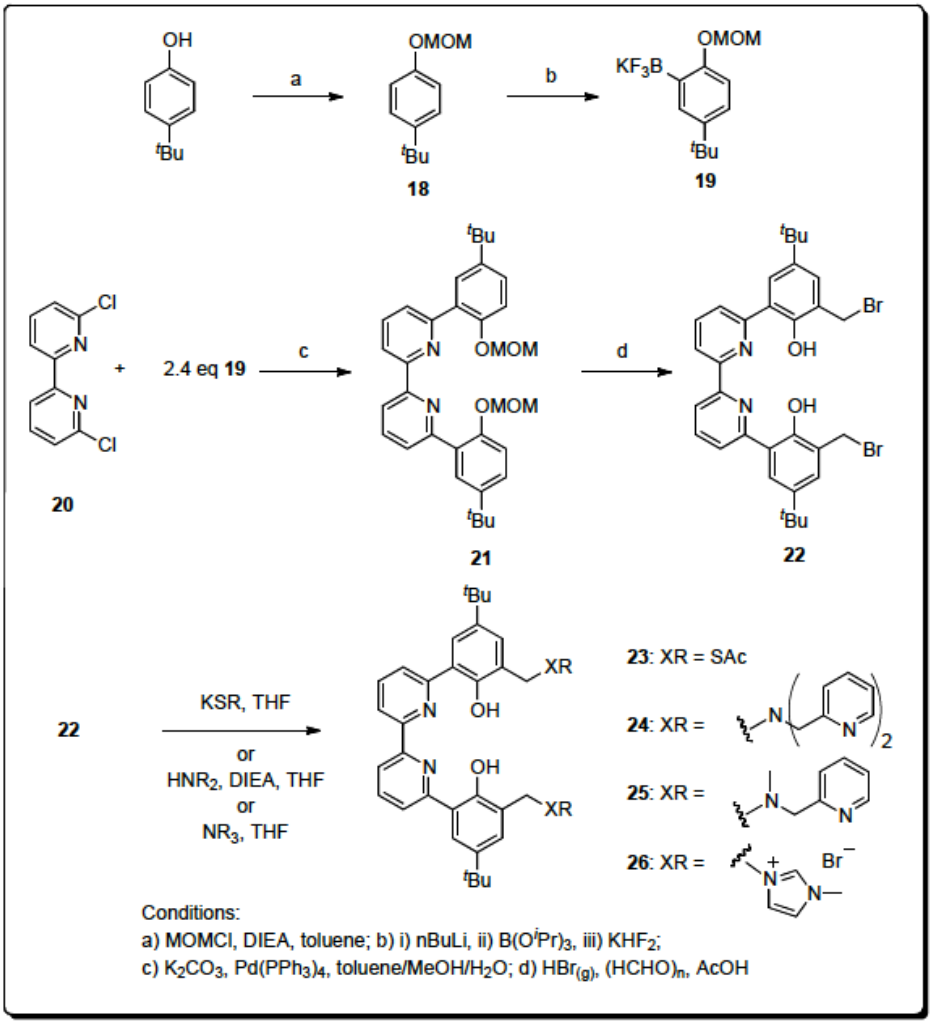


Unfortunately, numerous attempts at installing phosphines onto the ligand framework were unsuccessful. It was postulated that while sulfur and nitrogen are sufficiently nucleophilic to displace the bromide, phosphines are more bulky and instead deprotonate this reactive orthobromomethylphenol moiety, even though other ortho-bromomethylphenol phosphine compounds have been reported in the literature38,39. Disappointingly, the acetyl-protected variant of compound **22** also failed to yield phosphine-substituted products.

**Scheme B.5.** Toward accessing a mixed thiolate/thioether bimetallic compound.

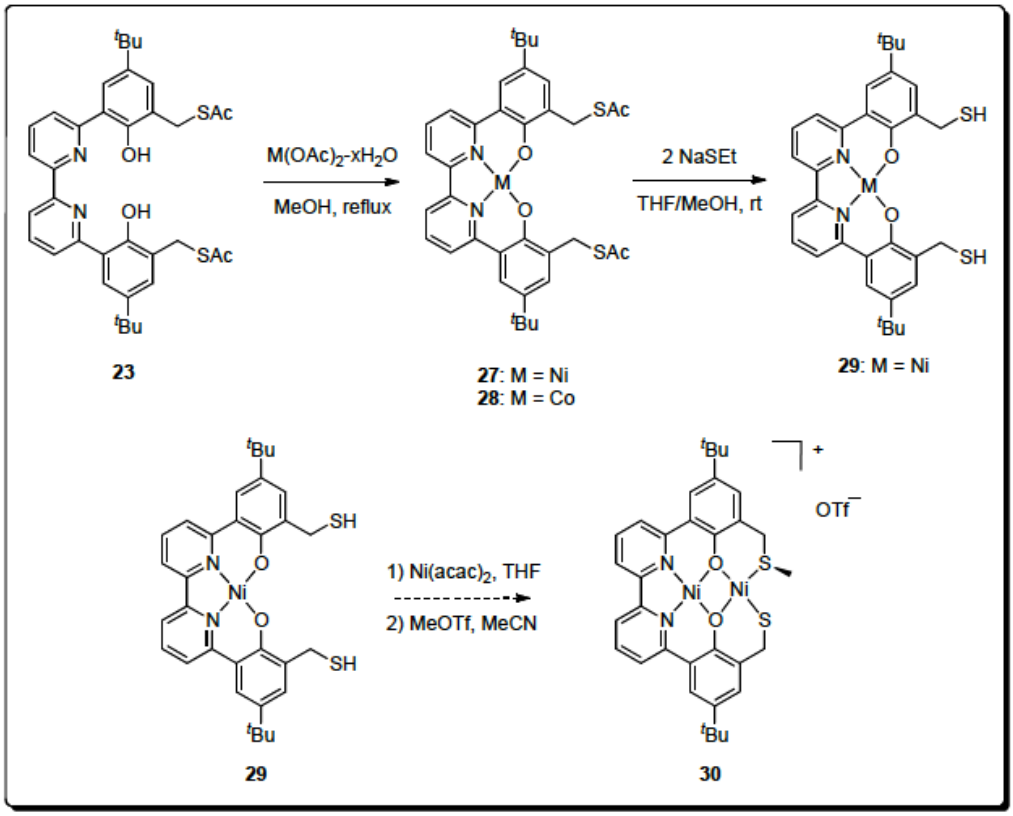


Toward accessing a mixed thiolate/thioether bimetallic compound, reaction of the thioester compound **23** suspended in refluxing methanol with $M^{II}(OAc)_2$-$xH_2O$ and two equivalents of $Et_3N$ over the course of 12 hours led to a color change from tan to yellow, red/orange, and brown for M = Zn, Ni, and Co, respectively (see Scheme B.5). After cooling to room temperature and collecting the colored precipitates, the yellow product from the Zn reaction proved insoluble in most solvents, however it was solubilized by pyridine, suggesting that the product forms oligomers that can be broken up by strongly coordinating solvent. Similar bisphenol-pyridine Cu and Zn compounds have been shown to exhibit dimerization and oligomerization in the solid state[40]. This yellow Zn product has yet to be characterized further by either $^1$H NMR spectroscopy

in $d_5$-pyridine or ESI-MS.

The products of the Ni and Co reactions, however, showed solubility in chlorinated solvents and THF. The $^1$H NMR spectrum of the Ni product in $CDCl_3$ revealed diamagnetic resonances consistent with a $C_{2v}$ symmetric molecule and displayed aromatic resonances similar to those observed in compound **13**. The absence of a phenol resonance and the lack of a shift in the benzylic methylene and the thioester acetyl resonances suggest Ni is bound in the bipyridine pocket. ESI-MS data from a solution of the red/orange solid in 1:1 $CH_2Cl_2$:MeOH revealed a peak at 707. This mass is assigned as the $[M + Na]^+$ ion where M is compound **27**. The $^1$H NMR spectrum of the Co product in $CDCl_3$ only revealed resonances assignable to trace solvents and no resonances assignable to the diamagnetic starting material. The observed color change and the absence of diamagnetic $^1$H NMR resonances are consistent with the formation of a paramagnetic $Co^{II}$ complex. ESI-MS data from a solution of the brown solid in 1:1 $CH_2Cl_2$:MeOH revealed a peak at 708. This mass is assigned as the $[M + Na]^+$ ion where M is compound **28**.

The Ni compound **27** was taken on and deprotection of the thioester moieties was attempted with two equivalents of NaSEt in THF/MeOH at room temperature. After stirring for 10 minutes, removal of the volatiles in vacuo followed by treatment of the crude reaction product with a saturated aqueous NaHCO3 solution and extraction with DCM led to the isolation of a red solid. The $^1$H NMR spectrum of this red solid revealed resonances consistent with a $C_{2v}$ symmetric molecule. The absence of a phenolic signal suggests that Ni remains bound to a phenoxide moiety. The absence of the benzylic methylene and thioester acetyl resonances and the appearance of a new doublet at 3.86 ppm and a new triplet at 3.10 ppm that integrate as 4:2 (against the 18H

tert-butyl resonance at 1.35 ppm) suggest clean conversion to the bis-thiol compound **29** in which 3-bond coupling is observed through the sulfur heteroatom. ESI-MS data of a solution of this product in $CH_2Cl_2$ failed to yield any assignable signals, possibly due to the reactive and oxygen-sensitive thiol moieties assumed present. It was found that the cleanest deprotections were affected with very short reaction times, on the order of 10 minutes, while slightly longer reaction times resulted in the appearance of downfield resonances in the $^1$H NMR spectra assigned as phenolic protons, presumably corresponding to loss of Ni.

Reaction of the Ni-bisthiol compound **29** as a solution in THF with one quivalent of $Ni(acac)_2$ at room temperature led to a color change from dark red to brown over the course of 12 hours. Removal of the volatiles in vacuo led to the isolation of a brown solid. This brown product demonstrated incredibly low solubility in most common solvents; however, a suspension of this solid in MeCN was subsequently solubilized over the course of 3 hours upon addition of 1.5 equivalents of MeOTf. Removal of the volatiles in vacuo resulted once again in the isolation of a brown solid. The $^1$H NMR spectrum of this product in $CD_3CN$ revealed only broad resonances in the diamagnetic region. ESI-MS data of a solution of this brown solid in MeCN revealed a peak at 688. This mass is assigned as the $[M + O + H]^+$ ion, where M corresponds to the cation of compound **30**.

**Scheme B.6.** Synthesis of multimetallic Cu-containing complexes.

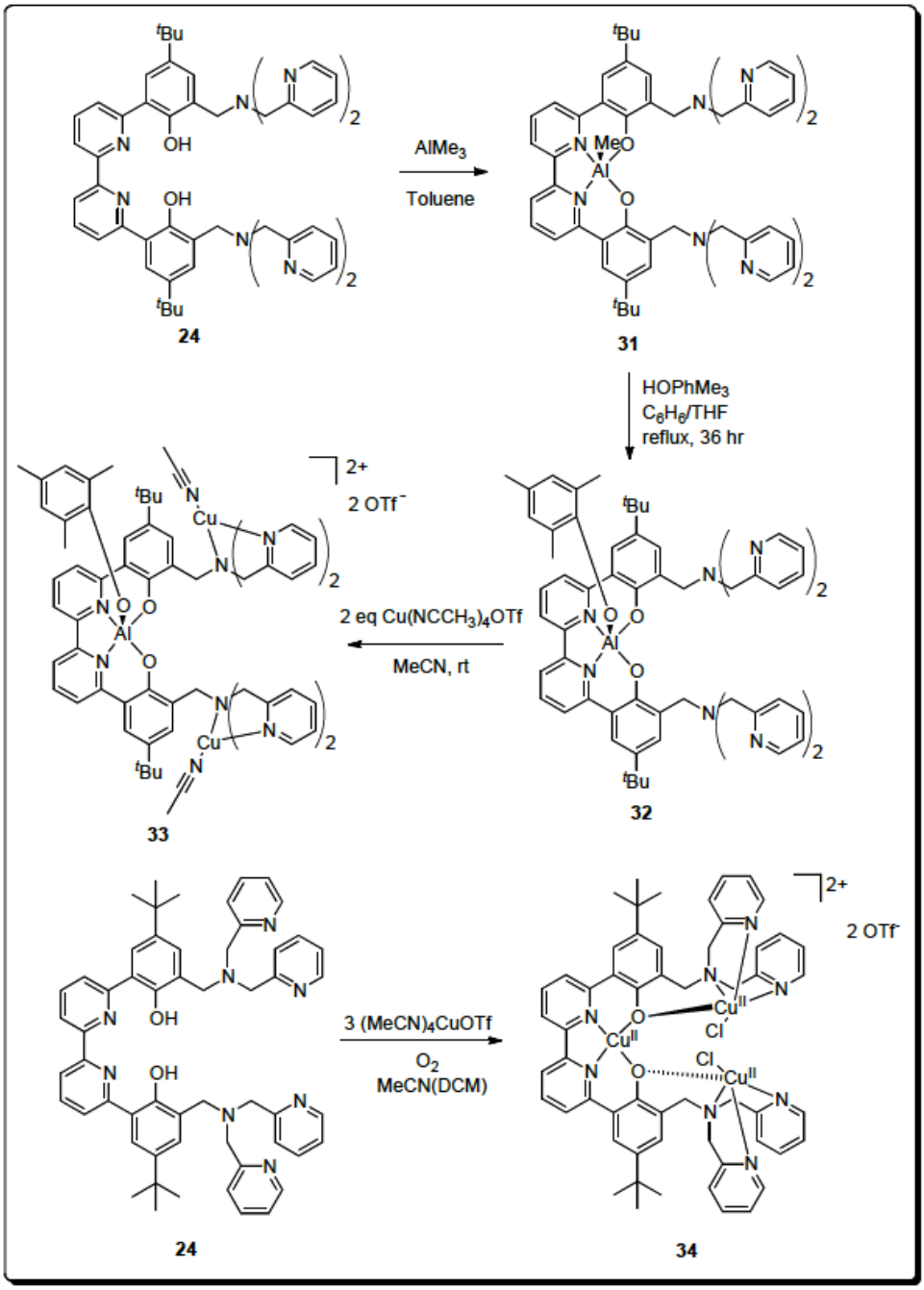


Attempts at crystallizing this product are currently underway. If this product is indeed a di-Ni compound, it seems that either the Ni centers adopt pseudo-tetrahedral

geometries or in solution the Ni centers are able to distort away from square-planarity quickly on the NMR timescale, giving rise to broad resonances. One can imagine a fluxional process in which the phenoxides rotate in and out of the bipyridine plane that could account for this distortion from square-planar geometry. Variable temperature $^1$H NMR experiments have yet to be performed to investigate this phenomenon further.

Inspired by the active site of Tyrosinase, other multi-metallic compounds (see 2 in Figure B.1) were pursued in which pendant amine arms could bind two $Cu^I$ atoms in close proximity to a third metal center (see Scheme B.6). If the two $Cu^I$ centers could cooperatively react with dioxygen intramolecularly, a reactive $Cu_2O_2$ intermediate could be held in close proximity to a pendant lewis acid that could facilitate substrate-based C–H bond oxidation. Pursuant to this goal, addition of a solution of one equivalent of $AlMe_3$ in Toluene upon thawing to a frozen solution of compound **24** in Toluene followed by warming the solution slowly to room temperature resulted in a color change from orange to brown and subsequent lightening to a red/orange after stirring at room temperature for 3 hours. Upon removal of the volatiles in vacuo, $^1$H NMR of the resulting yellow solid in $CD_2Cl_2$ revealed resonances consistent with a $C_s$ symmetric molecule. The absence of a phenolic resonance and the lack of significant shifts in the pyridyl and benzylic methylene signals suggest binding of aluminum in the bipyridine pocket. The appearance of a signlet at -1.5 ppm that integrates as 3H against the tert-butyl 18H singlet at 1.3 ppm is assigned as the Me-Al peak and is consistent with similar bisphenoxide-Al-Me species reported in the literature[41]. The benzylic methylene protons have split due to the break in symmetry created by the presence of the proposed 5-coordinate Me-Al moiety in compound **31**. Based on integration, the picolyl methylene protons exhibit diastereotopicity, while the phenolic benzyl protons demonstrate

coincidental resonance.

Heating this product in the presence of one equivalent of 2,4,6-trimethylphenol in THF or a mixture of THF/$C_6D_6$ for 36 hours at 60 °C resulted in the loss of the Al-Me resonance by 1H NMR and the growth of several new resonances consistent with a $C_s$ symmetric molecule. The resulting orange product was washed with $Et_2O$ to remove unreacted 2,4,6-trimethylphenol as well as other minor impurities, and the resulting orange precipitate exhibited an $^1$H NMR spectrum consistent with Aluminum-phenoxide compound **32**. Addition of a solution of 2 equivalents of $Cu(NCCH_3)_4OTf$ in MeCN to a suspension of compound **32** in MeCN resulted in a homogeneous orange solution after 5 minutes. Removal of the solvents in vacuo resulted in isolation of an orange solid.

Analysis of the $^1$H NMR spectrum of this compound revealed resonances consistent with a $C_s$ symmetric molecule in which the benzylic signals have split further, with both the picolyl and phenolic methylene protons exhibiting diastereotopicity. The chemical shifts of the pyridyl resonances in the aromatic region are also consistent with binding to $Cu^I$, thus this product has been assigned as the desired Al-$Cu_2$ complex **33**.

Reactivity with dioxygen of this compound was investigated next to determine the feasibility of intramolecular Cu-$O_2$ reactivity and consequential C–H bond oxygenation of the bound trimethylphenoxide. Exposure of a solution of compound **33** to an atmosphere of $O_2$ at -40 °C in MeCN resulted in a color change from light orange to dark brownorange. After warming to room temperature and removal of the volatiles in vacuo, the resulting brown-orange solid exhibited only broad resonances in the diamagnetic region by $^1$H NMR spectroscopy, consistent with oxidation of $Cu^I$ to a paramagnetic product. Protonolysis of this dark brown-orange product with excess HCl,

extraction with $Et_2O$ and analysis by GC-MS revealed only 2,4,6-trimethylphenol in the organic fraction, and nothing that could be assigned as an oxidized product of the phenol. Since free ligand **24** cannot be detected by GC-MS, the organic extract was then analyzed by $^1H$ NMR spectroscopy. Aside from the 2,4,6-trimethylphenol and free ligand, no other products could be readily identified.

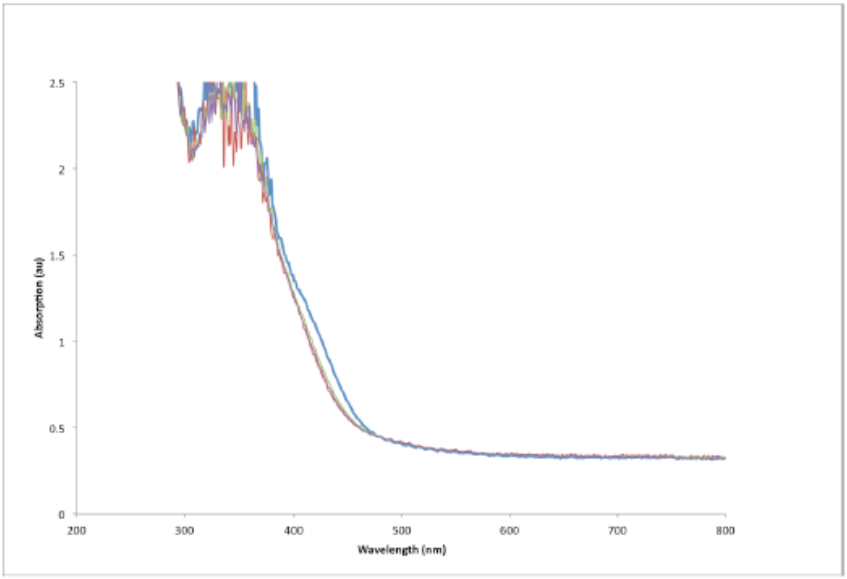


**Figure B.5:** UV-vis absorption of the reaction of **33** with $O_2$ at -80 °C in 1:1 EtCN:Toluene at ~0.05 mM. The blue line is the absorption of **33** under $N_2$. The other traces are after the addition of an oxygenated solution of 1:1 EtCN:Toluene, and show only the expected decrease is absorption corresponding to the dilution. No detectable change appears over 30 minutes.

Monitoring of the reaction of compound **33** with dioxygen at -80 °C in a 1:1 mixture of EtCN and toluene by UV-vis spectroscopy revealed no change in absorption (see Figure B.5). Various $Cu_xO_y$ intermediates (see Figure B.6) that result upon reaction

of x equivalents of $Cu^{I}$ with dioxygen exhibit specific UV-vis and Resonance Raman spectral features that have been investigated in the literature[42] for other $Cu^{I}$ complexes. None of the possible $Cu_xO_y$ intermediates listed in Figure B.6 were observed by UV-vis monitoring. Upon warming to room temperature, analysis of the oxidized product by GC-MS in a manner similar to the NMR reaction revealed only 2,4,6-trimethylphenol.

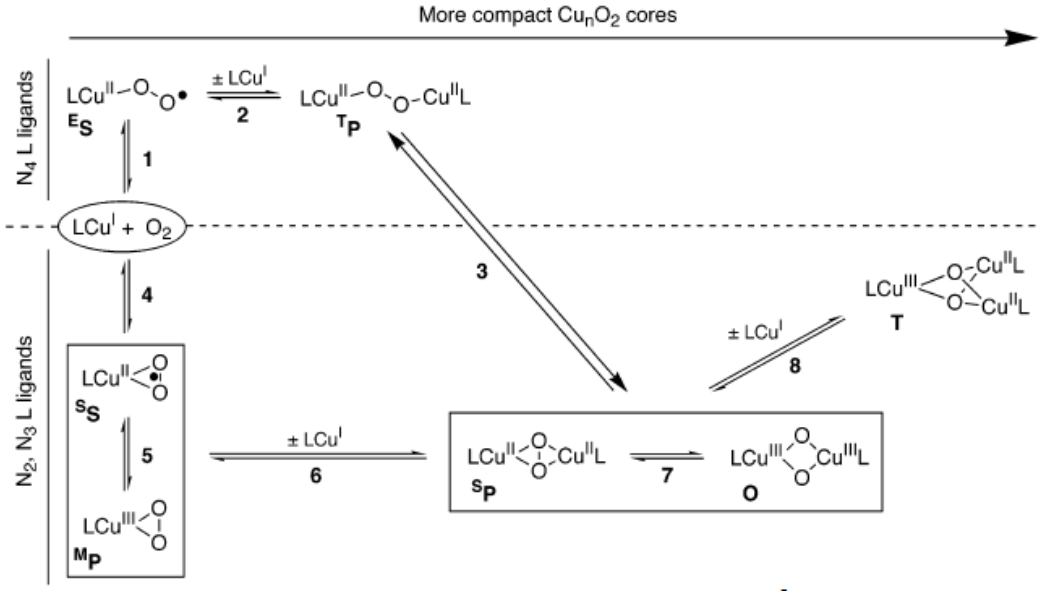


**Figure B.6:** Possible $Cu_xO_y$ intermediates formed upon reaction of $O_2$ with $Cu^{I}$ compounds supported by di-, tri-, and tetra-dentate amine ligands ($N_2$, $N_3$, and $N_4$ L ligands). Taken from the literature[42].

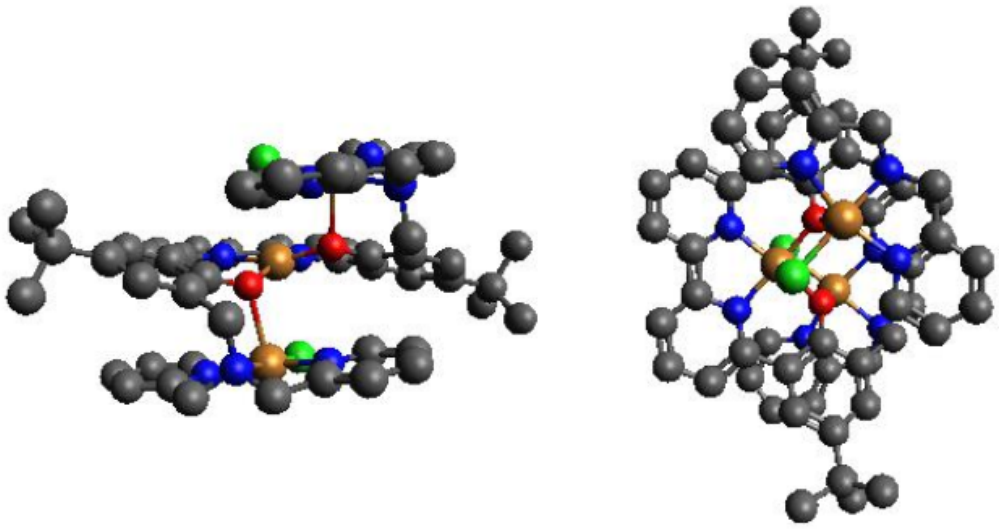

**Figure B.7:** Crystal structure of **34**, top view (right) and side-on view (left). For clarity, hydrogen atoms and outer-sphere triflates have been omitted. Atoms correspond to nitrogen (blue), oxygen (red), copper (orange), chloride (green), and carbon (grey).

Insight into the lack of observable cooperative, intramolecular reactivity of compound **33** with dioxygen was gained by the reaction of dioxygen with a mixture of free ligand **24** and 3 equivalents of $Cu(NCCH_3)_4OTf$ in MeCN (see Scheme B.6). Upon exposure to an atmosphere of $O_2$ at -40 °C, the light orange solution of the mixture of free ligand and three equivalents of $Cu^I$ turned dark green. Upon warming to room temperature, $^1H$ NMR analysis of the resulting dark green product revealed only broad resonances in the diamagnetic region, suggestive of oxidation of $Cu^I$. Crystals of this dark green product suitable for X-ray Diffraction studies were grown by slow evaporation of a concentrated MeCN solution at room temperature. The corresponding crystal structure reveals a tri-metallic complex composed of three $Cu^{II}$ centers (see Figure B.7); one Cu is bound in the bpy-bisphenol pocket, while the other two Cu atoms are each bound by a

dipicolylamine arm, with a fourth interaction with a phenoxide oxygen atom. The sterically accessible nature of the phenoxide moiety and the visible interaction present in **34** seems to suggest that an oxidized Cu atom bound to a dipicolylamine arm can easily be coordinated by these oxygen atoms. While it has been suggested previously that phenoxides bound to $Cu^{II}$ or $Ni^{II}$ exhibiting fairly covalent M–O bonds would only weakly bridge to a second metal center, this crystal structure indicates that an interaction is possible, at least in the solid state. Considering compound **33** contains Al-O bonds, which are more ionic in nature than the Cu-O bonds in compound **34**, it is possible that this exposed phenoxide atom could rapidly bridge to an oxidized copper species supported by one of the dipicolylamine moieties.

Based on these results, the mechanism proposed in Scheme B.7 could account for the lack of observable cooperative, intramolecular reactivity of compound **33** with dioxygen. The initial step involves reaction of one CuI center with $O_2$ to form either the side-on superoxo-$Cu^{II}$ **33-$^{S}$S** or the mono-nuclear peroxo-$Cu^{III}$ **33-$^{M}$P-1**, which are likely in equilibrium with one another. As soon as it is formed, this equilibrium oxidized-Cu center then rapidly and irreversibly binds to the aluminum-bound phenoxide oxygen, generating the **33-$^{M}$P-2**. This bound species is unable to react further with another $Cu^{I}$ center intramolecularly as it is sterically inaccessible to the second dipicolylamine arm. This species then thermally decomposes, yielding some oxidized copper product **33ox**. While Cu-superoxo and peroxo species **$^{S}$S** and **$^{M}$P** do typically exhibit distinct spectroscopic absorptions in the UV-visible region, the extinction coefficients associated with these species are usually quite low (~1000 $M^{-1}cm^{-1}$)[43-46] and the more intense absorptions likely overlap with the main absorption of **33** at ~350 nm, which exhibits a very large extinction coefficient (~30,000 $M^{-1}cm^{-1}$). Thus assuming this

proposed mechanism is operative, it is not surprising that a Cu-peroxo or superoxo species is not detected by UV-vis spectroscopy at these low concentrations (~0.05 mM). Resonance Raman experiments have not yet been performed to observe any O–O or Cu–O vibrations associated with a Cu-superoxo or peroxo species.

**Scheme B.7.** Proposed mechanism of $O_2$ reactivity for **33**.

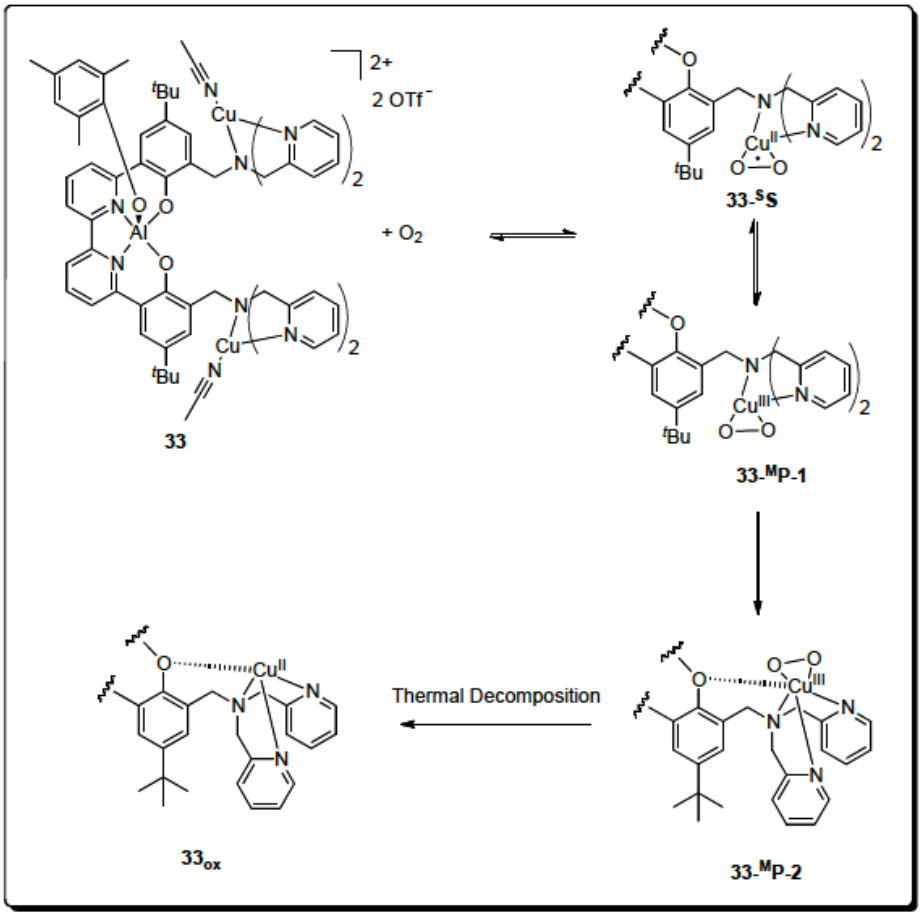


Finally, as the thioether's present in **11** were posited to be both inadequate sigma donors and pi-acceptors for stabilizing either a $Ni^{II}$ or a $Ni^{0}$ center, the possibility of using N-heterocyclic carbenes (NHCs) in the terminal donor position was pursued (see Scheme B.8) as NHCs have been shown to readily bind both Ni(II)[47] and Ni(0)[48]. Initial

access to the methyl-substituted bis-imidazolium bromide 26 was gained via simple $S_N2$ displacement of the benzylic bromide in 22 with methylimidazole (Scheme B.4), resulting in precipitation of the pale yellow product out of THF. The resulting solid proved insoluble in MeCN, but was readily solubilized in MeOH, and revealed $^1$H NMR resonances consistent with structure **26** in $CD_3OD$.

**Scheme B.8.** Towards N-heterocyclic carbene compounds.

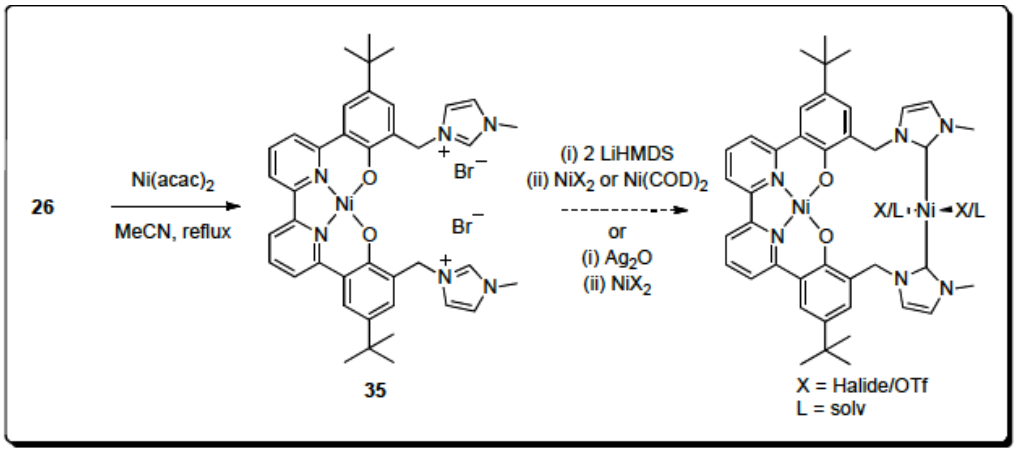


Analogous to complexes **27** and **28**, reaction of compound **26** suspended in refluxing MeCN with $Ni(acac)_2$ resulted in a color change from pale yellow to red over the course of 12 hours. Collection of the red precipitate via filtration and analysis by $^1$H NMR in $CD_3OD$ revealed diamagnetic aromatic resonances consistent with the formation of the desired Ni compound **35**. ESI-MS data of a solution of this red product in MeOH revealed a peak at 698, assigned as $[M - 2Br]^+$ where M is compound **35**. Initial attempts at accessing a di-Ni compound via either deprotonation of the imidazolium to form the free NHC followed by metallation with $Ni^{II}$ or $Ni^0$, or formation of the NHC-AgBr compound by reaction with $Ag_2O$ followed by transmetallation with $Ni^{II}$ have proved unsuccessful. This may be due to the relative instability of methyl-substituted NHCs as

compared to the bulkier arylsubstituted NHCs[49].

## CONCLUSIONS

A series of substituted bipyridine-bisphenol compounds were synthesized incorporating various sulfur- and nitrogen-donor functional groups. Using these ligands, multi-metallic complexes of relevance to biological systems were pursued. Multi-metallic $Ni_2$ systems were not readily accessed from bis-thioether compound **11**, however the thioether donors may better stabilize a softer metal like $Ag^+$. Hetero-bimetallic first-row transition metal $M^{II}$-$Ag^+$ complexes supported by compound **11** could be pursued and their structural and electrochemical properties investigated. The use of the thioester group in compound **23** allowed easy access to mono-metallic bis-thiol compound **29**, suggesting site-selective access to a series of hetero-bimetallic compounds can be gained through use of this protected thiol moiety. Furthermore, access to mixed thiolate/thioether bi-metallic complexes similar to **30** in which the bipyridine-bound metal is varied across the first row could be pursued and substrate-based reactivity investigated related to ACS.

The ability of bpy-bisphenol compounds to generate mulit-metallic complexes was demonstrated through the dipicolylamine-functionalized compound **24**, as both the hetero-metallic Al-$Cu_2$ compound **33** and tri-metallic $Cu_3$ compound **34** were synthesized from this ligand precursor. The structural characterization of **34** revealed unanticipated interactions between the oxidized dipicolylamine-bound Cu centers and the phenoxide moieties, which was interpreted as a contributing factor in the lack of demonstrated cooperative intramolecular reactivity of **33** with $O_2$. Use of bulkier, tetradentate amine ligands ($N_4$) supporting Cu in place of the dipicolylamine moiety may circumvent this phenoxide bridging and allow intramolecular dioxygen reactivity between the Cu centers. Additionally, further investigations into ligands bearing more

robust NHC moieties and their corresponding multi-metallic complexes could be pursued.

## EXPERIMENTAL SECTION

### General considerations.

All procedures were carried out using standard Schlenk techniques or in a M. Braun glovebox filled with purified nitrogen unless stated otherwise. All reactions involving metal reagents were carried out in the glovebox. Anhydrous THF was purchased from Aldrich in 18 L Pure-PacTM containers. Anhydrous dichloromethane, acetonitrile, diethyl ether, and THF were purified by sparging vigorously with nitrogen for 15 minutes and then passing under nitrogen pressure through a column of activated A2 alumina (Zapp's). Anhydrous DMF was purchased from Sigma-Aldrich and stored under nitrogen over 4 Å molecular sieves. Spectrophotometric grade acetone was purchased from Sigma-Aldrich, dried over calcium sulfate, vacuum-transferred onto additional calcium sulfate, vacuum-transferred a second time, and stored in the glovebox. All non-dried solvents used were reagent grade or better. All NMR solvents were purchased from Cambridge Isotope Laboratories, Inc. NMR solvents were dried as follows: $CD_3CN$, $CD_2Cl_2$, and $CDCl_3$ over calcium hydride, $C_6D_6$ over sodium benzophenone ketyl. All NMR solvents were degassed by three freeze-pump-thaw cycles and vacuum-transferred prior to use. $^1H$ NMR spectra were recorded on a Varian 300 MHz instrument, with shifts reported relative to TMS as determined by observation of the residual solvent peak. Unless otherwise noted, all commercially available materials were used as received. Compounds **4**[50] , **10**[51] , and **20**[52] were prepared according to literature procedures. UV-Vis spectra were collected on a Varian 50 Bio spectrophotometer using a Schlenk-adapted 1 cm quartz cuvette. Low-temperature UV-Vis spectra were obtained using a Varian dip-probe (661.202-UV, 10 mm).

**Synthesis of 2-bromo-4-(tert-butyl)-6-((isopropylthio)methyl)phenol (5)**

In a 100 mL round bottom, NaH (2.0746 g, 86 mmol) was suspended in THF (50 mL). To this suspension was added isopropyl mercaptan (15 mL, 160 mmol) dropwise, stirring until hydrogen formation had ceased. Next 4 was added neat, and the mixture stirred at room temperature for 2 hours. The volatiles were then removed in vacuo and the residue washed with a saturated solution of $NH_4Cl$ (50 mL). The organics were extracted with $CH_2Cl_2$ (3 x 50 mL), dried over $MgSO_4$ , filtered and concentrated in vacuo. The residue was then purified by kugelröhr distillation, yielding 11.2277 g (85%) of a pale yellow oil. $^1$H NMR (300 MHz, $CDCl_3$, 25 °C): δ (ppm) 7.37 (d, 2.1 Hz, 1H), 7.15 (d, 2.1 Hz, 1H), 6.24 (s, 1H), 3.82 (s, 2H), 2.85 (septuplet, 6.6 Hz, 1H), 1.26-1.29 (m, 15H).

**Synthesis of 1-tert-butyl-3-((isopropylthio)methyl)-4-(methoxymethyloxy)-benzene (6)**

A solution of MOMCl (~70 mmol) in toluene (~50 mL) was prepared according to the literature[53] . To this solution was added **5** (11.2277g, 35 mmol) and N,N-diisopropylethylamine (12 mL, 70 mmol). The resulting mixture was then heated at 50 ° C for 12 hours. After cooling to room temperature, the volatiles were removed in vacuo. The residue was dissolved in a saturated aqueous solution of $NH_4Cl$ (50 mL) and extracted with $CH_2Cl_2$ (1 x 50 mL; 2 x 25 mL). The combined organics were then washed with $NaHCO_3$ (50 mL), dried over $MgSO_4$, filtered, and concentrated in vacuo. The residue was then purified by kugelröhr distillation to yield 10.6829 g (84%) of a yellow oil. $^1$H NMR (300 MHz, $CDCl_3$, 25 °C): δ (ppm) 7.42 (d, 2.4 Hz, 1H), 7.34 (d,

2.4 Hz, 1H), 5.12 (s, 2H), 3.85 (s, 2H), 3.66 (s, 3H), 2.86 (septuplet, 6.9 Hz, 1H), 1.27 (d, 6.9 Hz, 6H), 1.28 (s, 9H).

**Synthesis of potassium (2-(methoxymethyloxy)-3-(isopropylthio)methyl-5-(tert-butyl)-phenyl)-trifluoroborate (7)**

In a 100 mL round bottom 6 (2.0155 g, 5.6 mmol) was stirred in THF (50 mL) and cooled to -78 ° C. Next, $^{n}$BuLi (2.4 mL, 2.65 M, 6.4 mmol) was added dropwise. After complete addition, the solution was stirred for 15 minutes at this temperature, then $B(O^{i}Pr)_3$ (1.6 mL, 6.9 mmol) was added neat. The solution was stirred at -78 °C for 1 hour and then allowed to warm to room temperature over night. The volatiles were then removed in vacuo, and $KHF_2$ (2.6784 g, 34.3 mmol) was added as a solution in $H_2O$ (10 mL) and MeOH (10 mL). The mixture was stirred for 1 hour at room temperature, and the resulting precipitate was then filtered on a glass frit, rinsing with $H_2O$ and then hexanes. The resulting white solid was then dried under vacuum, yielding 0.9686 g (45%) of the desired compound. $^{1}$H NMR (300 MHz, $(D_3C)_2CO$, 25 °C): δ (ppm) 7.52 (d, 2.7 Hz, 1H), 7.18 (d, 2.7 Hz, 1H), 5.14 (s, 2H), 3.86 (s, 2H), 2.89 (septuplet, 6.9 Hz, 1H), 1.27 (s, 9H), 1.25 (d, 6H). $^{19}$F NMR (300 MHz, $(D_3C)_2CO$, 25 °C): δ (ppm) -139.2 (broad multiplet).

**Synthesis of 6,6'-bis-(2-(methoxymethyloxy)-3-(isopropylthio)methyl-5-(tert-butyl)-phenyl)-2,2'-bipyridine (9)**

In a schlenk bomb was combined 6,6'-dibromo-2,2'-bipyridine (0.3091 g, 0.98 mmol), **7** (0.9083 g, 2.3 mmol), $K_2CO_3$ (1.3028 g, 9.4 mmol), toluene (40 mL), MeOH (10 mL),

$H_2O$ (5 mL) and a stir bar. The vessel was degassed using the freeze-pump-thaw method (3 cycles), and then under an atmosphere of $N_2$ a suspension of $Pd(PPh_3)_4$ (0.0679 g, 0.06 mmol) in degassed toluene (5 mL) was transferred to the reaction mixture. The bomb was sealed and refluxed at 80 °C for 12 hours. After cooling to room temperature, $H_2O$ (50 mL) was added to the reaction mixture and the organic material was extracted with $CHCl_3$ (50 mL). The aqueous layer was then washed with $CHCl_3$ (2 x 25 mL), and the combined organic washes were dried over $MgSO_4$, filtered, and concentrated in vacuo. The crude yellow solid was then suspended in a minimal amount of MeOH, sonicated for 5 minutes, cooled to -20 ° C for one hour, and then filtered on a glass frit. The yellow powder was then collected and dried under high vacuum, yielding 0.7059 g (80%) of the desired product. $^1$H NMR (300 MHz, $CDCl_3$, 25 ° C): δ (ppm) 8.50 (dd, 7.5 Hz, 1.2 Hz, 2H), 7.86 (t, 7.5 Hz, 2H), 7.80 (dd, 7.5 Hz, 1.2 Hz, 2H), 7.72 (d, 2.7 Hz, 2H), 7.48 (d, 2.7 Hz, 2H), 4.78 (s, 4H), 3.94 (s, 4H), 3.30 (s, 6H), 2.96 (septuplet, 6.9 Hz, 2H), 1.39 (s, 18H), 1.33 (d, 6.9 Hz, 12H).

**Synthesis of 6,6'-([2,2'-bipyridine]-6,6'-diyl)-bis-(2-(isopropylthio)methyl-4-(tert-butyl))phenol (10)**

In a 50 mL round bottom, **9** (0.5035 g, 0.7 mmol) was suspended in MeOH (20 mL). Then concentrated HCl (0.40 mL, 12 N, 4.8 mmol) was added and the mixture stirred for 1 hour at room temperature. The volatiles were then removed in vacuo and the residue treated with $H_2O$ (20 mL). The organics were extracted with $CHCl_3$ (3 x 20 mL). The combined extracts were dried over MgSO4 , filtered, and concentrated in vacuo to yield 0.2806 g (60%) of the desired product. $^1$H NMR (300 MHz, $CDCl_3$, 25 ° C): δ (ppm) 14.39 (s, 2H), 8.15 (dd, 6.6 Hz, 2.1 Hz, 2H), 8.04 (m, 4H), 7.77 (d, 2.1 Hz,

2H), 7.44 (d, 2.1 Hz, 2H), 3.94 (s, 4H), 2.97 (septuplet, 6.9 Hz, 2H), 1.38 (s, 18H), 1.33 (d, 6.6 Hz, 12H).

**Synthesis of LSiPrNi (11)**

In a 20 mL scintillation vial, **10** ( 0.02 g, mmol) was dissolved in THF (5 mL). To this solution was added $Ni(acac)_2$ (0.01 g, mmol) as a solution in THF (2 mL). A color change from pale yellow to dark red was observed over the course of 30 minutes. After stirring for 3 hours, the volatiles were removed in vacuo, and the resulting salmon-orange solid washed with $Et_2O$ (5 mL). The salmon-orange precipitate was then collected and dried in vacuo yielding (60%) of the desired product. $^1$H NMR (300 MHz, $CDCl_3$, 25 ° C): δ (ppm) 14.39 (s, 2H), 8.15 (dd, 6.6 Hz, 2.1 Hz, 2H), 8.04 (m, 4H), 7.77 (d, 2.1 Hz, 2H), 7.44 (d, 2.1 Hz, 2H), 3.94 (s, 4H), 2.97 (septuplet, 6.9 Hz, 2H), 1.38 (s, 18H), 1.33 (d, 6.6 Hz, 12H). ESI-MS .

**Synthesis of 4-tert-butyl-1-(methoxymethyloxy)-benzene (18)**

A solution of MOMCl (~500 mmol) in toluene (~220 mL) was prepared according to the literature[53]. To this solution was added 4-tert-butylphenol (50.6929 g, 337 mmol) and N,N-diisopropylethylamine (80 mL, 460 mmol). The resulting mixture was then heated at 50 ° C for 12 hours. After cooling to room temperature, the volatiles were removed in vacuo. The residue was dissolved in a saturated aqueous solution of $NH_4Cl$ (150 mL) and extracted with $CH_2Cl_2$ (1 x 150 mL; 2 x 100 mL). The combined organics were then washed with $NaHCO_3$ (150 mL), dried over $MgSO_4$, filtered, and concentrated in vacuo. The residue was then purified by kugelröhr distillation to yield 63.0975 g (96%) of a colorless oil. $^1$H NMR (300 MHz, $CDCl_3$, 25 °C): δ (ppm) 7.31 (d,

8.7 Hz, 2H), 6.98 (d, 8.7 Hz, 2H), 5.16 (s, 2H), 3.48 (s, 3H), 1.30 (s, 9H).

**Synthesis of potassium (2-(methoxymethyloxy)-5-tert-butyl-phenyl)trifluoroborate (19)**

In a 3-neck, 500 mL round bottom fitted with $N_2$ inlet and 60 mL dropping funnel was added TMEDA (9.3 mL, 62.0 mmol) in $Et_2O$ (250 mL). The solution was cooled to -40 ° C and $^n$BuLi (24 mL, 2.61 M, 62.6 mmol) was added dropwise, flushing with Et2 O (20 mL). After stirring for 15 minutes, 1-tert-butyl-4-(methoxymethoxy)-benzene (10.0105 g, 51.5 mmol) was added dropwise, flushing with $Et_2O$ (20 mL). After stirring for 1 hour at -40 ° C, the cooling bath was removed and the mixture allowed to warm to room temperature for 1 to 2 hours. The reaction mixture was then cooled to -78 ° C and $B(O^iPr)_3$ (16 mL, 69.3 mmol) was added neat. The solution was stirred for 1 hour at this temperature and then warmed to room temperature and left stirring over night. The solution was then concentrated in vacuo and quenched with a solution of $KHF_2$ (24.0255 g, 308 mmol) in $H_2O$ (100 mL) and MeOH (100 mL), stirring for 1 hour. The resulting precipitate was then filtered on a coarse glass frit, washing with $H_2O$ followed by washing with hexanes. The resulting white solid was then collected and dried under high vacuum for several hours, yielding 13.6358 g (88%) of the desired product. $^1$H NMR (300 MHz, $(D_3C)_2CO$, 25 °C): δ (ppm) 7.59 (d, 2.7 Hz, 1H), 7.06 (dd, 8.7 Hz, 2.7 Hz, 1H), 6.78 (d, 8.7 Hz, 1H), 5.13 (s, 2H), 3.44 (s, 3H), 1.26 (s, 9H). $^{19}$F NMR (300 MHz, $(D_3C)_2CO$, 25 °C): δ (ppm) -140.5 (broad multiplet).

**Synthesis of 6,6'-bis-(5-tert-butyl-2-(methoxymethyloxy)phenyl)-2,2'-bipyridine (21)**

In a schlenk bomb was combined 6,6'-dichloro-2,2'-bipyridine (2.0174 g, 9.0 mmol), **19** (6.4166 g, 21.4 mmol), $K_2CO_3$ (8.8966 g, 64.4 mmol), toluene (160 mL), MeOH (40 mL), $H_2O$ (20 mL) and a stir bar. The vessel was degassed using the freeze-pump-thaw method (3 cycles), and then under an atmosphere of $N_2$ a suspension of $Pd(PPh_3)_4$ (0.3001 g, 0.26 mmol) in degassed toluene (20 mL) was transferred to the reaction mixture. The bomb was sealed and refluxed at 80 ° C for 12 hours. After cooling to room temperature, $H_2O$ (100 mL) was added to the reaction mixture and the organic material was extracted with $CHCl_3$ (160 mL). The aqueous layer was then washed with $CHCl_3$ (2 x 50 mL), and the combined organic washes were dried over $MgSO_4$, filtered, and concentrated in vacuo. The crude yellow solid was then suspended in a minimal amount of MeOH, sonicated for 5 minutes, cooled to -20 ° C for one hour, and then filtered on a glass frit. The white powder was then collected and dried under high vacuum, yielding 3.9948 g (82%) of the desired product. $^1$H NMR (300 MHz, $CDCl_3$, 25 °C): δ (ppm) 8.51 (dd, 6.4 Hz, 2.4 Hz, 2H), 8.00 (d, 2.4 Hz, 2H), 7.85 (m, 4H), 7.40 (dd, 8.7 Hz, 2.4 Hz, 2H), 7.19 (d, 8.7 Hz, 2H), 5.19 (s, 4H), 3.44 (a, 6H), 1.40 (s, 18H).

**Synthesis of 6,6'-([2,2'-bipyridine]-6,6'-diyl)bis(2-(bromomethyl)-4-(tert-butyl)phenol) (22)**

In a 3-neck 250 mL round bottom was combined **21** (3.1500 g, 5.8 mmol), paraformaldehyde (0.5371 g, 17.9 mmol), glacial acetic acid (50 mL), and a stir bar. $HBr_{(g)}$ was bubbled through the suspension with vigorous stirring for 15 minutes. Then

the reaction flask was sealed and heated at 90 °C over 8 hours, turning from a yellow heterogenous mixture to an orange homogenous solution. After cooling to room temperature, the acetic acid was distilled in vacuo, the residue washed with $H_2O$ (50 mL), and extracted with $CHCl_3$ (3 x 50 mL). The combined organic washes were dried over MgSO4 , filtered, and concentrated in vacuo. The resulting residue was then triturated with hexanes, filtered, and dried under vacuum yielding 3.6696 g (98%) of a yellow powder. $^1$H NMR (300 MHz, $CDCl_3$, 25 °C): δ (ppm) 14.62 (bs, 2H), 8.17 (dd, 7.5 Hz, 1.5 Hz, 2H), 8.09 (t, 7.5 Hz, 2H), 8.05 (dd, 8.1 Hz, 1.5 Hz, 2H), 7.86 (d, 2.4 Hz, 2H), 7.48 (dd, 2.4 Hz, 2H), 4.74 (s, 4H), 1.39 (s, 18H).

**Synthesis of S-5-(tert-butyl)-3-(6'-(5-(tert-butyl)-2-hydroxy-3-methylphenyl)-[2,2'-bipyridin]-6-yl)-2-hydroxybenzyl ethanethioate (23)**

In a 50 mL round bottom equipped with a stir bar was combined **22** (1.0153 g, 1.6 mmol), KSAc (0.5567 g, 4.8 mmol), and DMF (30 mL). The flask was sealed and heated at 80 °C over 12 hours. After cooling to room temperature, the DMF was distilled in vacuo, and the residue washed with $H_2O$ (20 mL), and extracted with $CH_2Cl_2$ (3 x 20 mL). The combined organic washes were dried over $MgSO_4$, filtered, and concentrated in vacuo, yielding 0.8276 g (83%) of a tan powder. $^1$H NMR (300 MHz, $CDCl_3$, 25 °C): δ (ppm) 14.41 (s, 2H), 8.0 – 8.15 (m, 6H), 7.79 (d, 2.1 Hz, 2H), 7.50 (d, 2.1 Hz, 2H), 4.28 (s, 4H), 2.35 (s, 6H), 1.37 (s, 18H).

**Synthesis of 6,6'-([2,2'-bipyridine]-6,6'-diyl)bis(2-((bis(pyridin-2-ylmethyl)amino)methyl)-4-(tertbutyl)phenol) (24)**

In a 25 mL round bottom was combined diisopropylethylamine (0.3578 g, 2.8 mmol), di-(2-picolyl)amine (0.5101 g, 2.6 mmol), THF (10 mL), and a stir bar. To this stirred solution was added dropwise a solution of **22** (0.7488 g, 1.2 mmol) in THF (10 mL), with precipitate forming upon addition. After complete addition, the mixture was left stirring at room temperature for 3 hours. Then, the precipitate was filtered and the filtrate concentrated in vacuo. The crude solid was then dissolved in a minimal amount of 1:1 EtOAc:$Et_2O$, and washed with $H_2O$ (3 x 30 mL). The organic layer was then dried over $MgSO_4$, filtered, and concentrated in vacuo, yielding 0.4432 g (43%) of an orange solid. $^1$H NMR (300 MHz, $CDCl_3$, 25 °C): δ (ppm) 13.72 (bs, 2H), 8.53 (m, 4H), 8.19 (d, 7.5 Hz, 2H), 8.05 (t, 7.5 Hz, 2H), 8.00 (t, 7.5 Hz, 2H), 7.82 (d, 2.4 Hz, 2H), 7.63 (m, 10H), 7.13 (m, 4H), 3.95 (bs, 8H), 3.93 (bs, 4H), 1.37 (s, 18H).

**Synthesis of 6,6'-([2,2'-bipyridine]-6,6'-diyl)bis(2-((N-methyl-N-(pyridin-2-ylmethyl)amino)methyl)-4-(tert-butyl)phenol) (25)**

In a 25 mL round bottom was combined diisopropylethylamine (0.4131 g, 3.2 mmol), N-methyl-(2-picolyl)amine (0.2070 g, 1.7 mmol), THF (10 mL), and a stir bar. To this stirred solution was added dropwise a solution of **22** (0.5012 g, 0.8 mmol) in THF (10 mL), with precipitate forming upon addition. After complete addition, the mixture was left stirring at room temperature for 3 hours. Then, the solvent was removed in vacuo. The residue was then dissolved in DCM, and washed with aqueous NaOH (1M, 1 x 20 mL) and $H_2O$ (3 x 30 mL). The organic layer was then dried over $MgSO_4$, filtered, and concentrated in vacuo. The resulting residue was then triturated with pentane, yielding

0.4432 g (43%) of an orange solid. $^1$H NMR (300 MHz, $CDCl_3$, 25 °C): δ (ppm) 13.77 (bs, 2H), 8.55 (m, 2H), 8.22 (d, 7.5 Hz, 2H), 8.07 (d, 7.5 Hz, 2H), 8.00 (t, 7.5 Hz, 2H), 7.85 (d, 2.1 Hz, 2H), 7.66 (m, 2H), 7.50 (m, 4H), 7.16 (m, 2H), 3.85 (bs, 4H), 3.82 (bs, 4H), 2.37 (s, 6H), 1.39 (s, 18H).

**Synthesis of 6,6'-([2,2'-bipyridine]-6,6'-diyl)bis(2-((N-methyl-N-(pyridin-2-ylmethyl)amino)methyl)-4-(tert-butyl)phenol) (26)**

In a 25 mL round bottom was combined diisopropylethylamine (0.4131 g, 3.2 mmol), N-methyl-(2-picolyl)amine (0.2070 g, 1.7 mmol), THF (10 mL), and a stir bar. To this stirred solution was added dropwise a solution of **22** (0.5012 g, 0.8 mmol) in THF (10 mL), with precipitate forming upon addition. After complete addition, the mixture was left stirring at room temperature for 3 hours. Then, the solvent was removed in vacuo. The residue was then dissolved in DCM, and washed with aqueous NaOH (1M, 1 x 20 mL) and $H_2O$ (3 x 30 mL). The organic layer was then dried over MgSO4 , filtered, and concentrated in vacuo. The resulting residue was then triturated with pentane, yielding 0.4432 g (43%) of an orange solid. $^1$H NMR (300 MHz, $CDCl_3$, 25 °C): δ (ppm) 13.77 (bs, 2H), 8.55 (m, 2H), 8.22 (d, 7.5 Hz, 2H), 8.07 (d, 7.5 Hz, 2H), 8.00 (t, 7.5 Hz, 2H), 7.85 (d, 2.1 Hz, 2H), 7.66 (m, 2H), 7.50 (m, 4H), 7.16 (m, 2H), 3.85 (bs, 4H), 3.82 (bs, 4H), 2.37 (s, 6H), 1.39 (s, 18H).

**Synthesis of LSAcNi (27)**

In a schlenk tube, **23** (0.2112 g, 0.3 mmol), $Ni(OAc)_2$-$4H_2O$ (0.0981 g, 0.4 mmol), and $NEt_3$ (0.1031 g, 1.0 mmol) were suspended in MeOH (20 mL). The suspension was then heated at 60 °C for 12 hours, during which the color changed from tan to red. After cooling to room temperature, the red precipitate was filtered and washed with MeOH (3 x 10 mL). The precipitate was then collected and dried in vacuo yielding (60%) of the desired product. $^1$H NMR (300 MHz, $CDCl_3$ , 25 °C): δ (ppm) 7.72 (d, 7.5 Hz, 2H), 7.57 (d, 7.5 Hz, 2H), 7.46 (t, 7.5 Hz, 2H), 7.40 (d, 2.1 Hz, 2H), 7.34 (d, 2.1 Hz, 2H), 4.25 (s, 4H), 2.35 (s, 6H), 1.33 (s, 18H). ESI-MS (DCM/MeOH): m/z = 707 $[M + Na]^+$.

**Synthesis of LSacCo (28)**

In a schlenk tube, **23** (0.1999 g, 0.3 mmol), $Co(OAc)_2$-$4H_2O$ (0.0889 g, 0.4 mmol), and $NEt_3$ (0.0685 g, 0.7 mmol) were suspended in MeOH (20 mL). The suspension was then heated at 60 °C for 12 hours, during which the color changed from tan to brown. After cooling to room temperature, the brown precipitate was filtered and washed with MeOH (3 x 10 mL). The precipitate was then collected and dried in vacuo yielding (60%) of the desired product. ESI-MS (DCM/MeOH): m/z = 708 $[M + Na]^+$ .

**Synthesis of LSHNi (29)**

In a 20 mL scintillation vial, **27** (0.0380 g, 0.055 mmol) and NaSEt (0.0099 g, 0.12 mmol) were combined with THF (9 mL) and a magnetic stir bar. MeOH (1 mL) was added and the red solution stirred for 10 minutes at room temperature. Then the volatiles were removed in vacuo, the residue was washed with saturated aqueous $NaHCO_3$ (10 mL), and the product extracted with excess $CHCl_3$. The combined organic

extracts were dried over $MgSO_4$, filtered and concentrated in vacuo, yielding g (%) of the desired product. $^1$H NMR (300 MHz, $CDCl_3$, 25 °C): δ (ppm) 7.81 (d, 7.5 Hz, 2H), 7.74 (d, 7.5 Hz, 2H), 7.62 (t, 7.5 Hz, 2H), 7.44 (d, 2.1 Hz, 2H), 7.28 (d, 2.1 Hz, 2H), 3.86 (d, 8.1 Hz, 4H), 3.10 (t, 8.1 Hz, 2H), 1.35 (s, 18H).

**Synthesis of LAlMe (31)**

In a 20 mL scintillation vial, **17** (0.1085 g, mmol) was dissolved in Toluene (4 mL). In a separate vial $AlMe_3$ (0.0095 g, mmol) was dissolved in Toluene (1 mL). In a cold well, the two vials were cooled using liquid $N_2$. After freezing the solutions, the vials were removed and allowed to thaw. Upon thawing, the $AlMe_3$ solution was added to the solution of **17** with stirring. The mixture was allowed to warm to room temperature and stirred for another 3 hours. The mixture first darkened, then lightened again over this time period. The volatiles were then removed in vacuo, giving the desired compound in quantitative yield. $^1$H NMR (300 MHz, $CD_2Cl_2$, 25 °C): δ (ppm) 8.41 (m, 4H), 7.93 (bs, 6H), 7.88 (d, 2.4 Hz, 2H), 7.78 (d, 7.8 Hz, 2H), 7.67 (td, 7.5 Hz, 1.8 Hz, 4H), 7.59 (d, 2.4 Hz, 2H), 7.13 (m, 4H), 4.10 (bs, 4H), 4.06 (d, 15 Hz, 4H), 3.99 (d, 15 Hz, 4H), 1.41 (s, 18H), –1.44 (s, 3H).

**Synthesis of LAl(OPh$Me_3$) (32)**

In a schlenk tube was combined **18** (0.0732 g, mmol), 2,4,6-trimethylphenol (0.0101 g, mmol), THF (10 mL), and a stir bar. The sealed tube was then heated at 60 ° C over 24 hours. The solvents were removed in vacuo and the crude solid was washed with $Et_2O$ (5 mL). The precipitate was then redissolved in THF (5 mL), filtered through celite, and

concentrated in vacuo, yielding 0.0781 g (94 %) of an orange solid. $^1$H NMR (300 MHz, $CD_2Cl_2$, 25 °C): δ (ppm) 8.56 (m, 4H), 7.9 – 8.0 (m, 8H), 7.78 (d, 7.8 Hz, 4H), 7.69 (td, 7.8 Hz, 1.8 Hz, 4H), 7.58 (d, 2.4 Hz, 2H), 7.16 (m, 4H), 6.19 (s, 2H), 4.21 (d, 15.6 Hz, 2H), 4.02 (s, 8H), 4.00 (d, 15.6 Hz, 2H), 1.87 (s, 3H), 1.37 (s, 18H), 1.35 (s, 6H).

**Synthesis of $LAl(OPhMe_3)Cu_2(NCMe)_2(OTf)_2$ (33)**

In a 20 mL scintillation vial (19 ) (0.0763 g, mmol) was suspended in MeCN (4 mL). To this stirred suspension was added a solution of $(MeCN)_4Cu(OTf)$ (0.0554 g, mmol) in MeCN (2 mL). Upon addition the orange suspension turned homogeneous. After stirring for 15 minutes, the solvent was removed in vacuo, yielding the desired complex in quantitative yield. $^1$H NMR (300 MHz, $CD_3CN$, 25 °C): δ (ppm) 8.35 – 8.50 (m, 8H), 8.28 (d, 8.1 Hz, 2H), 7.70 (d, 2.4 Hz, 2H), 7.45 – 7.55 (m, 6H), 7.22 (m, 4H), 6.95 (bs, 4H), 6.31 (s, 2H), 4.50 (d, 12 Hz, 2H), 4.12 (d, 12 Hz, 2H), 3.77 (bs, 6H), 3.38 (s, 1H), 3.17 (s, 1H), 1.99 (s, 6H), 1.70 (s, 3H), 1.48 (s, 6H), 1.31 (s, 18H).

## REFERENCES


[1] Gordon, J.C.; Kubas, G.J. *Organometallics* **2010**, *29*, 4682-4701.

[2] Crossland, J.L.; Tyler, D.R. *Coord. Chem. Rev.* **2010**, *254*, 1883-1894.

[3] Himes, R.A.; Karlin, K.D. *Curr. Opin. Chem. Biol.*, **2009**, *13*, 119-131.

[4] Ragsdale, S.W. *Crit. Rev. in Bioch. and Mol. Biol.* **2004**, *39*, 165-195.

[5] Harrop, T.C.; Mascharak, P.K. *Coord. Chem. Rev.*, **2005**, *249*, 3007-3024.

[6] Jeoung, J.H.; Dobbek, H. *Science* **2007**, *318*, 1461-1464.

[7] Hegg, E.L. *Acc. Chem. Res.* **2004**, *37*, 775-783.

[8] Dobbek, H.; Gremer, L; Kiefersauer, R.; Huber, R.; Meyer, O. *Proc. Nat. Acad. Sci.* **2002**, *99*, 15971-15976.

[9] Rolff, M.; Schottenheim, J.; Decker, H.; Tuczek, F. *Chem. Soc. Rev.* **2011**, *40*, 4077-98.

[10] Volbeda, A.; Charon, M.H.; Piras, C.; Hatchikian, E.C.; Frey, M.; Fontecilla-Camps, J.C. *Nature*, **1995**, *373*, 580-587.

[11] Volbeda, A.; Martin, L.; Cavazza, C.; Matho, M.; Faber, B.W.; Roseboom, W.; Albracht, S.P.J.; Garcin, E.; Rousset, M.; Fontecilla-Camps, J.C. *J. Biol. Inorg. Chem.*, **2005**, *10*, 239-249.

[12] Peters, J.W.; Lanzilotta, W.N.; Lemon, B.J.; Seefeldt, L.C. *Science*, **1988**, *282*, 1853-1858.

[13] Nicolet, Y.; Piras, C.; Legrand, P.; Hatchikian, C.E.; Fontecilla-Camps, J.C. *Structure*, **1999**, *7*, 13-23.

[14] Nicolet, Y.; de Lacey, A.L.; Vernede, X.; Fernandez, V.M.; Hatchikian, E.C.; Fontecilla-Camps, J.C. *J. Am. Chem. Soc.*, **2001**, *123*, 1596-1601.

[15] Shima, S.; Pilak, O.; Vogt, S.; Schick, M.; Stagni, M.S.; Meyer-Klaucke, W.; Warkentin, E.; Thauer, R.K.; Ermler, U. *Science*, **2008**, *321*, 572-575.

[16] Hiromoto, T.; Warkentin, E.; Moll, J.; Ermler, U.; Shima, S. *Angew. Chem., Int. Ed.*, **2009**, *48*, 6457-6460.

[17] Okawa, H.; Furutachi, H.; Fenton, D.E. *Coord. Chem. Rev.* **1998**, *174*, 51-75.

[18] Brooker, S. Coord. *Chem. Rev.* **2001**, *222*, 33-56.

[19] Gagne, R.R.; Spiro, C.L. *J. Am. Chem. Soc.* **1980**, *102*, 1443-1444.

[20] Gagne, R.R.; Spiro, C.L.; Smith, T.J.; Hamann, C.A.; Thies, W.R.; Shiemke, A.K. *J. Am. Chem. Soc.* **1981**, *103*, 4073-4081.

[21] Lambert, S.L.; Spiro, C.L.; Gagne, R.R.; Hendrickson, D.N.; *Inorg. Chem.* **1982**, *21*, 68-72.

[22] Fraser, C.; Johnston, L.; Rheingold, A.L.; Haggerty, B.S.; Williams, G.K.; Whelan, J.; Bosnich, B. *Inorg. Chem.* **1992**, *31*, 1835-1844. An example of a bimetallic $Mn_2$ macrocyclic complex catalyzing epoxidation of styrene by iodosobenzene.

[23] Arora, H.; Philouze, C.; Jarjayes, O.; Thomas, F. *Dalton Trans.*, **2010**, *39*, 10088-10098.

[24] Hsiao, Y.M.; Chojnacki, S.S.; Hinton, P.; Reibenspies, J.H.; Darensbourg, M.Y. *Organometallics*, **1993**, *12*, 870-875.
[25] Kim, J.S.; Ewivwnapiwa, J.H.; Darensbourg, M.Y. *Inorg. Chim. Act.*, **1996**, *250*, 283-294.
[26] Kim, J.S.; Reibenspies, J.H.; Darensbourg, M.Y. *J. Am. Chem. Soc.*, **1996**, *118*, 4115-4123.
[27] Nakane, D.; Kuwasako, S.; Tsuge, M.; Kubo, M.; Funahashi, Y.; Ozawa, T.; Ogura, T.; Masuda, H. *Chem. Comm.*, **2010**, *46*, 2142-2144.
[28] Machan, C.W.; Spokoyny, A.M.; Jones, M.R.; Sarjeant, A.A.; Stern, C.L., Mirkin, C.A. *J. Am. Chem. Soc.*, **2011**, *133*, 3023-3033.
[29] Mills, D.K.; Reibenspies, J.H.; Darensbourg, M.Y. *Inorg. Chem.*, **1990**, *29*, 4355-4368.
[30] Goodman, D.C.; Buonomo, R.M.; Farmer, P.J.; Reibenspies, J.H.; Darensbourg, M.Y. *Inorg. Chem.*, **1996**, *35*, 4029-4037.
[31] Bellefeuille, J.A.; Grapperhaus, C.A.; Derecskei-Kovacs, A.; Reibenspies, J.H.; Darensbourg, M.Y. *Inorg. Chim. Act.*, **2000**, *300-302*, 73-81.
[32] Sylvestre, I.; Wolowska, J.; Kilner, C.A.; McInnes, E.J.L.; Halcrow, M.A. *Dalton Trans.*, **2005**, 3241-3249.
[33] Gennari, M.; Retegan, M.; DeBeer, S.; Pecaut, J.; Neese, F.; Collomb, M.N.; Duboc, C. *Inorg. Chem.*, **2011**, *50*, 10047-10055.
[34] Akine, S.; Shimada, T.; Nagumo, H.; Nabeshima, T. *Dalton Trans.*, **2011**, *40*, 8507-8509.
[35] Bai, X.L.; Liu, X.D.; Wang, M.; Kang, C.Q.; Gao, L.X. *Synthesis*, **2005**, *3*, 458-464.
[36] Su, W. P.; Urgaonkar, S.; Verkade, J. G. Org. Lett. **2004**, 6, 1421–1424.
[37] Tagata, T.; Nishida, M. *J. Org. Chem.*, **2003**, *68*, 9412-9415.
[38] Vigalok, A.; Rybtchinski, B.; Gozin, Y.; Koblenz, T.S.; Ben-David, Y.; Rozenberg, H.; Milstein, D. *J. Am. Chem. Soc.*, **2003**, *125*, 15692-15693.
[39] Boom, M.E.; Liou, S.Y.; Ben-David, Y.; Shimon, L.J.W.; Milstein, D. *J. Am. Chem. Soc.*, **1998**, *120*, 6531-6541.
[40] Zhang, H.Y.; Ye, K.Q.; Zhang, J.Y.; Liu, Y.; Wang, Y. *Inorg. Chem.*, **2006**, *45*, 1745-1753.
[41] Atwood, D.A.; Hill, M.S.; Jegier, J.A.; Rutherford, D. *Organometallics*, **1997**, *16*, 2659-2664.
[42] Mirica, L.M.; Ottenwaelder, X.; Stack, T.D.P. *Chem. Rev.*, **2004**, *104*, 1013-1045.
[43] Fujisawa, K.; Tanaka, M.; Moro-Oka, Y.; Kitajima, N. *J. Am. Chem. Soc.*, **1994**, *116*, 12079-12080.
[44] Chen, P.; Root, D. E.; Campochiaro, C.; Fujisawa, K.; Solomon, E. I. *J. Am. Chem. Soc.*, **2003**, *125*, 466-474.
[45] Spencer, D.J.E.; Aboelella, N.W.; Reynolds, A.M.; Holland,P. L.; Tolman, W. B. *J. Am. Chem. Soc.*, **2002**, *124*, 2108-2109.

[46] Aboelella, N. W.; Lewis, E. A.; Reynolds, A. M.; Brennessel, W. W.; Cramer, C. J.; Tolman, W. B. *J. Am. Chem. Soc.*, **2002**, *124*, 10660-10661.
[47] Li, W.F.; Sun, H.M.; Wang, Z.G.; Chen, M.Z.; Shen, Q.; Zhang, Y. *J. Organomet. Chem.*, **2005**, *690*, 6227-6232.
[48] Wu, J.; Faller, J.W.; Hazari, N.; Schmeier, T.J. *Organomet*allics **2012**, *31*, 806-809.
[49] Crudden, C.M.; Allen, D.P. *Coord. Chem. Rev.*, **2004**, 248, 2247-2273.
[50] Zetta, L.; Wolff, A.; Vogt, W.; Platt, K.L.; Boehmer, V. *Tetrahedron* **1991**, 47, 1911-1924.
[51] Bai, X.L.; Liu, X.D.; Wang, M.; Kang, C.Q.; Gao, L.X. *Synthesis* **2005**, 0458-0464.
[52] Ogawa, S.; Shiraishi, S. *J. Chem. Soc. Perkin Trans. 1* **1980**, 2527-2530.
[53] Berliner, M.A.; Belecki, K. *J. Org. Chem.* **2005**, *70*, 9618-9621.

# APPENDIX C

SPECTRA

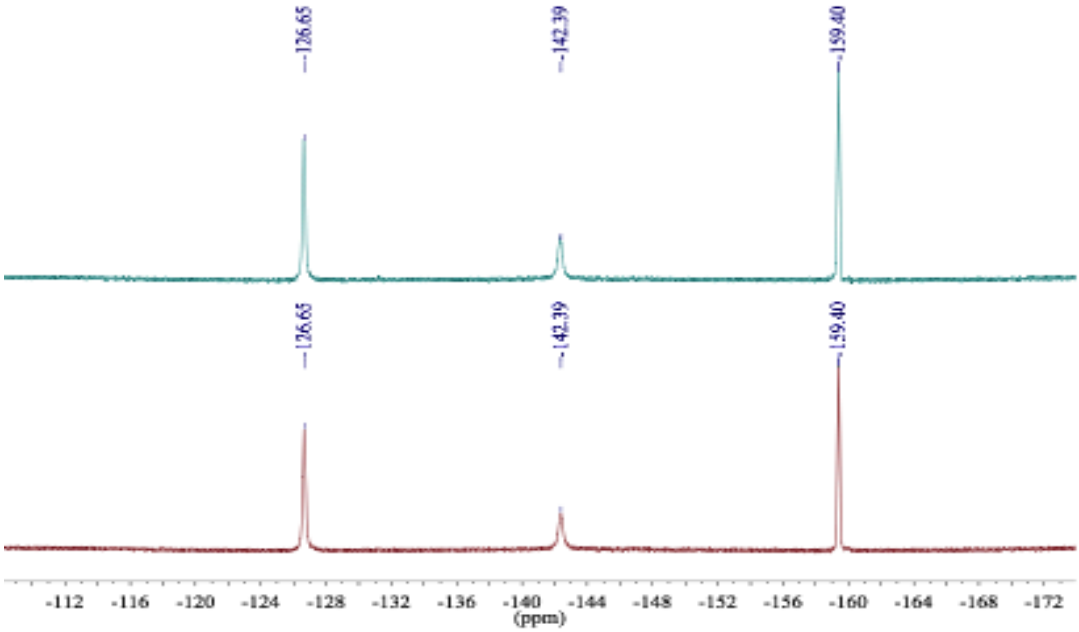


**Figure C2.1**. $^{19}F$ NMR spectra of $B(C_6F_5)_3$ under $O_2$ (1 atm) at 5 min. (bottom) and 24 hours (top) in $CD_2Cl_2$ at 25 °C.

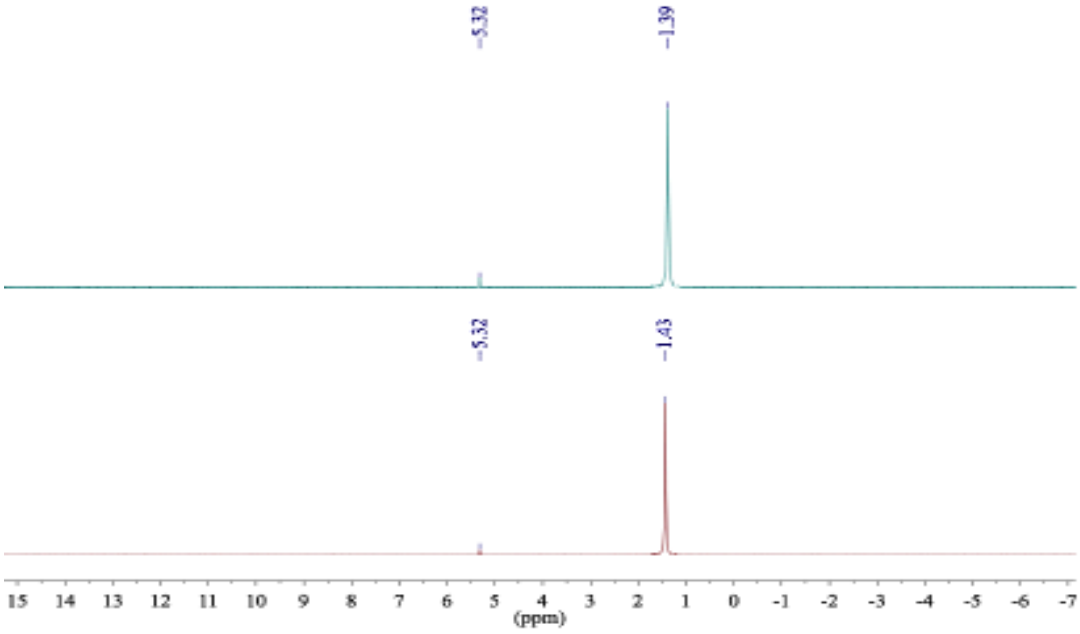


**Figure C2.2.** $^1H$ NMR spectra of $Cp^*_2Fe$ under $O_2$ (1 atm) at 5 min. (bottom) and 24 hours (top) in $CD_2Cl_2$ at 25 °C.

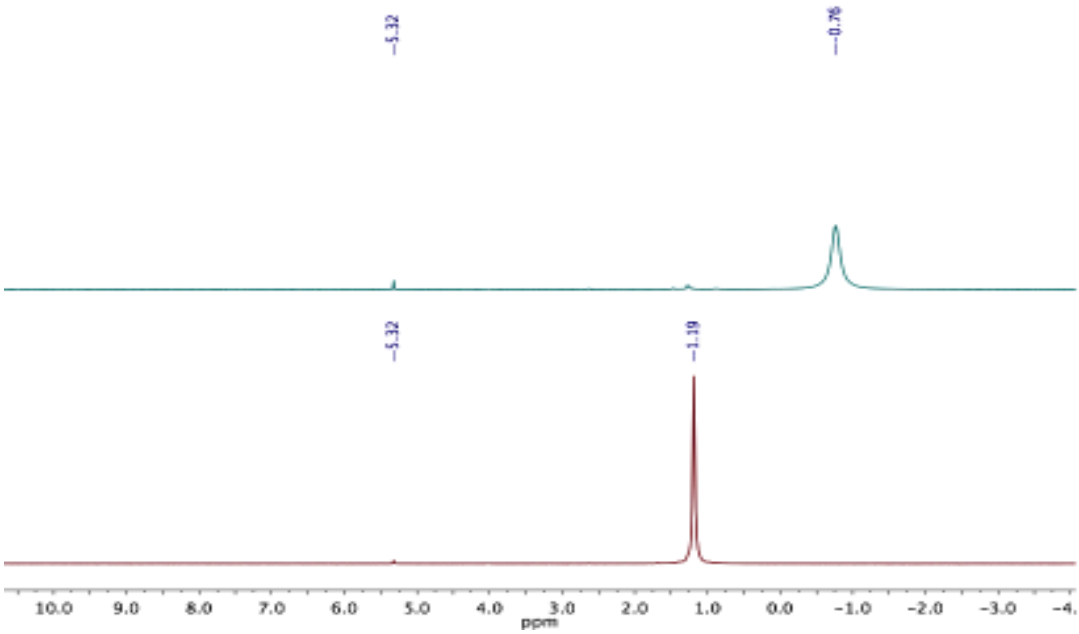


**Figure C2.3.** $^{1}H$ NMR spectra of $Cp^{*}_{2}Fe$ and $B(C_6F_5)_3$ under $N_2$ at 15 min. (bottom) and 12 hours (top) $CD_2Cl_2$ at 25 °C.

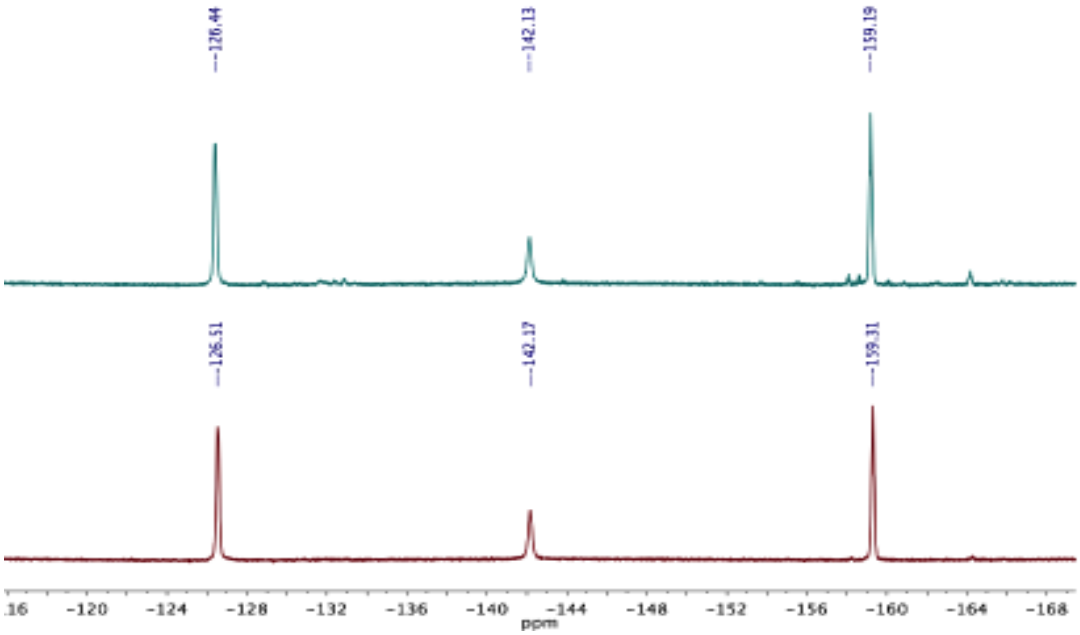


**Figure C2.4.** $^{19}F$ NMR spectra of $Cp^{*}_{2}Fe$ and $B(C_6F_5)_3$ under $N_2$ at 15 min. (bottom) and 12 hours (top) $CD_2Cl_2$ at 25 °C.

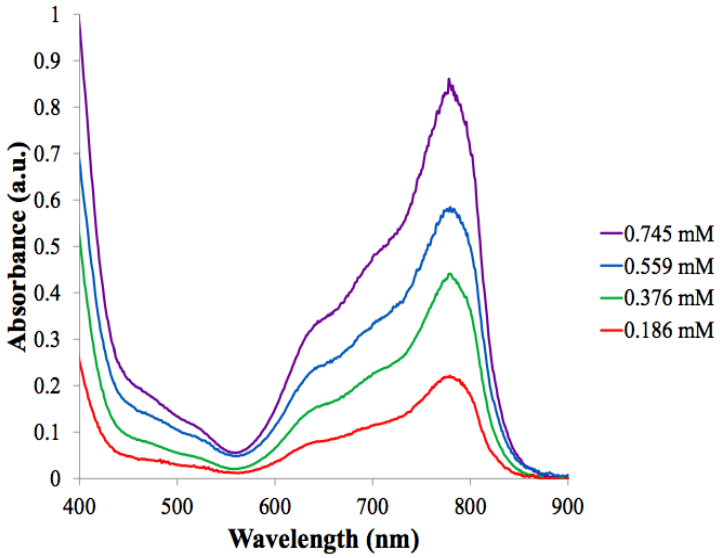


**Figure C2.5.** UV-vis spectrum of $[\mathbf{1}^{2-}][Cp^*_2Fe^+]_2$ in DCM with varying concentration.

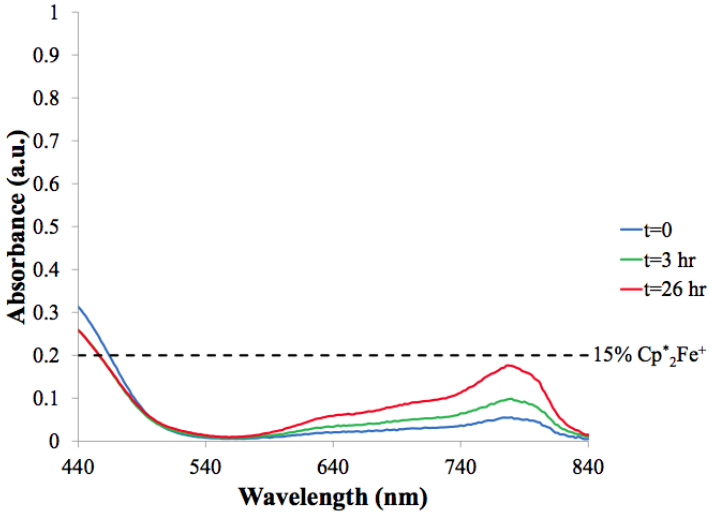


**Figure C2.6.** UV-vis monitoring of the NMR concentration reaction of $Cp^*_2Fe$ and $B(C_6F_5)_3$ in DCM under $N_2$. Aliquots of the reaction were taken over time and diluted by a factor of 0.06. The absorption at 780 nm was measured to determine the amount of $Cp^*_2Fe^+$ generated. After 26 hours at room temperature, less than 15% of the total $Cp^*_2Fe$ had been oxidized to $Cp^*_2Fe^+$.

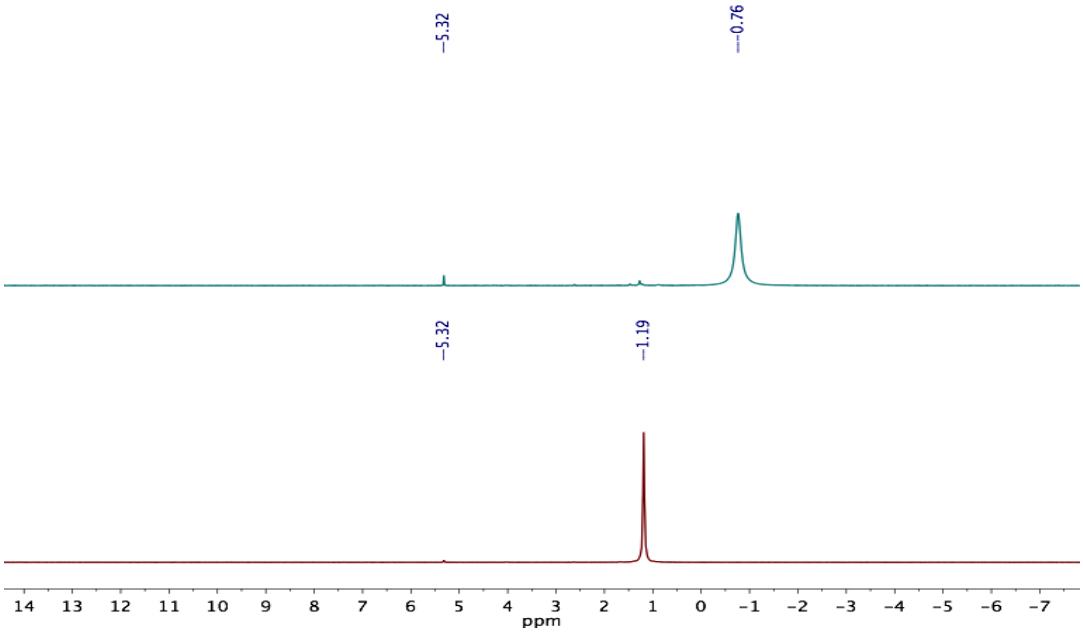


**Figure C2.7.** $^{1}$H NMR spectra of $Cp^{*}_{2}Fe$ and $B(C_6F_5)_3$ under vacuum at 15 min. (bottom) and 12 hours (top) $CD_2Cl_2$ at 25 °C.

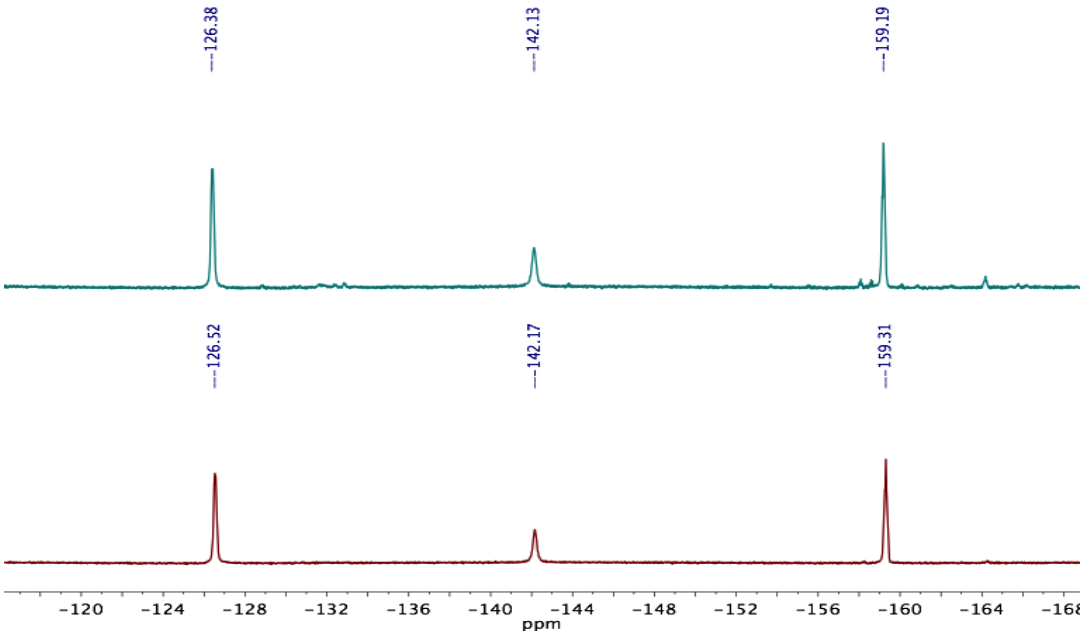


**Figure C2.8.** $^{19}$F NMR spectra of $Cp^{*}_{2}Fe$ and $B(C_6F_5)_3$ under vacuum at 15 min. (bottom) and 12 hours (top) $CD_2Cl_2$ at 25 °C.

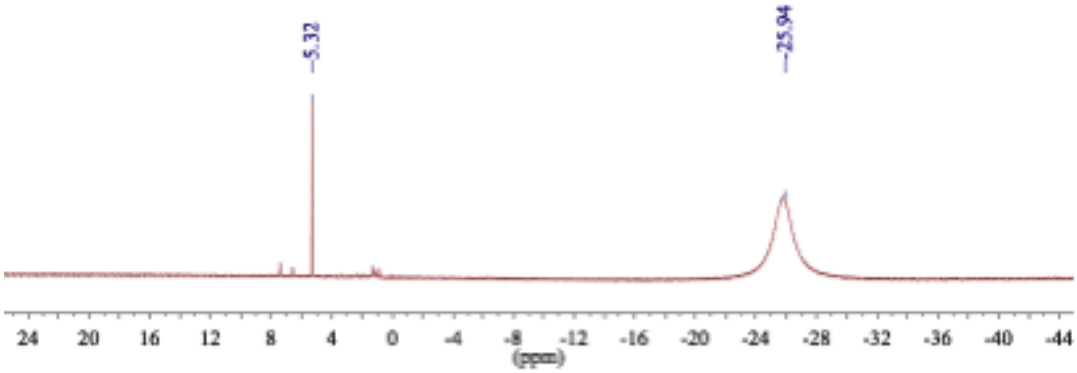


**Figure C2.9.** $^{1}$H NMR spectrum of $Cp^{*}_{2}Fe$ and $B(C_6F_5)_3$ under $O_2$ (1 atm) in $CD_2Cl_2$ at 25 °C.

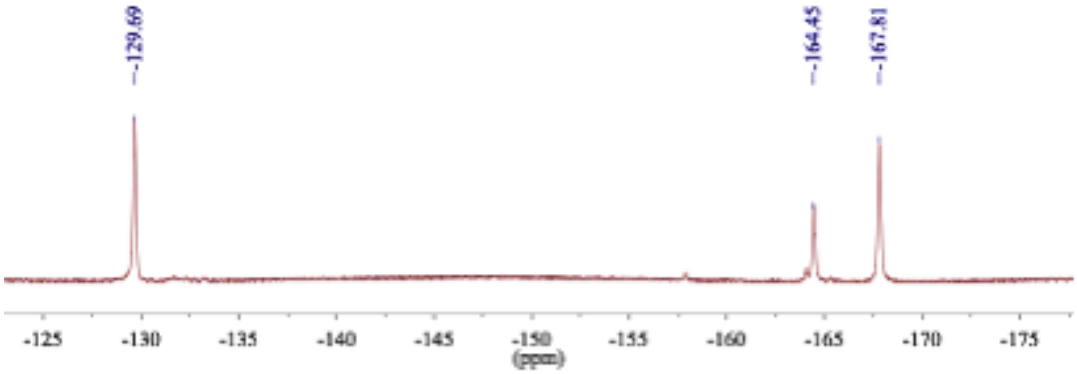


**Figure C2.10.** $^{19}$F NMR spectrum of $Cp^{*}_{2}Fe$ and $B(C_6F_5)_3$ under $O_2$ (1 atm) in $CD_2Cl_2$ at 25 °C.

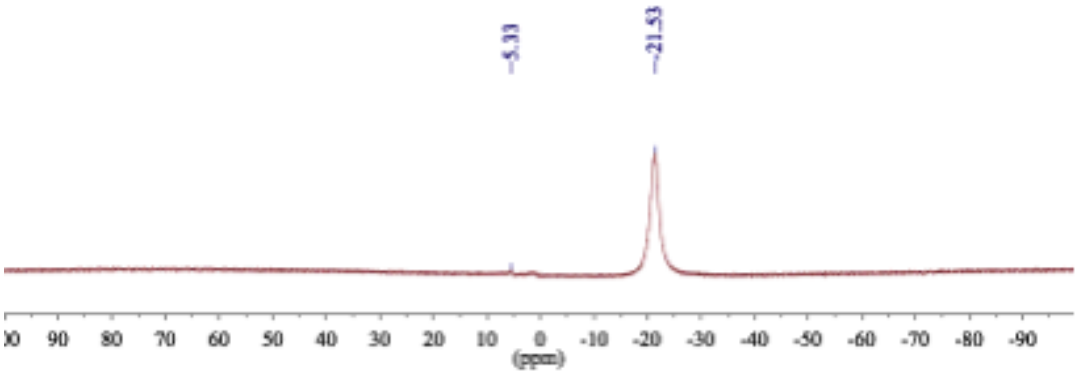


**Figure C2.11.** $^{1}$H NMR spectrum of $Cp^{*}_{2}Fe$ and $B(C_6F_5)_3$ in the dark under $O_2$ (1 atm) in $CD_2Cl_2$ at 25 °C.

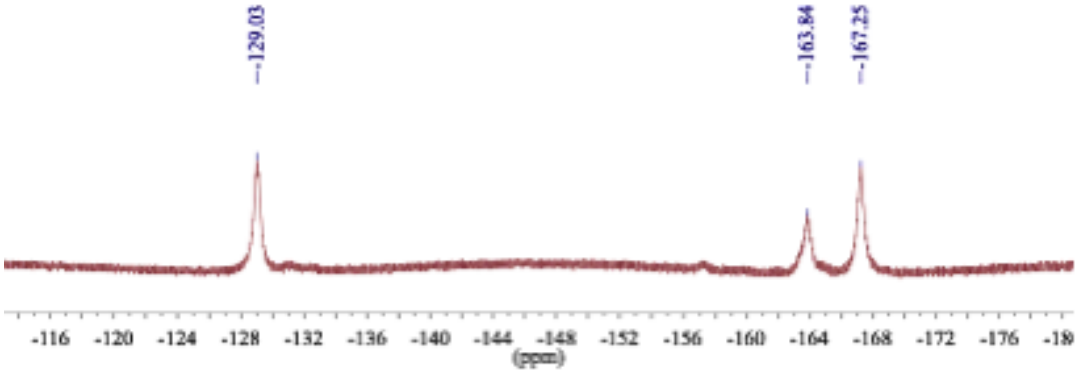


**Figure C2.12.** $^{1}$H NMR spectrum of $Cp^{*}_{2}Fe$ and $B(C_6F_5)_3$ in the dark under $O_2$ (1 atm) in $CD_2Cl_2$ at 25 °C.

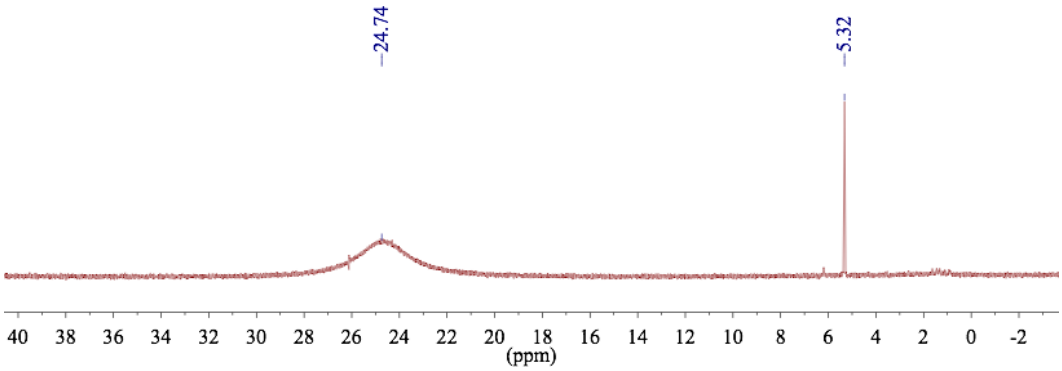


**Figure C2.13.** $^{1}$H NMR spectrum of $Cp_2Fe$ and $B(C_6F_5)_3$ under $O_2$ (1 atm) after 7 hours in $CD_2Cl_2$ at 25 °C.

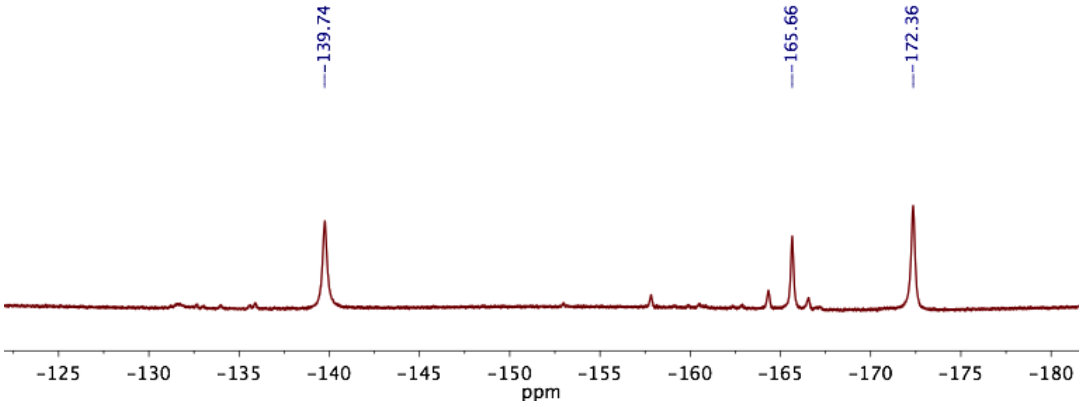


**Figure C2.14.** $^{19}$F NMR spectrum of $Cp_2Fe$ and $B(C_6F_5)_3$ under $O_2$ (1 atm) after 7 hours in $CD_2Cl_2$ at 25 °C.

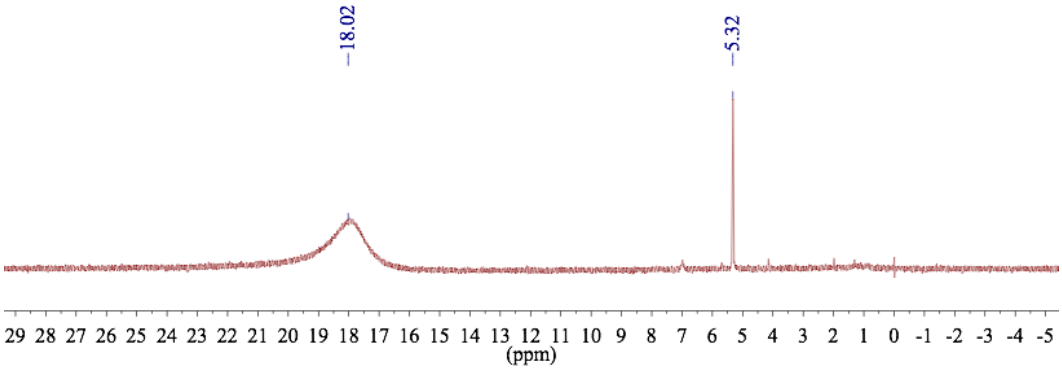


**Figure C2.15.** $^{1}$H NMR spectrum of $Cp_2Fe$ and $B(C_6F_5)_3$ under $O_2$ (1 atm) after degassing in $CD_2Cl_2$ at 25 °C.

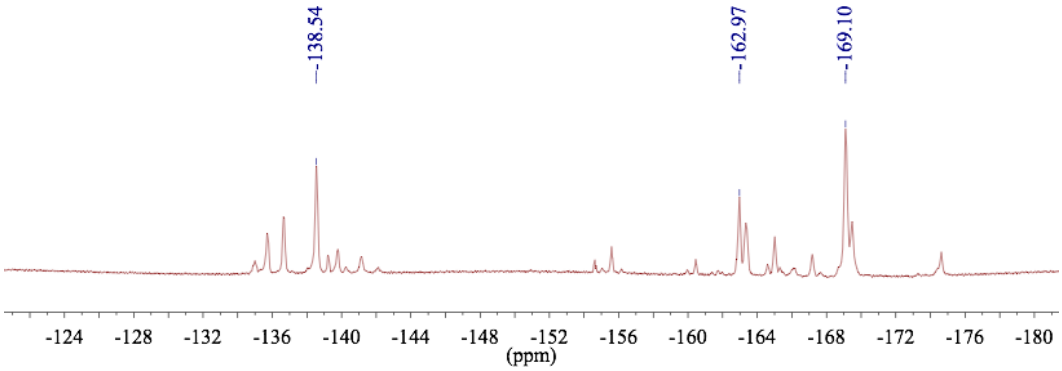


**Figure C2.16.** $^{19}$F NMR spectrum of $Cp_2Fe$ and $B(C_6F_5)_3$ under $O_2$ (1 atm) after degassing in $CD_2Cl_2$ at 25 °C.

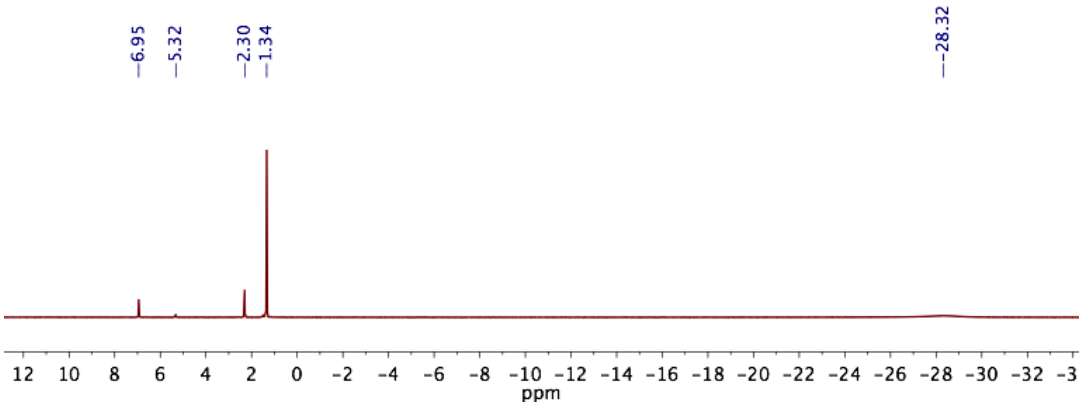


**Figure C2.17.** $^{1}$H NMR spectrum of $Cp^{*}_2Fe$, $B(C_6F_5)_3$, and DTBMP under $O_2$ (1 atm) in $CD_2Cl_2$ at 25 °C.

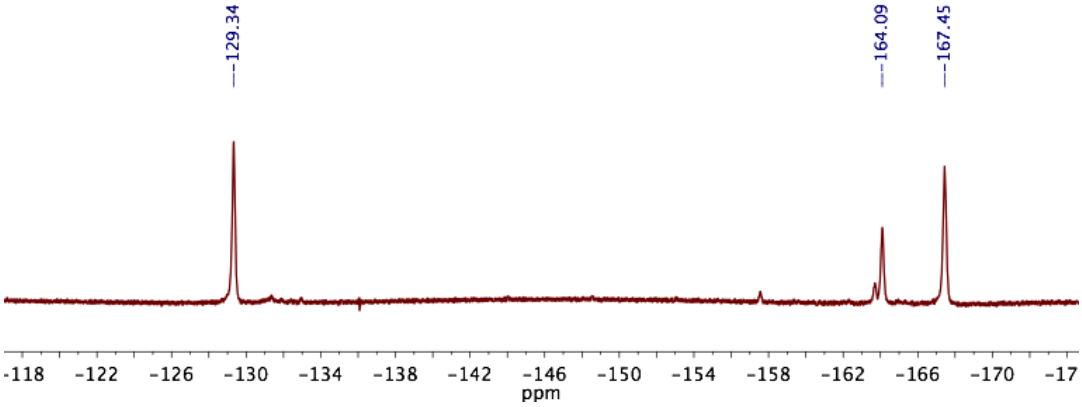


**Figure C2.18.** $^{19}F$ NMR spectrum of $Cp^*_2Fe$, $B(C_6F_5)_3$ and DTBMP under $O_2$ (1 atm) in $CD_2Cl_2$ at 25 °C.

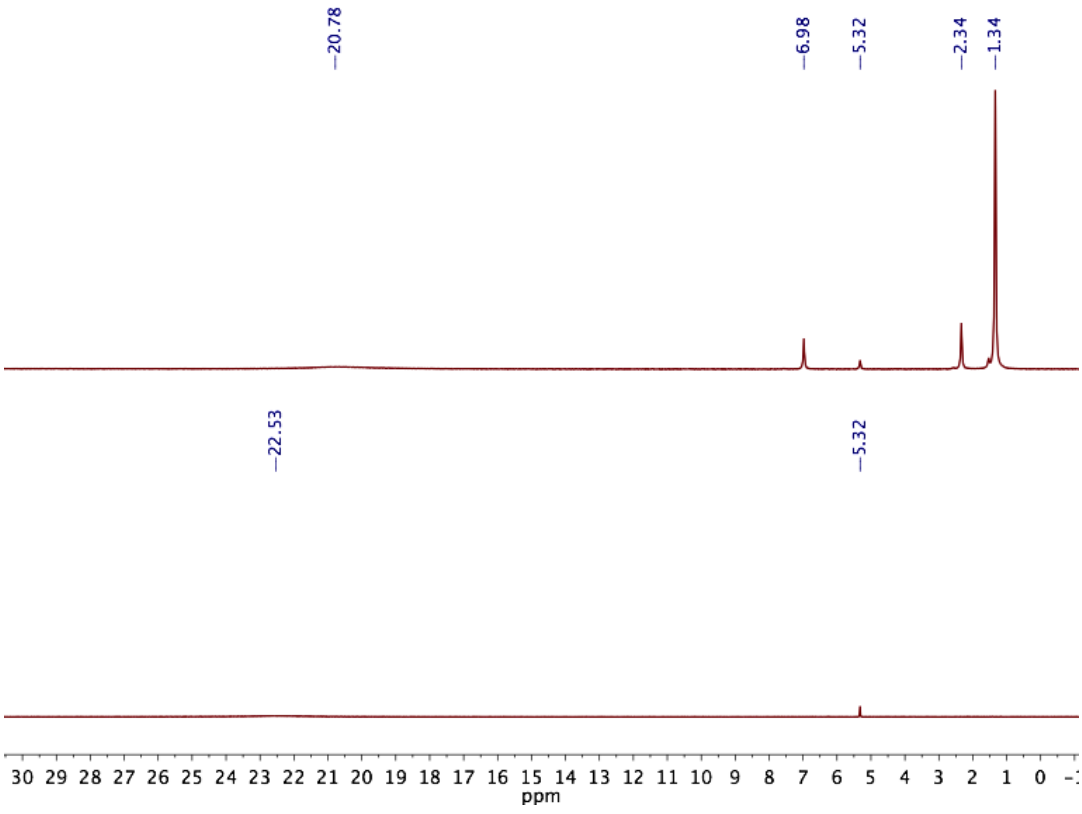


**Figure C2.19.** $^1H$ NMR spectrum of $Cp_2Fe$ and $B(C_6F_5)_3$ under $O_2$ (1 atm) after 3 hours in $CD_2Cl_2$ at 25 °C (bottom) and $Cp_2Fe$, $B(C_6F_5)_3$ and DTBMP under $O_2$ (1 atm) after 3 hours in $CD_2Cl_2$ at 25 °C (top).

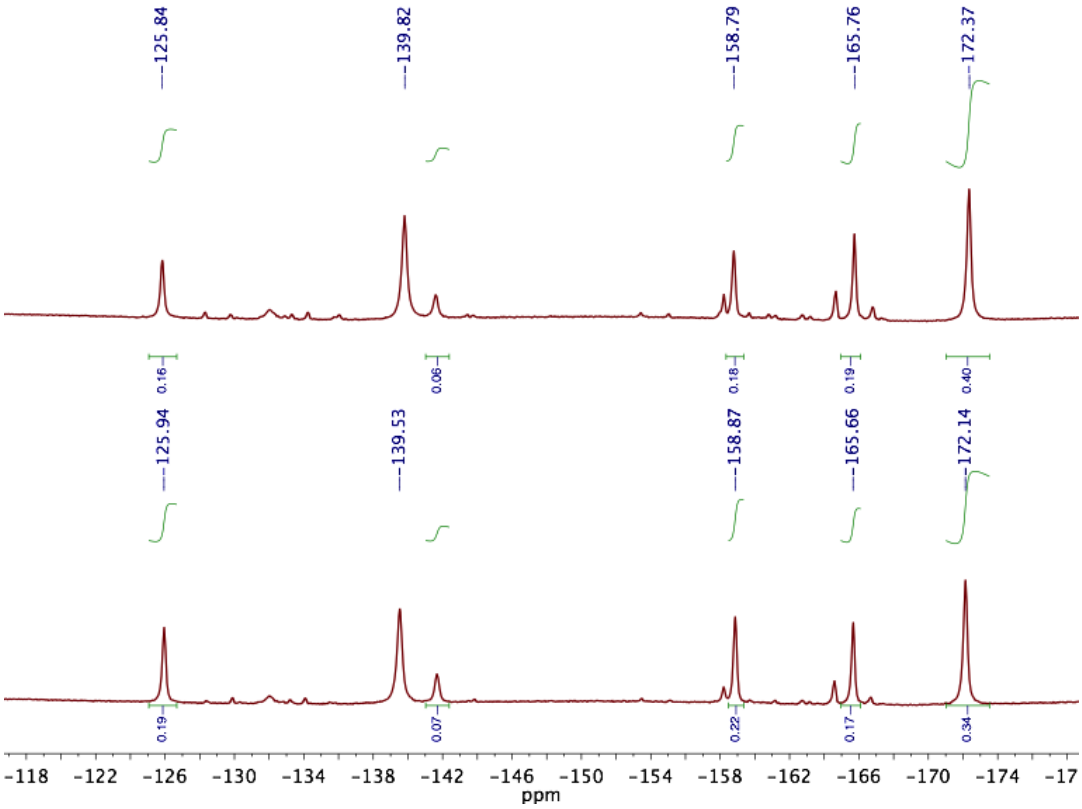


**Figure C2.20.** $^{19}F$ NMR spectrum of $Cp_2Fe$ and $B(C_6F_5)_3$ under $O_2$ (1 atm) after 3 hours in $CD_2Cl_2$ at 25 °C (bottom) and $Cp_2Fe$, $B(C_6F_5)_3$ and DTBMP under $O_2$ (1 atm) after 3 hours in $CD_2Cl_2$ at 25 °C (top).

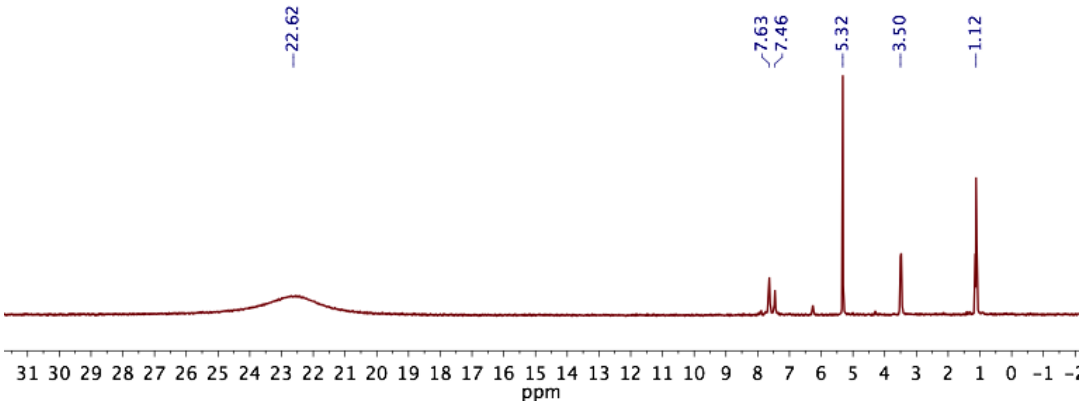


**Figure C2.21.** $^1H$ NMR spectrum of $Cp_2Fe$, $B(C_6F_5)_3$ and $H(OEt_2)_2BArF^{24}$ under $O_2$ (1 atm) after 3 hours in $CD_2Cl_2$ at 25 °C.

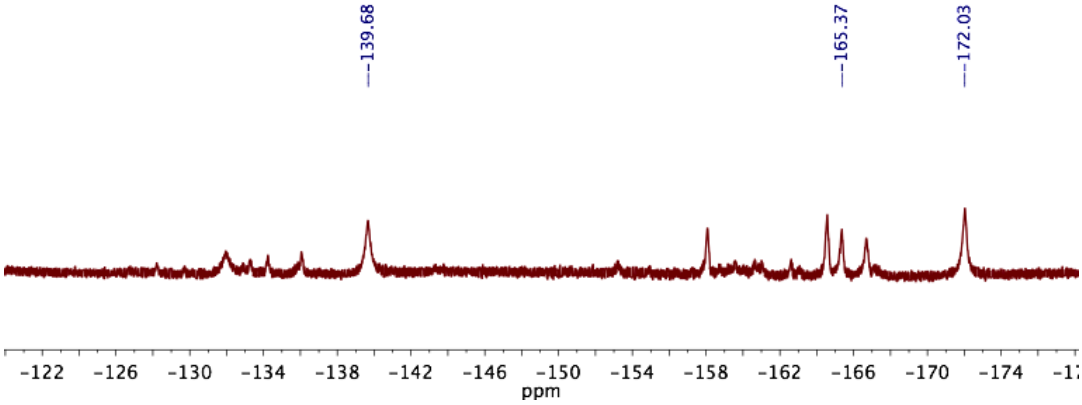


**Figure C2.22.** $^{19}F$ NMR spectrum of $Cp_2Fe$, $B(C_6F_5)_3$ and $H(OEt_2)_2BArF^{24}$ under $O_2$ (1 atm) after 3 hours in $CD_2Cl_2$ at 25 °C.

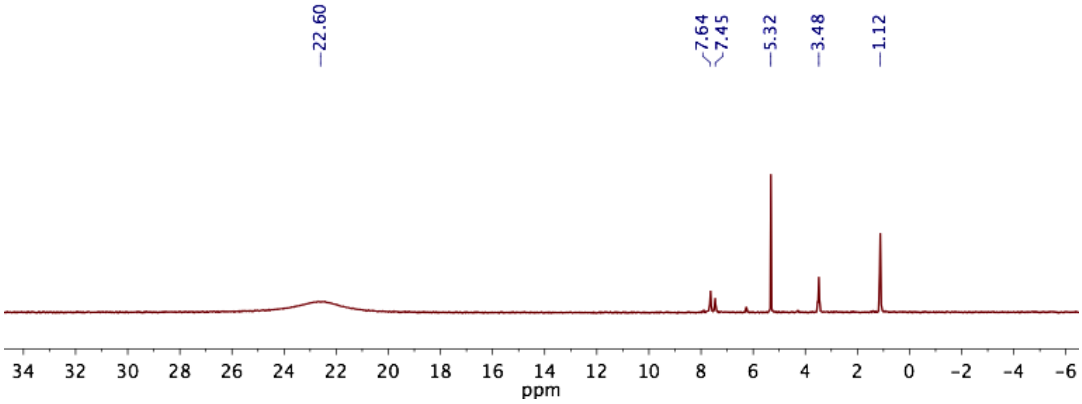


**Figure C2.23.** $^{1}H$ NMR spectrum of $Cp_2Fe$, $B(C_6F_5)_3$ and $H(OEt_2)_2BArF^{24}$ under $O_2$ (1 atm) after 2 hours in $CD_2Cl_2$ at 25 °C.

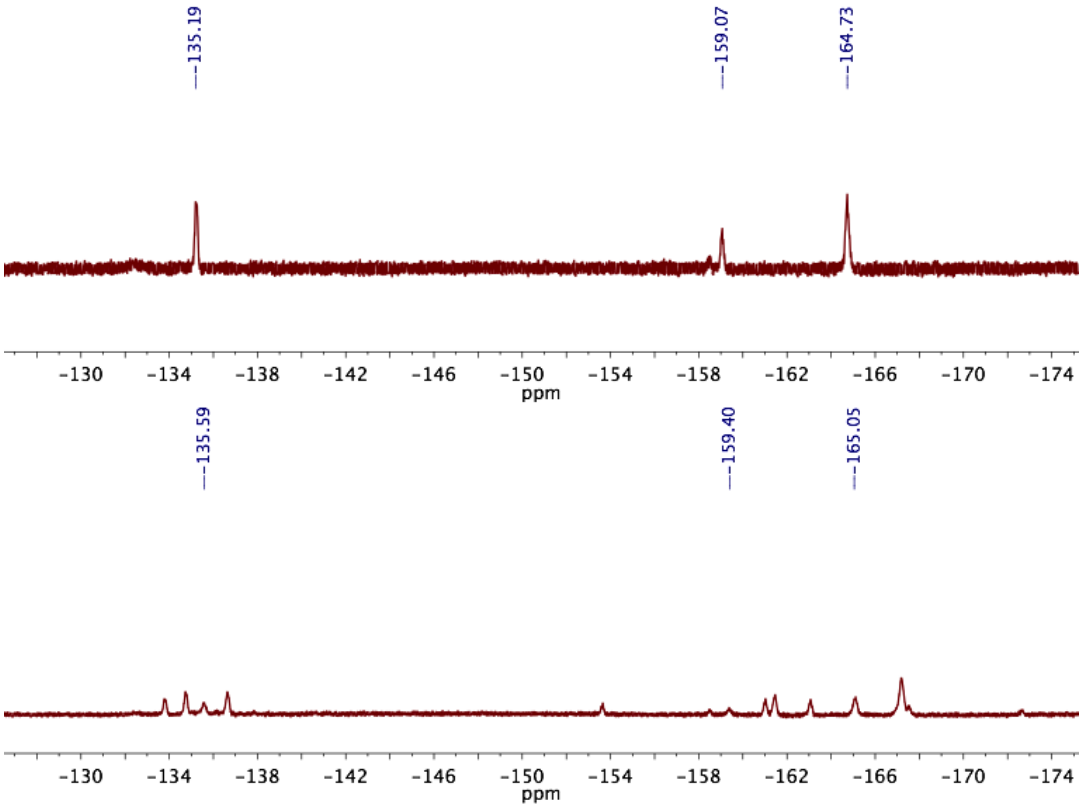


**Figure C2.24.** $^{19}F$ NMR spectrum of $Cp_2Fe$, $B(C_6F_5)_3$ and $H(OEt_2)_2BArF^{24}$ under $O_2$ (1 atm) after 3 hours in $CD_2Cl_2$ at 25 °C (bottom) and crystals of $[\{(F_5C_6)_3B\}_2OH^-][Cp_2Fe^+]$ isolated from the reaction mixture in $CD_2Cl_2$ at 25 °C (top).

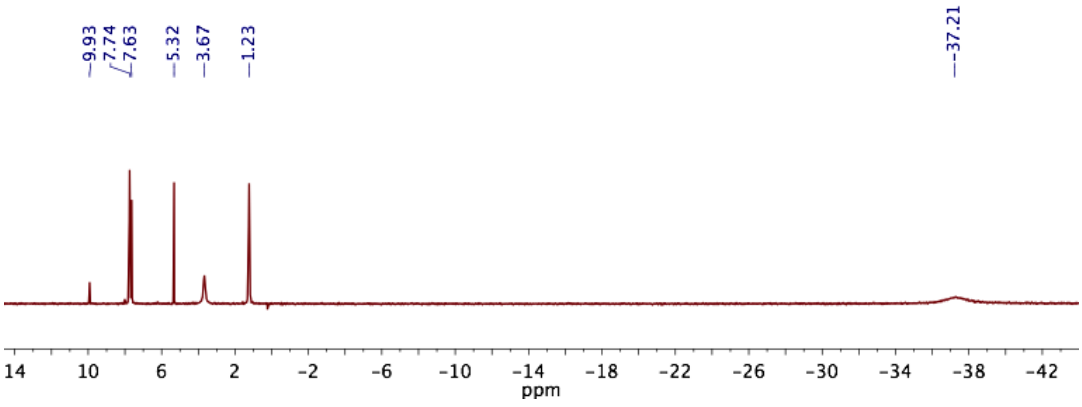


**Figure C2.25.** $^1H$ NMR spectrum of $[\mathbf{1}^{2-}][Cp^*_2Fe^+]_2$ and $H(OEt_2)_2BArF^{24}$ in $CD_2Cl_2$ at 25 °C.

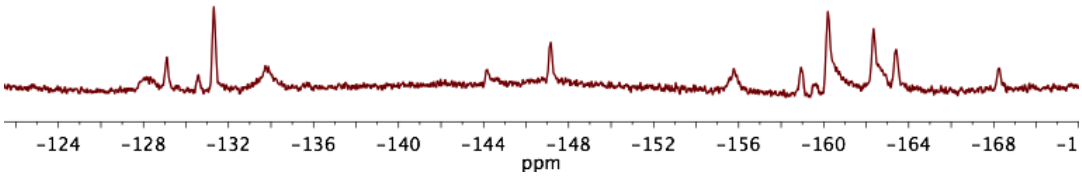


**Figure C2.26.** $^{19}F$ NMR spectrum of [**1**$^{2-}$][$Cp^*_2Fe^+$]$_2$ and H(OEt$_2$)$_2$BArF$^{24}$ in $CD_2Cl_2$ at 25 °C.

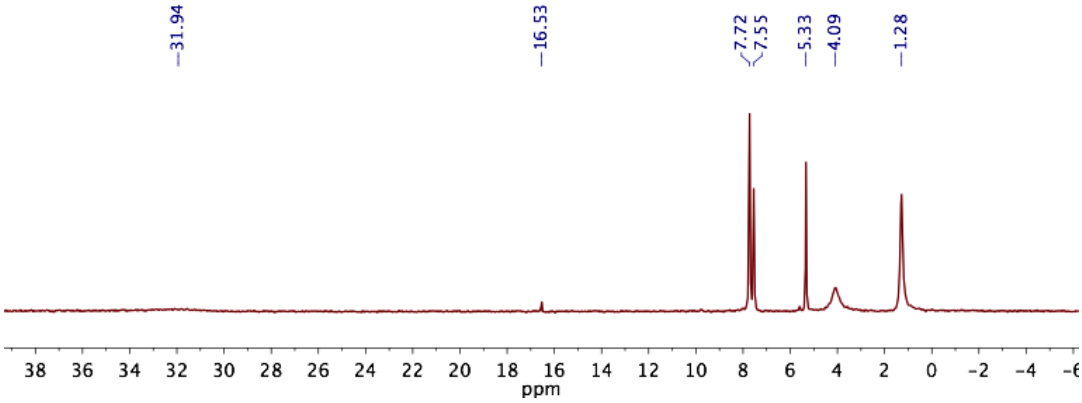


**Figure C2.27.** $^{1}H$ NMR spectrum of [**1**$^{2-}$][$Cp_2Fe^+$]$_2$ and H(OEt$_2$)$_2$BArF$^{24}$ in $CD_2Cl_2$ at 25 °C.

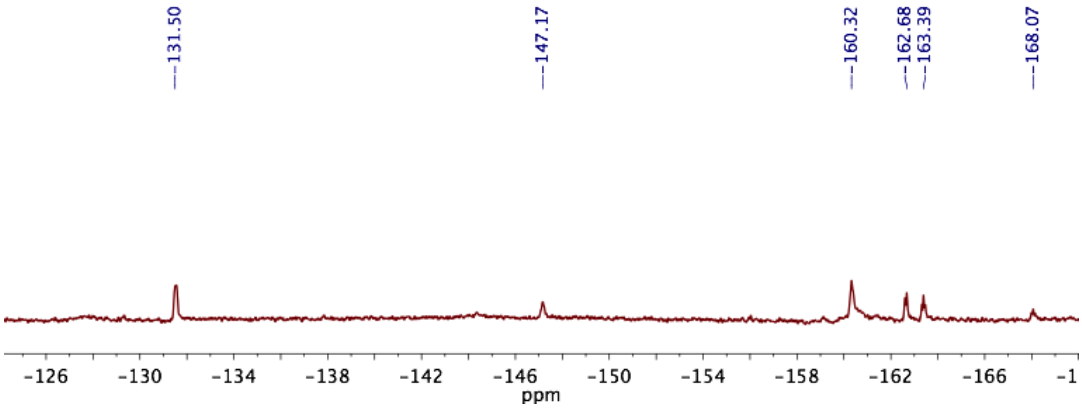


**Figure C2.28.** $^{19}F$ NMR spectrum of [**1**$^{2-}$][$Cp_2Fe^+$]$_2$ and H(OEt$_2$)$_2$BArF$^{24}$ in $CD_2Cl_2$ at 25 °C.

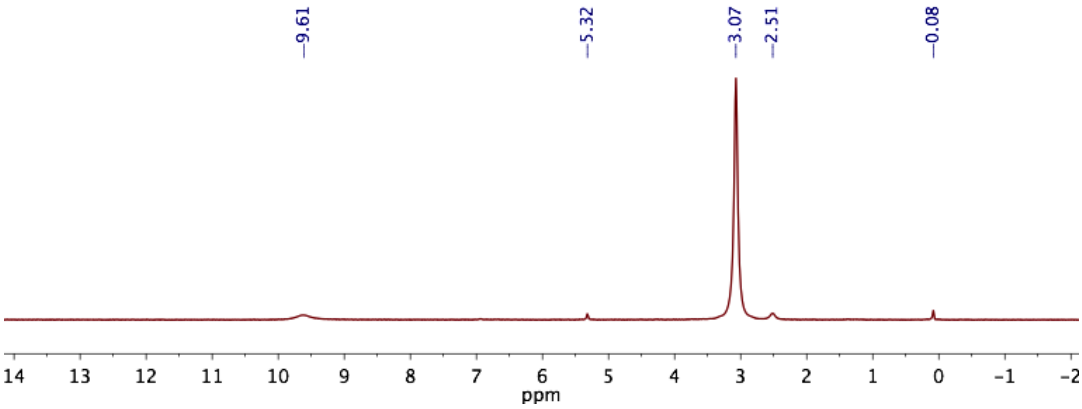


**Figure C2.29.** $^{1}$H NMR spectrum of $B(C_6F_5)_3$, DABCO•$2H_2O_2$, and DABCO in $CD_2Cl_2$ at 25 °C.

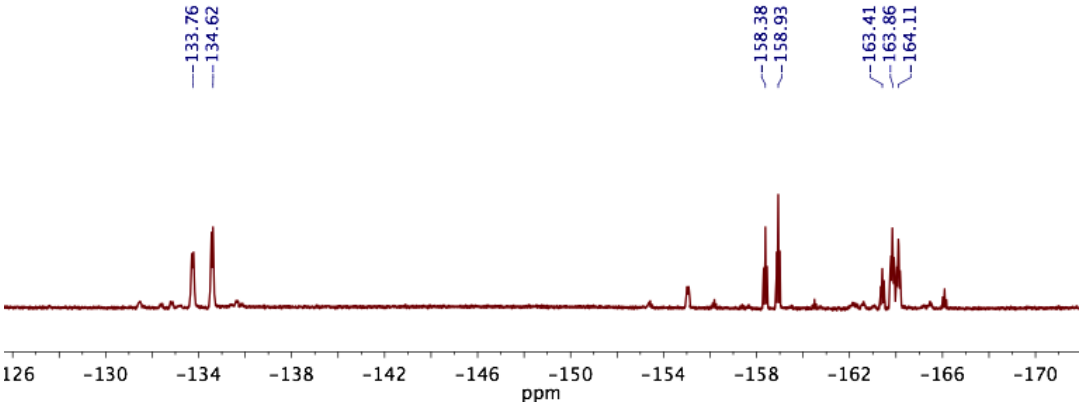


**Figure C2.30.** $^{19}$F NMR spectrum of $B(C_6F_5)_3$, DABCO•$2H_2O_2$, and DABCO in $CD_2Cl_2$ at 25 °C.

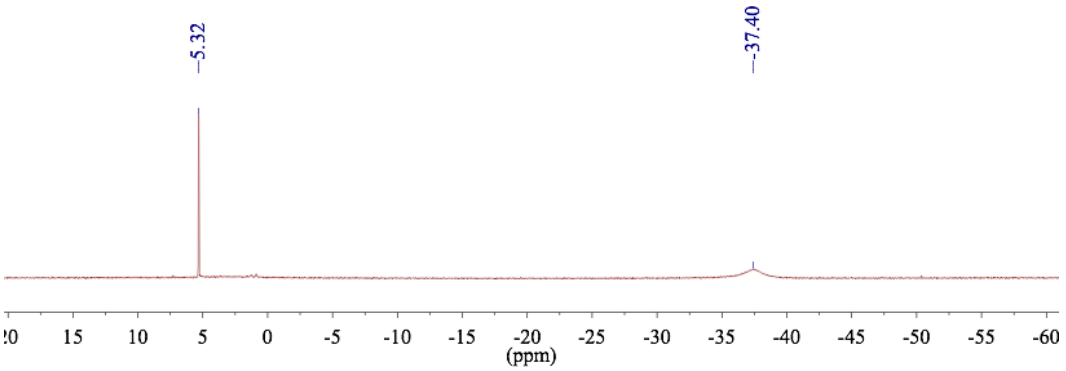


**Figure C2.31.** $^{1}$H NMR spectrum of [**1**$^{2-}$][$Cp^{*}_2Fe^{+}$]$_2$ in $CD_2Cl_2$ at 25 °C.

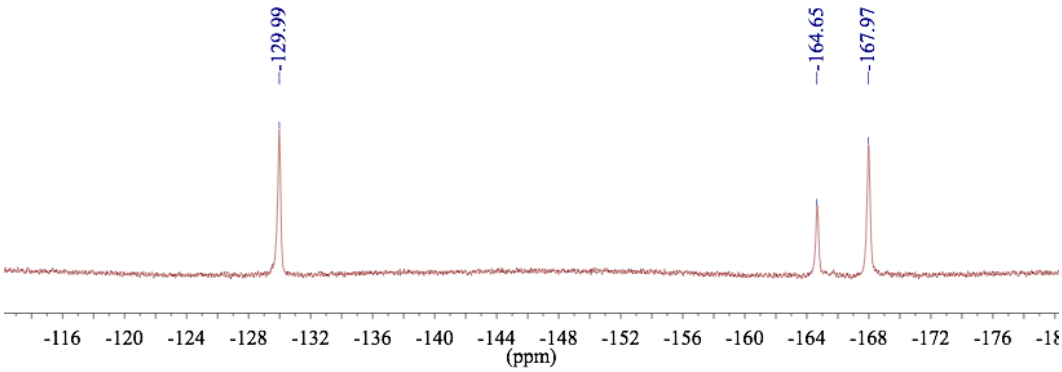


**Figure C2.32.** $^{19}F$ NMR spectrum of [**1**$^{2-}$][$Cp^{*}_{2}Fe^{+}$]$_2$ in $CD_2Cl_2$ at 25 °C.

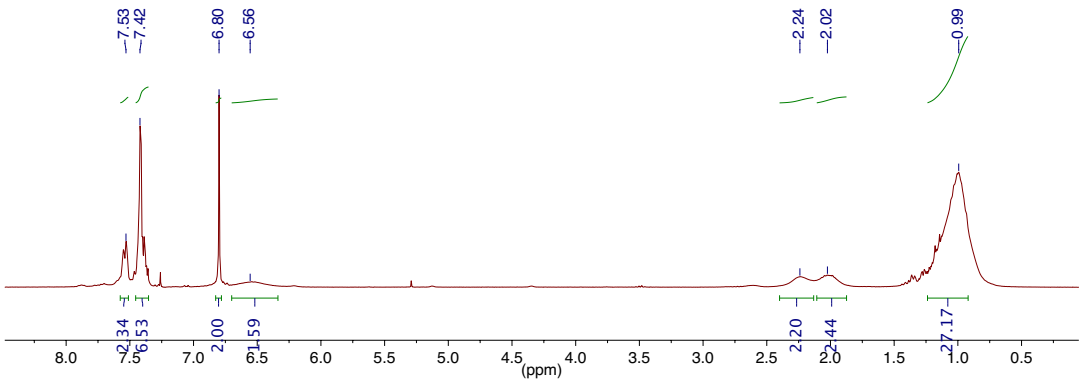


**Figure C3.1.** $^{1}H$ NMR spectrum of **3.1a** in $CDCl_3$ at 25 °C.

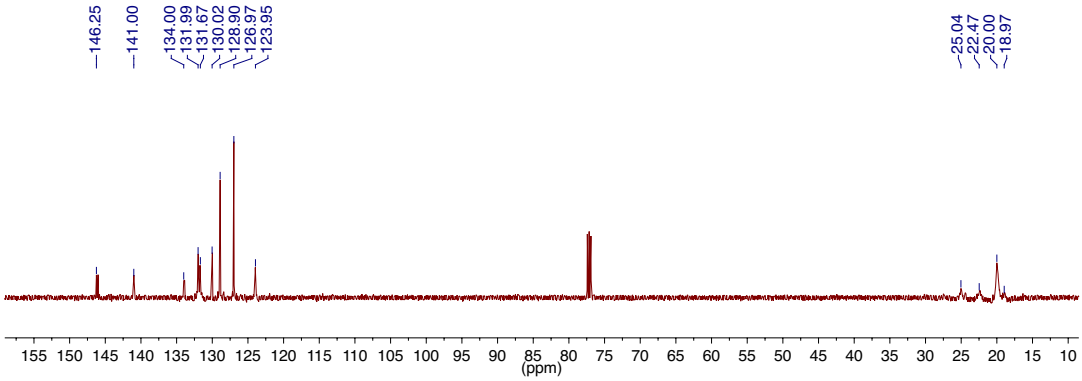


**Figure C3.2.** $^{13}C\{^{1}H\}$ NMR spectrum of **3.1a** in $CDCl_3$ at 25 °C.

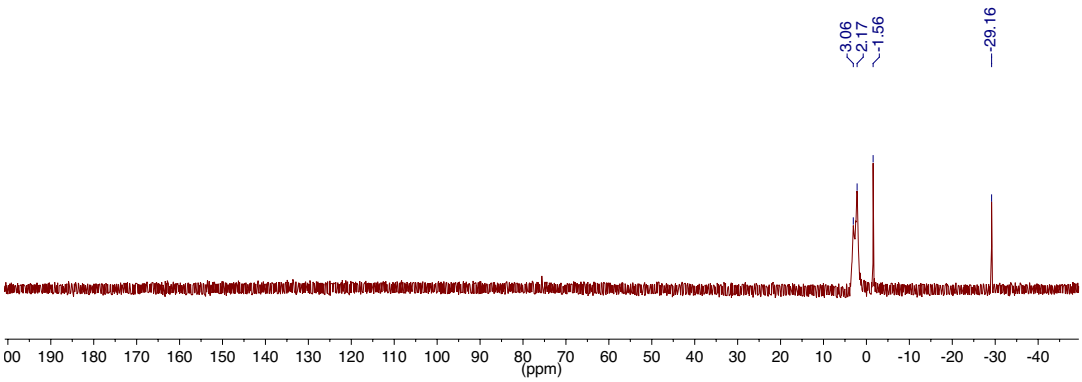


**Figure C3.3.** $^{31}P\{^{1}H\}$ NMR spectrum of **3.1a** in $CDCl_3$ at 25 °C.

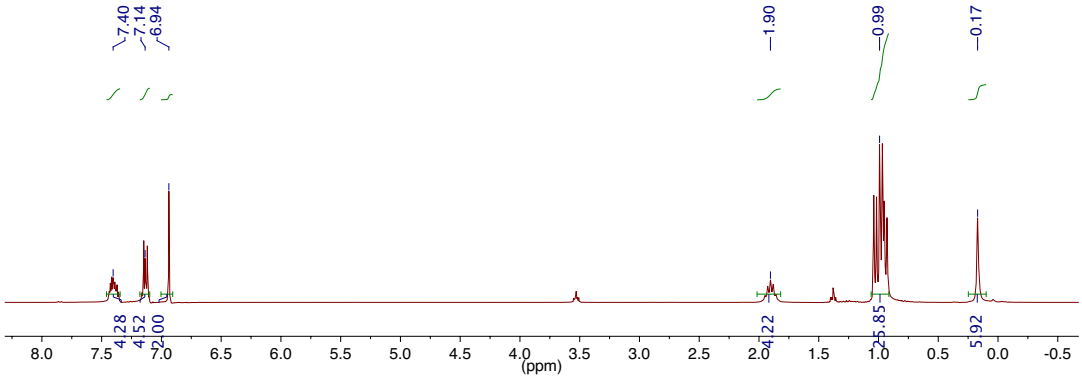


**Figure C3.4.** $^{1}H$ NMR spectrum of **3.1b** in $C_6D_6$ at 25 °C.

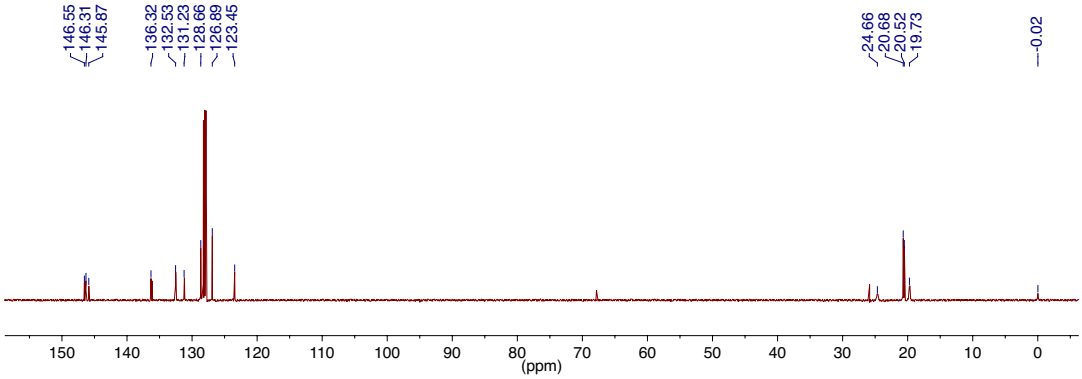


**Figure C3.5.** $^{13}C\{^{1}H\}$ NMR spectrum of **3.1b** in $C_6D_6$ at 25 °C.

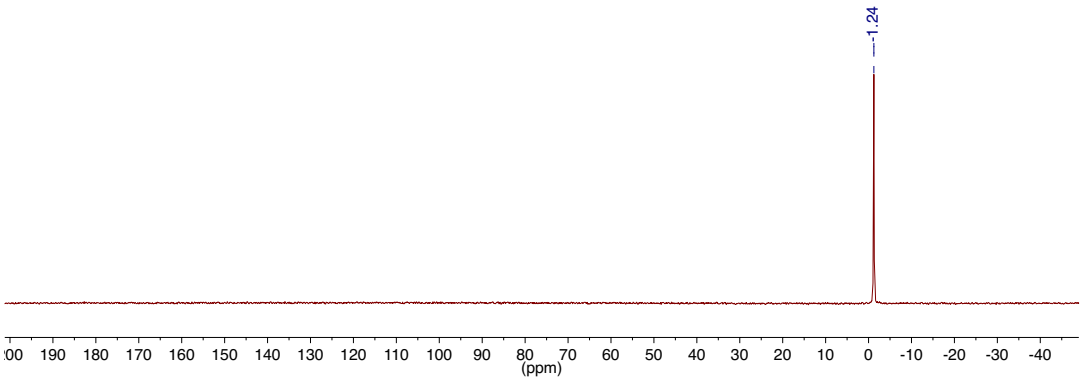


**Figure C3.6.** $^{31}P\{^{1}H\}$ NMR spectrum of **3.1b** in $C_6D_6$ at 25 °C.

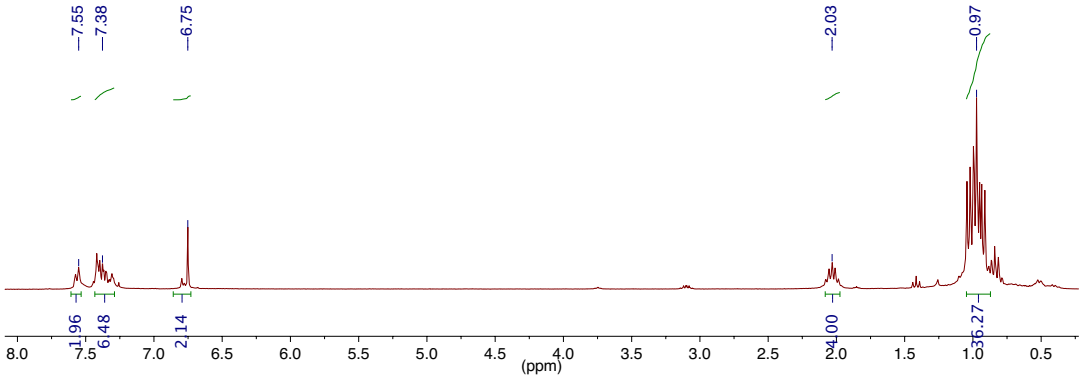


**Figure C3.7.** $^{1}H$ NMR spectrum of **3.1c** in $CDCl_3$ at 25 °C.

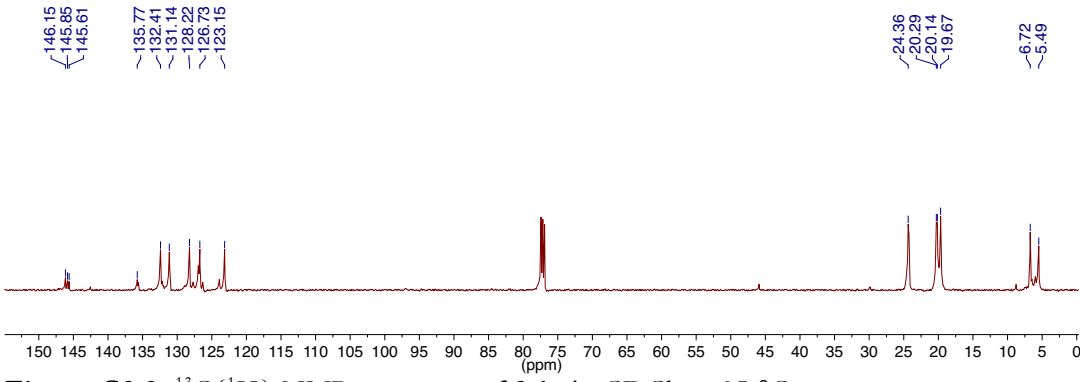


**Figure C3.8.** $^{13}C\{^{1}H\}$ NMR spectrum of **3.1c** in $CDCl_3$ at 25 °C.

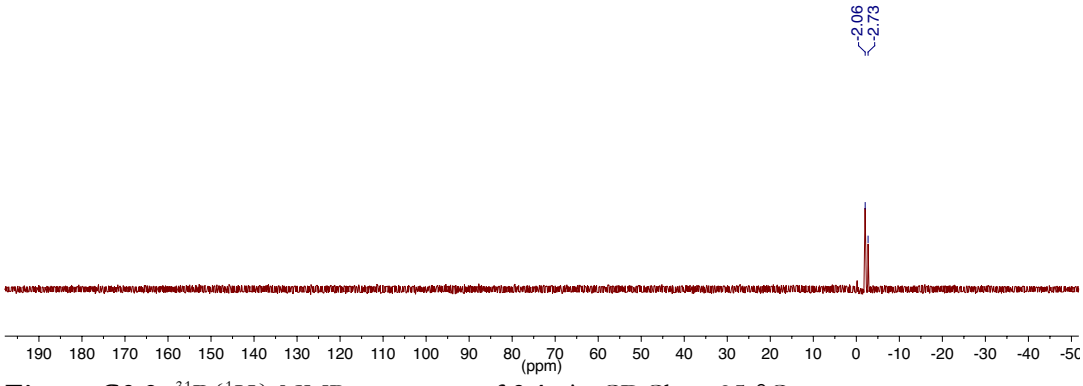


**Figure C3.9.** $^{31}P\{^{1}H\}$ NMR spectrum of **3.1c** in $CDCl_3$ at 25 °C.

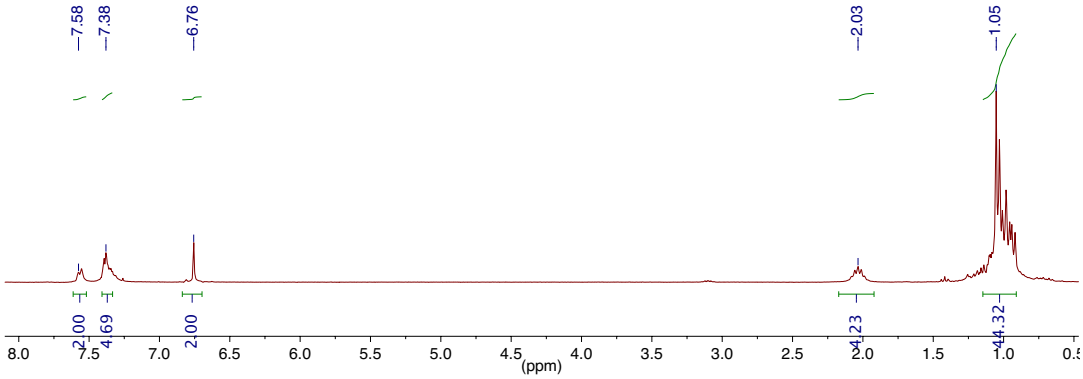


**Figure C3.10.** $^{1}H$ NMR spectrum of **3.1d** in $CDCl_3$ at 25 °C.

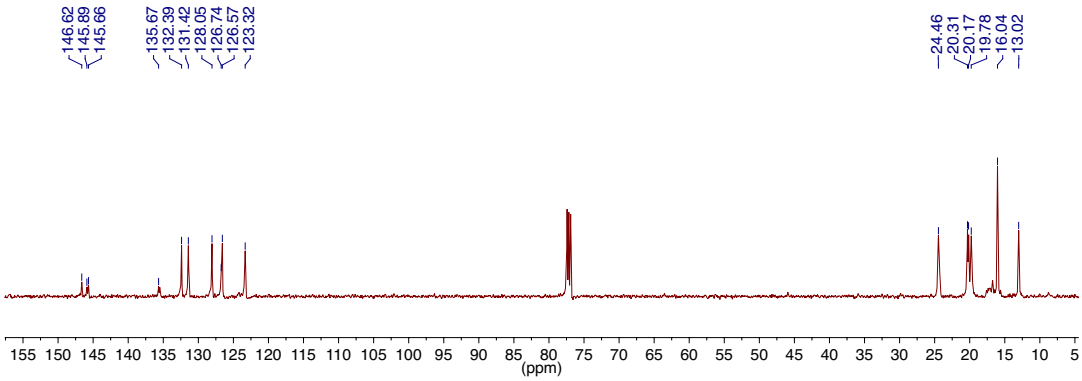


**Figure C3.11.** $^{13}C\{^{1}H\}$ NMR spectrum of **3.1d** in $CDCl_3$ at 25 °C.

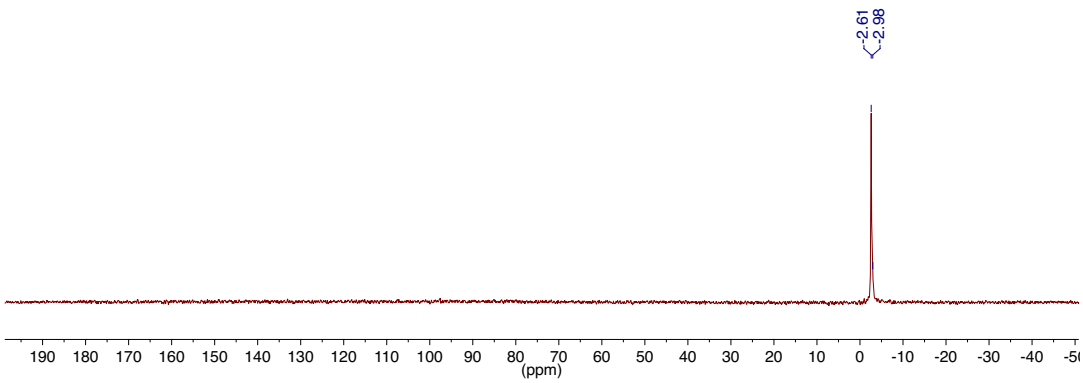


**Figure C3.12.** $^{31}P\{^{1}H\}$ NMR spectrum of **3.1d** in $CDCl_3$ at 25 °C.

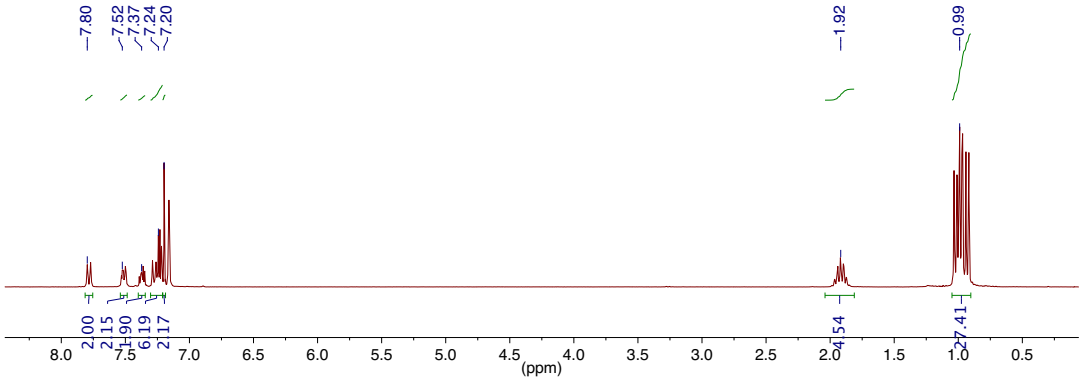


**Figure C3.13.** $^{1}H$ NMR spectrum of **3.1e** in $C_6D_6$ at 25 °C.

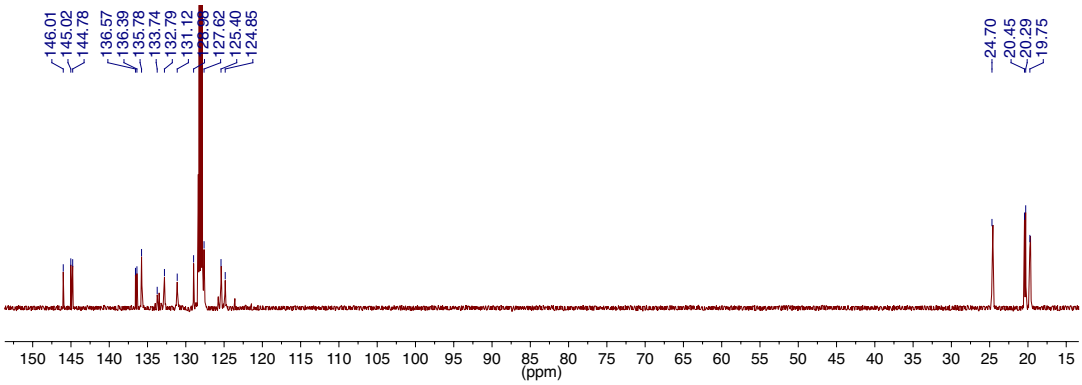


**Figure C3.14.** $^{13}C\{^{1}H\}$ NMR spectrum of **3.1e** in $C_6D_6$ at 25 °C.

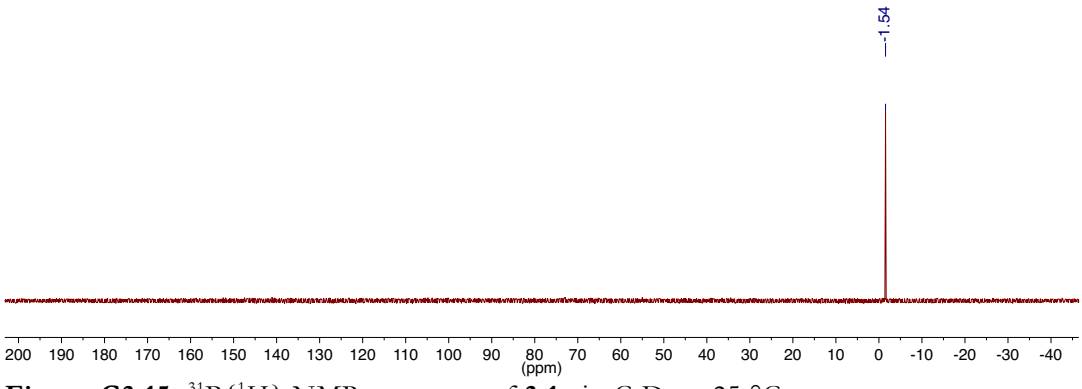


**Figure C3.15.** $^{31}P\{^{1}H\}$ NMR spectrum of **3.1e** in $C_6D_6$ at 25 °C.

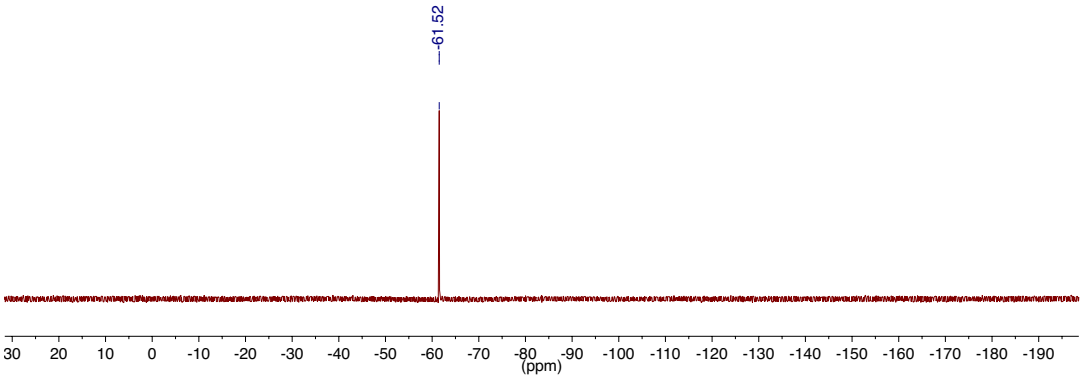


**Figure C3.16.** $^{19}F$ NMR spectrum of **3.1e** in $C_6D_6$ at 25 °C.

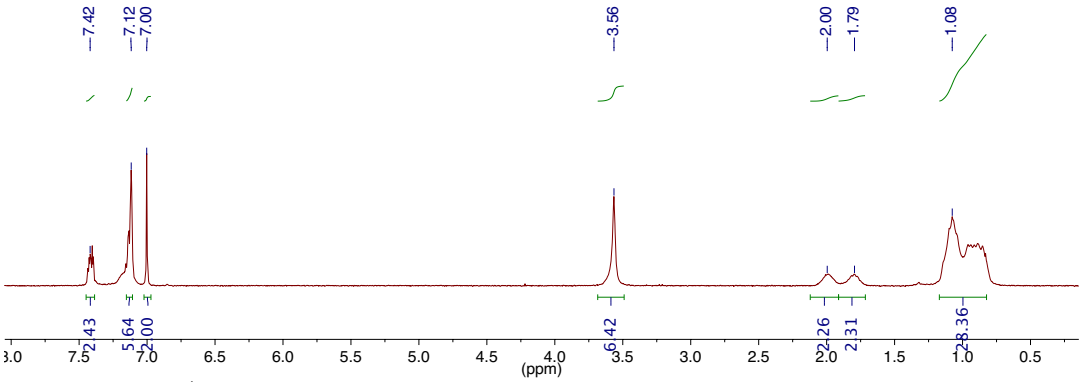


**Figure C3.17.** $^{1}H$ NMR spectrum of **3.1f** in $CDCl_3$ at 25 °C.

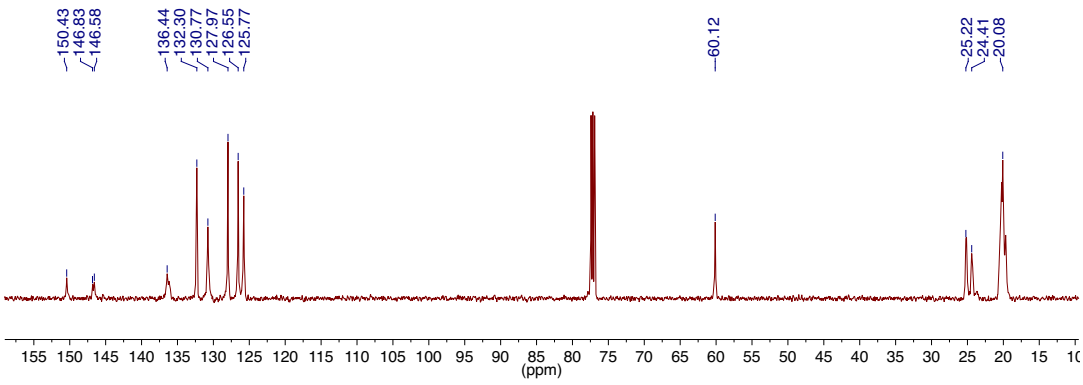


**Figure C3.18.** $^{13}C\{^{1}H\}$ NMR spectrum of **3.1f** in $CDCl_3$ at 25 °C.

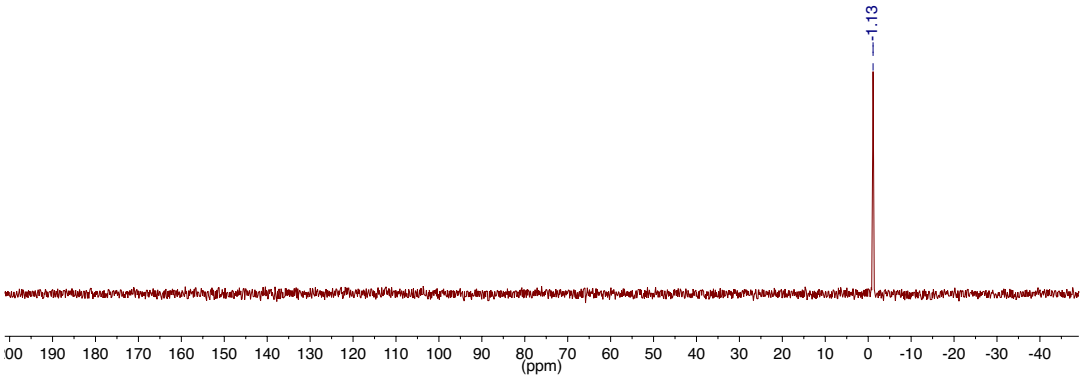


**Figure C3.19.** $^{31}P\{^{1}H\}$ NMR spectrum of **3.1f** in $CDCl_3$ at 25 °C.

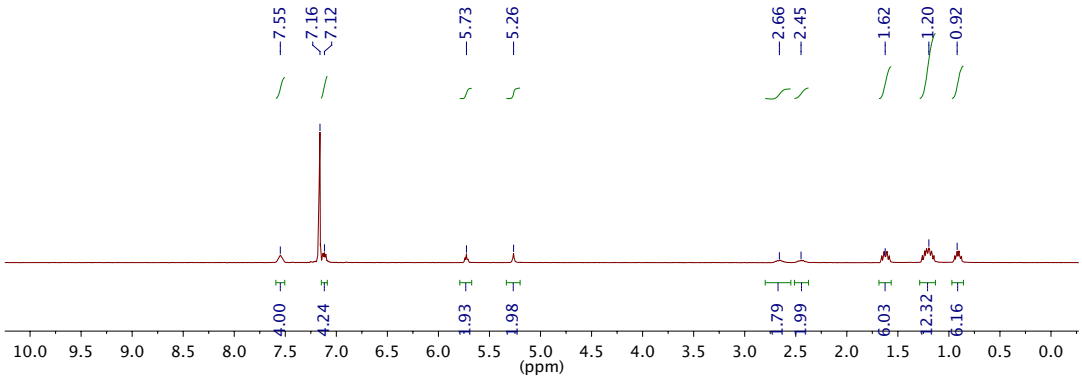


**Figure C3.20.** $^{1}H$ NMR spectrum of **3.2a** in $C_6D_6$.

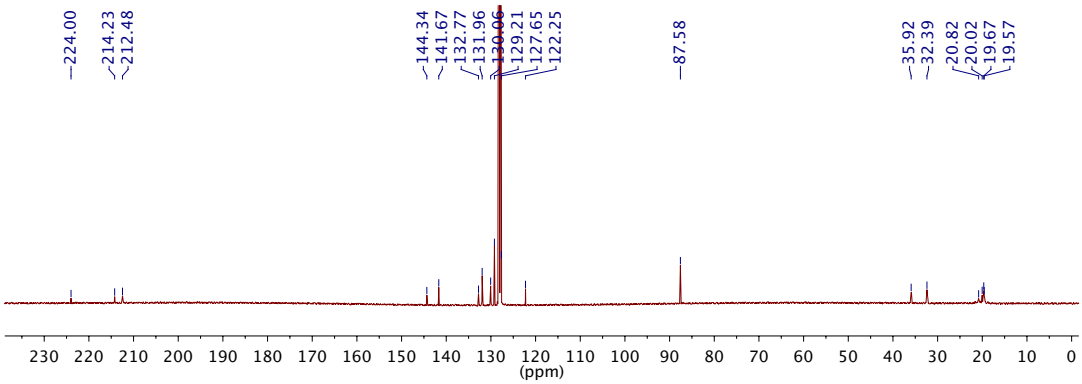


**Figure C3.21.** $^{13}C\{^{1}H\}$ NMR spectrum of **3.2a** in $C_6D_6$ at 75 °C.

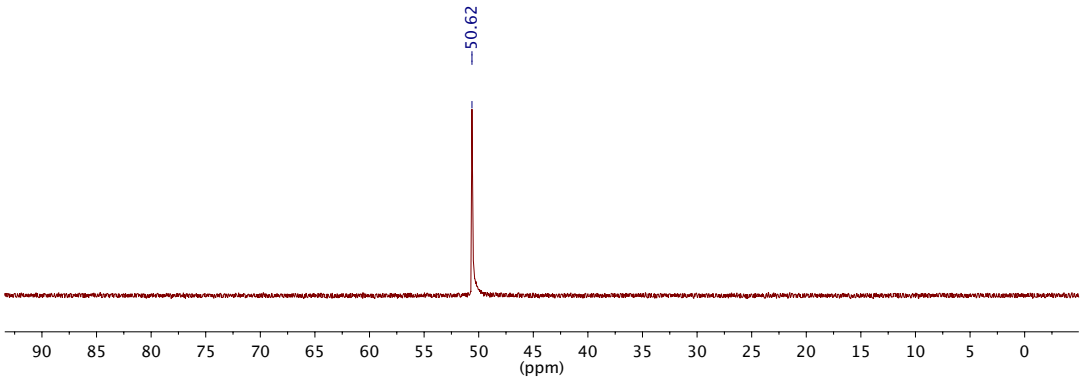


**Figure C3.22.** $^{31}P\{^{1}H\}$ NMR spectrum of **3.2a** in $C_6D_6$.

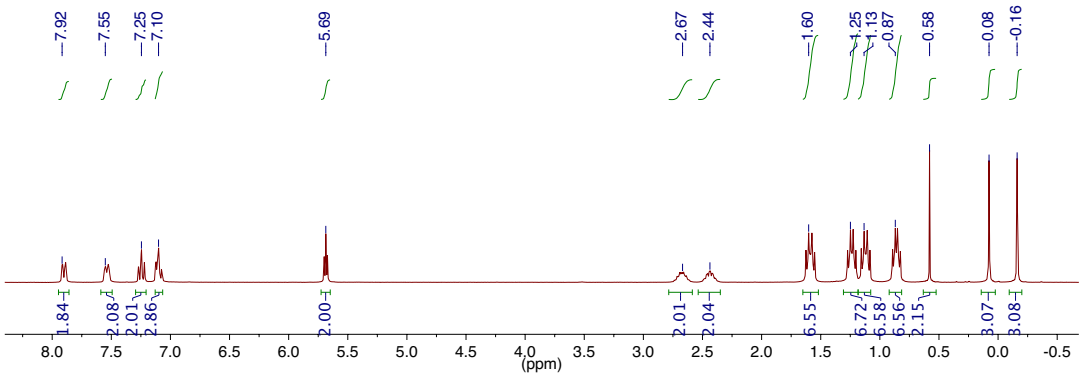


**Figure C3.23.** $^{1}H$ NMR spectrum of **3.2b** in $C_6D_6$ at 25 °C.

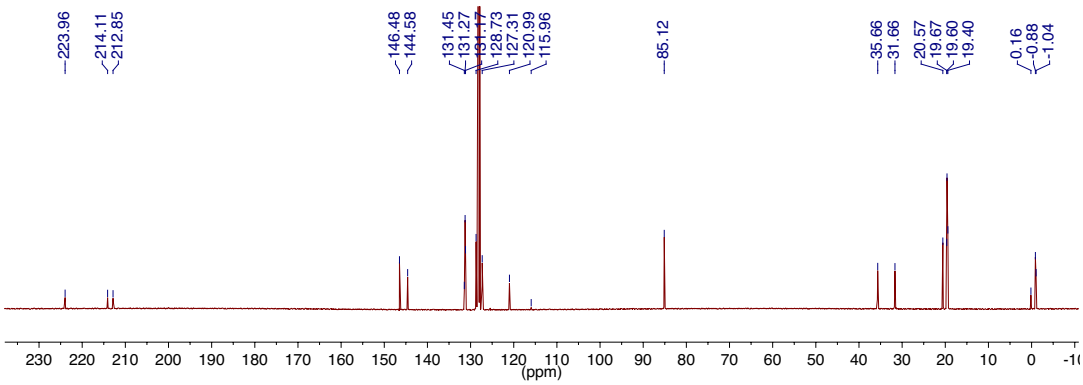


**Figure C3.24.** $^{13}C\{^{1}H\}$ NMR spectrum of **3.2b** in $C_6D_6$ at 25 °C.

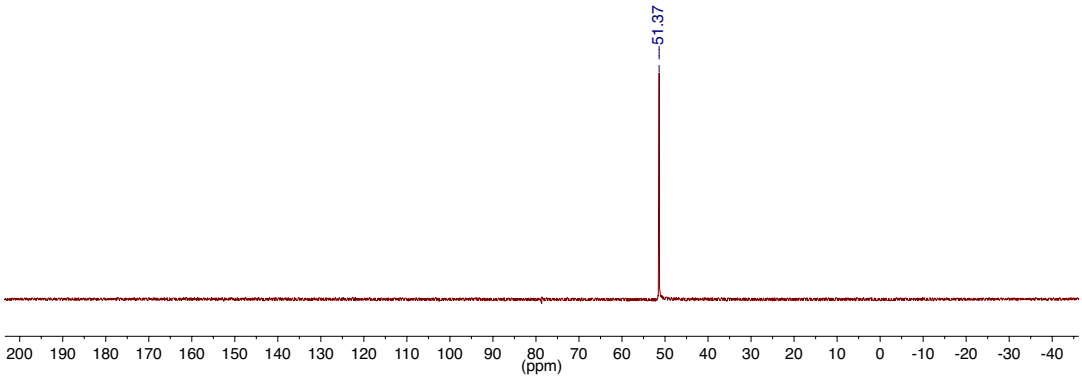


**Figure C3.25.** $^{31}P\{^{1}H\}$ NMR spectrum of **3.2b** in $C_6D_6$ at 25 °C.

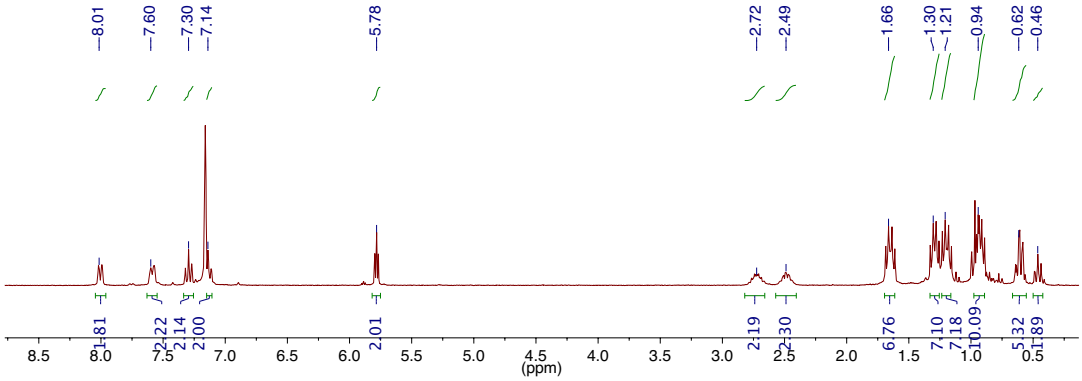


**Figure C3.26.** $^{1}H$ NMR spectrum of **3.2c** in $C_6D_6$ at 25 °C.

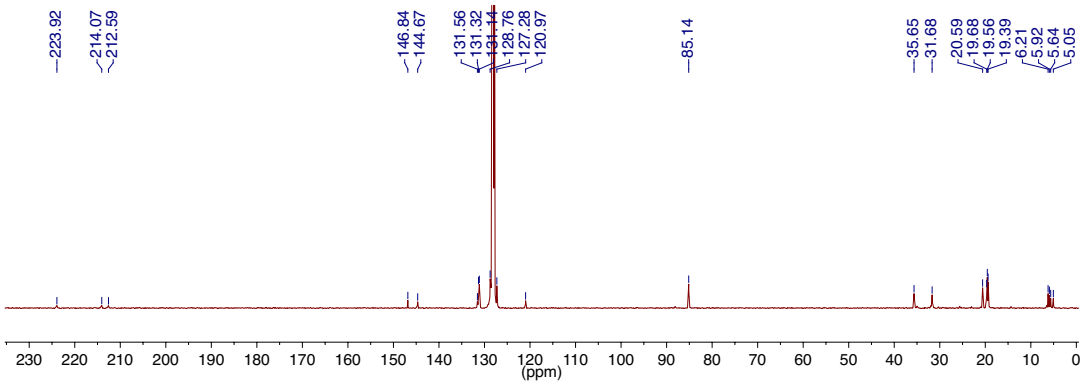


**Figure C3.27.** $^{13}C\{^{1}H\}$ NMR spectrum of **3.2c** in $C_6D_6$ at 25 °C.

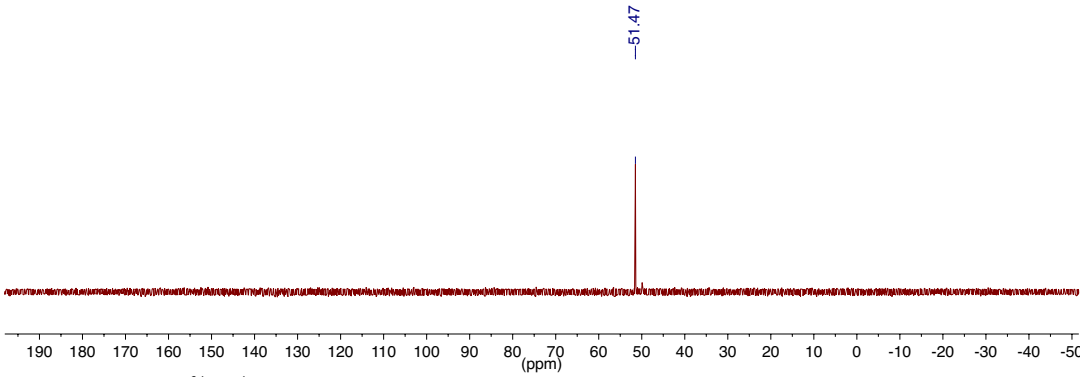


**Figure C3.28.** $^{31}P\{^{1}H\}$ NMR spectrum of **3.2c** in $C_6D_6$ at 25 °C.

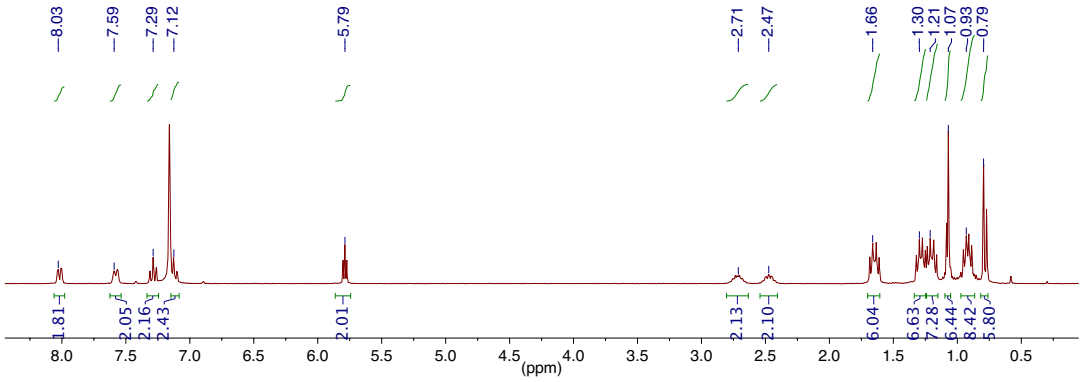


**Figure C3.29.** $^{1}H$ NMR spectrum of **3.2d** in $C_6D_6$ at 25 °C.

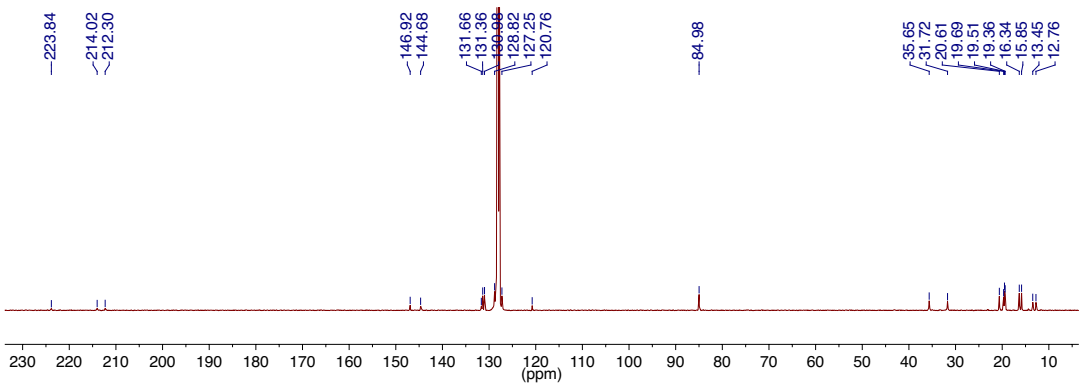


**Figure C3.30.** $^{13}C\{^{1}H\}$ NMR spectrum of **3.2d** in $C_6D_6$ at 25 °C.

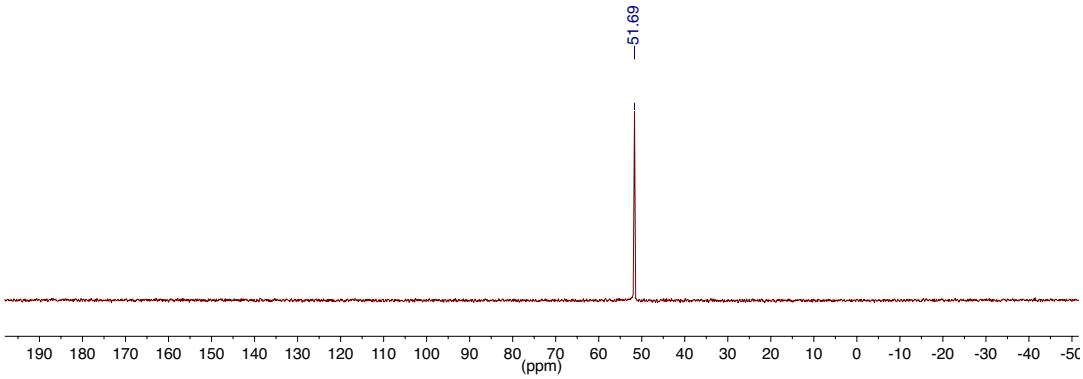


**Figure C3.31.** $^{31}P\{^{1}H\}$ NMR spectrum of **3.2d** in $C_6D_6$ at 25 °C.

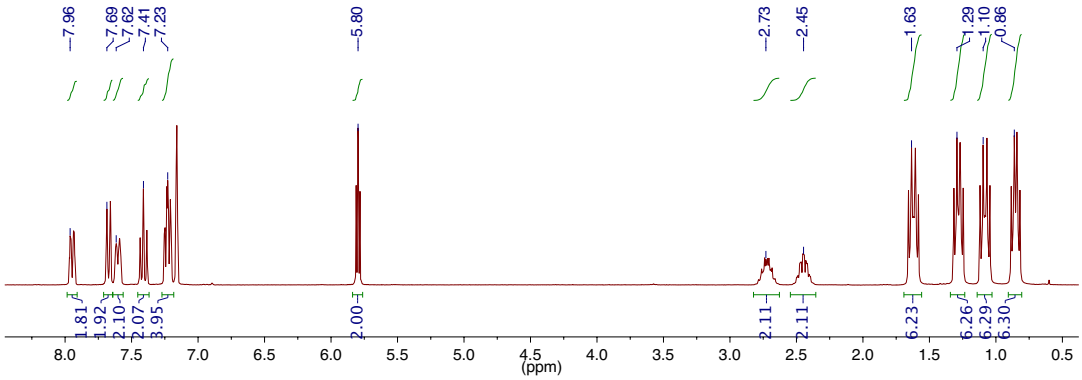


**Figure C3.32.** $^{1}H$ NMR spectrum of **3.2e** in $C_6D_6$ at 25 °C.

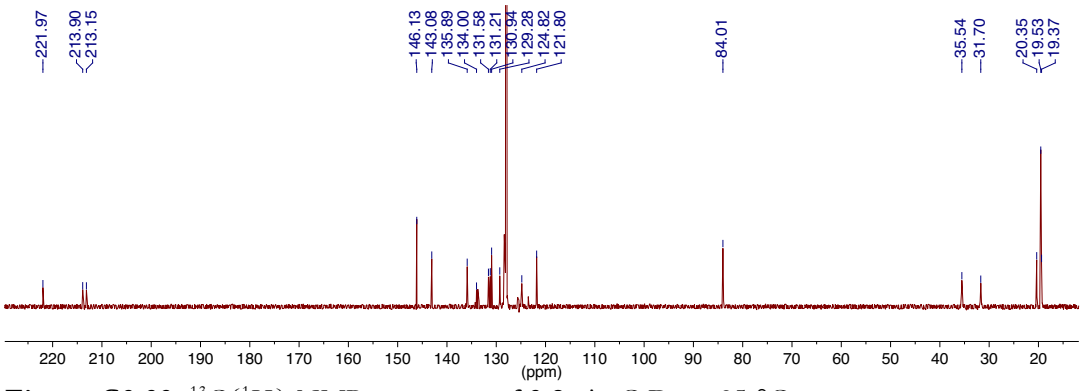


**Figure C3.33.** $^{13}C\{^{1}H\}$ NMR spectrum of **3.2e** in $C_6D_6$ at 25 °C.

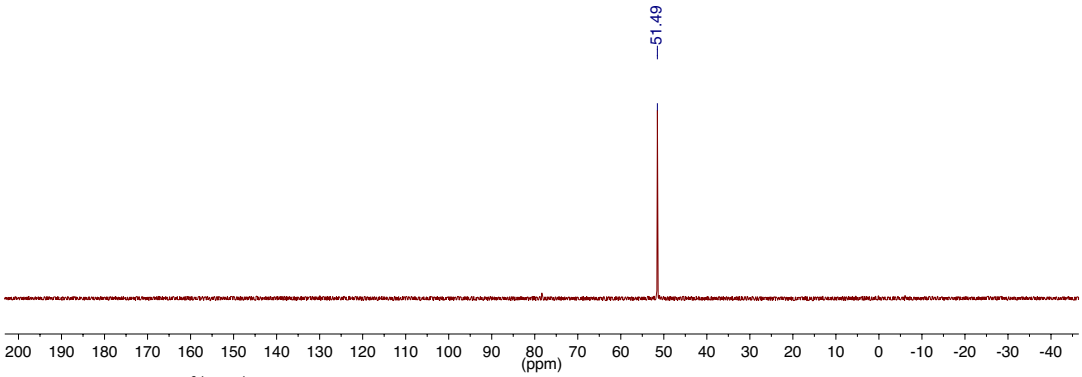


**Figure C3.34.** $^{31}P\{^{1}H\}$ NMR spectrum of **3.2e** in $C_6D_6$ at 25 °C.

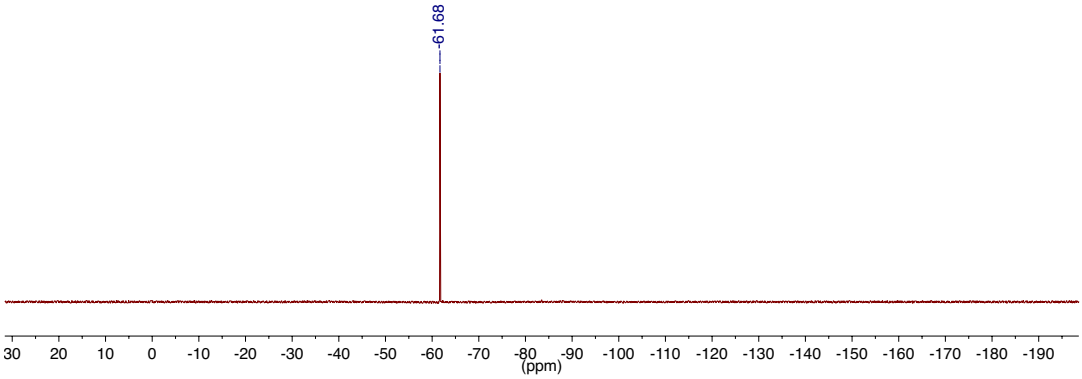


**Figure C3.35.** $^{19}F$ NMR spectrum of **3.2e** in $C_6D_6$ at 25 °C.

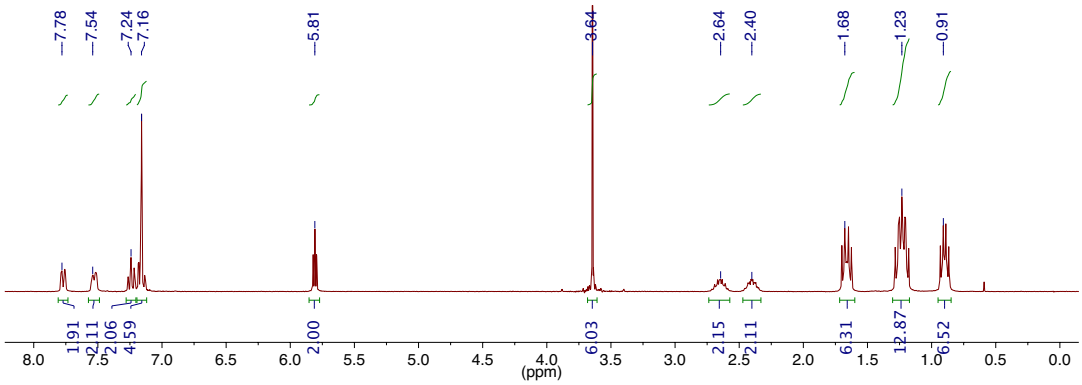


**Figure C3.36.** $^{1}H$ NMR spectrum of **3.2f** in $C_6D_6$ at 25 °C.

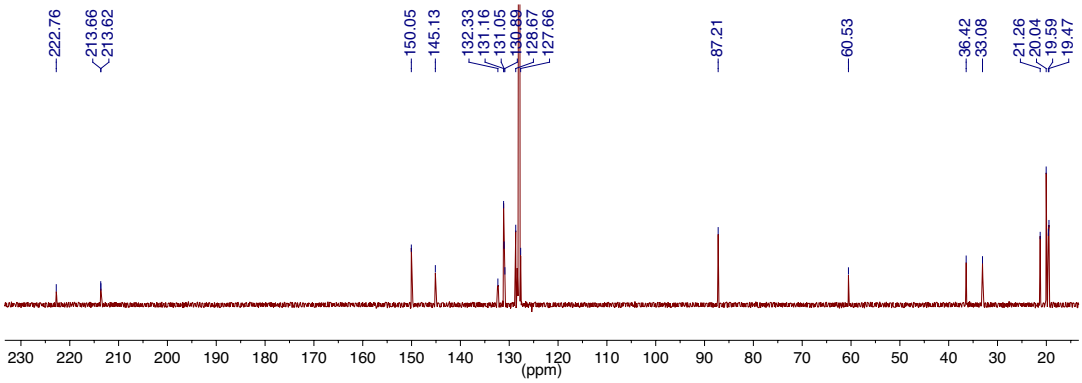


**Figure C3.37.** $^{13}C\{^{1}H\}$ NMR spectrum of **3.2f** in $C_6D_6$ at 25 °C. Solvent peaks off scale.

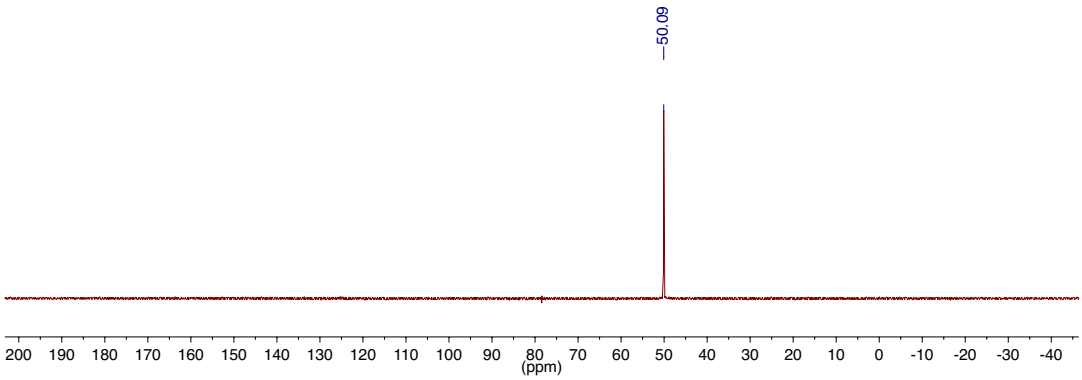


**Figure C3.38.** $^{31}P\{^{1}H\}$ NMR spectrum of **3.2f** in $C_6D_6$ at 25 °C.

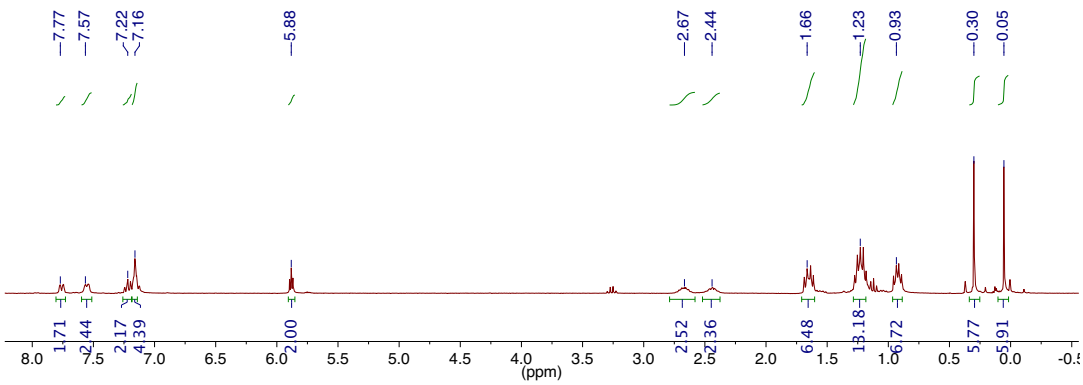


**Figure C3.39.** $^{1}H$ NMR spectrum of **3.2h** in $C_6D_6$ at 25 °C.

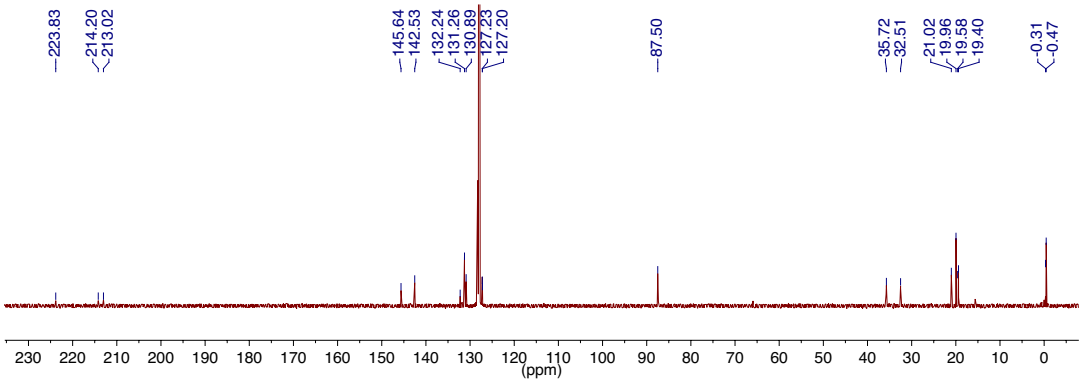


**Figure C3.40.** $^{13}C\{^{1}H\}$ NMR spectrum of **3.2h** in $C_6D_6$ at 25 °C. Solvent peaks off scale

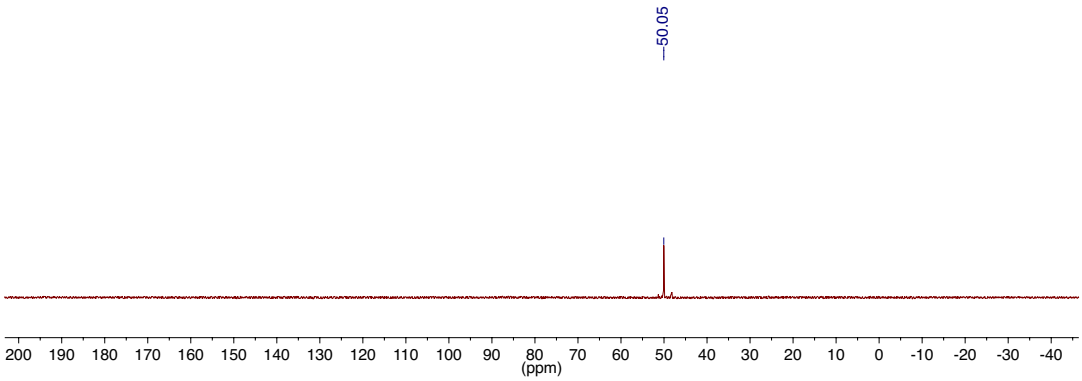


**Figure C3.41.** $^{31}P\{^{1}H\}$ NMR spectrum of **3.2h** in $C_6D_6$ at 25 °C.

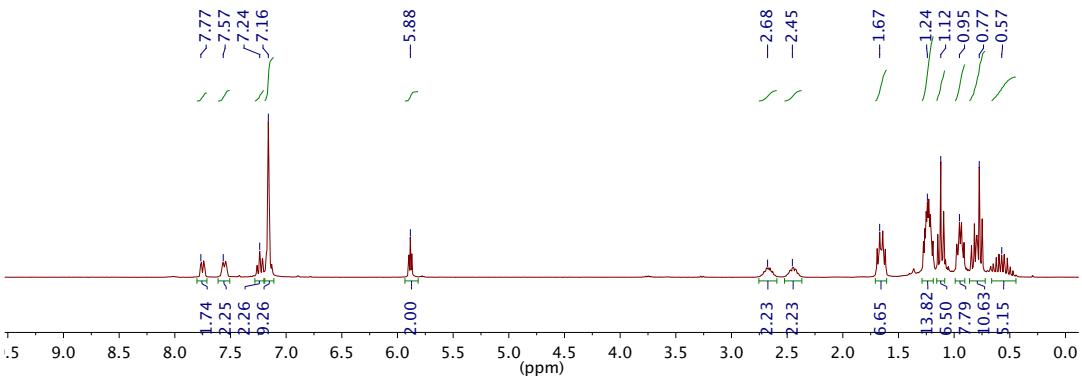


**Figure C3.42.** $^{1}H$ NMR spectrum of **3.2i** in $C_6D_6$ at 25 °C.

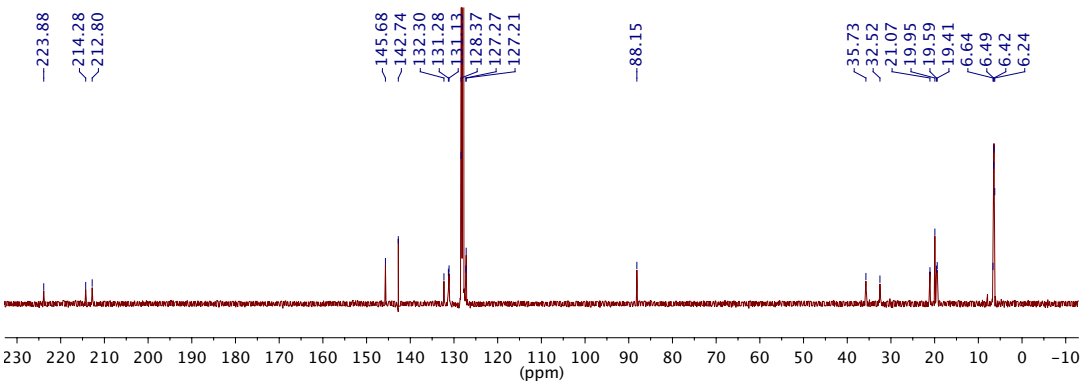


**Figure C3.43.** $^{13}C\{^{1}H\}$ NMR spectrum of **3.2i** in $C_6D_6$ at 25 °C. Solvent peaks off scale

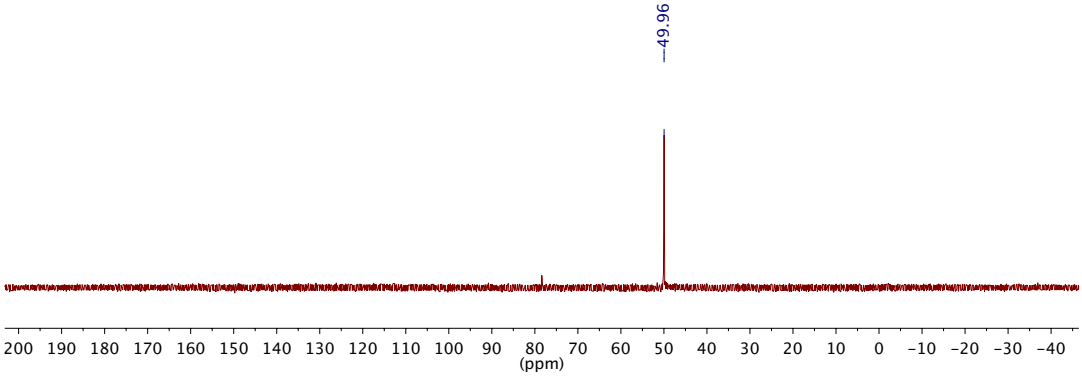


**Figure C3.44.** $^{31}P\{^{1}H\}$ NMR spectrum of **3.2i** in $C_6D_6$ at 25 °C.

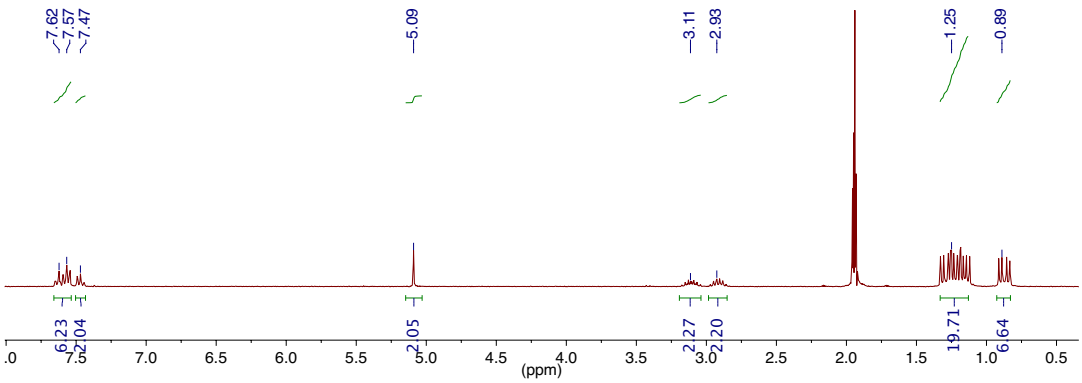


**Figure C3.45.** $^{1}H$ NMR spectrum of **3.3** in $CD_3CN$ at 25 °C.

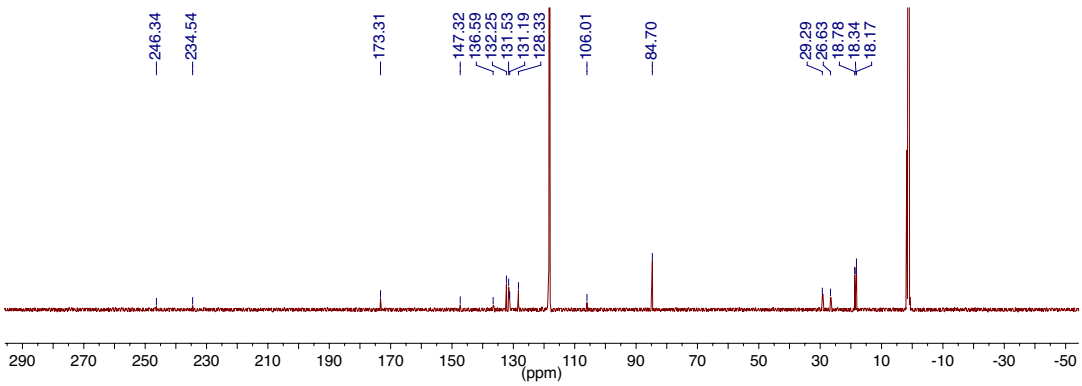


**Figure C3.46.** $^{13}C\{^{1}H\}$ NMR spectrum of **3.3** in $CD_3CN$ at 25 °C. Solvent peaks off scale.

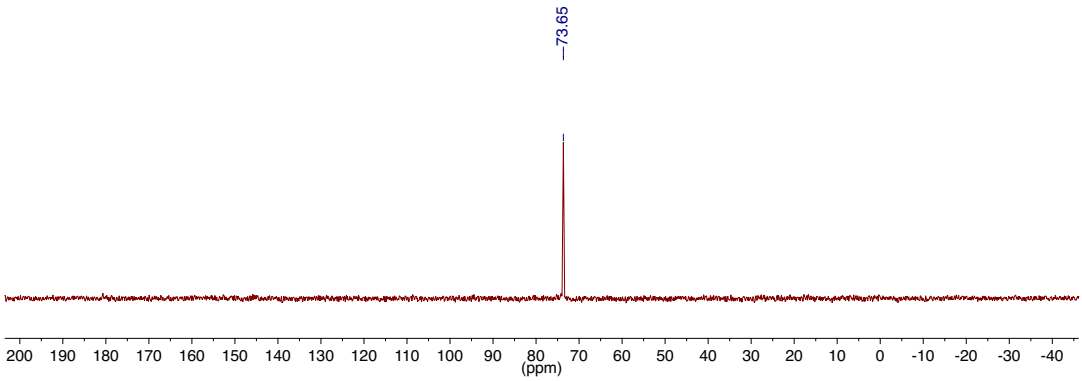


**Figure C3.47.** $^{31}P\{^{1}H\}$ NMR spectrum of **3.3** in $CD_3CN$ at 25 °C.

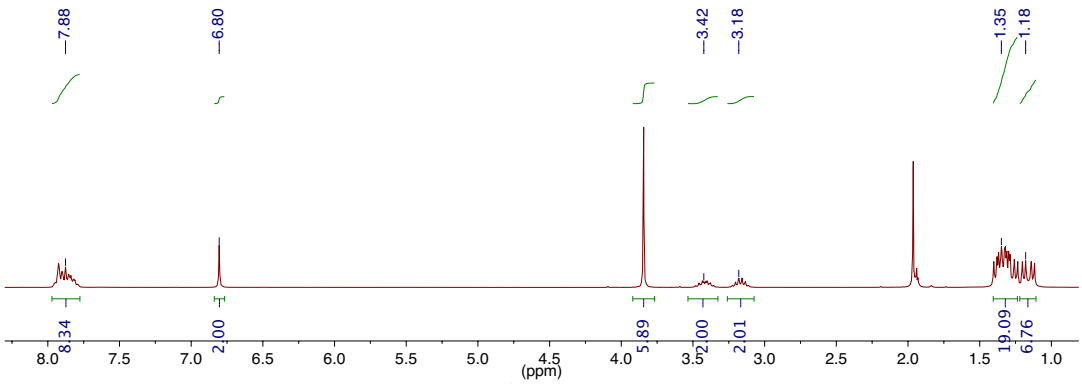


**Figure C3.48.** $^{1}H$ NMR spectrum of $[\mathbf{3.5}^{2+}][OTf]_2$ in $CD_3CN$ at 25 °C.

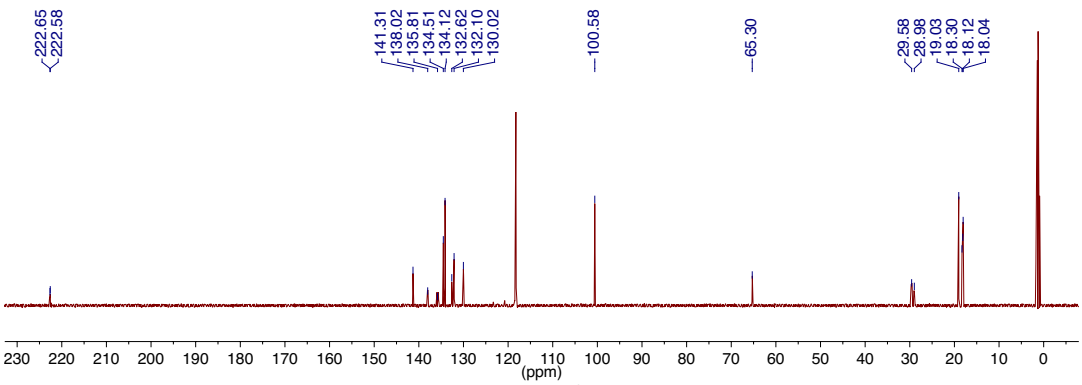


**Figure C3.49.** $^{13}C\{^{1}H\}$ NMR spectrum of [**3.5**$^{2+}$][OTf]$_2$ in $CD_3CN$ at 25 °C.

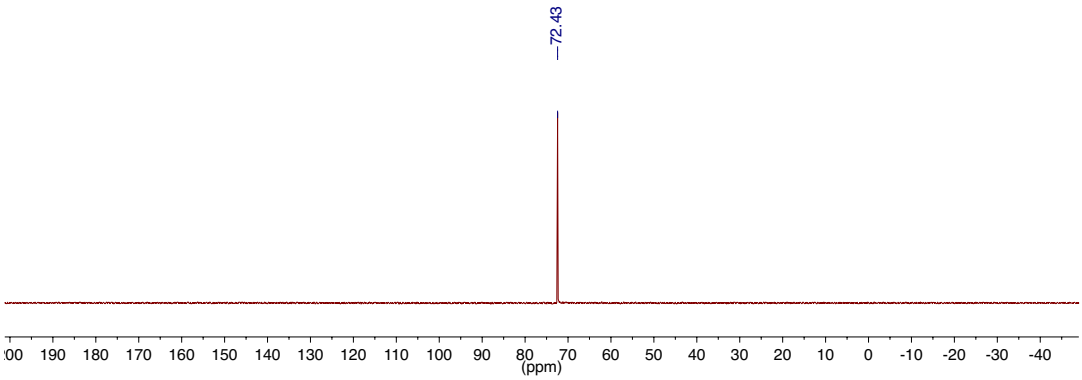


**Figure C3.50.** $^{31}P\{^{1}H\}$ NMR spectrum of [**3.5**$^{2+}$][OTf]$_2$ in $CD_3CN$ at 25 °C.

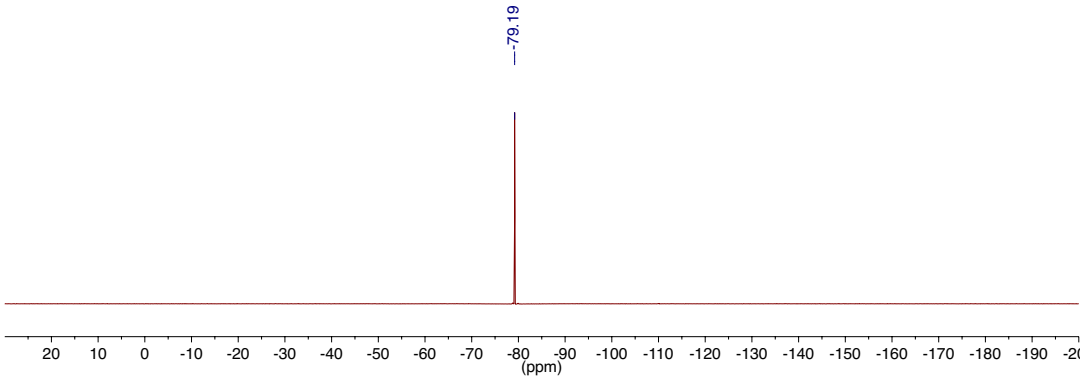


**Figure C3.51.** $^{19}F$ NMR spectrum of [**3.5**$^{2+}$][OTf]$_2$ in $CD_3CN$ at 25 °C.

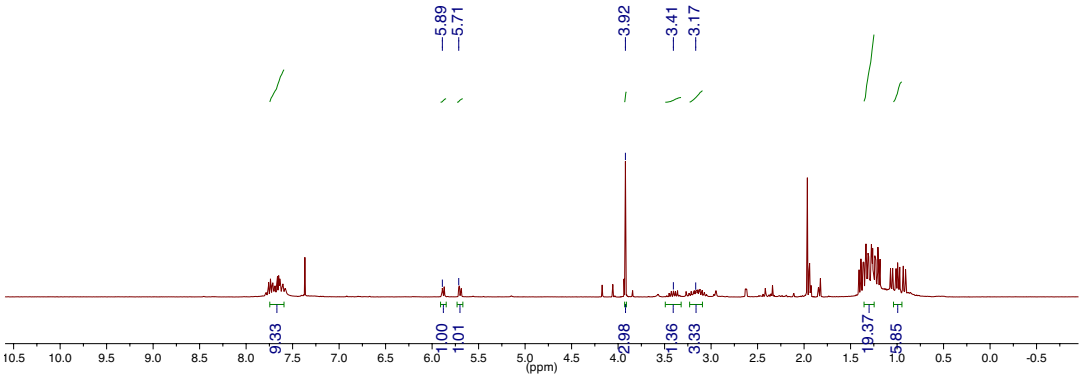


**Figure C3.52.** $^{1}$H NMR spectrum of [**3.6**$^{+}$][OTf$^{-}$] in $CD_3CN$ at 25 °C.

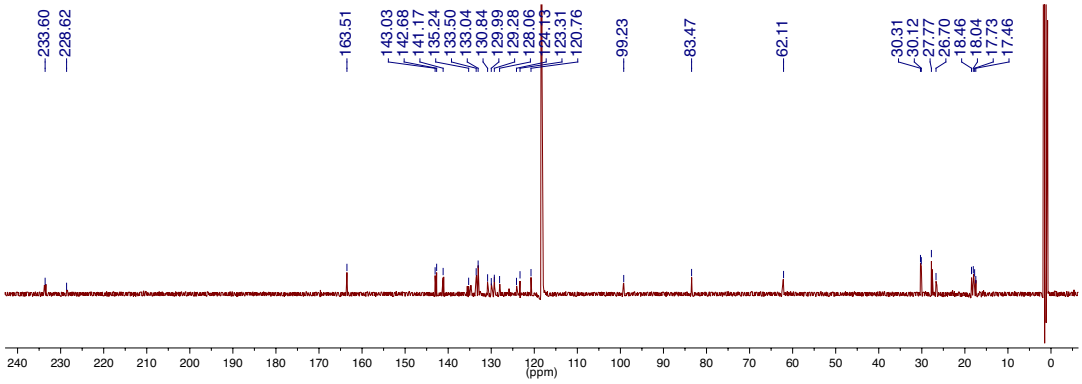


**Figure S3.53.** $^{13}$C{$^{1}$H} NMR spectrum of [**3.6**$^{+}$][OTf$^{-}$] in $CD_3CN$ at 25 °C.

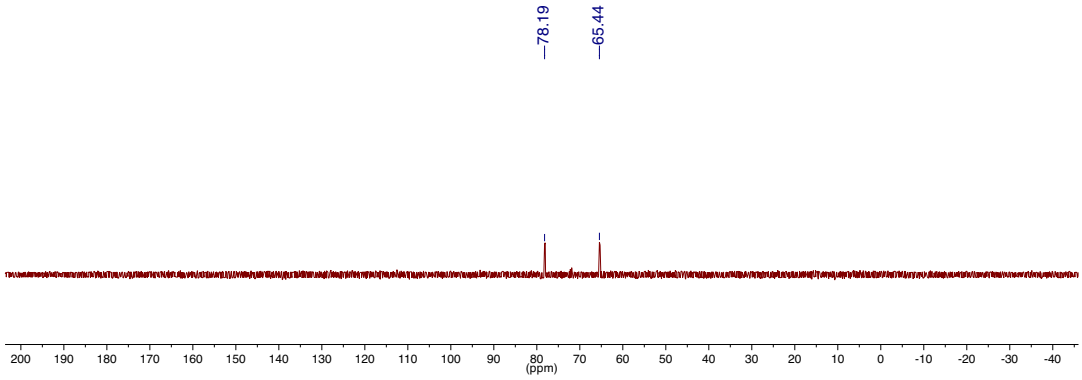


**Figure C3.54.** $^{31}$P{$^{1}$H} NMR spectrum of [**3.6**$^{+}$][OTf$^{-}$] in $CD_3CN$ at 25 °C.

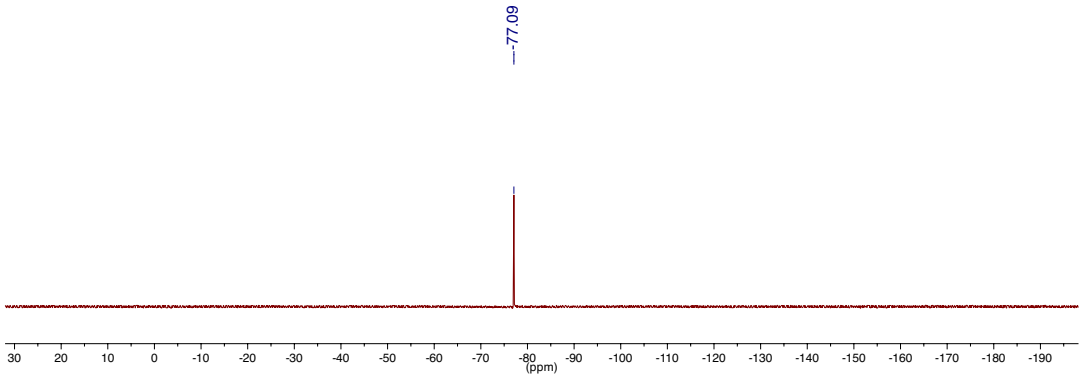


**Figure C3.55.** $^{19}F$ NMR spectrum of [**3.6**$^{+}$][OTf] in $CD_3CN$ at 25 °C.

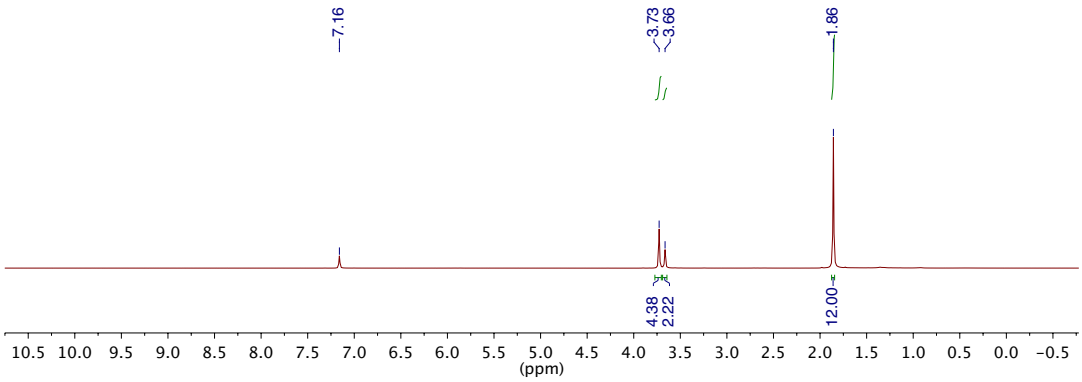


**Figure C3.56.** $^{1}H$ NMR spectrum of $Me_4Fc$ in $C_6D_6$ at 25 °C.

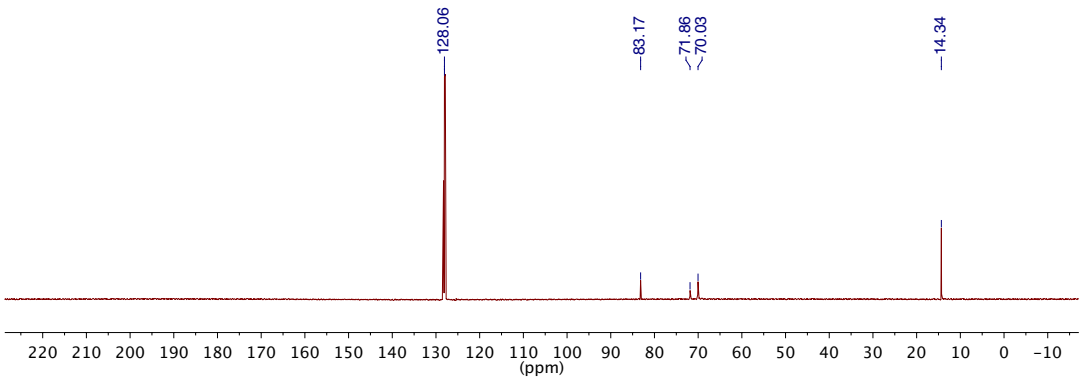


**Figure C3.57.** $^{13}C\{^{1}H\}$ NMR spectrum of $Me_4Fc$ in $C_6D_6$ at 25 °C.

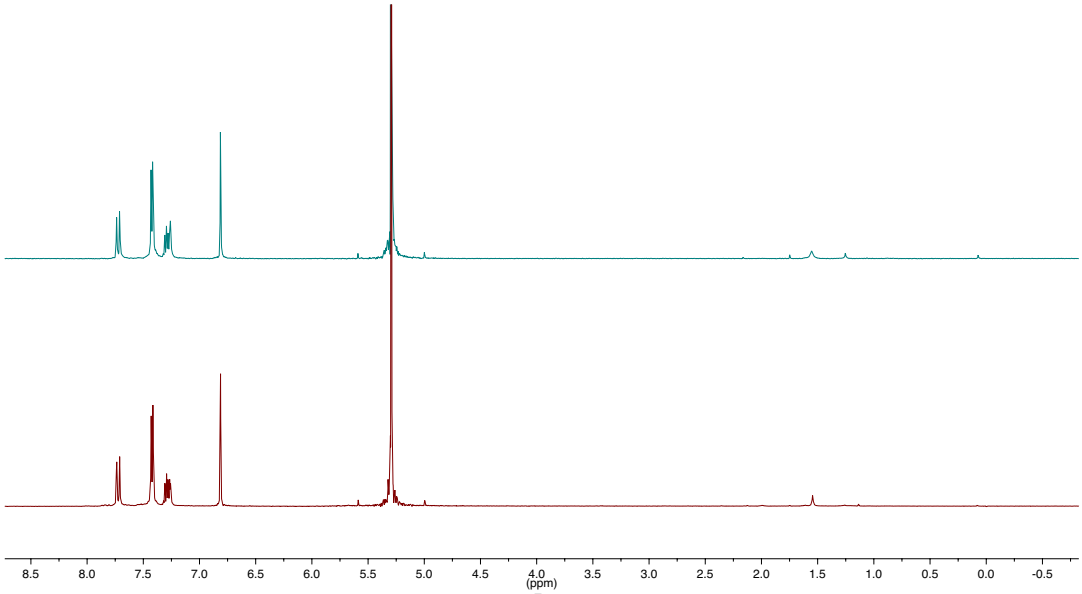


**Figure C3.58.** $^{1}$H NMR spectrum of **3.1$^{Br}$a** in $CD_2Cl_2$ under $O_2$ at 25 °C after 10 minutes (bottom) and 24 hours (top). Solvent peak off scale.

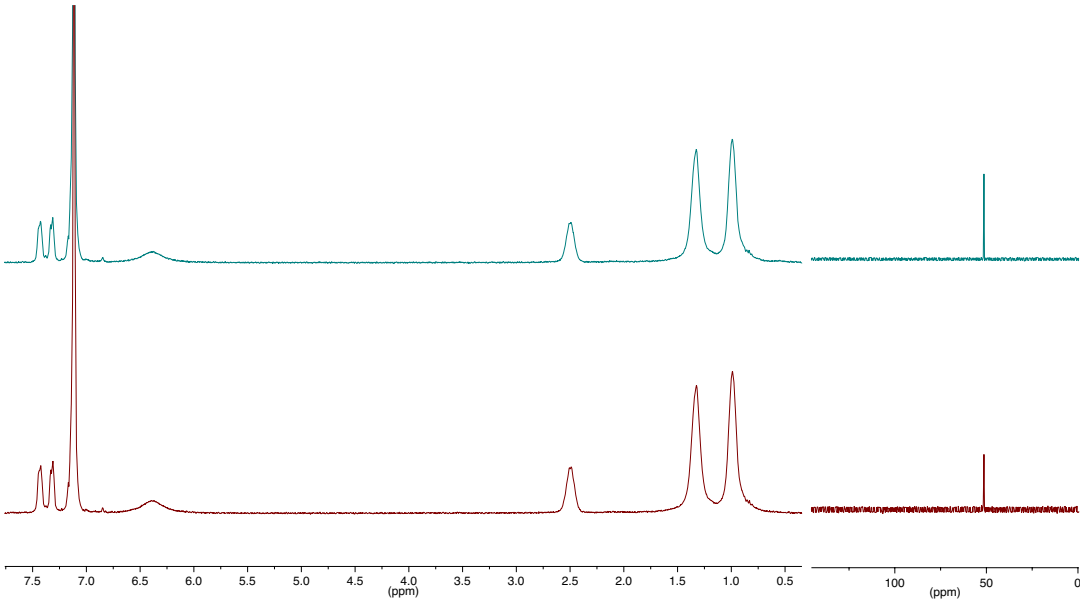


**Figure C3.59.** $^{1}$H NMR spectra (left) and $^{31}$P{$^{1}$H} NMR spectra (right) of **3.2g** in $C_6D_6$ under $O_2$ at 25 °C after 10 minutes (bottom) and 24 hours (top). Solvent peak off scale.

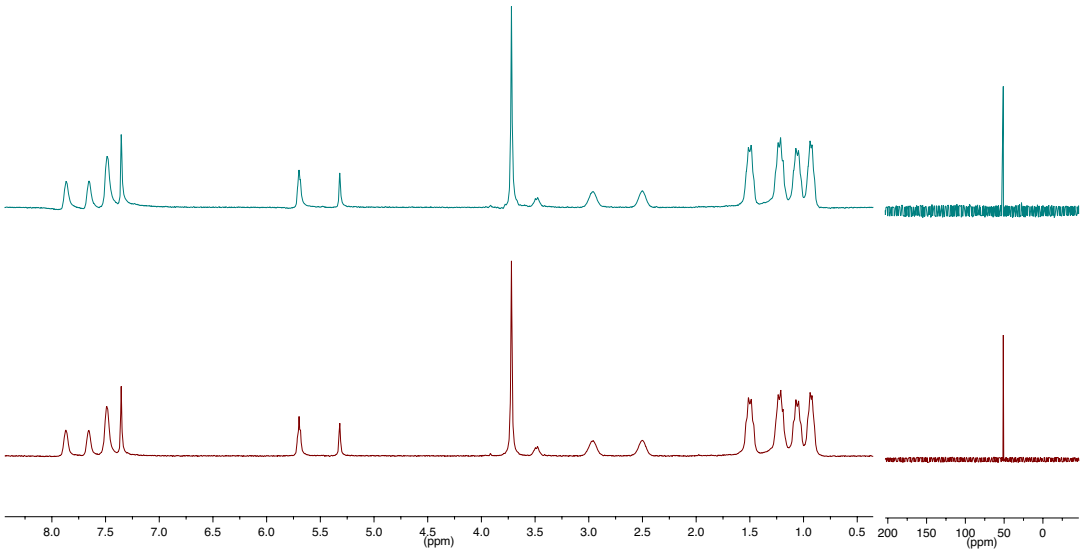


**Figure C3.60.** $^{1}$H NMR spectra (left) and $^{31}$P{$^{1}$H} NMR spectra (right) of **3.2f** in $CD_2Cl_2$ under $O_2$ at 25 °C after 10 minutes (bottom) and 24 hours (top).

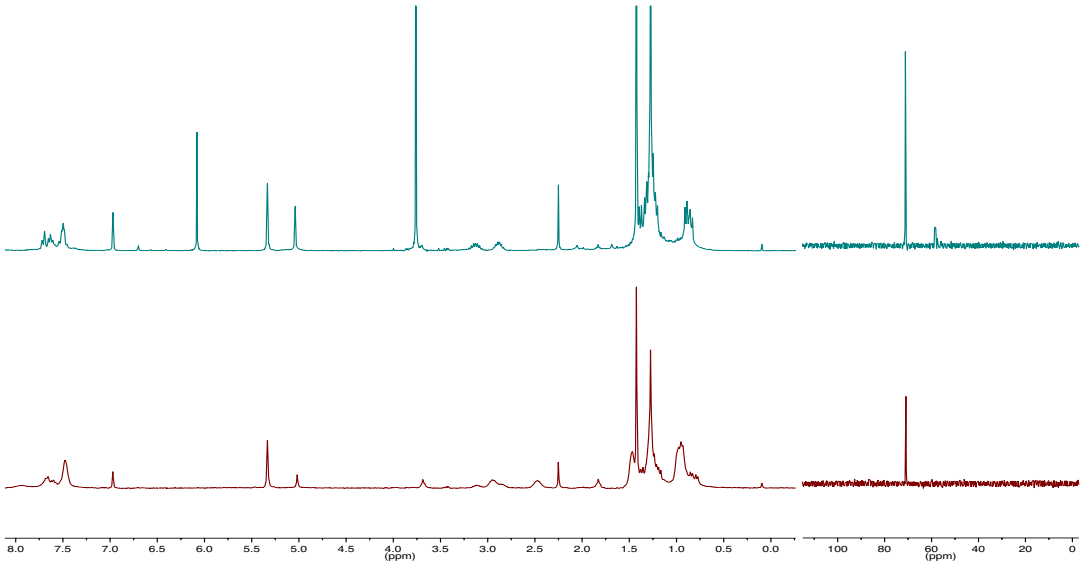


**Figure C3.61.** $^{1}$H NMR spectra (left) and $^{31}$P{$^{1}$H} NMR spectra (right) of **3.2a** + $H_2O_2$ after 1 hour (bottom) and **3.3** + $H_2O_2$ after 1 hour (top) in $CD_2Cl_2$ at 25 °C.

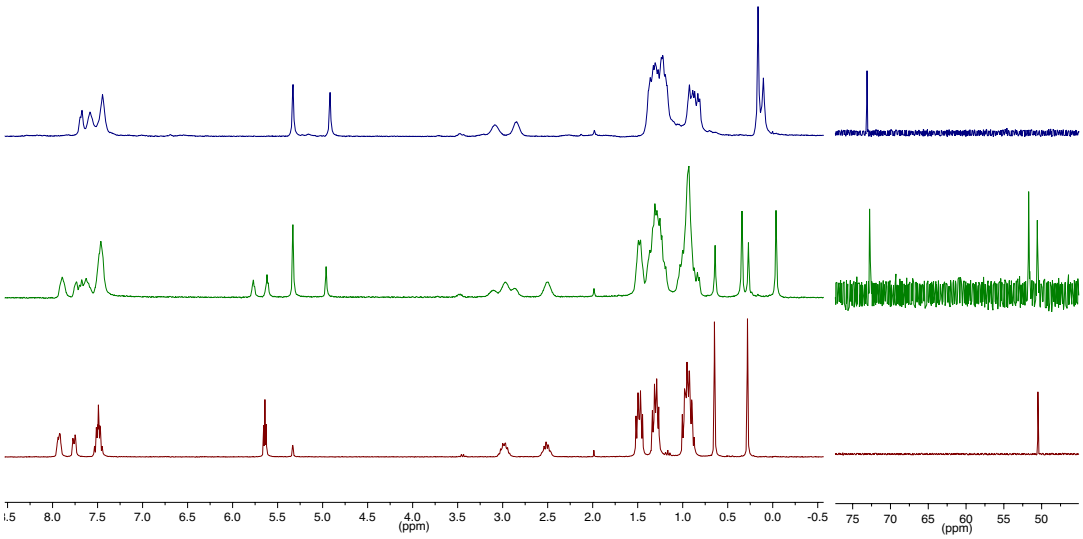


**Figure C3.62.** $^{1}$H NMR spectra (left) and $^{31}$P{$^{1}$H} NMR spectra (right) of **3.2b** under $N_2$ (bottom) and under $O_2$ after 1.5 hours (middle) and after 3 hours (top) in $CD_2Cl_2$ at 25 °C.

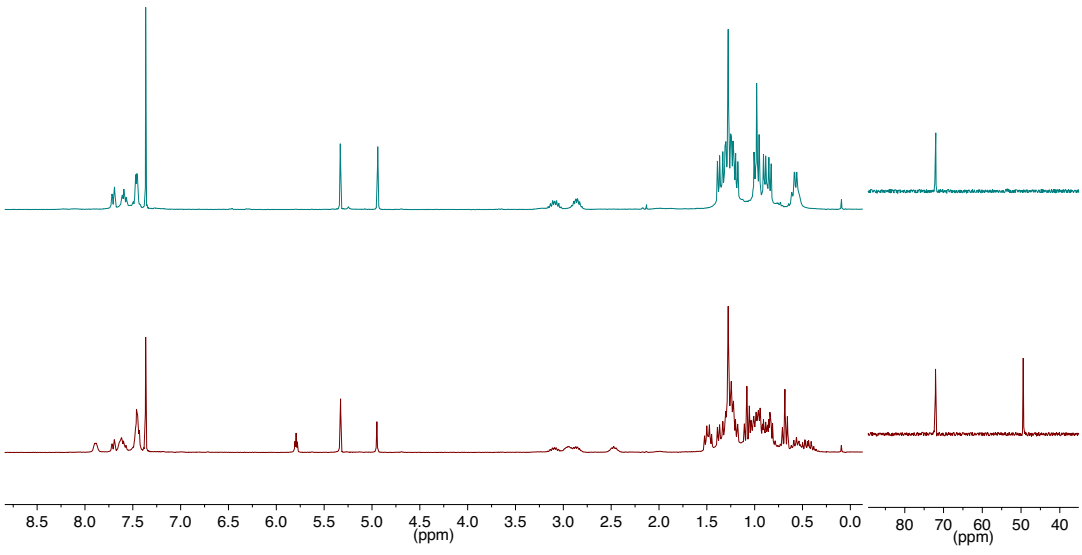


**Figure C3.63.** $^{1}$H NMR spectra (left) and $^{31}$P{$^{1}$H} NMR spectra (right) of **3.2c** under $O_2$ for 8 hours (bottom) and 48 hours (top) in $CD_2Cl_2$ at 25 °C.

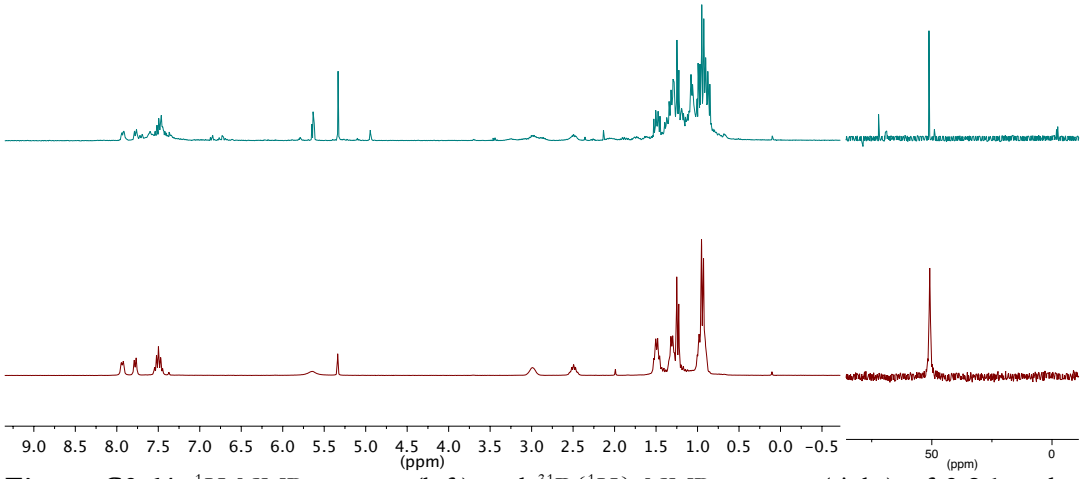


**Figure C3.64.** $^{1}H$ NMR spectra (left) and $^{31}P\{^{1}H\}$ NMR spectra (right) of **3.2d** under $O_2$ for 10 minutes (bottom) and 5 days (top) in $CD_2Cl_2$ at 25 °C.

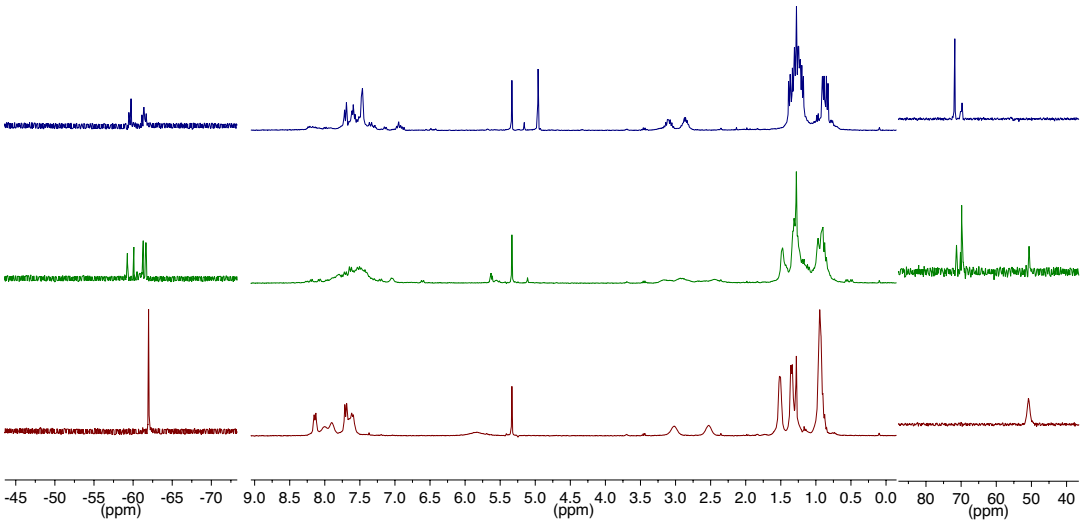


**Figure C3.65.** $^{19}F$ NMR spectra (left), $^{1}H$ NMR spectra (center) and $^{31}P\{^{1}H\}$ NMR spectra (right) of **3.2e** under $O_2$ after 10 minutes (bottom), 6 hours (middle), and 36 hours (top) in $CD_2Cl_2$ at 25 °C.

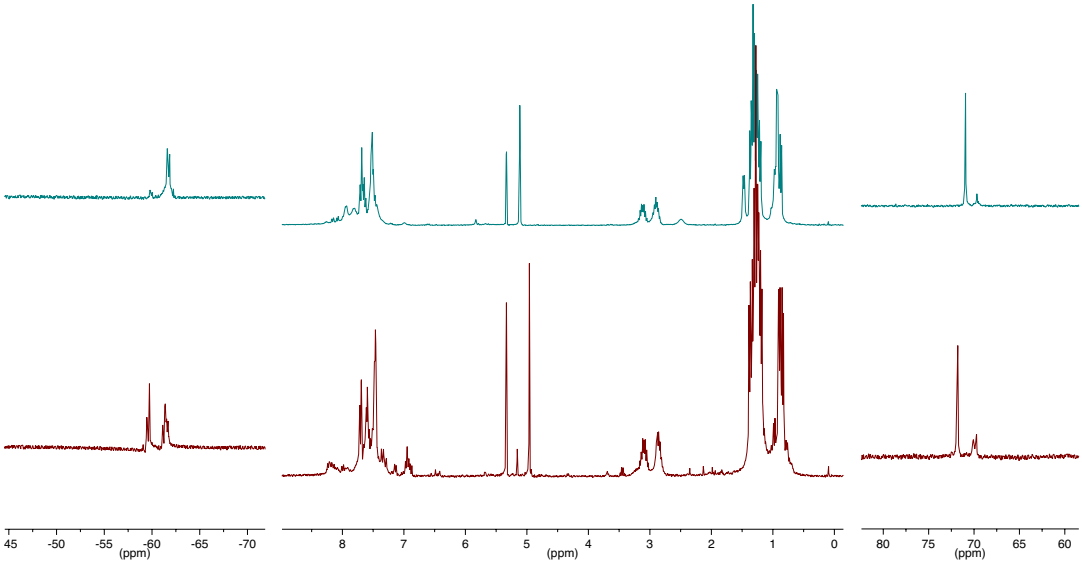


**Figure C3.66.** $^{19}F$ NMR spectra (left), $^{1}H$ NMR spectra (center) and $^{31}P\{^{1}H\}$ NMR spectra (right) of **3.2e** under $O_2$ (bottom) and **3.3** + $(p CF_3C_6H_4BO)_3$ under $N_2$ (top) in $CD_2Cl_2$ at 25 °C.

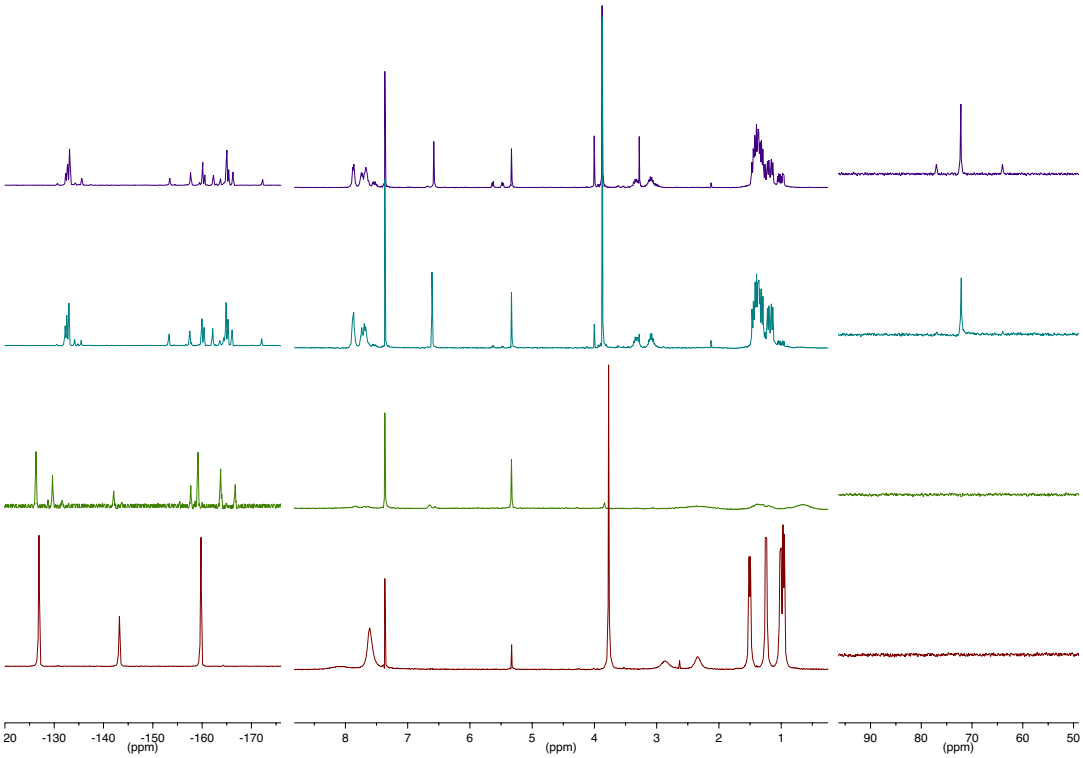


**Figure C3.67.** $^{19}F$ NMR spectra (left), $^{1}H$ NMR spectra (center) and $^{31}P\{^{1}H\}$ NMR

spectra (right) of **3.2f** and 2 equivalents $B(C_6F_5)_3$ under $N_2$ (maroon), under $O_2$ for 10 minutes (green), 7 hours (teal), and 24 hours (purple) in $CD_2Cl_2$ at 25 °C.

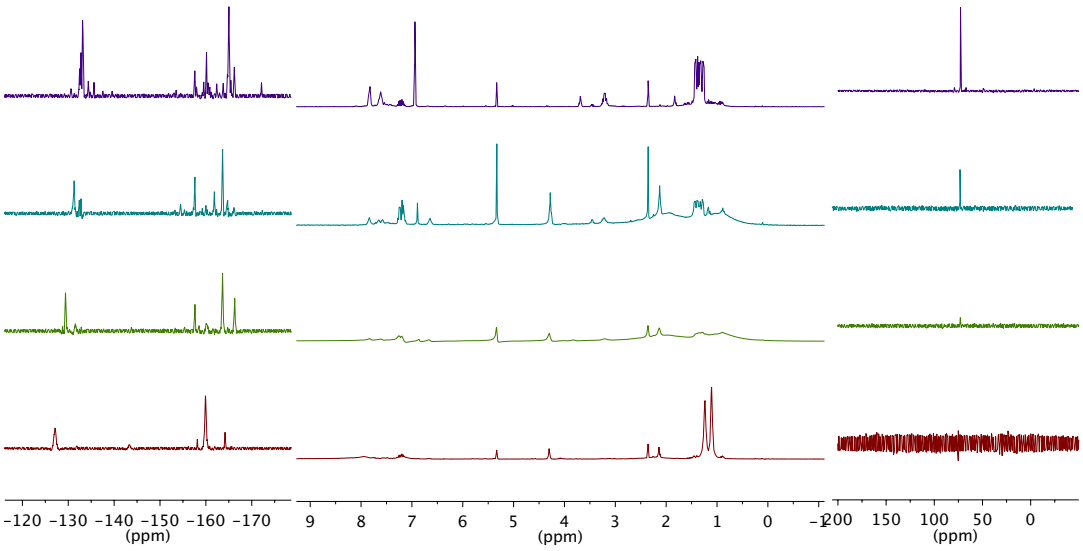


**Figure C3.68.** $^{19}F$ NMR spectra (left), $^{1}H$ NMR spectra (center) and $^{31}P\{^{1}H\}$ NMR spectra (right) of **3.2g** and 2 equivalents $B(C_6F_5)_3$ under $N_2$ (maroon), under $O_2$ for 15 minutes (green), 12 hours (teal), and 36 hours (purple) in $CD_2Cl_2$ at 25 °C.

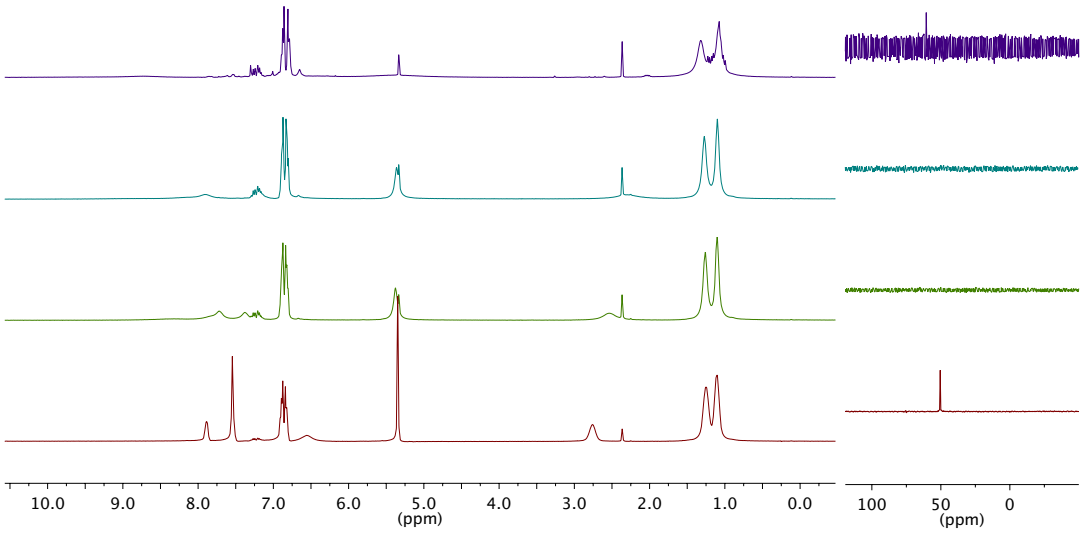


**Figure C3.69.** $^{1}H$ NMR spectra (left) and $^{31}P\{^{1}H\}$ NMR spectra (right) of **3.2g** and catechol under $N_2$ (maroon), under $O_2$ for 10 minutes (green), 3 hours (teal), and 36 hours (purple) in $CD_2Cl_2$ at 25 °C.

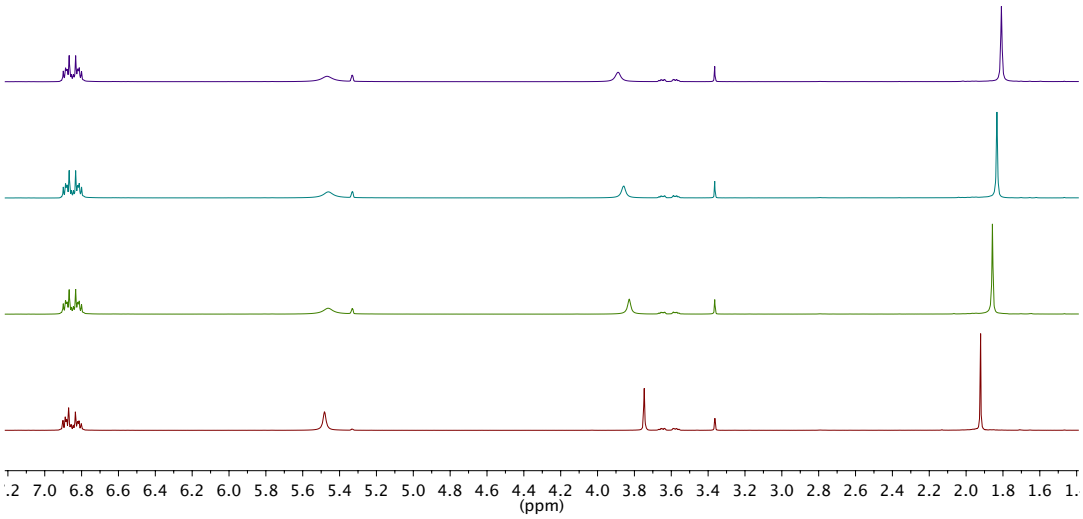


**Figure C3.70.** $^{1}H$ NMR spectra of $Me_4Fc$ and catechol under $N_2$ (maroon), under $O_2$ for 10 minutes (green), 90 minutes (teal), and 3 hours (purple) in $CD_2Cl_2$ at 25 °C.

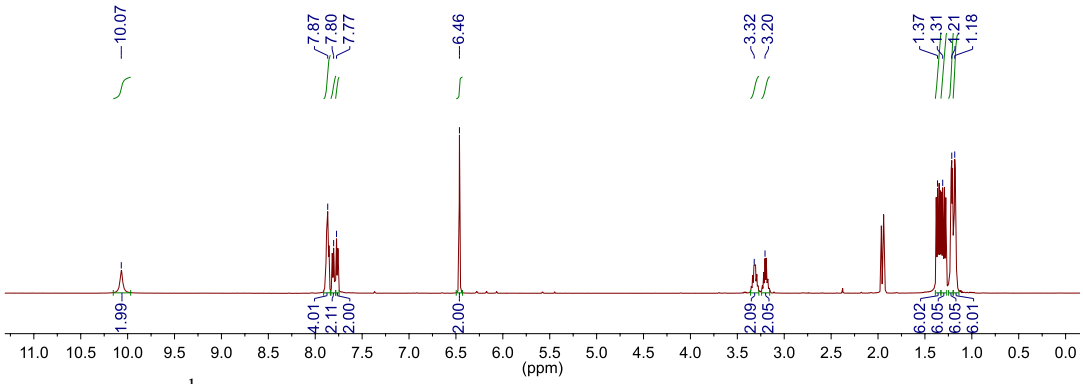


**Figure C4.1.** $^{1}$H NMR spectrum of **4.2** in $CD_3CN$ at 25 °C.

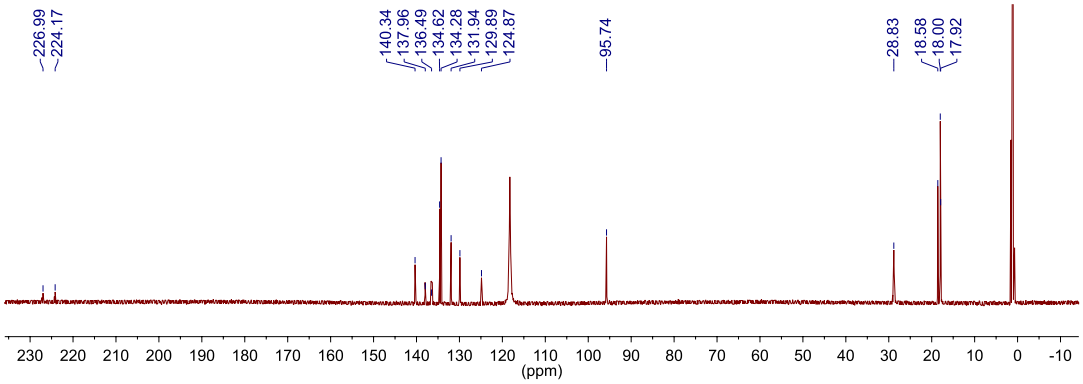


**Figure C4.2.** $^{13}$C{$^{1}$H} NMR spectrum of **4.2** in $CD_3CN$ at 25 °C.

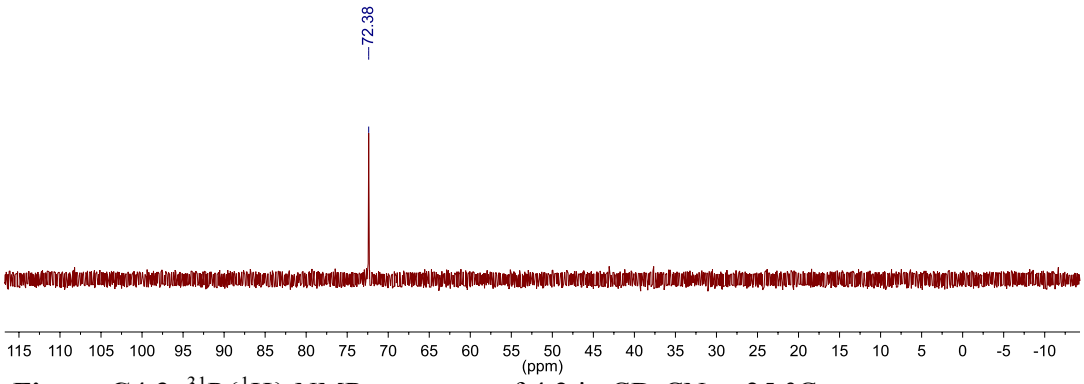


**Figure C4.3.** $^{31}$P{$^{1}$H} NMR spectrum of **4.2** in $CD_3CN$ at 25 °C.

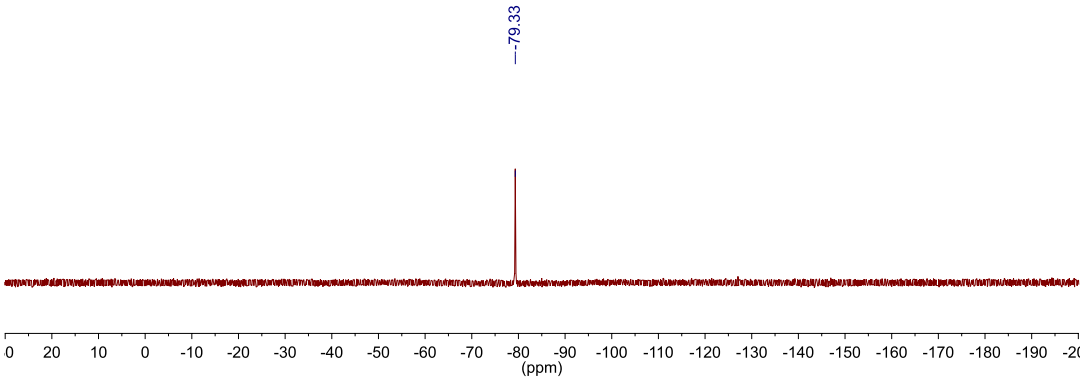


**Figure C4.4.** $^{19}F$ NMR spectrum of **4.2** in $CD_3CN$ at 25 °C.

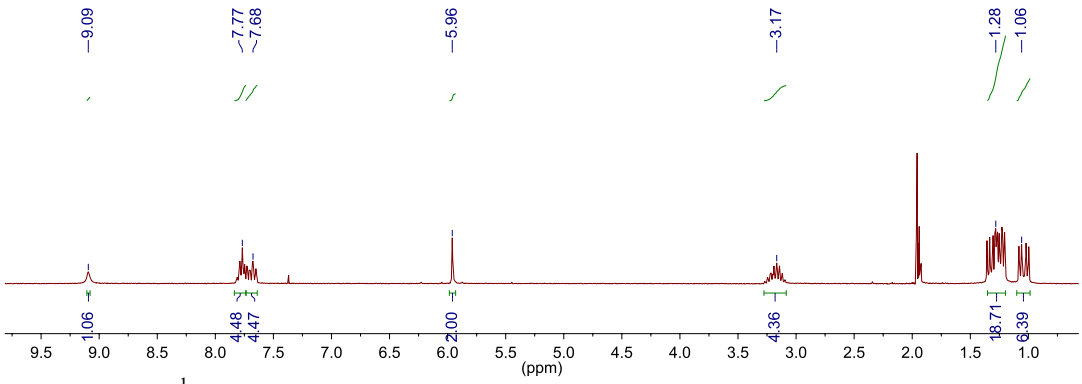


**Figure C4.5.** $^{1}H$ NMR spectrum of **4.3** in $CD_3CN$ at 25 °C.

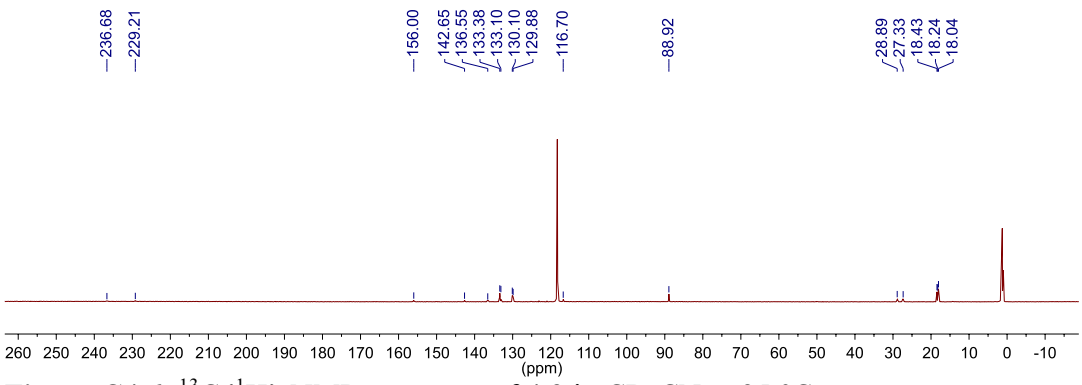


**Figure C4.6.** $^{13}C\{^{1}H\}$ NMR spectrum of **4.3** in $CD_3CN$ at 25 °C.

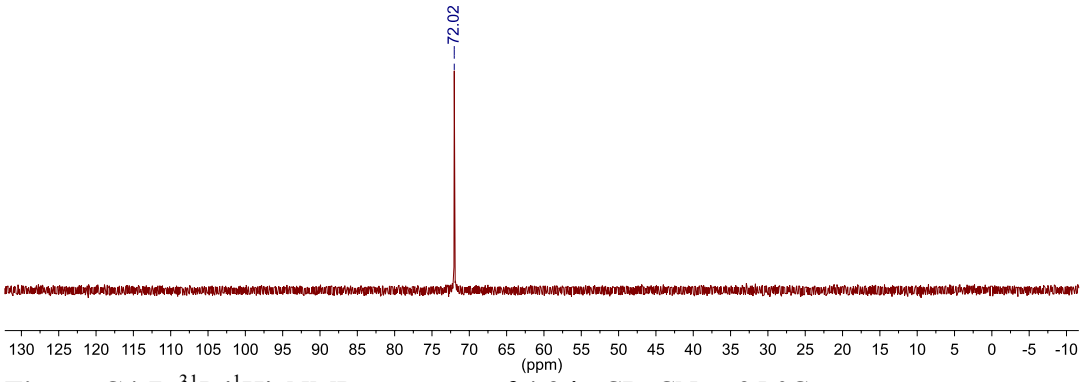


**Figure C4.7.** $^{31}P\{^{1}H\}$ NMR spectrum of **4.3** in $CD_3CN$ at 25 °C.

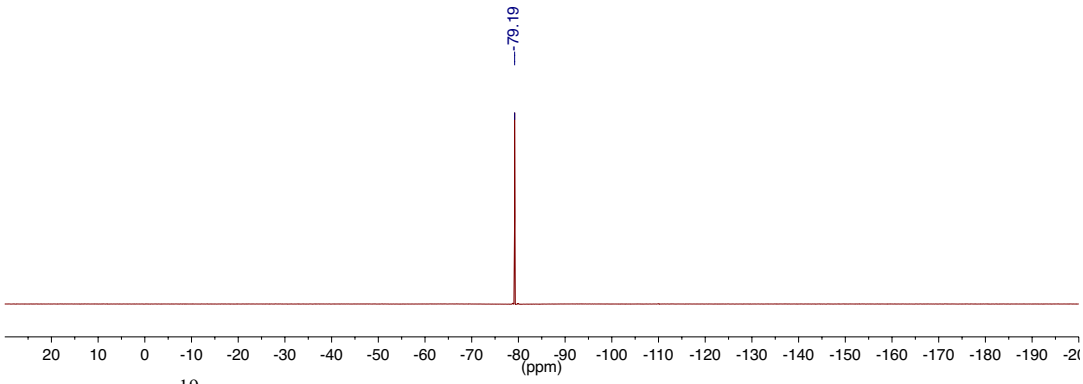


**Figure C4.8.** $^{19}F$ NMR spectrum of **4.3** in $CD_3CN$ at 25 °C.

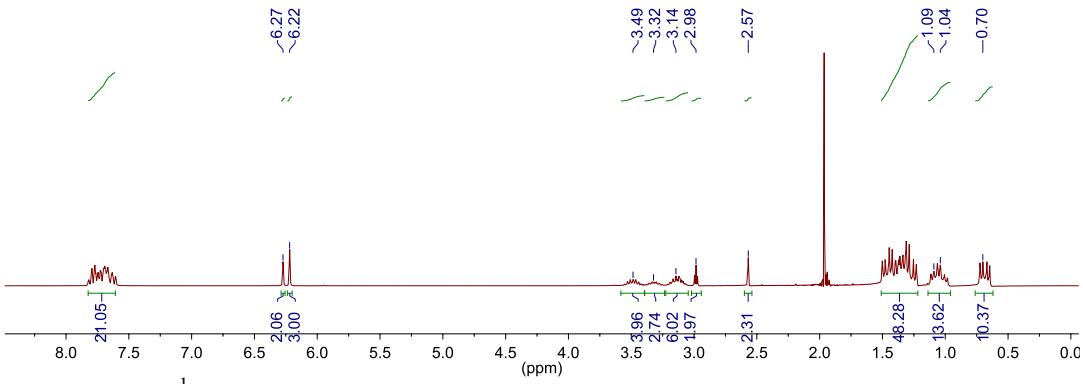


**Figure C4.9.** $^{1}H$ NMR spectrum of mixture of **4.5a** and **4.5b** in $CD_3CN$ at 25 °C.

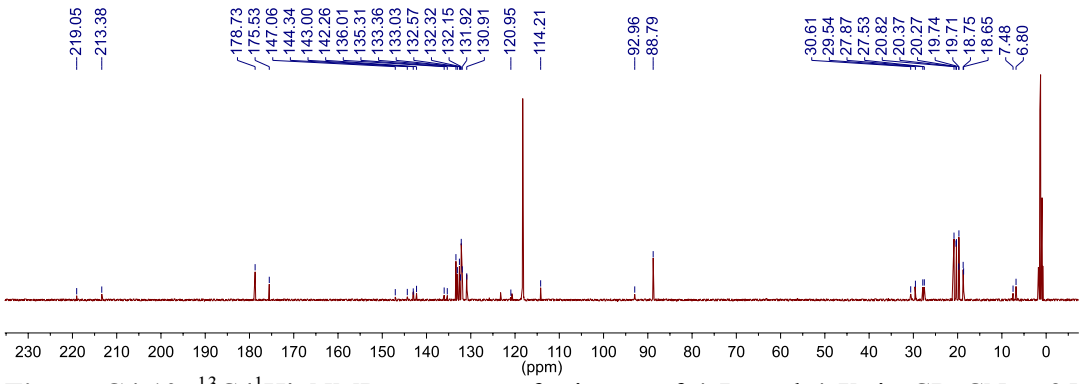


**Figure C4.10.** $^{13}C\{^{1}H\}$ NMR spectrum of mixture of **4.5a** and **4.5b** in $CD_3CN$ at 25 °C.

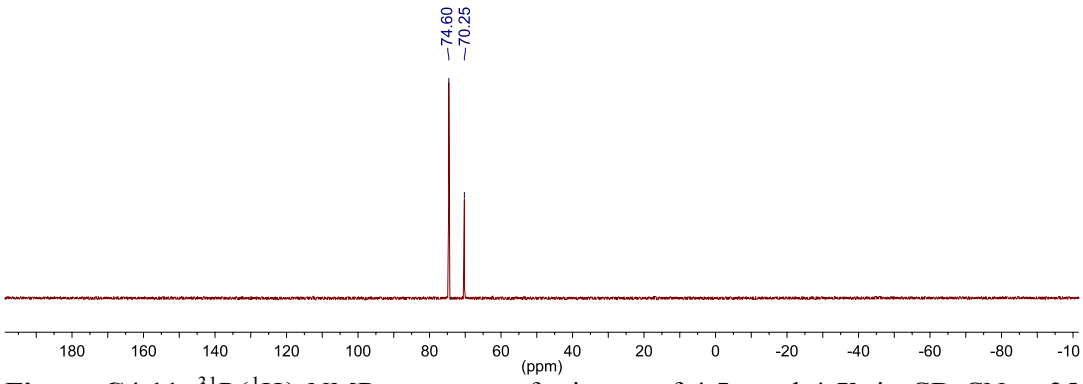


**Figure C4.11.** $^{31}P\{^{1}H\}$ NMR spectrum of mixture of **4.5a** and **4.5b** in $CD_3CN$ at 25 °C.

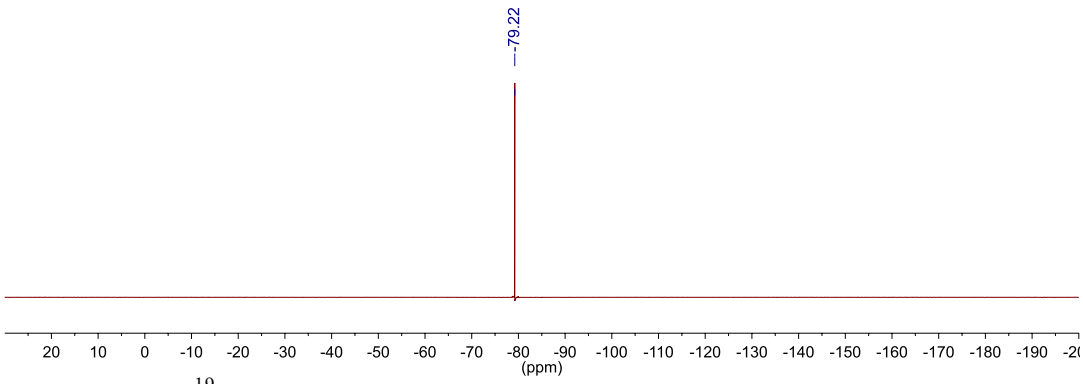


**Figure C4.12.** $^{19}F$ NMR spectrum of mixture of **4.5a** and **4.5b** in $CD_3CN$ at 25 °C.

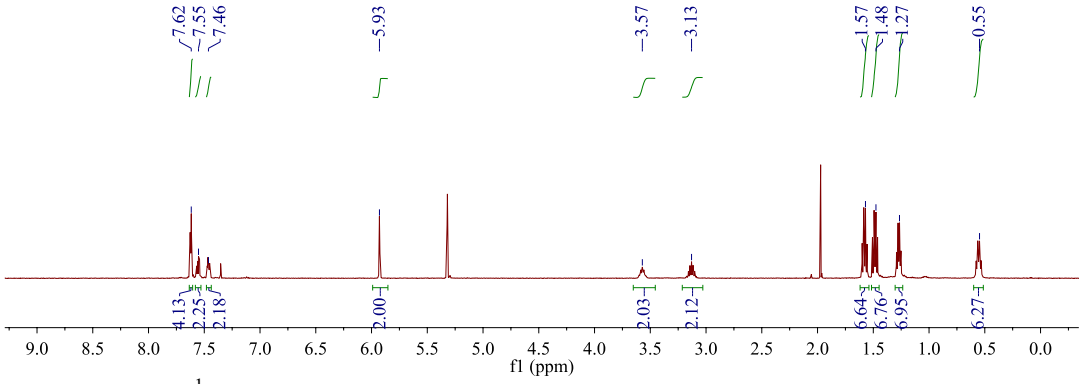


**Figure C4.13.** $^{1}H$ NMR spectrum of **4.6** in $CD_2Cl_2$ at 25 °C.

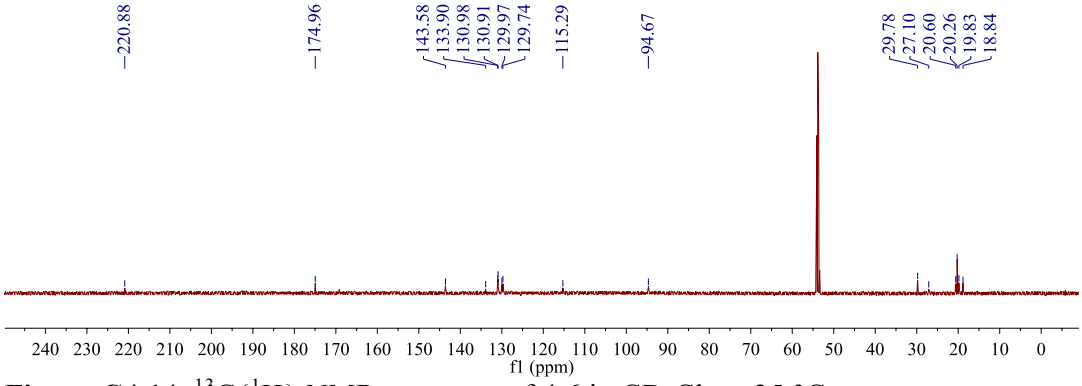


**Figure C4.14.** $^{13}C\{^{1}H\}$ NMR spectrum of **4.6** in $CD_2Cl_2$ at 25 °C.

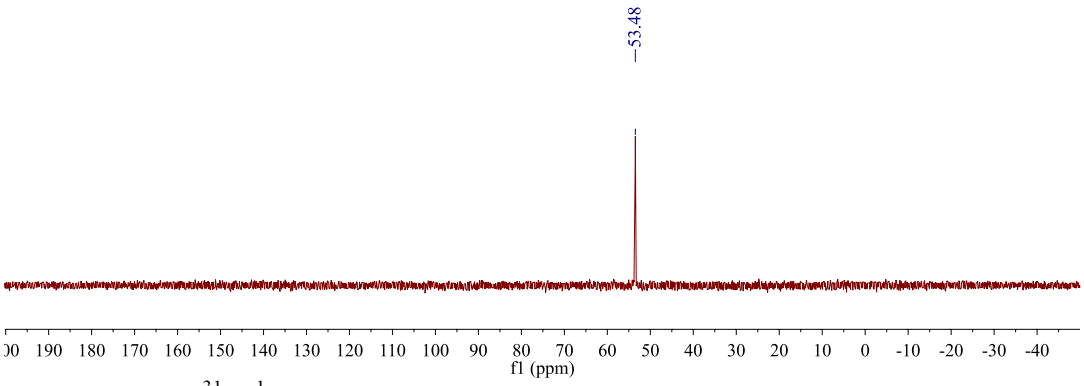


**Figure C4.15.** $^{31}P\{^{1}H\}$ NMR spectrum of **4.6** in $CD_2Cl_2$ at 25 °C.

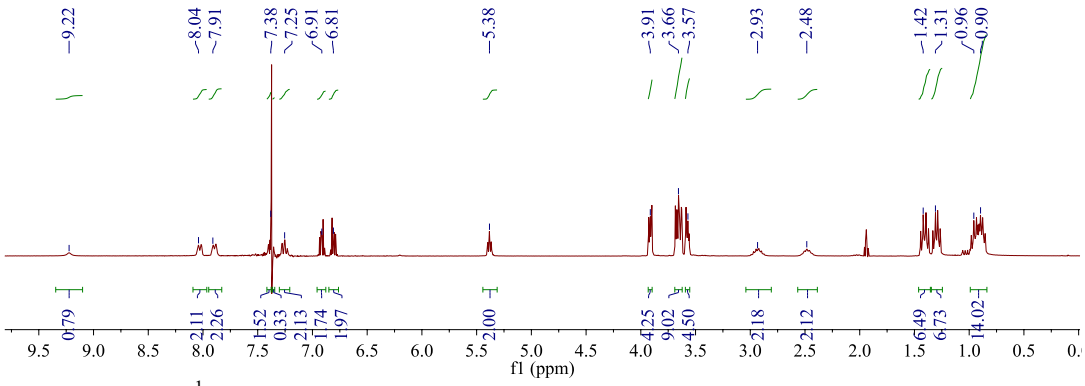


**Figure C4.16.** $^{1}$H NMR spectrum of **4.9** in $CD_3CN$ at 25 °C.

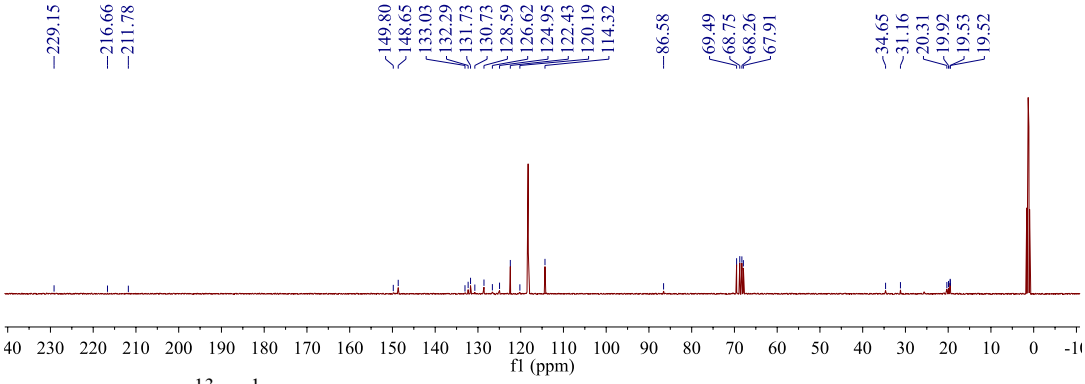


**Figure C4.17.** $^{13}$C{$^{1}$H} NMR spectrum of **4.9** in $CD_3CN$ at 25 °C.

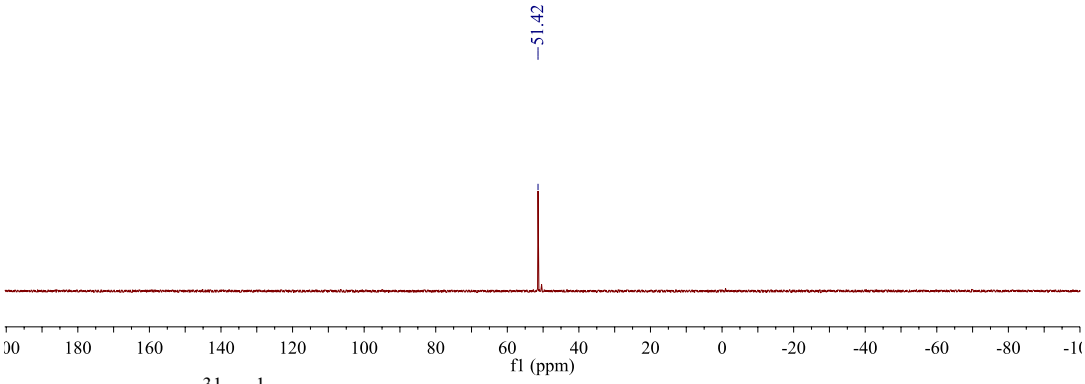


**Figure C4.18.** $^{31}$P{$^{1}$H} NMR spectrum of **4.9** in $CD_3CN$ at 25 °C.

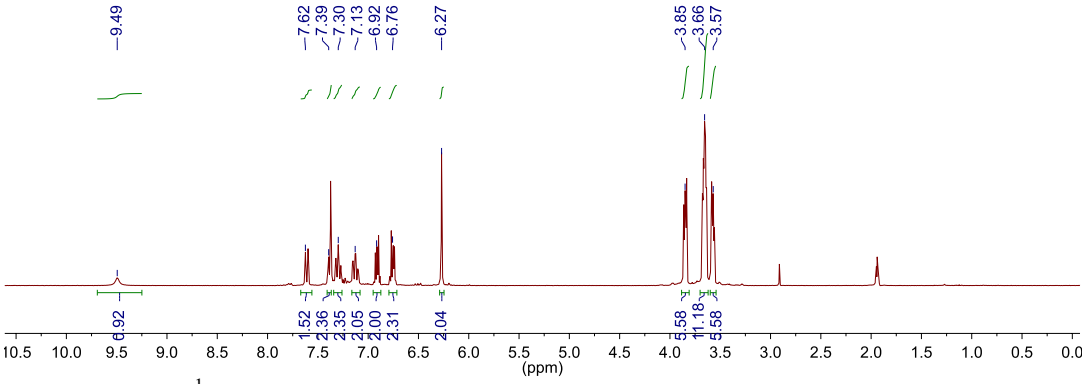


**Figure C4.19.** $^{1}$H NMR spectrum of **4.10** in $CD_3CN$ at 25 °C.

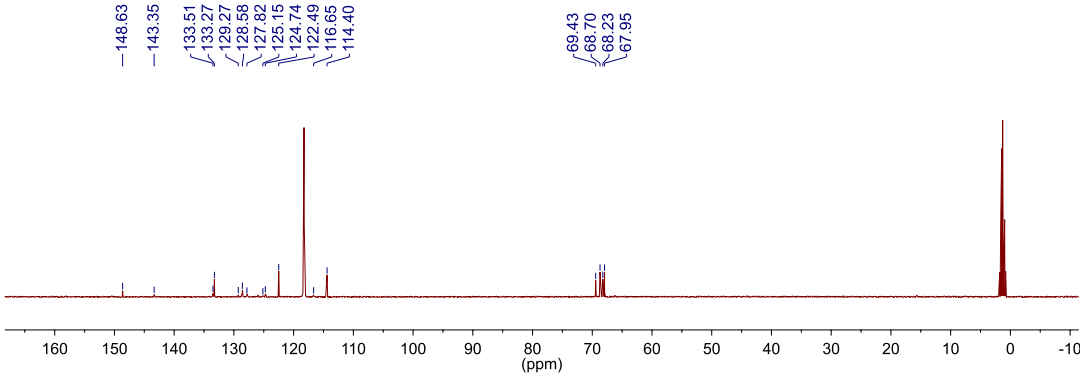


**Figure C4.20.** $^{13}$C NMR spectrum of **4.10** in $CD_3CN$ at 25 °C.

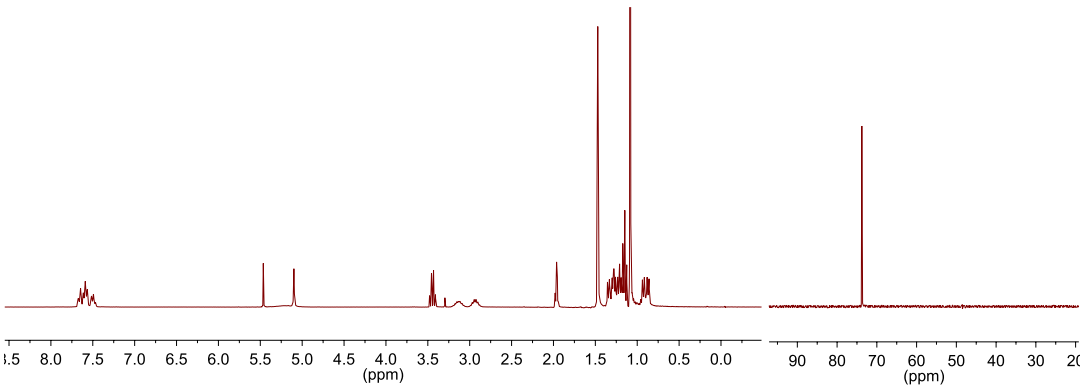


**Figure C4.21.** $^{1}$H NMR spectrum (left) and $^{31}$P NMR spectrum (right) of **4.1** and 2 equiv. TEMPO in $CD_3CN$ at 25 °C after 10 min.

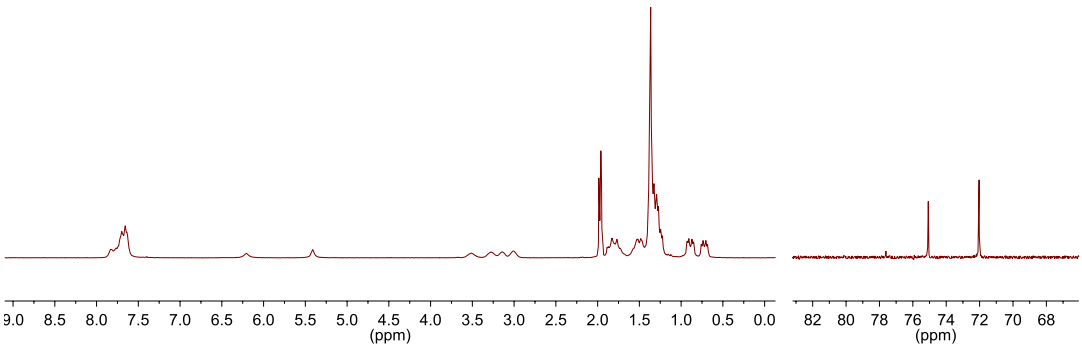


**Figure C4.22.** $^{1}$H NMR spectrum (left) and $^{31}$P NMR spectrum (right) of **4.2** and 2 equiv. TEMPO in $CD_3CN$ at 25 °C after 10 min.

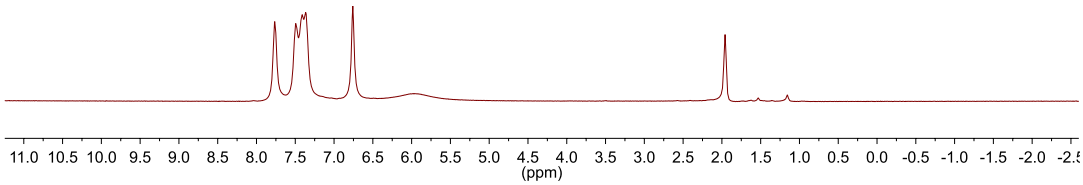


**Figure C4.23.** $^{1}$H NMR spectrum of **4.8** and 2 equiv. TEMPO in $CD_3CN$ at 25 °C after 10 min.

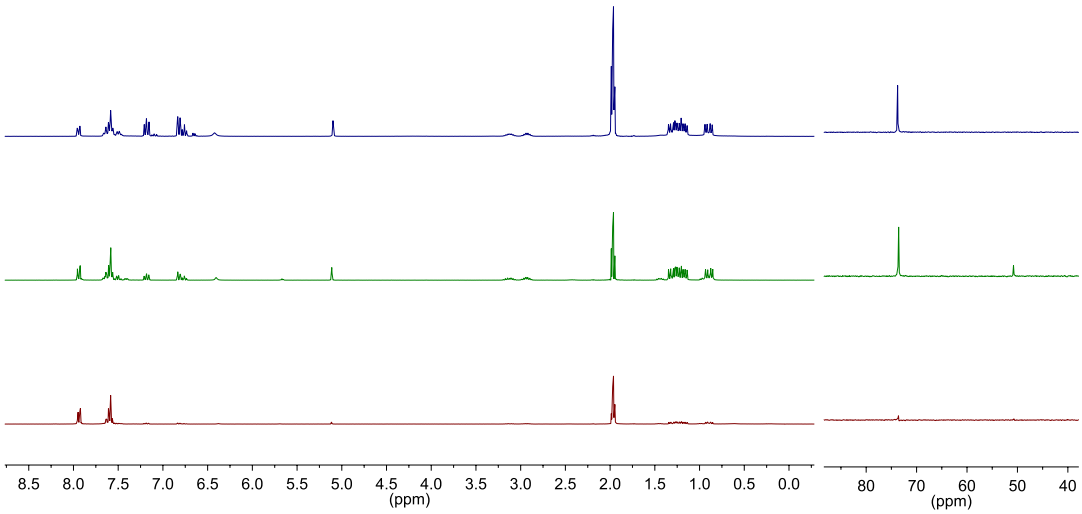


**Figure C4.24.** $^{1}$H NMR spectrum (left) and $^{31}$P NMR spectrum (right) of **4.1** and azobenzene in $CD_3CN$ after 15 min room temperature (bottom), 1 hour 80 °C (middle), and 3 hours 80 °C (top) all recorded at 25 °C. Note: the low signal corresponding to **1** in the bottom and middle spectra is due to the low solubility of **4.1** in $CD_3CN$.

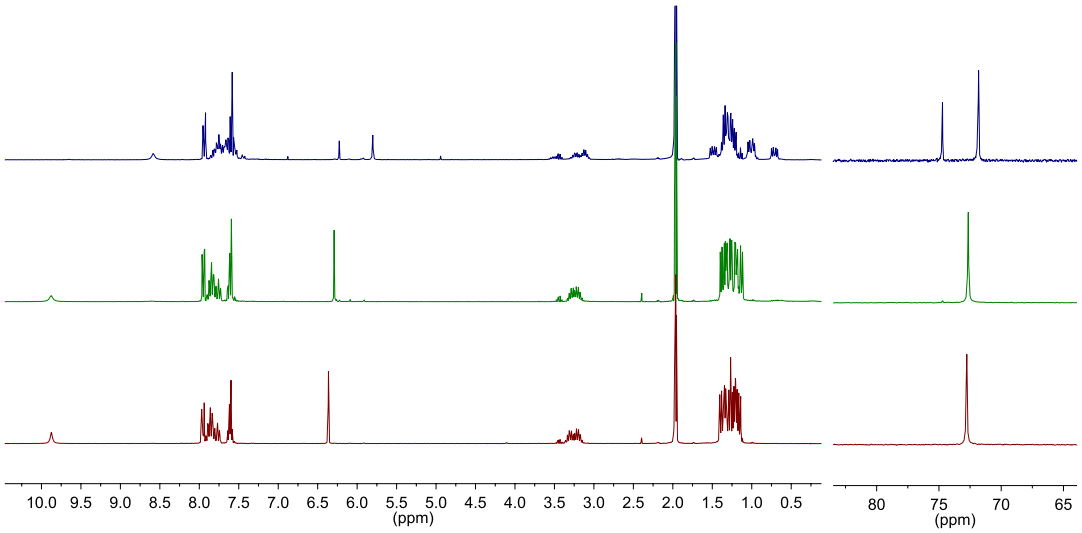


**Figure C4.25.** $^{1}$H NMR spectrum (left) and $^{31}$P NMR spectrum (right) of **4.2** and azobenzene in $CD_3CN$ after 15 min room temperature (bottom), 3 hour 80 °C (middle), and 24 hours 80 °C (top) all recorded at 25 °C.

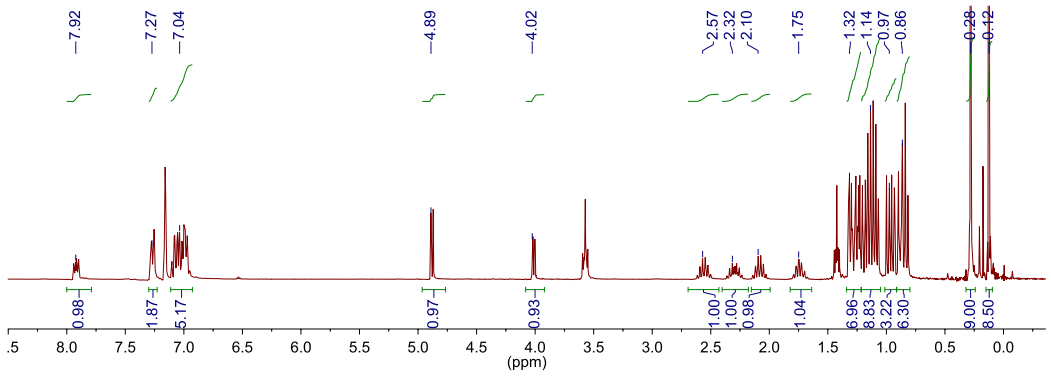


**Figure C5.1.** $^{1}$H NMR spectrum of **5.2** in $C_6D_6$ at 25 °C.

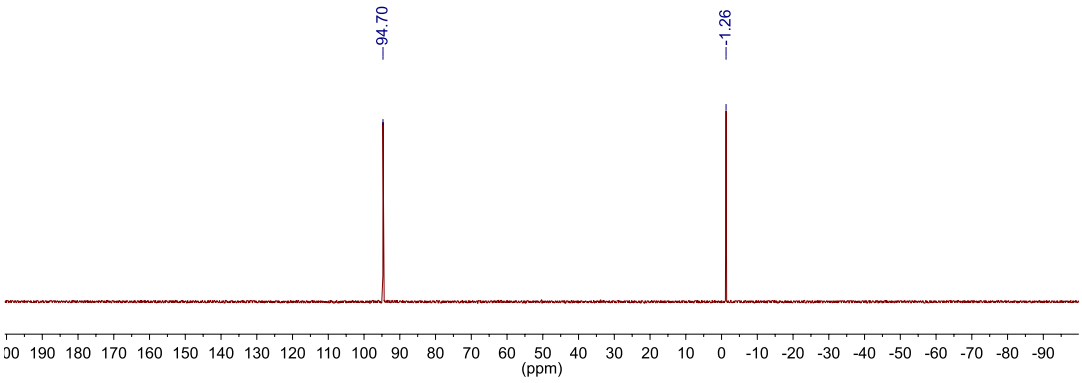


**Figure C5.2.** $^{31}$P{$^{1}$H} NMR spectrum of **5.2** in $C_6D_6$ at 25 °C.

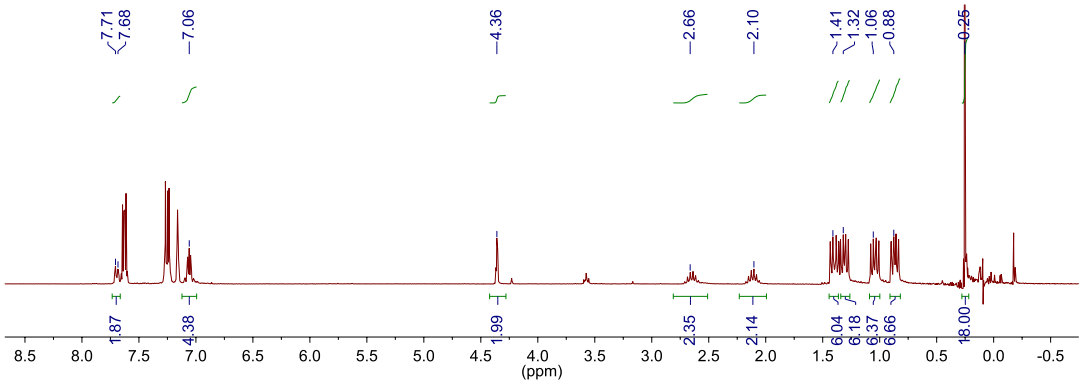


**Figure C5.3.** $^{1}$H NMR spectrum of **5.4a** in $C_6D_6$ at 25 °C.

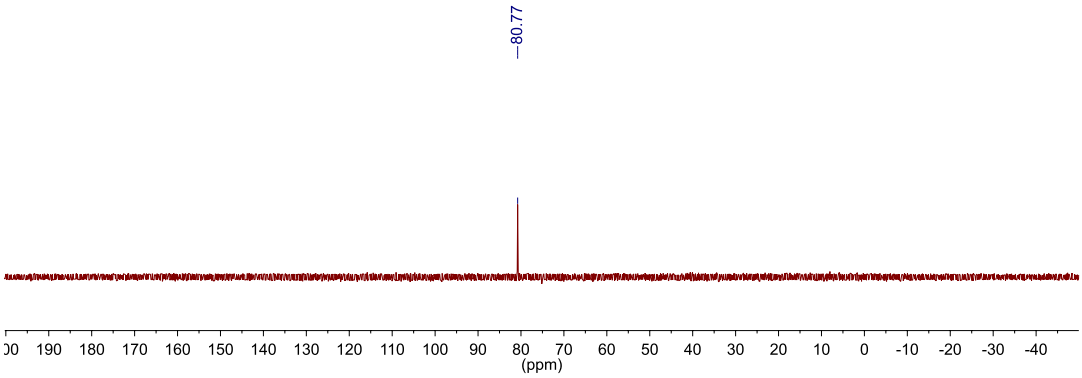


**Figure C5.4.** $^{31}P\{^{1}H\}$ NMR spectrum of **5.4a** in $C_6D_6$ at 25 °C.

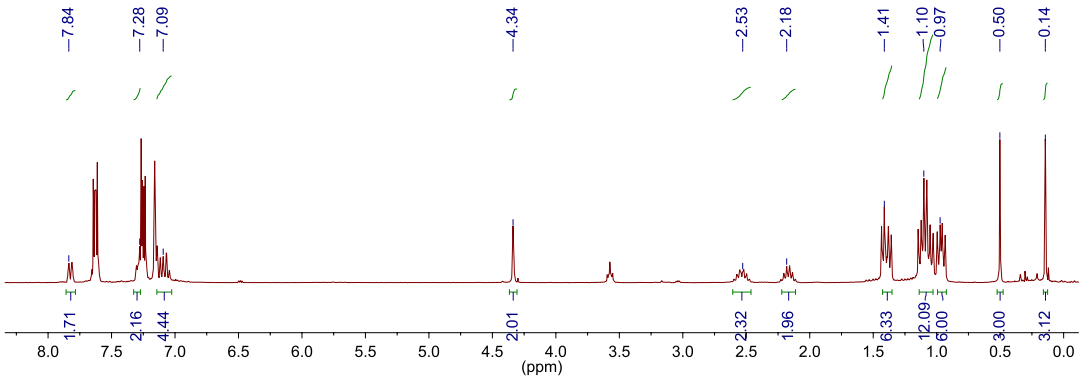


**Figure C5.5.** $^{1}H$ NMR spectrum of **5.4b** in $C_6D_6$ at 25 °C.

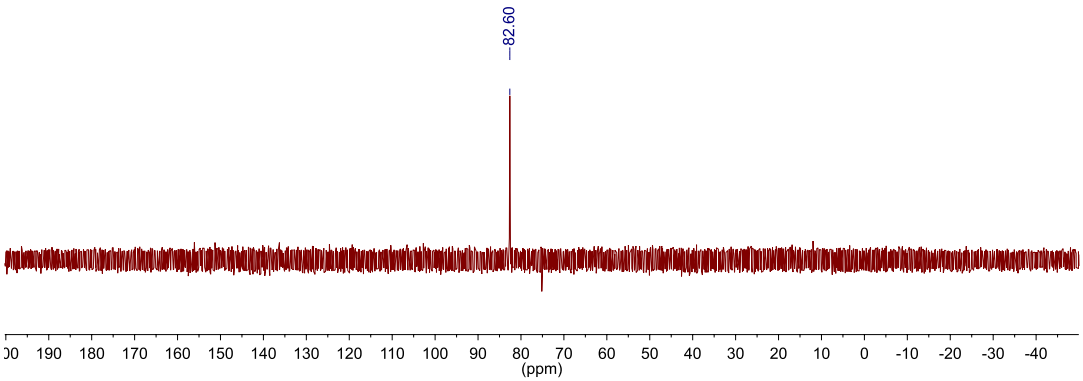


**Figure C5.6.** $^{31}P\{^{1}H\}$ NMR spectrum of **5.4b** in $C_6D_6$ at 25 °C.

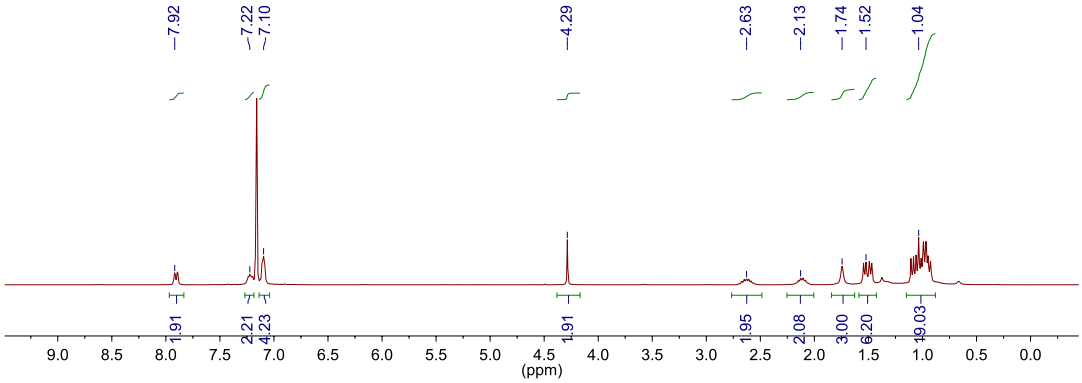


**Figure C5.7.** $^{1}$H NMR spectrum of **5.6a** in $C_6D_6$ at 25 °C.

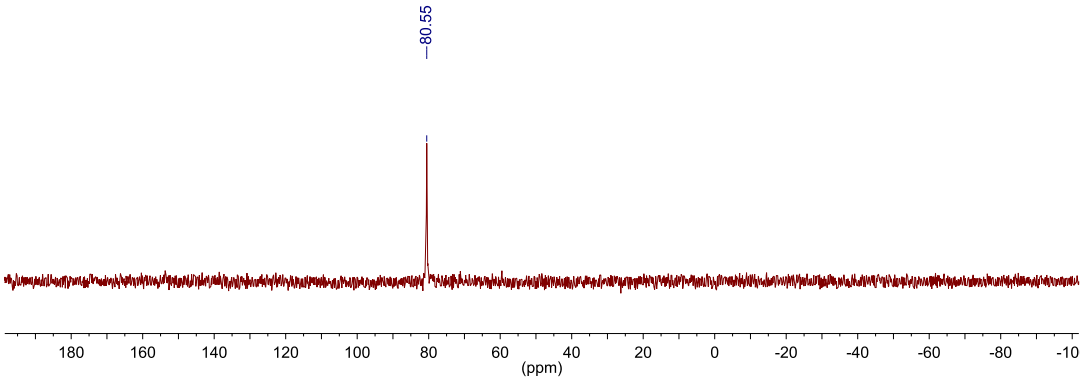


**Figure C5.8.** $^{31}$P{$^{1}$H} NMR spectrum of **5.6a** in $C_6D_6$ at 25 °C.

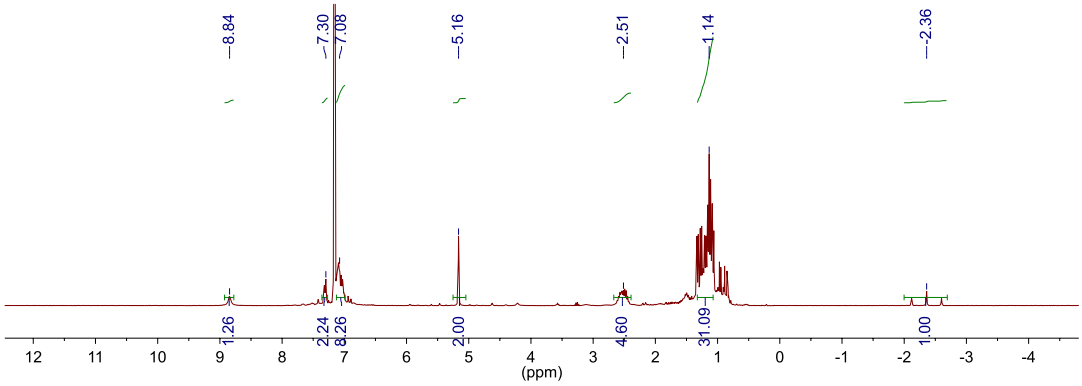


**Figure C5.9.** $^{1}$H NMR spectrum of **5.7** in $C_6D_6$ at 25 °C.

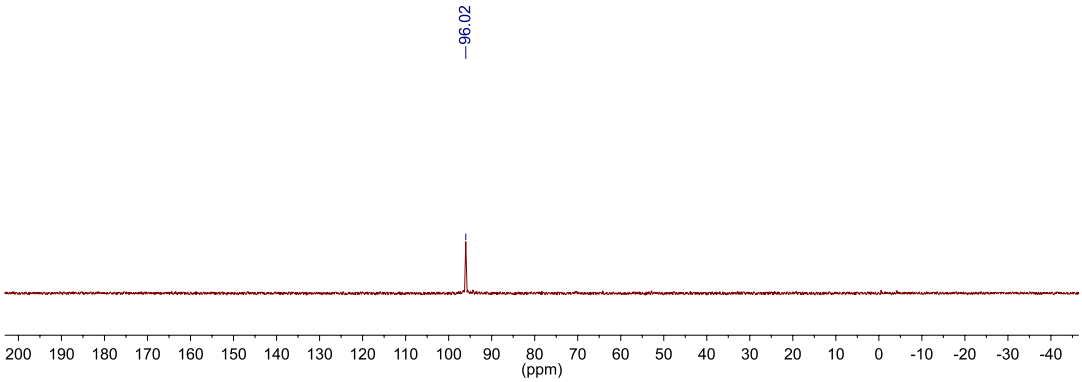


**Figure C5.10.** $^{31}P\{^{1}H\}$ NMR spectrum of **5.7** in $C_6D_6$ at 25 °C.

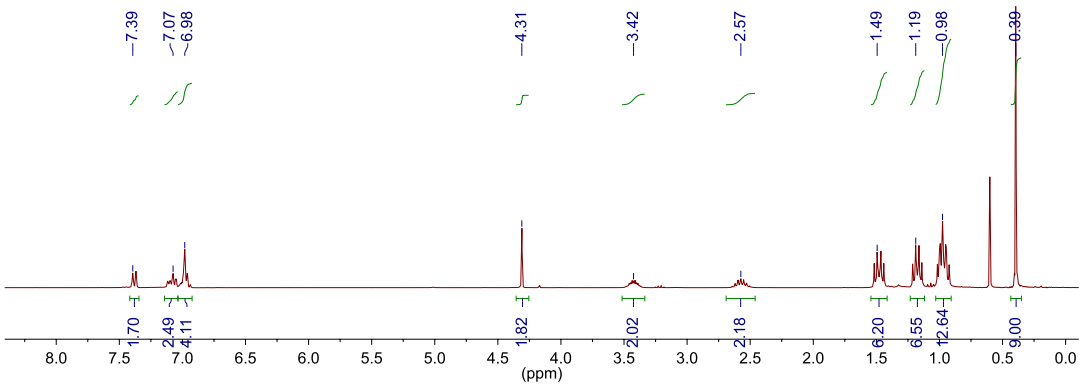


**Figure C5.11.** $^{1}H$ NMR spectrum of **5.8** in $C_6D_6$ at 25 °C.

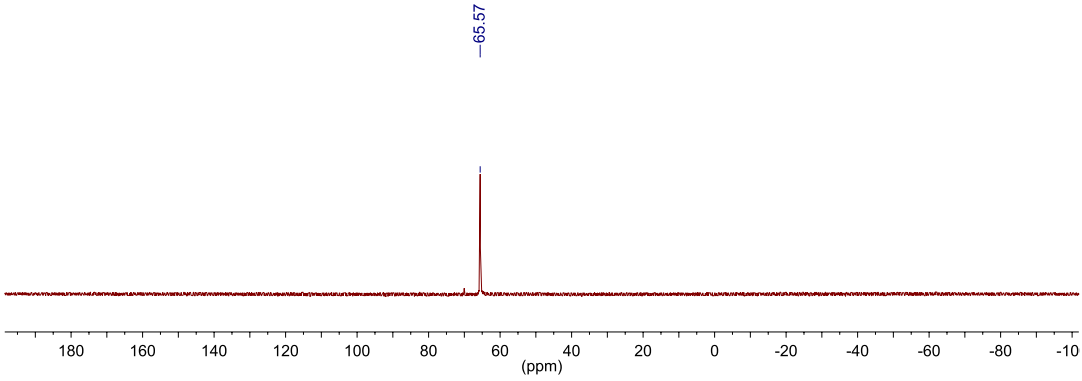


**Figure C5.12.** $^{31}\{^{1}H\}$ NMR spectrum of **5.8** in $C_6D_6$ at 25 °C.